The Pennsylvania State University

The Graduate School

Department of Veterinary and Biomedical Sciences

METABOLOMICS REVEALS THE IMPACT OF XENOBIOTICS ON THE HOST-METABOLITE-MICROBIOME INTERACTION

A Dissertation in

Molecular Toxicology

by

Jingwei Cai

Submitted in Partial Fulfillment
of the Requirements
for the Degree of

Doctor of Philosophy

August 2018

The dissertation of Jingwei Cai was reviewed and approved* by the following:

Andrew D. Patterson
Tombros Early Career Professor
Associate Professor of Molecular Toxicology
Associate Professor of Biochemistry and Molecular Biology
Dissertation Advisor
Chair of Committee

Gary H. Perdew
John T. and Paige S. Smith Professor in Agricultural Sciences
Interim Department Head

Curtis J. Omiecinski
Professor of Veterinary & Biomedical Sciences
H. Thomas and Dorothy Willits Hallowell Endowed Chair in Agricultural Sciences
Co-chair of the Intercollege Graduate Degree Program in Molecular Toxicology

Matam Vijay-Kumar
Associate Professor of Physiology and Pharmacology

*Signatures are on file in the Graduate School

ABSTRACT

The diversity and composition of the bacterial community inhabiting the human gastrointestinal tract contributes to the evolutionary fitness of the host through its role in extracting energy from diet and producing signaling molecules (e.g., short chain fatty acid [SCFA] and bile acid) to regulate metabolic and immunological function. Further, the gut microbiome composition and function can be perturbed by environmental stressors (xenobiotics, toxicants, drugs), change in diet (nutrition) or lifestyle (smoking, exercise, stress), and thus greatly influence the host metabolic phenotype and disease risk. A better understanding of how the xenobiotic-microbiome-host interaction contributes to disease risk may identify new therapeutic targets for metabolic and inflammatory disorders like obesity and diabetes.

High-throughput metabolomics approaches including liquid chromatography coupled with mass spectrometry (LC-MS), gas chromatography coupled with mass spectrometry (GC-MS) and nuclear magnetic resonance (NMR) spectroscopy inform metabolic changes by creating a “metabolite dictionary” to decipher the metabolite chatter between the host and the gut microbiota. Moreover, robust genomics approaches, including 16S rRNA gene sequencing, metagenomics and metatranscriptomics, provide an additional perspective to view and understand the microbiome community structure and function. By combining those approaches, the correlation between microbial community structure, metabolic profiles and phenotypes of microbiome and host can be established to develop a deeper understanding of microbiota-host interaction. Therefore, the central hypothesis of the dissertation is metabolomics in addition with other

informative techniques enables the comprehensive and complementary understanding of the mechanistic interplay between the host and microbiome.

Given the biological and clinical significance of microbiota and microbial-derived metabolites like SCFAs and bile acids, reliable and efficient metabolomics platforms and methods to provide robust detection and quantitation results with improved analytical confidence is highly demanded. Four different methods for SCFA extraction and quantitation were evaluated and compared using two independent platforms GC-MS and ^{1}H NMR spectroscopy. MS-based methods, especially after derivatization, have incomparable sensitivity and precision thus they are highly recommended for trace/ultratrace detection. GC-MS acidified water method, because of the easier sample preparation and short run time is most suitable for studies with large sample numbers. Alternatively, NMR-based methods, while exhibiting high repeatability and relatively low sensitivity, are suitable for cecal and fecal samples with both global and target analysis purpose. The application of three mutually independent methods, GC-MS, NMR, and bomb calorimetry in the germ free (GF) mice study showed consistent results, demonstrating the feasibility of the techniques used in metabolomics studies and the critical role that gut microbiome play in host energy balance and metabolic status.

To investigate the metabolic functional roles of gut microbiome and how to target the microbiome for potential pharmaceutical application, a typical xenobiotic and antioxidant tempol (4-hydroxy-2,2,6,6-tetramethylpiperidine-N-oxyl) with anti-obesity and microbiome-modulation effect was investigated in conventionally-raised (CONV-R) and GF mouse models. The metabolic changes were evaluated with metabolomics tools combined with biochemistry and molecular biological techniques. The results

demonstrated tempol exerts its metabolic regulatory role on host through changing gut microbiota metabolism. Tempol decreases gut energy availability by inhibiting bacterial SCFAs production in a dose-dependent manner, and the restricted gut SCFAs availability impacts overall host metabolism by promoting energy expenditure. This study provides insight into a possible mechanism for the anti-obesity effect of tempol mediated by gut-microbiota, which sheds light on the pharmaceutical and therapeutic potential of tempol for obesity treatment and prevention.

The gut microbiome affects the bioavailability and toxicity of xenobiotics and can be modulated physiologically, compositionally and metabolically by xenobiotics. To further investigate the causal relationship between xenobiotic exposure and changes in gut microbiota metabolism, a novel approach combining in vitro bacterial incubation, single-cell flow cytometry, and global metabolomics tools including Orbitrap LC-MS and ^{1}H NMR were developed to elucidate the direct impact of xenobiotics on the microbiome physiology and metabolism. This multi-platform approach identified the unique physiological and metabolic biomarkers for microbial membrane damage and metabolism disruption. The result also revealed that the disrupted metabolic activity of the gut microbiota is strongly correlated with the bacterial membrane damage by direct xenobiotic exposure. Importantly, in vitro and in vivo results were highly consistent thus indicating the in vitro methods can be a convenient, economic approach to better understand and/or predict in vivo physiological and metabolic responses to xenobiotics for future screening and risk assessment application.

Together, the research presented in the dissertation demonstrates valuable metabolomics tools combined with other techniques are elegant approaches to study

xenobiotics-microbiome-host interactions, therefore opening up avenues for better risk assessment and toxicity study during drug discovery to minimize undesirable side effects.

TABLE OF CONTENTS

LIST OF FIGURES

LIST OF TABLES

ABBREVIATIONS

%R: percent recovery
HUMAnN2: **H**uman microbiome project **U**nified **M**etabolic **An**alysi**s** **N**etwork
1α,25-(OH)2-D_3: 1,25-dihydroxyvitamin D_3
3α-HSD: 3α-hydroxysteroid dehydrogenase
ABC/Abc: ATP-binding cassette
ACC/Acc: acetyl coenzyme A carboxylase
Acly: ATP citrate lyase
AHR: aryl hydrocarbon receptor
Akt: protein kinase B
AMPK: AMP-activated protein kinase
APO/Apo: apolipoprotein
ASBT: apical sodium dependent transporter
BAT: brown adipose tissue
BCAA: branched-chain amino acid
BHI: brain heart infusion
BSEP/Bsep: bile salt excretory pump
BSH: bile salt hydrolase
C/EBPβ: CCAAT enhancer binding protein β
CA: cholic acid
CAPE: caffeic acid phenethyl ester
CAR: constitutive androstane receptor
Cd36: cluster of differentiation 36
CDCA: Chenodeoxycholic acid
Ceh: cholesteryl ester hydrolase
CFDA: carboxyfluorescein diacetate
CFSE: carboxyfluorescein diacetate succinimidyl ester
CFU: colony-forming units
ChREBP: carbohydrate responsive element-binding protein
Cidea: cell death activator
CONV-R: conventionally-raised
COSY: ^{1}H–^{1}H correlation spectroscopy
COX: cycloxygenase
CV-ANOVA: ANOVA of the cross-validated residuals
CXCL: CXC chemokine ligand
CYP: Cytochrome P450
CYP27A1: sterol-27-hydrolase
CYP7A1: 7α-hydroxylase

DC: dendritic cell
DCA: deoxycholic acid
DiBAC: Bis-(1,3-Dibutylbarbituric Acid) Trimethine Oxonol
DIO2: deiodinase-2
ERK: extracellular signal-regulated kinase
FABP/Fabp: fatty acid binding protein
Fas: fatty acid synthethase
FFAR: free fatty acid receptor
FGF 19: fibroblast growth factor 19
FGF-R4: FGF receptor type 4
FID: flame ionization detection
Fmo: flavin Containing Monooxygenase
Foxo: forkhead box protein O1
FXR: farnesoid X receptor
G6pase: glucose 6-phosphatase
GC-MS: gas chromatography coupled with mass spectrometry
GF: germ free
GLC: gas-liquid chromatography
GLP-1: glucagon-like peptide-1
Glut: glucose transporter
GMCA: glycine-β-muricholic acid
GPBAR1/TGR5: G protein-coupled bile acid receptor 1
GPR: G protein-coupled receptors
Gsk3β: glycogen synthase kinase 3β
GST/Gst: glutathione S-Transferase
HDL: high density lipoprotein
HFD: high fat diet
HMBC: ^{1}H-^{13}C heteronuclear multiple-bond correlation
HNF4/Hnf4: hepatocyte nuclear factor 4
HPLC: high Performance Liquid Chromatography
HSDH: hydroxysteroid dehydrogenase
HSQC: ^{1}H-^{13}C heteronuclear single quantum correlation
I-BABP: intestine bile acid-binding protein
IBD: inflammatory bowel disease
ICP: intrahepatic cholestasis of pregnancy
IFN-γ: interferon gamma
IgA: immunoglobulin A
IGN: gluconeogenesis
IL: interleukin
iNKT: natural killer T cell

LAGB: laparoscopic adjustable gastric banding
LCA: lithocholic acid
LC-MS/MS: liquid chromatography-electrospray tandem mass spectrometry
LC-MS: liquid chromatography coupled with mass spectrometry
LEfSe: **L**inear discriminant analysis **Ef**fect **S**iz**e**
Lkb: liver kinase
LOD: limit of detection
LOQ: limit of quantitation
LPL: lipoprotein lipase
LPS: lipopolysaccharide
LR: linear range
LRH-1: liver-related homolog-1
LXR: liver X receptor
MARK: mitogen-activated protein kinase
MCA: muricholic acid
MDR/Mdr: multidrug resistance protein
ME: matrix effect
MRM: multiple reaction monitoring
MRP/Mrp: multi drug resistant protein
NAFLD: nonalcoholic liver disease
NASH: non-alcoholic hepatosteatosis
NF-κB: nuclear factor kappa B
NMR: nuclear magnetic resonance
NOS: nitric oxide synthase
NTCP: Na+ taurocholate co-transporting peptide
OATP/Oatp: organic anion transport polypeptide
OCA: obeticholic acid
Olfr78: Olfactory Receptor 78
OPLS-DA: orthogonal projection to latent structures with discriminant analysis
OST: organic solute transporter
PCA: principal component analysis
Pepck: phosphoenolpyruvate carboxykinase
Pfk-1: phosphofructokinase
PGC-1α/Pgc-1α: proliferator-activated receptor gamma coactivator 1-alpha
Pi: propidium iodide
PKA: protein kinase A
PPAR: peroxisome proliferator-activated receptor
Ppargc : proliferator-activated receptor γ coactivator
PPY: peptide YY
PXR: pregnane X receptor

RSD: relative standard deviation
RXR: retinoid X receptor
RYGB: Roux-en-Y gastric bypass
Scd: stearoyl CoA desaturase
SCFA: short chain fatty acid
Scp: sterol carrier protein
SHP: small heterodimer partner
SrebI: scavenger receptor BI
Srebp-1c: sterol regulatory element-binding protein 1
SULT: sulfotransferase
T2D: type 2 diabetes
Tempol: 4-hydroxy-2,2,6,6-tetramethylpiperidine-N-oxyl
Th1: T helper 1
TLC: Thin-Layer Chromatography
TNF-α: tumor necrosis factor alpha
TOCSY: ^{1}H–^{1}H total correlation spectroscopy
Tregs: regulatory T cells
TRPV6: transient receptor potential vanilloid
TSP-d_4: sodium 3-trimethylsilyl [2,2,3,3-d4] propionate
TβMCA: tauro-β-muricholic acid
UCP/Ucp: uncoupling protein
UDCA: ursodeoxycholic acid
UGT: UDP-glucuronosyltransferase
UHPLC: ultra-high pressure liquid chromatography
UPLC: ultra-performance liquid chromatography
UV: ultraviolet
VDR: vitamin D receptor
VLDL: very low density lipoprotein
VSG: visceral sleeve gastrectomy

ACKNOWLEDGEMENTS

There are so many people I want to acknowledge for the help I received during my doctoral work at Penn State. I would like to thank my advisor Dr. Andrew Patterson and the rest of my committee members Dr. Gary Perdew, Dr. Curtis Omiecinski, and Dr. Matam Vijay-Kumar for their patience and support in overcoming numerous difficulties I have faced through my research. I would like to express my gratitude to the technical and spiritual support that my labmates offered. Also, I want to thank my family, especially my parents and my husband for the greatest support and encouragement to turn me into a responsible and full-grown individual.

I would like to express my sincere gratitude to my advisor Dr. Andrew Patterson for the continuous and utmost support of my doctoral work. His caring, patience, motivation, and immense knowledge helped me throughout my research and life in America. The freedom, respect and patience he gave me and the artistic, hands-on techniques for teaching has developed me into a critical and self-motivated researcher, which will benefit me for the rest of my life. His support extends to my life as well which makes me feel at home working in the lab. I could not have imagined a better advisor, mentor and friend in my life.

Next, I would also like to thank the rest of my committee members: Dr. Gary Perdew, Dr. Curtis Omiecinski and Dr. Matam Vijay-Kumar for their insightful comments and suggestions for my research, for the hard question which helped me to widen my research from various perspectives, and for the supporting letters they provided with their best enthusiasm whenever is needed.

My sincere thanks also goes to my current and previous fellow labmates, Dr. Yuan Yian, Dr. Jingtao Zhang, Dr. Limin Zhang, Dr. Imhoi Koo, Robert Nichols, Anitha Vijay and Jared Correll, for the brainstorming discussions, the skills and experience advising, the comprehensive work collaborations, and for all the fun and laughter shared during my entire doctoral research. Moreover, I would like to thank Dr. Philip Smith, Dr. Emmanuel Hatzakis and Dr. Tapas Mal for the MS- and NMR- based technical support and patient assistant, which make my metabolomics research easier and enjoyable.

I want to give my highest gratitude to my family, I could not have accomplished anything without their sacrifice and support. I am so lucky to be a member of my loving family and even though we are spread out across the globe, it hasn't stopped me from continuously receiving their spiritual support. Everything they have done for me made me who I am today, and still inspires me to become what I want to be in the future.

Finally, I want to acknowledge the financial support in part from the National Institutes of Health and Huck Institutes of the Life Sciences, which helped make this dissertation possible. [Disclaimer: The findings and conclusions in this dissertation do not necessarily reflect the view of these funding agencies.] Moreover, I want to thank Penn State, for having the best program and the greatest research atmosphere. I would also like to thank the facility and staff support from the Huck Institutes of the Life Sciences, the College of Agricultural Sciences, the Department of Veterinary and Biomedical Sciences, the Centralized Biological Laboratory, and the Animal Resource Program.

From the depths of my heart, I offer a final sincere and heartfelt thank you to everyone who has helped me through my hardest, happiest and unforgettable doctoral research at Penn State.

Chapter 1

Literature Review

Select paragraphs have been published in:

The Anti-Oxidant Drug Tempol Promotes Functional Metabolic Changes in the Gut Microbiota

Published in the Journal of Proteome Research

J Proteome Res 2016,15(2),563-71.

DOI:10.1021/acs.jproteome.5b00957

Jingwei Cai[1], Limin Zhang[1,2], Richard A. Jones[1], Jared B. Correll[1], Emmanuel Hatzakis[4], Philip B. Smith[3], Frank J. Gonzalez[5], Andrew D. Patterson[1]

Affiliations: [1]Center for Molecular Toxicology and Carcinogenesis, Department of Veterinary and Biomedical Sciences, Pennsylvania State University, University Park, State College, Pennsylvania, 16802, USA; [2]CAS Key Laboratory of Magnetic Resonance in Biological Systems, State Key Laboratory of Magnetic Resonance and Atomic and Molecular Physics, National Centre for Magnetic Resonance in Wuhan, Wuhan Institute of Physics and Mathematics, Chinese Academy of Sciences (CAS), Wuhan 430071, China; [3]Metabolomics Facility, Huck Institutes of Life Sciences, Pennsylvania State University, University Park, State College, Pennsylvania, 16802, USA; [4]Department of Chemistry, Pennsylvania State University, University Park, Pennsylvania, 16802, USA; [5]Laboratory of Metabolism, National Cancer Institute, NIH, Bethesda, Maryland, 20892, USA

Orthogonal Comparison of GC-MS and ^{1}H NMR Spectroscopy for Short Chain Fatty Acid Quantitation

Published in the Analytical Chemistry

Anal. Chem., 2017, 89 (15), pp 7900–7906

DOI: 10.1021/acs.analchem.7b00848

Jingwei Cai[1], Jingtao Zhang[1], Yuan Tian[1,2], Limin Zhang[2], Emmanuel Hatzakis[4], Kristopher W. Krausz[5], Philip B. Smith[3], Frank J. Gonzalez[5], Andrew D. Patterson[1]

Affiliations: [1]Center for Molecular Toxicology and Carcinogenesis, Department of Veterinary and Biomedical Sciences, Pennsylvania State University, University Park, State College, Pennsylvania, 16802, USA; [2]CAS Key Laboratory of Magnetic Resonance in Biological Systems, State Key Laboratory of Magnetic Resonance and Atomic and Molecular Physics, National Centre for Magnetic Resonance in Wuhan, Wuhan Institute of Physics and Mathematics, Chinese Academy of Sciences (CAS), Wuhan 430071, China; [3]Metabolomics Facility, Huck Institutes of Life Sciences, Pennsylvania State University, University Park, State College, Pennsylvania, 16802, USA; [4]Department of Chemistry, Pennsylvania State University, University Park, Pennsylvania, 16802, USA; [5]Laboratory of Metabolism, National Cancer Institute, NIH, Bethesda, Maryland, 20892, USA

Microbiome is Important for Human Health

The microbiome consists of microbial organisms that reside in the human body, making up to approximately 1-5 pounds of the human body weight. The microbiome plays essential roles in development, nutrition, metabolism, physiology, and immunity of the host. The gut microbiome is the most well-studied community compared to microbiomes at other body sites (e.g., skin, lung). Disrupted gut microbiome-host interactions have been implicated in numerous diseases including metabolic disorders (obesity, diabetes), immune disorders (inflammatory bowel disease (IBD), allergies, asthma), cancer, and, potentially, autism (1). As the diversity and composition of gut microbiome can be perturbed by environmental factors including diet composition, xenobiotic exposure (drugs, environmental toxicants, antibiotics) and life-style (smoking, exercise, stress, social interactions) (2-4), a better understanding of functional role of microbiome and its regulation of host metabolic responses is an important prerequisite for designing microbiome-specific therapeutic strategies to combat disease.

Dynamic Distribution of Normal Microbiota

Microbes start colonizing the human body at birth, newborn handling (e.g., through contact with the caregiver including nurses, doctors and parents), and feeding after birth, leading to a stable, regular community. The microbiome remains throughout life and participates in maintaining health without causing disease under normal circumstances (5). In the healthy human body, the microbiome resides at surface tissues like skin, the digestive tract (mouth, stomach, and intestinal tract), respiratory tract (nose and lung), genital tract (urinary and vaginal tract) and other mucous membranes

(conjunctiva), while the internal tissues like brain, circulation system (blood, heart), muscles are considered microorganism-free (**Figure 1-1**). Importantly, the microbiome is characterized by relatively stable, body region-specific microbial inhabitants during particular life periods of an individual. For example, major inhabitants of the skin include *Staphylococcus epidermidis*, *Staphylococcus aureus*, *Micrococcus luteus* and *Diphtheroids*. The resident oral microbiota include a wide spectrum of anaerobic bacteria including *Streptococcus mutans, Viridans streptococci, Staphylococci, Fusiform bacilli, Treponemes* and *Lactobacilli*. The predominate inhabitants *Staphylococcus epidermidis*, *Staphylococcus aureus* and diphtheroids are found in the oropharynx and nose. The resident microbiota in the vagina depends on pH, hormonal level, and life stage of the female. *Lactobacillus* spp. is the predominate bacteria in female infant (vaginal pH=5) during the first month after birth. As the pH changes during the prepubescent phase (vaginal pH=7), diphtheroids, *Staphylococcus epidermidis*, Streptococci, and *E. coli* become the major inhabitants. At puberty, pH drops and adult vaginal microbiota contains *Lactobacillus acidophilus*, *Peptostreptococci*, *Staphylococci*, *Streptococci*, *Corynebacterium* and *Bacteroides*. After menopause, pH increases to neutral level similar to prepubescent, and the postmenopausal microbiota resembles that before puberty (5).

Microbiota in the gastrointestinal tract is the most diverse and relatively well-explored region. Currently more than 1000 gut microbial species have been characterized (6). Compared to the stomach where the acidic environment is hostile for bacteria, the intestinal tract is a relative hospitable environment for bacteria growth especially anaerobic genera such as *Bacteroides*, *Bifidobacterium*, *Streptococcus*,

Eubacterium, *Peptostreptococcus*, and *Clostridium* (5, 7, 8). Actinobacteria and Proteobacteria are the dominate phyla at early development stage, then the microbial diversity increases and resembles normal adult human microbial community, which is dominated by Bacteroidetes and Firmicutes at the end of the first 3-5 developmental years (9, 10). Notably, it has been suggested early life microbial development is critical for adulthood metabolic phenotypes. Microbial disruption during critical early developmental windows by antibiotics can cause tremendous and enduring metabolic consequences in later life, even though the microbial community recovers to normal after cessation of antibiotic treatment in mice model (11). In addition to pH and age, the quantity, distribution and composition of the microbiome are influenced by chemical, nutritional, and immunological gradients along the gut. In the small intestine of mice, the environment is hostile with higher concentrations of acidic digestive juices, oxygen, antimicrobials (host-derived bile acids and antimicrobial peptides) and a shorter transit time. The resistant, facultative, fast growing bacteria like Lactobacillaceae with the ability to adhere to epithelia or mucus thrives in the challenging environment (12). On the contrary, the cecum and colon environment are more hospitable to support a denser and more diverse microbial community, where the lower level of antimicrobials, slower transit time, and abundant complex carbohydrate sources favor the growth of fermentative polysaccharide-degrading anaerobic bacteria, like Bacteroidaceae and Clostridiaceae. The mouse cecum is dominated by Ruminococcaceae, Lachnospiraceae and Rikenellaceae, while Bacteroidaceae, Prevotellaceae and Rikenellaceae are enriched in the colon (12). In addition, the viscosity gradient of the mucus from the proximal to distal colon affects the local microbial composition, characterized with more abundant

mucus-associated bacteria in the proximal region (13). In addition to mucus-associated bacterial communities, digesta-associated and crypt-associated communities have been observed in different animal models and humans (14-17), indicating the complexity of the highly organized and niche-specific gut microbial community.

Functions of the Gut Microbiome

Normal gut microbiota usually exists as commensals and is relatively harmless providing benefit to the host, and thus separated from the pathogenic microbes, viruses, and parasites. However, a dysregulated and imbalance of the gut microbiome composition or function referred to as dysbiosis, has been linked to various human chronic diseases including IBD, colorectal cancer, asthma, diabetes and obesity (1, 18). The development of high throughput gene sequencing technology, metabolomics, and bioinformatics has enabled functional analysis of the gut microbiome thus providing mechanistic explanations of the beneficial or detrimental effect of gut microbiome to host (19).

Nutrient Metabolism

The gut microbiome directly participates in host nutrient metabolism. Comparison between conventionally-raised (CONV-R) and germ free (GF) rats revealed that with the help of microbial partners, CONV-R rats required 30% less caloric intake to maintain body weight relative to GF counterparts. This suggests the gut microbiome significantly contributes to host nutritional status (20). An important function of gut microbiome is metabolizing non-digestible carbohydrates to salvage extra energy from food to fuel the

host while producing short chain fatty acids (SCFAs) as end products. SCFAs play tremendous functional roles including energy sources (21), biosynthesis substrates and precursors (22), and signaling molecules for membrane receptors like G protein-coupled receptors (GPR) to regulate host metabolic and immunological pathways (23-25). An obese microbiome characterized with an increased ratio of Firmicutes to Bacteroidetes, and an increased energy harvest ability has been implicated into the pathophysiology of obesity (26). The gut microbiome can also metabolize proteins and amino acids with microbial enzymes including histamine decarboxylases encoded by microbial *hdcA* genes, which catalyze the conversion of histidine to histamine (27), and glutamate decarboxylases encoded by microbial *gadB* genes, which convert glutamate to γ-amino butyric acid (28). Some amino acid fermenting microbes (*Clostridium*, the *Bacillus-Lactobacillus-Streptococcus* groups, and *Proteobacteria*) are able to uptake and utilize peptides and amino acids to produce SCFAs, branched-chain amino acids (BCAAs) and ammonia (29, 30). It has been reported that ruminal bacteria (*Prevotella bryantii B14, Selenomonas ruminantium HD4, and Streptococcus bovis ES1*) contribute to *de novo* synthesis of amino acids (31). Moreover, metagenomics analysis has found that the human colonic microbiome is enriched with genes involved in essential amino acid biosynthesis (32), and a more recent study has identified biosynthetic genes in human microbiome for essential amino acid threonine biosynthesis (32). The gut microbiome is involved in the synthesis of vitamin K and water-soluble B vitamins, including biotin, cobalamin, folate, niacin, panthothenate, pyridoxine, riboflavin and thiamine (33, 34), which act as essential coenzymes and cofactors for numerous host metabolic functions such as DNA synthesis and regulation, glucose, fatty acid and amino acid metabolism (35,

36). Additional studies also revealed the gut microbiome is involved in breaking down and transforming dietary polyphenols to active compounds. The active products can be absorbed by the host via portal vein circulation to carry out antimicrobial and metabolic functions. For example, isoflavone is transformed to (S)-equol by a mixture of human microbes including *Bacteroides ovatus*, *Ruminococcus productus* and *Streptococcus intermedius* or *Lactobacillus mucosae*, *Enterococcus faecium*, *Finegoldia magna* and *Veillonella* spp. (37), which have anti-microbial, anti-oxidative, anti-androgenic, and anti-cancerous effects (38).

Drug and Xenobiotic Metabolism

Extensive evidence suggests that the gut microbiome affects the bioavailability and metabolism of drugs and xenobiotics through direct and indirect mechanisms. In vitro and in vivo evidence has revealed that the gut microbiome is capable of metabolizing at least 50 drugs (39, 40). Direct mechanisms involved in the microbial biotransformation of drugs into active, inactive, or toxic products occur primarily via reduction and hydrolysis with microbial enzymes. For example, the azo bond-containing prodrugs require microbial reduction for activation. The anti-inflammatory drug sulfasalazine and antibacterial drug prontosil contain azo bonds, which are reduced by microbial azoreductases, liberating the biologically active metabolites 5-aminosalicylic acid and sulfanilamide, respectively (40). Another typical example is the reduction/inactivation of digoxin by *Eggerthella lenta*. The cardiac glycoside digoxin used for the treatment of congestive heart failure and arrhythmias, was found to be reduced by *Eggerthella lenta* into the inactive metabolite dihydrodigoxin. The digoxin-

induced high cardiac glycoside reductase (*cgr*) operon activity in *Eggerthella lenta* was discovered and proven to be necessary for the reduction/inactivation of digoxin (41). Microbial hydrolysis of the chemotherapeutic drug by microbial β-glucuronidases can lead to undesirable side effects. The anti-cancer drug SN-38 and non-steroidal anti-inflammatory drugs are subject to host glucuronidation in the liver for detoxification, then are transported to the gut where glucuronides can be hydrolyzed by microbial β-glucuronidases to toxic metabolites, resulting in side effects such as diarrhea and small intestinal injuries (39, 40).

Besides directly impacting drug metabolism through microbial enzymes, the gut microbiome can affect host gene expression and receptor activity involved in xenobiotics metabolism. More than 100 differentially expressed genes have been identified between CONV-R and GF mice, predominately the cytochrome P450 family, the important enzymes involved in the metabolism of drugs, xenobiotics, chemical carcinogens and toxicants (42). Another RNA-sequencing study revealed the differentially expressed xenobiotic metabolism-associated genes in the GF mouse liver compared to CONV-R counterpart, as well as significantly altered xenobiotic receptor activity in GF mice liver, including increased peroxisome proliferator-activated receptor alpha (PPARα) and aryl hydrocarbon receptor (AHR), and decreased pregnane X receptor (PXR) and constitutive androstane receptor (CAR) (43). In addition, the gut microbiome can affect drug efficacy and xenobiotic metabolism indirectly through the disposition of bacterial-derived metabolites to compete with host xenobiotic-metabolizing enzymes, resulting in diminished host capacity to metabolize xenobiotics and drugs (44).

Immunological Function

It has been increasingly appreciated that gut microbiome plays a fundamental role in induction, education and regulation of the host immune system. The immune system consists of a complex network of innate and adaptive responses, which requires a delicate balance between attacking invading pathogens and maintaining tolerance to avoid harming self-tissue (45). The crosstalk between the host immune system and the gut microbiome is mediated by recognition of microbe-associated molecular patterns. Absence (germ free) or disruption (antibiotic-treated, deliberately colonized) of the gut microbiome has been implicated in the dysregulated innate and adaptive immune responses and autoimmune diseases (46). However, normal gut microbiome under homeostatic condition do not trigger inflammatory responses. This specific immunological tolerance is likely associated with the anti-inflammatory cytokine interleukin 10 (IL-10) secreting dendritic cells (DCs) at Peyers's patches (lymphoid follicles located in the ileum region) (47) and unique "inflammation anergy" phenotype of the intestinal macrophages (48). It has been suggested that the early interactions between commensals and immune system set the tone of the mucosal and systemic immune system for the appropriate response to pathogens and commensals long term. Microbial exposure during early life is critical for establishing persistent mucosal natural killer T cell (iNKT) tolerance to prevent autoimmune diseases later in life (49). A recent study suggested microbial inhibitory sphingolipids directly inhibited iNKT cell development during early life, and the restricted colonic iNKT cell number persisted and conferred protection against oxazolone-induced colitis in adulthood (50). Commensals contribute to secondary and lymphoid structure development postnatal, including a

smaller gut-associated lymphoid tissues, reduced number of CD4+T cells and immunoglobulin A (IgA) producing plasmocytes (51, 52). The gut microbiome is critical for the development and differentiation of naïve CD4+ cells, revealed by the bacterial polysaccharide-induced correction of systemic CD4+ cells deficiency and T helper 1 (Th1) and Th2 imbalance, and the consequently restored appropriate immunological functions in *Bacteroides fragilis*-colonized GF animal (53). Other studies have shown segmented filamentous bacteria is a key inducer of pro-inflammatory Th17 cell in the small intestine, and enhances the production of IgA (54, 55), while Clostridia clusters promote colonic regulatory T cells (Tregs) (56). These findings suggest different microbial members might have distinct regulatory roles in directing T cell responses, therefore a compositional change of gut microbiome might lead to either pathological or beneficial effects. Additional immune-regulatory roles mediated by microbial-derived metabolites (SCFAs and bile acids) important for directly sustaining or harming colonocytes, regulating mucosa proliferation, maintaining intestinal lining integrity and gut barrier function, modulating the anti-inflammatory activity of intestinal epithelial cells, macrophages and DCs, and activating receptor-dependent signaling pathways will be discussed in detail in the following sections.

Metabolic Signaling

The gut microbiome indirectly regulates host metabolic pathways including glucose, lipid, energy, xenobiotic metabolism and immunological functions through producing microbial-derived metabolic signaling molecules like SCFAs (23-25). Another group of critical microbial-derived metabolic and immunological signaling molecules are bile

acids (57), whose pool size and composition are intimately related to host physiological and metabolic health (58-62), and can be readily shaped by the microbiome through deconjugation, dehydroxylation, oxidation and epimerization, and other biotransformation reactions (63-66). The microbial-associated biosynthesis and biotransformation, functional significance, metabolism involvement, diseases association and therapeutic opportunity of microbial-derived metabolites (SCFAs and bile acids) will be reviewed below.

SCFAs: A Chemical Bridge Between Microbiota Activity to Host Physiology

SCFAs are those carboxylic acids with aliphatic tails less than six carbons. In human, SCFAs are largely derived from anaerobic bacterial activity in the gut referred to as "fermentation". During the fermentation process, bacteria utilize non-digestible dietary fibers, and resistant starches as energy sources for growth, producing SCFAs as end-products, which can be absorbed and utilized by the host to carry out a wide range of physiological, metabolic, and immunological functions (**Figure 1-2**). The primary fermentation-derived SCFAs are acetic acid (C2), propionic acid (C3) and butyric acid (C4). Ninety percent of SCFAs derived by bacterial fermentation are reabsorbed rapidly in the colon (67), utilized by the host as energy sources (21), anabolic substrates or precursors for biogenic synthesis (22) and signaling molecules for metabolic (23) and immunological regulation (24). Therefore, SCFAs are a chemical bridge to link bacteria activity to the host metabolic phenotype. Human fecal SCFAs levels vary however the molar ratio is fairly constant, approximately acetate:propionate:butyrate =60:20:20 (68). The physiological functions of three primary SCFAs are distinct but can overlap or

sometimes even counteract each other. Acetate is the most abundant SCFA in colon where it is transported to the liver and transformed into acetyl-CoA, a precursor for lipogenesis (22) and gluconeogenesis (69). Further, acetic acid is reported to be involved in central appetite regulation for energy intake control (70, 71). Propionic acid provides beneficial effects including anti-lipogenic (72, 73), anti-cholesterogenic (73, 74), anti-inflammatory (75, 76), anti-carcinogenic (75, 77) and energy homeostasis regulation activity . Butyric acid serves as a preferred nutrient for colonocytes (78, 79) and is implicated in colonic mucosa proliferation, intestinal lining integrity maintenance (79, 80), colonic inflammation attenuation (81, 82), and colonic cancer prevention (81, 83) and treatment (84, 85).

SCFAs are Preferable Energy Sources

Mammals are unable to digest dietary fibers and resistant starches due to lack of necessary enzymes; however, the gut bacteria possess the enzymes to break down non-digestible fibers readily. From the host perspective, the bacteria fermentation turns non-usable carbon molecules into absorbable, transportable, and usable SCFAs, thus helping the host to salvage more energy from food and fueling the physiological and metabolic activity. Bacterial-derived SCFAs account for about 5-10% of daily energy intake of the host (86). Colonocytes utilize SCFAs, especially butyrate as a preferred primary energy source (78). GF mice who are unable to produce SCFAs due to lack of microbiota are in a constant energy deprived state and show a significant downregulation of critical enzyme expression in the Krebs cycle and downstream consequences including decreased NADH/NAD+, oxidative phosphorylation, ATP levels, which lead to autophagy (87).

Interestingly, butyrate supplementation can rescue disrupted mitochondrial respiration and prevent autophagy occurrence (88). Additional evidence demonstrated butyrate is not only a preferred nutrition source, but also a prerequisite for colonocytes to maintain normal homeostasis and physiological function. Lacking luminal butyrate or lacking the ability to metabolize butyrate causes a nutritional deficiency of colonic epithelium, which might lead to mucosal atrophy in short term and "nutritional colitis" in long term (89). Recent evidence suggest SCFAs, especially butyrate is critical for intestinal epithelial to maintain gut barrier function (90, 91), which is essential to protect against intraluminal entities including foreign antigens, microorganisms and their toxic metabolites and to ensure the selective absorption of essential dietary nutrients, electrolytes and water (92). Microbial-derived acetate enters circulation, serves as an oxidizable substrate throughout the body (93), particularly 70% is taken up by the liver and undergoes further catabolism as energy substrates or biosynthesis as anabolic substrates (94).

SCFAs Serve as Building Blocks for Anabolism

SCFAs are not only direct energy substrates for tissues but also substrates for biosynthesis including glucose, cholesterol, and lipids. Propionate is a well-known precursor for hepatic gluconeogenesis (95, 96), which in the liver is first converted to propionyl-CoA and then to succinyl-CoA. Succinyl-CoA enters the Krebs cycle to generate oxaloacetate, the direct precursor for gluconeogenesis. Acetate and butyrate enter Krebs cycle as acetyl-CoA (butyrate is converted to acetyl-CoA through mitochondrial fatty acid oxidation), then is incorporated into oxaloacetate for synthesis of glucose, amino acids, cholesterol and fatty acids. Interestingly, palmitate and cholesterol

are mostly synthesized from acetate and butyrate but not propionate, suggesting the distinct metabolic fate of propionate versus acetate and butyrate (68). Additional evidence using stable isotopes showed gut-derived SCFAs reached to the liver and incorporated into long chain fatty acid palmitate aggravated metabolic syndrome in toll-like 5 receptor knockout mice, suggesting excessive gut-derived SCFAs promote augmented hepatic lipogenesis might potentiate metabolic syndrome (97).

SCFAs Act as Signaling Molecules through Receptors

SCFAs can function as integrated signaling regulators which trigger signaling cascades systemically via GPRs like free fatty acid receptor FFAR2 (GPR43), FFAR3 (GPR41), GPR109a and Olfactory Receptor 78 (Olfr78) (25, 98). FFAR2 and FFAR3 are two main SCFAs sensors with different affinity for different SCFAs. Specifically, FFAR2 preferentially binds to shorter SCFAs, the order of affinity for FFAR2 is acetate = propionate > butyrate. Whereas FFAR3 is favorably activated by relatively longer SCFAs with the order of affinity butyrate = propionate > acetate (25, 99). Besides the SCFAs binding specificity, FFAR2 and FFAR3 also differ by tissue distribution and activation mechanism. FFAR2 and FFAR3 are generally expressed broadly throughout the human body including spleen, intestine, liver, immune cells and adipocytes (99). FFAR2 is highly expressed in immune cells, especially neutrophils, monocytes, and polymorphonuclear cells (100, 101), suggesting FFAR2 could have important function in the SCFAs-mediated differentiation and activation of immune cells. FFAR3 is abundantly expressed in white adipose tissue and has been implicated in SCFAs-stimulated leptin secretion in adipocytes (102). The two receptors showed different

coupling preference during activation. Upon activation, FFAR3 only couples to pertussis toxin sensitive Gai/o family while FFAR2 couples to both Gai/o and pertussis toxin-insensitive Gaq family (100). The SCFAs-FFAR signaling pathways regulate glucose, lipid and energy homeostasis and immunological response extensively. GPR109a is a nicotinate receptor that recognizes butyrate as a ligand with low affinity. A recent study suggested colon tumor suppressive effect of butyrate is mediated via GPR109a activation (103). A newly discover SCFA receptor Olfr78 activated by acetate and propionate might play a potential role in SCFAs-mediated blood pressure control (104). There is an increasing appreciation of SCFAs receptors as pivotal mediators that mediating the crosstalk between gut microbiome and host physiology, through regulating glucose, lipid, energy metabolism and modulating immune response of the host.

SCFA Regulation of Lipid Metabolism

SCFAs play significant roles in fatty acid synthesis, fatty acid oxidation lipogenesis and cholesterol metabolism. In the liver, acetate transforms into acetyl-CoA and contributes to *de novo* lipogenesis and cholesterogenesis while propionate exhibits anti-lipogenic effects and inhibits hepatic fatty acid and cholesterol synthesis (105, 106). Therefore, the ratio of pro-lipogenic acetate and anti-lipogenic propionate in the liver might be critical for the overall physiological effect of SCFAs in lipid synthesis. Another independent study demonstrated SCFAs supplemented with a high propionate ratio inhibits hepatic lipogenesis and improves insulin-sensitivity in high-fat diet induced obesity (107). The anti-lipogenic property of propionate was confirmed with an acute randomized, controlled cross-over human study, wherein 10 g/day inulin-propionate ester

supplementation significantly reduced weight gain, visceral and liver fat in overweight adult humans (72). Propionate also inhibits cholesterol synthesis in vivo and in vitro, likely through suppressing 3-hydroxy-3-methylglutaryl CoA synthase and 3-hydroxy-3-methylglutaryl-CoA reductase, the critical enzymes for cholesterol biosynthesis (108, 109). The lipid modulatory effect of SCFAs is largely carried out through FFAR signaling. It is indicated that SCFAs-mediated FFAR2 activation promotes leptin secretion (110), stimulates adipogenesis (111), while inhibiting lipolysis in adipocytes, resulting in reduced plasma free fatty acids, energy control, and improved metabolic phenotype (112). A recent study using mice lacking FFAR2 and overexpressing FFAR2 in adipocytes demonstrated the lipid, glucose and energy metabolism is associated with suppressed insulin signaling via SCFAs-mediated activation FFAR2 in adipocytes (113). FFAR3 is also found in high expression in human adipose tissue (25) and reported to promote leptin production in primary mouse white adipose tissue (114). However, other studies unable to detect FFAR3 in murine adipose tissue suggested FFAR2, rather than FFAR3 is the leptin inducer (110, 111).

SCFA Regulation of Glucose Metabolism

SCFAs supplementation improved glycemic control in animal studies (115-117), although the human studies showed inconclusive and somehow contradictory results (118-120). Oral administration of acetic acid improved fasting plasma glucose and HbA1c levels in diabetic KK-A(y) mice is likely associated with AMP-activated protein kinase (AMPK) -dependent inhibition of hepatic enzyme involved in gluconeogenesis and lipogenesis including glucose-6-phosphatase (G6pase), phosphoenolpyruvate

carboxykinase (Pepck) and sterol regulatory element binding protein-1 (Srebp-1c). A recent study suggested SCFAs ameliorate high fat diet (HFD)-induced obesity and insulin resistance by promoting fat oxidation via peroxisome proliferator-activated receptor γ (PPARγ) dependent activation of uncoupling protein 2 (UCP2) -AMPK- acetyl coenzyme A carboxylase (ACC) pathway (121). In addition, SCFAs are involved in appetite, glucose and insulin regulation by stimulating enteroendocrine L cells-secreted gut hormone glucagon-like peptide-1 (GLP-1) and peptide YY (PPY) via FFAR2 and FFAR3 (122). GLP-1 is incretin hormone which is strongly insulintropic and plays a critical regulatory role in energy balance and glucose homeostasis (123). PPY is a satiety hormone for appetite regulation and improves insulin sensitivity (124). Intracolonic infusion of SCFAs or intake of fibers increases circulating GLP-1 and PPY and enhances hormonal physiological effects (125-127). In addition, *Ffar2* and *Ffar3* knockout mice showed a reduction in SCFA-induced GLP-1 secretion in vitro and in vivo, and impaired glucose tolerance (123), suggesting FFAR2 and FFAR3 are critical for SCFA-induced gut hormone secretion. Moreover, SCFAs-activated FFAR2 and FFAR3 play crucial physiological roles on pancreatic β cell functions, including glucose stimulated insulin secretion, response to insulin resistance, and mass regulation of pancreatic β cells, another possible mechanism of SCFAs to impact glucose and energy metabolism dependent on FFAR activity (128). A recent study suggested propionate and butyrate exert body weight and glucose control through activating intestinal gluconeogenesis (IGN) via complementary mechanisms (129). Glucose released by IGN induces a nervous signal through portal vein glucose sensor and transmits to the brain for food intake and glucose regulation (130). Dietary SCFAs and fructo-oligosaccharides markedly

stimulated intestinal glucose production and ING gene expression including G6pase and Pepck, and significantly improved glucose tolerance and insulin sensitivity. Interestingly, butyrate activates IGN gene expression via cAMP-dependent mechanism while propionate induce IGN via a gut-brain neural circuit mediated by FFAR3.

SCFA Regulation of Energy Homeostasis

SCFAs increase energy expenditure and regulate energy homeostasis through multiple pathways. First, SCFAs induced FFAR-dependent leptin secretion improves metabolic rate and regulates energy homeostasis. Leptin is a potent adipose-derived hormone that regulates the appetite, metabolic rate and variety of other physiological and immunological functions (131). Leptin is involved in regulation of energy expenditure by controlling feeding behavior to reduce food intake (131) while stimulating fatty acid oxidation and thermogenesis through increasing the AMP/ATP ratio and AMPK activity in liver and muscle tissue (132, 133). Second, SCFAs activate AMPK in liver and muscle (134, 135), a critical enzyme that induces peroxisome proliferator-activated receptor gamma coactivator 1-alpha (PGC-1α) -dependent regulation of critical transcription factors including PPARα, PPARβ/δ, farnesoid X receptor (FXR) and liver X receptor (LXR), all play critical roles in the maintenance of glucose, lipid and energy homeostasis (136). The SCFAs-mediated AMPK activation promotes hepatic fatty acid oxidation, ketogenesis, skeletal muscle fatty acid oxidation and glucose uptake, inhibits lipolysis and lipogenesis in the adipocytes and modulates insulin secretion by pancreatic β-cells (137). SCFAs activate AMPK either via SCFAs-FFAR2 mediated leptin pathway aforementioned or via leptin-independent mechanism by directly increase AMP/ATP

ratio (138). Lastly, SCFAs promote metabolic and energy homeostasis via neural system. SCFAs regulate appetite via central homeostatic mechanism, wherein hypothalamus, acetate increases the glutamate–glutamine, gamma-aminobutyric acid neuroglial cycles and changes the expression profiles of the regulatory neuropeptides that favor appetite suppression (70). It is also shown SCFAs initiate neural gut-brain circuits involving sympathetic activity and intestinal gluconeogenesis to exert glucose and energy control (129).

SCFA Regulation of Immune Response

Gut-derived SCFAs have been greatly appreciated in the regulation of intestinal homeostasis and pathogenesis of IBD (24). Butyrate and propionate supplementation or fiber-rich diets have been demonstrated to ameliorate IBD in both animal and human studies (139, 140). The anti-inflammatory properties of SCFAs, especially butyrate, has been associated with: 1) preferred energy substrates for colonocytes proliferation and differentiation and gut barrier maintenance; 2) inhibition of histone deacetylase to regulate the anti-inflammatory activity of intestinal epithelial cells, macrophages and DCs; and, 3) activation of GPCRs to regulate the gene expression, proliferation differentiation, chemotaxis and apoptosis of different immune cells. A lack of SCFAs often lead to rectosigmoid colitis, suggesting local nutritional deficiency in the gut leads to an inflammatory state, while local application of SCFAs significantly ameliorates inflammatory symptoms in colitis patients (139). As a histone deacetylase inhibitor, butyrate directly modulates macrophage function by inhibiting lipopolysaccharide (LPS)-induced pro-inflammatory mediators including nitric oxide production of IL-6 and IL-10

via histone deacetylase inhibition independent of toll-like receptor and GPR signaling (141). Through inhibition of histone deacetylation, butyrate also prevents the proteasome-dependent degradation of IκBα to suppress pro-inflammatory transcription factor nuclear factor κB (NF-κB) (142). The suppression of NF-κB results in downregulation of proinflammatory factors including tumor necrosis factor alpha (TNF-α), IL-1β, and IL-6 to achieve anti-inflammatory effect (143). SCFAs modify the recruitment, chemotaxis and effector function of neutrophils, another critical component of the innate immune response, dependent on the activation of GPRs (144). Acetate induced apoptosis in neutrophils a dose-dependent and a GPR43-dependent manner. Also inflammatory response and surface expression of pro-inflammatory receptors such as complement fragment 5a receptor and C-X-C chemokine receptor were markedly reduced with acetate stimulation (145). SCFAs modulate neutrophil recruitment through regulating the pro-inflammatory cytokines like TNF-α and neutrophil-chemoattractants including cytokine-induced neutrophil chemoattractant-2 released by neutrophil (146). SCFAs modulate the function of DCs, a critical cell population that initiates the adaptive immune response by processing and presenting antigens to T cells, and producing cytokine response to immunological signals. In vitro studies demonstrated that propionate and butyrate significantly reduced pro-inflammatory cytokines and chemokines including TNF-α, IL-12B, IL-6, C-C motif chemokine ligand-5, CXC chemokine ligand (CXCL)-9, CXCL-10, CXCL-11 released by LPS-induced human monocyte-derived DC (147). Another in vitro study indicates non-toxic doses of butyrate inhibited the cytokine-driven phenotypic differentiation process of monocyte-derived DCs and macrophages, and altered the terminal maturation of DC with a decreased ability to prime alloreactive naive T cells,

thus exerting anti-inflammatory effect (148). A recent study suggested that butyrate and propionate-dependent induction of indoleamine 2,3-dioxygenase 1 and aldehyde dehydrogenase 1A2 in DCs potentiates the ability of DCs to encourage naïve T cells convert into immunosuppressive Tregs than pro-inflammatory interferon gamma (IFN-γ)-producing cells (149). Consistent with the in vitro results, animal studies confirmed that SCFAs ameliorate central nervous system autoimmunity through promoting Tregs differentiation via suppression of the c-Jun N-terminal protein kinase 1 and p38 pathway (150). A possible mechanism of butyrate-regulated Tregs differentiation is the upregulation of histone H3 acetylation of Foxp3 locus by butyrate (151). GPRs might have a chemoattractant effect for Tregs, as SCFAs induced anti-inflammatory cytokine secretion and Tregs suppressor activity is FFAR3 (GPR41) dependent (152). SCFAs, especially butyrate, have shown anti-carcinogenic effects in vitro and in vivo. Multiple animal and cell line studies have demonstrated the butyrate prevents the development of colon adenoma and cancer (81, 83, 153, 154). Possible molecular mechanisms by which butyrate inhibits colon carcinogenesis include: 1) histone deacetylases inhibition-mediated regulation of carcinogenesis-related transcription factors including p53, retinoblastoma protein, Stat3, NF-κB and estrogen receptors (155); 2) GPR signaling dependent apoptotic, anti-proliferative and anti-inflammatory effects (103, 156); and, 3) the acidic colonic environment due to accumulation of SCFAs decreases the level of toxic and tumorigenic secondary bile acids through promoting calcium binding of free bile acids, decreasing solubility of bile acids, and inhibiting bacterial 7a-dehydroxylase to prevent secondary bile acids formation from primary bile acids (68).

In summary, the anti-inflammatory and anti-cancerous roles of SCFAs can be achieved via multiple mechanisms, including nutritional function, direct immune-modulatory effects, receptor-mediated effects, oxidative stress remission effects, benefiting immune cell proliferation, differentiation, migration, activation and cytokine expression.

Metabolomics Methods for SCFAs quantitation

Reliable, reproducible, and affordable methods for SCFAs quantitation are highly important for experimental and clinical application. Multiple techniques have been employed for SCFA quantitation, including capillary electrophoresis (157, 158), high pressure liquid chromatography coupled with ultraviolet detection (HPLC-UV) (159, 160), liquid chromatography coupled with mass spectrometry (LC-MS) (161), gas chromatography coupled with flame ionization (GC-FID) and mass spectrometry (GC-MS) (162, 163), and nuclear magnetic resonance (NMR) spectroscopy (164, 165). Among these techniques, gas chromatography is most widely employed for its separation power, choice of detectors, and the relatively inexpensive cost of the instrumentation. Multiple extraction methods have been developed based on GC-MS techniques including acidified water extraction (166, 167), organic reagent extraction (168), ultrafiltration (169, 170), steam distillation (171, 172), vacuum evaporation stripping (173), purge and trap (174, 175), headspace single-drop microextraction (176), and derivatization to decrease polarity and improve volatility (177, 178). NMR spectroscopy is commonly used in metabolomic fingerprinting studies due to its high reproducibility and simple preparation process(179). NMR spectroscopy has been used for SCFAs profiling in

extracts from mouse cecal content and feces as well (180, 181). A combination of MS- and NMR- based SCFAs quantitation method has been employed to provide comprehensive and complementary views of SCFAs status and overall metabolic changes in the CONV-R and GF mice feces study (182).

Bile Acids: Microbial-derived Signals in Host Homeostasis and Disease

Bile acids are a group of steroid acids, which are initially synthesized from cholesterol in the liver and then undergo extensively bacterial transformation as they move along the intestinal tract. The combined host and microbiota enzymatic activities give rise to a bile acid pool with great diversity. Bacterial-transformed bile acids profoundly impact host metabolic and immunological functions as they are able to activate different bile acid receptors to regulate signaling pathways with a broad coverage of complex symbiotic metabolism networks, including lipid metabolism, glucose metabolism, xenobiotics metabolism and energy homeostasis. Disrupted bile acid signaling due to perturbed gut microbiome or dysregulated gut microbiome-host interaction has been associated with pathogenesis and progression of metabolic disorders. Given the physiological significance of bile acids signaling, bile acids might represent novel and exciting therapeutic solutions in the treatment of metabolic and immunological diseases.

Bacterial modulation of bile acid *de novo* synthesis and biotransformation

The gut microbiota plays a well-documented role in the synthesis, transformation and regulation of bile acids (63). Bile acids are hydroxylated sterols which are initially

synthesized from cholesterol in the liver via either the classical (neutral) pathway initiated by 7α-hydroxylase (CYP7A1) (183) or alternative (acidic) pathway initiated by sterol-27-hydroxylase (CYP27A1) (184), and released into duodenum to aid in the solubilization and absorption of dietary lipids and lipid-soluble nutrients (63, 185). In a process known as enterohepatic circulation, more than 95% of bile acids are reabsorbed into the portal circulation and returned to liver by active transport in the ileum and passive transport throughout the length of the gastrointestinal tract (186). Bile acids escaping reabsorption are secreted mainly into feces (~0.2-0.6 g/day) and urine (~0.5 mg/day), and replenished by *de novo* bile acid synthesis from cholesterol in the liver, a process which is regulated by a bile acid controlled feedback mechanism via FXR (185). At least 17 enzymes are involved in bile acid *de novo* synthesis and the gut microbiota participates in the regulation of some of these key participant enzymes, including CYP7A1 (rate-limiting enzyme), CYP7B1, CYP8B1 and CYP27A1 (187-189) (**Figure 1-3**). Importantly, primary bile acids (cholic acid (CA) and chenodeoxycholic acid (CDCA)) are conjugated with glycine (extensively in human, 75%) or taurine (exclusively in murine, 95%) in the liver (190, 191) before undergoing extensive biotransformation as they pass through the intestine as the result of bacterial mediated enzymatic activity, transformed into a variety of secondary bile acids (deoxycholic acid (DCA) and lithocholic acid (LCA)), deconjugated bile acids (removal of the glycine or taurine), bile acid isomers (ursodeoxycholic acid (UDCA), isodeoxycholic acid), bile acid esters, and unsaturated bile acids (**Table 1-1**).

Deconjugation

Microbial bile acid deconjugation was first identified in "*B.Coli*" in 1934 (65, 192) and occurs through the hydrolysis of amino acid side chain of taurine and glycine conjugates with the bacterial enzyme bile salt hydrolase (BSH). Through a bacteria culture supernatants assay and functional metagenomics analysis, functional BSH activity has been detected in *Lactobacillus* (193-196), *Bacteroides* (196-198), *Bifidobacterium* (193, 196, 199), *Clostridium* (196, 200, 201), *Listeria* (202, 203), and *Enterococcus* (204-206). As conjugated bile acids are antimicrobial (207, 208), the enriched gut microbiota BSH is a microbial adaptation to detoxify intestinal bile acids (196). Importantly, microbial deconjugation regulates host metabolism via FXR, which will be reviewed in detail in next section. Deconjugated free bile acids are subsequently available to various microbial mediated biotransformation activities, including dehydroxylation, epimerization, desulfatation, esterification and unsaturation (**Table 1-1**), which generates bile acid pools with great structural diversity.

Dehydroxylation

Specifically, deconjugated primary bile acids are transformed to secondary bile acids through dehydroxylation catalyzed by bacterial 7α-dehydroxylase possessed by mainly Firmicutes phylum genera *Clostridum* XIVa and XI (66, 209) and *Eubacterium* (210, 211). Bile acid-inducible genes which encode enzymes in the bile acid 7α-dehydroxylation pathways has been characterized in *Eubacterium* sp. strain VPI 12708 (212), *Clostridium hylemonae,* and *Clostridium scindens* (64). Importantly, the secondary bile acids DCA and LCA, which predominate in human feces (66) and have been associated with obesity (213), cholesterol gallstone disease (214, 215), liver and colon

cancer pathogenesis (216-220), indicate that 7α-dehydroxylation is the most quantitatively and physiologically important bacterial bile acid biotransformation in the human intestine. Importantly, deconjugation and dehydroxylation of bile acid increases the hydrophobicity and enhances absorption, thus slowing the bile acid turnover, which leads to multiple physiological and pathological effects. For example, conversion of primary bile acid into secondary bile acid via on gut bacteria alters host metabolism via bile acid receptor G protein-coupled bile acid receptor 1 (GPBAR1/TGR5), PXR and vitamin D receptor (VDR).

Oxidation and Epimerization

Another critical microbial transformation occurs through reversible oxidation of 3α-,7α-, or 12α- hydroxyl groups of bile acid catalyzed by bacterial hydroxysteroid dehydrogenase (HSDH) (65), generating ketonic (oxo-) bile acid, which can undergo epimerization through the subsequent stereospecific reduction of the oxo group to yield β-hydroxyl bile acid or iso-bile acid (66). Major bacterial phyla including Bacteroidetes (genus: *Bacteroides*), Firmicutes (genera: *Clostridium*, *Eubacterium*, *Peptostreptococcus* and *Ruminococcus*), Proteobacteria (genera: *Bifidobacterium*, *Egghertella*) and Proteobacteria (genera: *Enterobacter*, *Escherichia*) (65, 66, 221-223) are known to exhibit either α-, β- or both HSDH enzyme activity. Epimerization is a microbial adaptation mechanism results in more hydrophilic, less toxic iso-bile acids that in turn increase microbial resistance in the highly competitive and hostile intestinal environment (224, 225). Interestingly, iso-bile acids function as a potential modulator for both gut microbial composition and host metabolism. For example, iso-DCA was reported to favor

the growth of bacterial genus *Bacteroides* (224), a critical genus involves in obesity and metabolic disorders (226, 227). Of note, UDCA (iso-CDCA) was reported to protect against cytotoxicity in vitro studies (228, 229) and cholestatic liver diseases clinically (230) (231). Curiously, human liver class I alcohol dehydrogenase γγ isozyme presented 3β-HSDH activity (232), indicating the interplay between liver and bacterial biotransformation and the co-contribution of host and bacteria to the diversity of the bile acid pool.

Desulfatation, Esterification and Unsaturation

Bile acid ethyl esters account for approximately 10 to 30% of the human total bile acid pool in feces (221). In vitro human fecal isolates studies have shown the bacterial esterification activity to covert bile acids to C-24 ethyl esters present in genera *Bacteroides*, *Eubacterium*, *Lactobacillus*, *Citrobacter* and *Peptostreptococcus* (233, 234). Bile acid sulfatase activity was found in the bacteria genera *Clostridium*, *Peptococcus*, *Fusobacterium*, and *Pseudomonas* (221, 235-237), converting bile acid sulfates into less polar and more efficiently absorbed desulfated bile acids, indicating that the desulfating bacteria regulate enterohepatic circulation and lengthens metabolic half-life of bile acids (238, 239). Desulfation results in a more toxic and longer half-life substrate than the sulfated counterpart, which might be involved in hepatobiliary and intestinal toxicity, like cholestasis (a decrease in bile flow and biliary bile acid excretion) and colon cancer (239). In vitro studies have demonstrated that the gut bacteria genus *Clostridium* (240, 241) possesses dehydrogenase activity, which is capable of introducing a double bond in the bile acid nucleus. However, it is uncertain if bacterial unsaturation transformation

occurs in vivo given the fact that unsaturation reaction reported are from fecal isolates and the unsaturated bile acids are rarely found in human feces (65).

Bile Acid Activated Receptors and Signaling Metabolism Networks

Bile acids are not only detergents, but critical signaling molecules that activate nuclear receptors including FXR, PXR, LXR, VDR and GPBAR1/TGR5 (57). The receptor activated cell-signaling pathways regulate complex symbiotic metabolism networks, including lipid metabolism (58), glucose metabolism (59), xenobiotic metabolism (60, 61) and energy homeostasis (62). As the size and composition of the bile acid pool directly regulates *de novo* bile acid synthesis via negative feedback control (242) and affects receptors activation (57, 225), by modulating bile acid pool through microbial biotransformation, gut microbiota has an essential participation in bile acid self-regulation signaling and receptor-dependent symbiotic metabolism network signaling (225, 243) (**Table 1-2**).

Farnesoid X Receptor (FXR)

FXR is the major bile acid receptor in the liver and intestine, which regulates bile acid, glucose, insulin, lipoprotein, triglyceride, drug, xenobiotic, and energy metabolism upon activation (60, 244) . FXR regulates *de novo* bile acid synthesis through negative feedback (242). In the liver, activated FXR forms a heterodimeric complex with the retinoid X receptor (RXR) to target the nuclear receptor small heterodimer partner (SHP), which binds to and inactivates liver-related homolog-1 (LRH-1) and an oxysterol-activated nuclear receptor LXRα to inhibit transcription of *CYP7A1* and *CYP8B1*, both

encode critical enzymes in the classical (neutral) bile acid synthesis pathway. Besides inhibition of bile acid synthesis, FXR activation enhances bile acid elimination via induction of bile salt efflux pump bile salt excretory pump (BSEP) (known as triphosphate-binding cassette transporter (ABCB11)) (245), conjugate export pump multi drug resistant protein 2 (MRP2) (246), organic solute transporters α and β (OST α and β) (247), while downregulating hepatocyte basolateral bile acid uptake via repression Na+ taurocholate co-transporting peptide (NTCP/ SLC10A1) (248, 249) and organic anion transport polypeptides OATP1B1/SLCO1B1 (known as OATP-C) and OATP1B3/SLCO1B3 (formerly known as OATP8/ SLC21A8) (244, 250). Together, liver FXR activation negatively regulates hepatic bile acid pools by reducing bile *de novo* synthesis and influx while enhancing excretion. FXR activation in the distal ileum results in regulation of the expression of a series of ileal bile acid transporters, which move bile acids from the intestine into the portal circulation. Apical sodium dependent transporter (ASBT) transfers bile acids into the ileal enterocyte brush border membrane, and its expression is decreased upon bile acid mediated FXR activation via the SHP (251). Bile acids are shuttled from the apical to the basolateral membrane of enterocytes by intestinal bile acid-binding protein (I-BABP; also known as fatty acid-binding protein 6 (FABP6)), and transported into blood vessels by the OSTα and OSTβ, all of which are positively regulated by FXR (252). Additionally, intestinal enterocytes can directly suppress hepatic bile acid synthesis via fibroblast growth factor 19 (FGF19) in humans (its homolog Fgf15 in mouse), which is secreted and circulated to the liver in response to bile acid activation of FXR, binding to the FGF receptor type 4 (FGF-R4) and β-Klotho complex to trigger mitogen-activated protein kinase MARK /extracellular signal-regulated kinase ERK1/2

pathway, ultimately repressing expression of the gene encoding CYP7A1 (253, 254). FGF19 has also been shown to activate hepatic glycogen synthesis and inhibit hepatic gluconeogenesis independent of insulin signaling, directly linking FXR to the regulation of carbohydrate metabolism (255, 256). Notably, FGF19 also negatively regulates bile acid synthesis and intestinal and hepatic bile acid transporters, which mediate absorption of dietary lipids and adiposity (257), thus altered FXR-FGF signaling impacts lipid homeostasis was shown in *Fxr* null and *Fgf19* transgenic studies (258-260).

Bile acids are the endogenous ligands for FXR and show a striking diversity in FXR activation which is correlated with hydrophobicity (261). The bile acid ligands binding affinity of FXR in order of potency is CDCA>LCA=DCA>CA (262, 263). As gut microbiota readily transforms bile acids structurally, by altering the bile acid pool composition, the gut microbiota is capable of altering FXR signaling and tuning the host physiology and metabolism. Multiple studies revealed that the gut microbiota regulates bile acids and host metabolism in an FXR-dependent manner (187, 264). GF mice and *Fxr* knockout mice studies suggest the gut microbiota regulates FXR signaling not only by converting bile acids to more or less potent FXR ligands, but also by controlling bile acid synthesis and pool size. It was reported germ free and antibiotic-treated mice exhibited changes in the bile acid pool size and profile as well as the gene expression involved in FXR-dependent pathways like Cyp7a1 and Fgf 15 (187, 265), Bsep, Mrp2, multidrug resistance protein 3 (Mdr3) and ATP-binding cassette (Abcg5/Abcg8) (266). Tissue specific *Fxr* knockout studies have shown intestinal FXR inhibition by elevated FXR antagonist tauro-β-muricholic acid (TβMCA)(187) levels via modulating microbiota to reduce bacterial BSH activity (264, 267). Interestingly, the gut microbiota modulation

of FXR signaling is intestine-specific (264, 267). As intestinal FXR inhibition with elevated TβMCA ameliorates adiposity and attenuates hepatic gluconeogenesis, enhancing FXR antagonism by targeting BSH producing bacteria (e.g., *Lactobacillus* and *Clostridium* IV and XIV) provides a potential therapeutic treatment of obesity and diabetes (264, 268). However, the translational application to human remains unknown as muricholic acid (MCA) is restricted to mouse species (269).

FXR Signaling Mediated Glucose Metabolism

Emerging evidence suggests the regulatory role of bile acid-induced FXR activity in glucose metabolism. Activating FXR by administration of bile acids or synthetic FXR agonist inhibits gluconeogenesis by repressing the expression of gene encoding G6pase, Pepck, and fructose 1,6-bis phosphatase via hepatocyte nuclear factor 4 (Hnf4) and forkhead box protein O1 (Foxo1) in an SHP-dependent fashion (270, 271). Over expressed hepatic G6pase and Pepck were identified in response to suppressed FXR signaling in GF and antibiotic-treated rats (266). Diabetic model studies demonstrated FXR activation promotes glucose metabolism and enhances insulin sensitivity (272, 273). FXR promotes insulin sensitivity via protein kinase B (Akt) signaling cascade, which inactivate glycogen synthase kinase 3β (Gsk3β) through phosphorylation to upregulate glycogenesis (272) and activating glucose transporter Glut2 translocation at pancretic β cell membrane and Glut4 in hepatocyte to promote insulin transcription and secretion (274, 275). Interestingly and controversially, FXR deficiency through genetic knockouts or bile acid sequestrant administration appears to promote glucose metabolism through

activating GLP-1 synthesis, a critical hormone involving in glucose homeostasis and energy balance (276).

FXR Signaling Regulates Lipid Metabolism

FXR deficient mice have disrupted lipid homeostasis as shown by elevated levels of hepatic cholesterol, phospholipid, triglycerides, and pro-atherogenic lipoprotein-containing serum (277), indicating the regulatory role that FXR plays in lipid metabolism. Bile acid activated FXR/SHP pathway lowers triglyceride levels by negatively regulating the expression of enzyme involved in lipogenesis including fatty acid synthethase (Fas) via repression of lipogenic protein Srebp-1c (278). Moreover, bile acid-activated FXR promotes lipoprotein lipase (LPL)-mediated triglyceride clearance of triacylglycerol-rich lipoproteins such as very low density lipoprotein (VLDL) and chylomicrons through repression of LPL inhibitor apolipoprotein CIII (Apo-CIII) (279), while inducing LPL cofactor/activator ApoC-II (280) and APOA-V promotor (human) (281) dependent on FXR/RXR heterodimerization, and upregulates expression of VLDL receptor (282), and transmembrane protein syndecan-1 (283). In addition, a transgenic mice study described the lipoprotein regulatory role of FXR in mediating bile acid-induced transcriptional downregulation of thrombosis and atherogenesis-related lipoprotein(a) encoding human APOA by directly binding and repressing APOA promoter activity (284, 285). FXR activation also regulates PPARα, a nuclear receptor that upon activation promotes fat oxidation to reduce triglycerides (286). Together, hepatic FXR activation up-regulates the expression of genes involved in VLDL and chylomicron clearance such as syndecan-1, VLDL receptor, ApoC-II and APOA-V,

while reducing liver triacylglycerol levels through suppression of Fas expression via Srebp-1c and enhanced fatty acid β-oxidation via PPARα expression.

FXR Signaling Promotes Cholesterol Metabolism

FXR participates in cholesterol metabolism as it is the primary regulator of bile acid homeostasis and serves as the intimate linkage between bile acid *de novo* synthesis and biliary cholesterol elimination (287). Induction of CYP7A1 activity through bile acid regulated-FXR modulation stimulates cholesterol *de novo* synthesis and biliary cholesterol secretion (288). Bile acid-activated FXR enhances biliary and fecal cholesterol excretion by regulating transporters and enzymes, as evidence show FXR natural (bile acid) and synthesized ligands induce expression of ATP-binding cassette transporters Abcg5 and Abcg9 in mice and rat hepatoma cells (289), and promote macrophage reverse cholesterol transportation and hepatic CYP8B1 inhibition-dependent reduction of intestinal cholesterol absorption (290). Additional evidence in *Fxr* knockout mice has shown impaired cholesterol clearance indicated by increased plasma cholesterol, reduced hepatic high density lipoprotein (HDL)-mediated cholesterol ester clearance, and increased intestinal cholesterol absorption, resulting from a deceased cholesteryl ester hydrolase (Ceh)-mediated cholesterol mobilization, sterol carrier protein (Scp)-mediated intra-cellular transport, scavenger receptor BI (SrbI)-mediated HDL cholesterol ester clearance, and transporter Abcg5/8-mediated free cholesterol biliary secretion (287).

FXR Signaling Involves In Xenobiotics Metabolism

In human hepatocytes, bile acid mediated-FXR activation induced gene expression involve in bile acid and xenobiotics detoxification, including Cytochrome P450 Family 3A4 (CYP3A4) (291), DHEA sulfotransferase (SULT2A1) (292), UDP-glucuronosyltransferase 1A3 (UGT1A3) (293) and UDP-glucuronosyltransferase 2B4 (UGT2B4) (294). Long lived little mice studies revealed more FXR-activated xenobiotic genes enconding Abcb1, Flavin containing monooxygenase 3 (Fmo3) and Glutathione S-transferase A2 (Gsta2) (61). Together, these studies heightened the FXR-dependent bile acid regulation in phase I and II xenobiotics and drug metabolism.

FXR Signaling Modulates Energy Metabolism

FXR signaling regulates metabolism of glucose and lipid, which are two major energy sources in human and other organisms, thus serves as an important modulator in energy metabolism and homeostasis. The antioxidant drug tempol (4-hydroxy-2,2,6,6-tetramethylpiperidine-N-oxyl) inhibits BSH-producing bacteria *Lactobacillus* to favor T β MCA production (an FXR antagonist) and thus promote FXR inhibition, which leads to a more catabolic state to ameliorate obesity (264, 295). *Fxr* knockouts have revealed important regulatory roles that FXR plays in Ucp1-driven thermogenesis due to low metabolic fuels like glucose and triglyceride (296). Intestinal FXR agonism enhances thermogenesis and white adipose tissue browning via expression of genes involved in thermogenesis, mitochondrial biogenesis and fatty acid oxidation including peroxisome proliferator-activated receptor γ coactivator 1α and β (*Ppargc1α* and *Ppargc1β*, encoding Pcg1α and β), *Ucp1* and *Fabp1* (297). FGF19 (Fgf15 in mouse), is an FXR-dependent key regulator of energy expenditure to increase metabolic rate, restore mitochondrial

function, reduce adiposity and ameliorate hyperglycemia by upregulating expression of phosphofructokinase (Pfk-1), ATP citrate lyase (Acly), stearoyl CoA desaturase (Scd) and Pgc-1 while repressing Acc2 has been identified in transgenic and diet-induced obesity mice model (298, 299). The FXR agonist GW4046 attenuates mitochondrial dysfunction and oxidative injury via repression of microRNAs miR-199a-3p to increase liver kinase B1 (Lkb1) (300), while CDCA treatment induced antioxidant and detoxifying enzymes via AMPK and ERK-mediated CCAAT enhancer binding protein β (C/EBPβ) phosphorylation (301). However, activated FXR may induce mitochondrial dysfunction, apoptosis and cell death in certain cell lines with distinct phenotypes including cardiomyocyte and cancer cell line (302, 303). Together, FXR-dependent signaling pathways coordinate energy metabolism via regulating glucose and lipid metabolism to promote mitochondrial and cellular function and catabolism.

G-Protein-Coupled Receptor-1 (GPBAR1/TGR5)

TGR5 (GPBAR1), the first identified G-coupled protein receptor specific for bile acid ligand (304), is expressed extensively in tissues including liver, skeletal muscle, kidney, gall-bladder, with prominent expression in the enteric nervous system in the intestine (305). TGR5 is in low-affinity state at rest condition and is activated with greater potency by secondary bile acids LCA and DCA (304). Importantly, conversion of less potent primary bile acid ligands CA and CDCA to more potent secondary bile acid ligands DCA and LCA is bacterial deconjugation (to free primary bile acid) and dehydroxylation (to dehydroxylate primary bile acid)-dependent, therefore emphasizing the critical regulatory role that BSH and 7α-dehydroxylase active bacteria have in TGR5

signaling pathways. Bile acid-activated TGR5 stimulates intracellular cAMP level to activate protein kinase A (PKA), resulting in the cAMP-dependent upregulation of gene expression involves in energy expenditure, glucose and lipid metabolism and NO production (62, 306, 307).

TGR5 Regulates Energy Homeostasis and Inflammation

Bile-acid-activated TGR5 regulates lipid metabolism, energy homeostasis and prevents diet-induced obesity through activation of cAMP-dependent thyroid hormone activating enzyme deiodinase-2 (DIO2), which converts inactive thyroid hormone throxine (T_4) into its active counterpart (T_3), therefore promoting mitochondrial oxygen consumption and energy expenditure in mice brown adipose tissue (BAT) and human skeletal myocytes, the most thermogenically important tissues of rodents and human (62). The TGR5-dependent thermogenesis and energy expenditure boosting effect of bile acids was confirmed in a CDCA oral supplementation human study. Two-day CDCA supplementation to 12 healthy female promotes BAT activity and whole-body energy expenditure with an enhanced mitochondrial uncoupling UCP1 and DIO2 expression (308). FXR is unlikely involved in cAMP-DIO2 pathway as the FXR is neither expressed nor induced in the metabolic responding BAT tissue, plus the evidence suggests FXR specific agonist GW4046 fails to induce the similar energy expenditure promotion effect (309). Bile acid-activated TGR5 stimulates NO via upregulating expression of nitric oxide synthase (NOS) in liver sinusoidal endothelial cells, a possible protective mechanism to against oxidative stress and lipid peroxidation induced by excessive bile acids (307, 310). Bile acid activated TGR5/cAMP signaling also inhibits inflammatory

cytokines induced by LPS via repression NF-κB pathway and attenuates colon inflammation in colitis mouse model, revealing the anti-inflammatory role and intestinal barrier protection effect that bile acids have through TGR5-dependent signaling pathways (311, 312).

TGR5 Promotes Glucose Metabolism and Insulin Sensitivity

TGR5 signaling promotes glucose metabolism and insulin sensitivity mainly through stimulating incretin hormone GLP-1, which is driven by elevated intracellular ATP/ADP ratio and a subsequent intracellular calcium influx (293). GLP-1 regulates glucose metabolism and energy balance through promoting pancreatic insulin production, inhibiting gastric empty and acid secretion, delaying intestinal transit, and reducing food intake by enhanced satiety (313, 314). GLP-1-mediated physiological benefits can be achieved by bile acids (e.g., CDCA) and bile acid sequestrants (e.g., colesevelam) treatment through TGR5-dependent signaling pathway (315). Notably, gut microbiota regulates GLP-1 not only through bacterial modulated bile acid TGR5 signaling, but also via bacterial derived SCFAs signal through GPR41/43 (316), and microbial modifiable endocannabinoid-like compounds (e.g., 2-oleoylglycerol-activated GPR119 pathway (317, 318), emphasizing the importance of microbial tuning in host metabolic regulation.

Pregnane X Receptor (PXR)

PXR is highly expressed in the intestine and liver, functions as a master xenobiotic receptor as it transcriptionally regulates phase I and phase II enzymes and transporters (319). Evidence demonstrated RXR also serves as a bile acid sensor, which

can be activated by bile acid with the potency order: 3-keto-LCA > LCA > DCA= CA (246, 320). Upon activation by the efficacious and toxic LCA and its 3-keto metabolite, PXR coordinately regulates gene expression involved in bile acid biosynthesis (e.g., Cyp7a1), transport (e.g., Oatp2) and detoxification (e.g., Cyp3a) in mice (320). PXR regulated detoxification enzymes in human include UDP-glucuronosyltransferases (UGTs, UGT1A1, UGT1A6, UGT1A3 and UGT1A4), sulfotransferases (SULTs, SULT2A1), glutathione S-transferases (GSTs, GSTA1, GSTA2, GSTM1), cytochromes P450 family (CYP3A4, CYP3A11 and CYP1A) , multidrug resistance associated proteins (MRP2, MRP3, MRP4, and MRP5) and SLC/OATP family (SLCO1A2/OATP1A2, SLCO1B1/OATP1B1, SLCO1B3/OATP1B3), multidrug resistance 1 or P-glycoprotein (MDR1/P-gp) (320-323). Of note, the PXR ligand, synthetic pregnane pregnenolone 16α-carbonitrile and the antibiotic rifampicin, have anti-hepatotoxic and anti-cholestatic effects. The possible underlying mechanism involves PXR-mediated *de novo* bile acid synthesis regulation through CYP7A1 signaling pathway, and promoted bile acid transportation via upregulated basolateral transporters and bile acid detoxification through CYP3A-dependent 6-hydroxylation of the toxic bile acid. Recently studies revealed LCA or rifampicin activated PXR in bile acid and cholesterol metabolism is related to HNF4α/PGC-1α -induced CYP7A1 inhibition and FGF19-dependent CYP7A1 repression in human hepatocytes (324, 325). In addition to xenobiotic and bile acid metabolism, PXR activation has been associated with transcriptional regulation of gene expression involves in gluconeogenesis, thermogenesis, cholesterol, and fatty acid in high-fat diet-induced obesity and knockout

mice models, revealing the additional physiological function that PXR in glucose, lipid and energy metabolism (322, 323, 326).

Vitamin D Receptor (VDR)

VDR, a vitamin D hormone 1,25-dihydroxyvitamin D3 ($1\alpha,25\text{-}(OH)_2\text{-}D_3$) activated transcriptional factor also functions as a bile acid sensor which can be activated by secondary bile acids LCA and 3-keto-LCA (327). The responsive genes expression activated via VDR-dependent transactivation includes CYP2, CYP3A, SULT2A1, MDR1, MRP3, CYP7A1 (328-332), coordinately regulates xenobiotics and drugs, glucose, lipid, and energy metabolism with other bile acid-activated receptors like FXR and PXR in the nuclear receptor regulatory networks (185). LCA also upregulates vitamin D-induced gene expression of calbindin D_{9K}, Ca^{2+} ATPase, transient receptor potential vanilloid (TRPV6) and CYP24. LCA-treated vitamin D-deficient mice restored vitamin D-sufficient phenotype, indicating LCA might serve as a vitamin D substitute and regulates calcium absorption, mobilization and homeostasis in intestine, kidney, bone and serum (327, 333). Additionally, VDR is also participates in cell proliferation, differentiation, and immunomodulation, as VDR signaling induces apoptosis in keratinocytes, psoriatic plaques, breast cancer cells and pre-malignant colonic epithelium (334-337), inhibits antigen-induced T cell proliferation, enhances Tregs function, attenuates pro-inflammatory cytokine expression (338-340). These studies illustrated the anti-proliferative and anti-informatory effect of VDR, and the importance of natural or synthetic VDR agonists as immunoregulators for potential therapeutic applications against inflammatory and autoimmune diseases.

Gut Microbiota-Modulated Bile Acids and Associated Diseases

The diversity and composition of the bacterial community inhabiting the human gastrointestinal tract is a newly appreciated key factor that contributes to the evolutionary fitness of the host, and its quantity or structural perturbation caused by environmental stressors (xenobiotics, toxicants, drugs), change in diet (nutrition) or lifestyle (smoking, exercise, stress), will greatly influence the host metabolic phenotype and disease risk (2, 3). Microbial-modulated bile acids are major signaling molecules capable of fine-tuning host metabolism for the benefit of the microbiota. It is well appreciated that microbial composition perturbation and the resultant altered bile acid pool size and composition is involved in metabolic and immunological disorders. A better understanding of how microbiota-modulated bile acids contribute to disease risk and health will enlighten the way to new therapeutic applications for metabolic and inflammatory disorders, like obesity, diabetes, fatty liver disease, cholestatic disease and inflammation.

Obesity and Associated Metabolic Complications

The rising prevalence of obesity and obesity-associated metabolic complications like type 2 diabetes (T2D) has becoming an international epidemic, with a rate projected to increase by 33% in obesity and 54% in diabetes by 2030 in United States (341, 342). It is well established that the co-regulation of first genome (host) and second genome (microbiome) determines the host metabolic phenotype, and disrupted microbiome and microbiome-host interaction play a critical role for obesity and subsequent metabolic complications (343, 344). A diabetic animal study revealed the alterations in bile acid

pool size and composition while a clinical study confirmed elevated post-prandial circulating bile acids in obese patients with T2D compared to normoglycemic controls (345, 346). A discordant twin study demonstrated obese phenotype was correlated with a robust bile acid decrease, resulting from activated mouse host ileal FXR-Fgf15 signaling, and corresponding downregulation of liver bile acid *de novo* synthesis via suppression of Cyp7a1 (347).

Bile acids involved in obesity and related metabolic disorders mainly through three routes; 1) microbial-modulated bile acid signaling through bile acid receptor; 2) antimicrobial bile acids modulate the gut microbiome composition and function; 3) accumulation of toxic bile acids causes toxicity of the cells and organs. The first route highlights the microbial transformation of bile acid and the signaling role that certain transformed bile acids act through bile acid receptors to achieve metabolic regulatory function, especially through FXR, TGR5 and PXR (**Table 1-2**). Interestingly, controversial results showed *Fxr*-deficient mice are protected from diet- or genetic-induced obesity and hyperglycemia compared with wild-type counterparts. Recent studies demonstrated that intestinal upregulation of the FXR antagonist TβMCA by manipulating BSH active microbiome (e.g., *Lactobacillus*) or directly inhibiting bacterial BSH (caffeic acid phenethyl ester (CAPE)) improves obesity and hyperglycemia (264, 267). The second route emphasizes the microbial modulating effect of bile acids, which pool size and composition can regulate the structure of microbial community. The antimicrobial effect of bile acids can be achieved directly through damaging bacterial membrane, disturbing macromolecule stability and increasing oxidative stress, or indirectly through FXR-dependent antimicrobial peptides (348). Toxic and hydrophobic primary and

secondary bile acids directly damage the bacterial membrane, resulted in taxonomic alteration, which favors bile acid-metabolizing and resistant bacteria like Firmicutes, representing from 54% to 95% of the total microbiome while inhibiting bile acid intolerant bacteria like Bacteroidetes and Actinobacteria, reduced from 33% to less than 1% in CA-supplemented rats (349). It seems increased bile acid toxicity in the gut favors the growth of gram-positive bacteria as the protective peptidoglycan layer is thicker and more resistant to the harsh environment compared with gram-negative bacteria (350). Another study observed a 1000-fold increase of the bile acid 7α-dehydroxylating bacteria with CA treatment, which all belong to *Clostridium* cluster XIVa from Firmicutes phylum, indicating the conversion of primary bile acids to more toxic secondary bile acids by 7α-dehydroxylating bacteria might be an adaptation mechanism to inhibit nutrients competitors to favor their own growth in the highly competitive gut environment (351). Interestingly, expansion of Firmicutes and shrinkage of Bacteroidetes is the characteristic structure of an obesity-associated microbial community with an elevated energy-harvest ability (26). The third route accentuates the cytotoxic and genotoxic property of hydrophobic bile acids. In addition to membrane damage, bile acids disrupt intracellular activity by interfering with the transporters (352), inducing DNA damage, ER stress, protein malfolding and denaturation, which is involved in multiple diseases, including cholestasis and cancer (353, 354)

Nonalcoholic Liver Disease (NAFLD)

NAFLD refers to a broad spectrum of non-alcohol relevant liver pathologies (<20 g of alcohol intake/day) ranging from simple steatosis due to excessive hepatic lipid

accumulation to severe non-alcoholic hepatosteatosis (NASH), progressive fibrosis, cirrhosis and even hepatocellular carcinoma, which affects up to 25% of population worldwide with an astonishing estimated 33.5% prevalence among the adult population in 2030 (355, 356). NAFLD is highly correlated with obesity, insulin resistance and T2D mellitus. The co-occurrent rate of obesity/T2D and NAFLD is up to 70%-80%, and NAFLD is 100% presented in patients with combined obesity and T2D (357, 358). As pathogenesis of NAFLD is intimately associated with glucose, lipid, energy and immunity dysregulation, it is expected that bile acids are involved in NAFLD through modulating hepatic and extrahepatic lipid, carbohydrate and inflammation pathways by targeting bile acid receptors. *Fxr*-deficient mice exhibit the full spectrum of NAFLD pathology including hepatocellular carcinoma, and manipulating FXR expression or administering natural or synthetic FXR agonist improves NAFLD manifestation including steatosis, inflammation, fibrosis and carcinogenesis and regenerative capacity in both pre-clinical in vivo models and human clinical trials (359). Controversially, emerging evidence suggested intestine-specific *Fxr* deficiency might protect against HFD-induced NAFLD by reducing hepatic lipid accumulation via repression of ceramides/Srebp1-c/Cidea (cell death activator) pathway (360). *Tgr5* deficiency is implicated in obesity, hypercholesterolemia, NAFLD, and atherosclerosis mainly due to lack of glucose, energy metabolism and inflammation modulation with deficient TGR5/GLP-1 signaling, TGR5/cAMP/PKA thermogenesis signaling and TGR5/cAMP/NF-κB anti-inflammatory signaling. In agreement with the TGR5 deficiency phenotype, TGR5 agonist like INT-777 (a semisynthetic bile acid, also known as obeticholic acid (OCA); 6α-ethyl-CDCA), reverses HFD-induced hepatosteasosis and

LPS-induced atherosclerosis (306, 361). Additionally, bile acid transporters have been implicated in NAFLD pathogenesis, as the influx and efflux bile acid transporters control local and systemic bile acid levels, bile acid enterohepatic cycling and distribution, thus regulating the strength of the bile acid receptor activation and downstream signaling including glucose and lipid homeostasis. Evidence indicates bile acid transporters like BSEP, ASBT, NTCP and MRP2 are relevant in NAFLD pathogenesis in both animal and human studies (362, 363), while inhibition of ileal bile acid uptake by disrupting ASBT with ASBT inhibitor has protective effect against HFD-induced NAFLD, a potential therapeutic target to ameliorate NAFLD and NASH (364).

Hepatobiliary Diseases -Cholestasis and Gallstone Diseases

Cholestasis and gallstone disease are associated with impaired bile flow excretion due to impaired hepatocytes, bile duct or gallbladder, and dysregulated cholesterol metabolism. Cholestasis describes a medical condition characterized by a decrease in bile flow due to either impaired hepatocyte secretion or obstructed bile ducts (365). Cholestasis occurring during pregnancy is called obstetric cholestasis or intrahepatic cholestasis of pregnancy (ICP), a disorder with 1/140 incidence among UK pregnancies with an increased level of maternal and fetal circulating bile acids due to restriction of the hepatic bile excretion. ICP has been highly associated with incidence of stillbirth, perinatal complications and intra-uterine fetal death (366). Cholestasis is highly associated with cholestatic bile acids like CA, CDCA, LCA and DCA, which are highly hydrophobic thus eliminated inefficiently in the liver and cause hepatotoxicity and bile acid accumulation. Significant elevation of cholestatic bile acids in circulation is the

common manifestation with ICP conditions, indicating the impairment of the enterohepatic circulation (367, 368). Sufficient elimination of toxic bile acids relies on well-controlled bile acid *de novo* synthesis, enzymatic hydroxylation/detoxification to convert hydrophobic bile acids into more hydrophilic and less toxic molecules, and functional bile acid transportation system for efficient excretion. Both bile acid *de novo* synthesis, detoxification (Phase I and II enzymes) and transportation (Phase III transporters) are tightly regulated by bile acid receptors including FXR, PXR and VDR. Under cholestatic conditions, activation of those bile acid receptors exert protective effects by decreasing hepatic bile acid output and uptake, stimulating hepatic bile acid efflux, and inducing bile acid metabolizing, conjugating enzymes and transporters. Multiple studies have demonstrated bile acid receptor agonism is the potential therapeutic strategy for the treatment of cholestasis and hepatobiliary-related diseases (369).

Cholesterol gallstone formation is highly associated with hypersecretion of cholesterol resulting from dysregulated bile acid, which can obstruct the bile duct leading to diminished hepatic bile acid outflow and ultimately cholestasis. The inactivation of CYP7A1 (limiting enzyme of bile acid synthesis from cholesterol) has been reported to cause gallstone formation, proven by *Apobec-1*$^{-/-}$ mice with Cyp7a1 deficiency phenotype that readily develop lithogenic diet-induced gallstone, and the human hypercholesterolemic phenotype due to loss of CYP7A1 function with a homozygous deletion mutation (370, 371). A correlation has been established between decreased bile acid synthesis and increased biliary cholesterol secretion (372). Hydrophobic bile acid DCA and CA have been reported to promote cholesterol crystallization, a pre-stage of gallstone. Female gallstone patients showed a significantly smaller bile acid pool size

with an enhanced CA to DCA biotransformation comparing to the healthy female controls. Additional human studies confirmed cholesterol gallstone prevalence is associated with raised proportion of DCA and CA (373, 374). Bile acid receptor FXR, PXR and VDR are implicated in gallstone diseases by inhibiting bile acid synthesis to eliminate hepatic cholesterol through repressing transactivation or transcription of CYP7A1 (287, 324, 332). Moreover, studies revealed *Tgr5* knockout mice were protected from lithogenic diet-induced gallstone diseases, indicating TGR5 activation is involved in gallstone pathogenesis. The possible mechanism is related to promotion of gallbladder filling by inducing gallbladder smooth muscle relaxation via TGR5-cAMP-protein kinase A-K_{ATP} channel pathway (375, 376).

Interestingly, microbiota is involved in cholestasis and gallstone formation not only by regulating bile acid receptors, but also by directly converting bile acids to more or less cholestatic/hydrophobic forms. For example, microbiota contributes to hepatobiliary diseases pathogenesis by dehydroxylation of primary bile acid to more hydrophobic and toxic secondary bile acid via 7α-dehydroxylase activity, and deconjugation of more hydrophilic conjugated bile acids to free and toxic bile acids by BSH activity. Meanwhile, bacteria participates in the protection against cholestasis and gallstone by transforming cholestatic bile acids to less hydrophobic and toxic iso-bile acids form through oxidation and epimerization by HSDH activity.

Apoptosis, Inflammation and Autoimmunity

Bile acids are increasingly appreciated as immunological modulators in regulation of apoptosis, inflammation, and immunity. Accumulation of hydrophobic bile acids is the

major inducer of hepatic inflammation, cholestasis, fibrosis and carcinogenesis. Besides liver, systemic bile acids levels cause damage in extrahepatic organs including gut and kidney as well (377, 378). One mechanism, which bile acids lead to hepatocyte damage and inflammation involve bile acid-induced oxidative stress and endoplasmic reticulum stress through ligand independent epidermal growth factor receptor and FAS receptor-mediated caspase activation or hydrophobicity-caused direct mitochondria damage. (379). Another mechanism involves the bile acid-activated proinflammatory mediators including early growth response factor-1, which stimulates the proinflammatory signaling and effector including cytokine (TNF-α, IL-23, IL-17A), chemokine (Macrophage Inflammatory Protein-2) (380), and adhesion molecules (intercellular adhesion molecule-1) (380, 381). The most recognized mechanism that bile acids exert immunomodulatory effect is through bile acid receptors including FXR, TGR5, and VDR. Bile acid-activated FXR and TGR5 induce hepatic, colonic and cardiovascular anti-inflammatory signaling by inhibiting pro-inflammatory cytokines and enzymes including IL-1α, IL-1β, IL-6, TNF-α, IFN-γ, cycloxygenase (COX)-1, COX-2 and iNOS through antagonizing NF-kB dependent pathway (311, 312, 382). FXR modulates renal inflammation and fibrosis through repressing Srebp-1c-mediated fatty acid synthesis, profibrotic growth factor TGF-β, and pro-inflammatory cytokines and chemokines including TNF-α, IL-6 and monocyte chemoattractant protein-1 (383). VDR has been implicated in the prevention of IBD and colorectal cancer as it exhibits regulatory role in cell proliferation, differentiation, immunomodulation and pro-inflammatory signaling attenuation in epidermal cells, malignant breast cells, pre-malignant colonic epithelium and immune cells (334-337, 339). Due to the beneficial immunomodulatory effects, bile acid receptor

antagonism represents the promising therapeutic strategy in the treatment of inflammatory and autoimmune diseases.

Bile Acid Measurement Approaches

Bile acids have great clinical significance as the pool size and composition is intimately related to their metabolic and immunological function, and disrupted gut microbiome-host interaction. Increased serum bile acid especially hydrophobic bile acid indicates problems with intrinsic clearance and detoxification deficiency thus is critical for liver disease diagnosis including ICP, hepatitis and cirrhosis (384-386). Given the biological and clinical significance of bile acids, a reliable and efficient platform and method to provide robust detection and quantitation with improved analytical confidence is highly important for disease diagnosis and prognosis. However, the development of sensitive and accurate analytical methods remains challenging due to the structural diversity of BAs, broad spectrum of biological concentration (>10^6 magnitude), as well as the molecular complexity of the biological matrix like plasma, urine, bile, and stool, which can contain mixtures of lipid, protein, carbohydrates, mineral salts, vitamins ,various trace element, and other interfering components (387). Various methods using different platforms have been utilized for bile acid separation, detection and quantitation in the past decades, including enzymatic assays, thin layer chromatography, gas chromatography (GC), gas liquid chromatography (GLC), HPLC, GC-MS, LC-MS, and NMR spectroscopy. Reviewing and evaluating the analytical and practical performance of the emerging techniques will be advisable for clinical practice of bile acid measurement and disease diagnosis.

Enzymatic assays

Enzymatic assays offer a relative simple, specific and rapid measurement for total bile acids, thus they are most widely used in clinical laboratories for direct total bile acid measurement in patient serum with liver diseases. The general enzymatic reaction is initiated by adding dehydrogenase enzyme like NAD-linked 3α-hydroxysteroid dehydrogenase (3α-HSD) to catalyze the oxidation reaction of bile acid, either generating NADH to react with nitrotetrazolium blue to form fluorescent formazan dye with the presence of diaphorase enzymes (3rd generation method) or forming fluorescent reduced coenzyme thio-NADH with the presence of coenzyme thio-NADH (5th generation, also known as enzymatic cycling), followed by fluorometric measurement with ultraviolet spectrophotometry or fluorimetry (388, 389). Despite that enzymatic assays are extensively used for their cost and ease of use, the drawbacks that they are dependent on enzyme purification and certain bile acids may hinder the accuracy and thus reduce extensive application of the measurement (390).

Chromatography-based techniques

Besides total bile acid levels, individual bile acids serve important physiological function and clinical significance, especially hydrophobic secondary bile acids like LCA and DCA, which in high concentration are hepatotoxic and carcinogenic. Elevated LCA and DCA levels have been implicated in the promotion of colon cancer, chronic inflammation and hepatobiliary diseases like cholestasis and gallstone formation (369). Therefore, highly selective techniques for accurate specific bile acid quantitation is

required for clinical practice. Chromatographic techniques depend on the selective retention of the migrating components in the column by the stationary phase, thus providing good separation to purify individual bile acid from the complex biological matrices, which means this methodology can be extensively applied clinically for individual bile acid measurement (391).

Thin-Layer Chromatography (TLC)

TLC methods have mostly used in routine clinical separation of primary and secondary bile acids and their glycine or taurine conjugates for the relatively simple procedure (391). However, the relative low sensitivity and separation difficulties hinder the extensive application of this method to samples with low quantity and more complex constituents. High performance TLC, an over-pressured TLC technique with the improved separation, has been applied to the conjugated bile acid analysis of lower volume serum samples in children with cystic fibrosis (392). High performance TLC with fluorescence indicators has also been used for the rapid and accurate quantitation of free and conjugated bile acids in duodenal juices (393). In clinical practice, TLC is still a reliable, simple and time-effective alternative to other more advanced bile acid quantitation methods, like gas chromatography.

High Performance Liquid Chromatography (HPLC)

HPLC techniques with a high-pressure pump achieves better sensitivity and separation of the analytes in a complex matrix, thus HPLC has been developed extensively to analyze bile acids in biological fluids. Modification of chromatography

and choice of detectors and columns coupled with HPLC is dependent on sample type and analysis purpose. For samples with high bile acid concentrations (mM), HPLC coupled with refractive index or ultraviolet detectors yields satisfactory measurement. For samples with low bile acid concentrations (pM) or more unconjugated bile acids with poor spectroscopic absorption, the use of pre-column derivatization by esterification with derivatization reagent like 4-bromomethyl-7-methoxycoumarin and 1-bromoacetylpyrene, or the post–column immobilized 3α-HSD enzymatic reactions using octadecyl-silica column significantly improved the sensitivity and resolution of the bile acid detected by either UV or fluorescence detector (391). For determination of conjugated bile acid in serum, improved HPLC using paired-ion chromatography or ion-exchange chromatography on piperidinohydroxy-propyl-sephadex LH-20 were developed for better separation and selectivity (394, 395). However, the main disadvantages of HPLC including matrix effect and restricted specificity of the detectors limit the suitability for the measurement of the non-principal bile acid species in more complex biological matrix.

Gas/Gas-Liquid Chromatography (GC/GLC)

GC is a separation technique for volatile constituent in a mixed sample as it passes through carrier gas stream. The earliest GC application for bile acid series analysis was described in 1960, with only four methyl-bile acid derivatives detected (396). The development of capillary columns like glass or metal columns packed with liquid phase and inert fused-silica columns, improved the derivatization methods to derivatize the carboxyl group, hydroxyl group, or oxo group, and the diverse detection techniques

including electron capture detection, flame ionization detection and selected ion monitoring mass spectrometry enable the wider research application for bile acid derivatives analysis in bile, serum, urine and feces (391, 397). However, the time-consuming sample preparation procedure involving extraction, purification, hydrolysis, derivatization, and the inaccurate identification of stereoisomeric forms of bile acid with single column of GLC technique have posed practical difficulty for extensive application for bile acid quantitation.

Mass Spectrometry-based Techniques

The continuous utilization of mass spectrometry techniques for bile acid analysis is attributed to its structural elucidation, definitive quantitation and isotopic differentiation capacity. Various mass spectrometry ionization techniques have been used for bile acid analysis, including electron impact ionization, chemical ionization, fast atom bombardment, atmospheric pressure chemical ionization, matrix-assisted laser desorption ionization, thermospray ionization, ion spray and electrospray ionization (398). Choices of coupled mass analyzers are based on analytical purposes, including qualitative ion trap, orbitrap, time-of-flight and quantitative triple/tandem quadrupole.

Gas Chromatography-Mass Spectrometry (GC–MS)

GC-MS, as a robust, simple method, which has been extensively utilized for bile acid separation and quantitation, especially for bile acid structure elucidation (399). Compared to LC-MS, the obvious advantage of GC-MS is the relative inexpensive instrumentation and lower carry-over on columns. However, the drawbacks of GC-MS

for bile acid analysis include the requirement of time-consuming and variation-introducing conjugation cleavage and carboxyl or hydroxyl group derivatization/methylation. GC-MS recently has been used as a complementary approach to LC-MS to validate methods, increase metabolome coverage or to verify the biomarker identification (400, 401).

Liquid Chromatography-Mass Spectrometry (LC-MS)

LC-MS and LC-tandem mass spectrometry (LC-MS/MS) has been the most sensitive and widely used analytical tools for accurate bile acid quantitation in urine, plasma, serum, bile, intestinal content, liver and feces. Currently, most available LC-MS and LC-MS/MS methods are reverse-phase chromatography and atmospheric pressure ionization dependent, which allow wider choices of flow rates and column dimensions (387, 402). A buffered mobile phase is usually introduced to maintain a certain pH range to achieve better ionization and chromatographic response based on the analytical purpose. For example, bile acids are predominately in the deprotonated form under neutral pH environment. As the pH decreases to pH=4 by adding acetic or formic acid, taurine conjugated bile acids become deprotonated while glycine and free bile acids are in their ionized from predominately (403). Moreover, the highly specific and sensitive LC-MS/MS provides direct, reliable and accurate measurement of conjugated bile acid by simultaneous monitoring the parent and daughter ions with multiple reaction monitoring (MRM) method, which has been applied for bile acid profile screening and taurine, glycine, sulfated, and glucuronidated bile acid quantitation (387, 399, 401, 404). The improved ultra-high pressure liquid chromatography (UHPLC) system using columns

packed with particles smaller than 2 μm allows for faster flow rate, shorter elution time, better LC performance and increased peak capacity over HPLC. 21 and 55-66 different bile acids species in mouse and human samples have been quantified with UPLC-MS/MS system by different research groups, respectively (387, 405).

Nuclear Magnetic Resonance (NMR) Spectroscopy based Assays

As the most reproducible, reliable and simplest sample preparation analytical method, high field NMR spectroscopy has been exploited for bile acid identification and quantification. However, due to the relative low sensitivity and complexity of the matrix, the application has been limited to quantitation of total bile acids and several highly concentrated conjugated bile acid species (406, 407).

Manipulate Microbiome Therapeutically to Treat Metabolic Disease

The critical metabolic and immunological roles of microbial-derived metabolites for human health has led to therapeutic approaches to manipulate SCFAs and bile acids pool size, composition and function by targeting microbiome or microbial-derived metabolites like BSH via different strategies like bariatric surgery, dietary supplement and xenobiotic/drug intervention.

Bariatric Surgery

Bariatric surgery has been the most effective intervention for the treatment of obesity and glycemic control of T2D, with over 30,000 bariatric surgery procedures being undertaken annually (408). Roux-en-Y gastric bypass (RYGB), laparoscopic adjustable

gastric banding (LAGB) and vertical sleeve gastrectomy (VSG) operations are most common bariatric surgery procedures, which lead to glucose normalization, insulin resistance resolution and T2D remission strikingly within hours to days after the surgery, well before any significant weight loss has occurred (409). The molecular mechanisms underlying the metabolic improvement of bariatric surgery have not been well delineated, however recent data suggests that postsurgery improvement is not merely an effect of weight loss due to decreased stomach volume, but is intimately associated with significant alteration of gut microbiome, SCFAs and bile acid signals resulting from surgical re-routing of ingested nutrients and digestive juices (410-412). Increased anti-lipogenesis propionate and decreased pro-lipogenesis acetate in RYGB-recipient mice were likely responsible for the beneficial changes in lipid metabolism and promoted energy homeostasis(413). Elevated systemic bile acid following RYGB and VSG were reported in both clinical studies and animal models, suggesting an enhanced enterohepatic bile acid signaling after surgery (410, 414).

Emerging animal and human studies have shown a remodeling of gut microbiome structure after RYGB, with a substantial shift of the main phyla from predominant Firmicutes and Bacteroidetes towards γProteobacteria, specifically family Enterobacteriaceae (415, 416). Inoculation of GF recipients with gut microbes from RYGB donors resulted in significant lower fat mass and weight gain compared to recipients inoculated from sham surgery donors, indicating restructured gut microbiome after RYGB directly contributes to postsurgery metabolic improvement (413). The remodeling of microbiome after RYGB has been implicated in alteration of bile acid-regulated pathways through bile acid receptors. FXR and FGF19/21 signals, which are

known to modulate bile acid, glucose and lipid metabolism, have been observed in higher levels three months after RYGB (417). FXR-signaling was reported as a molecular target in mediating beneficial metabolic response to the gastric bypass alternative procedure VSG, and the genetic disruption of FXR lead to substantial reduction of therapeutic efficacy of VSG (418). Remarkably, the functional change of microbial community postsurgery is *Fxr*-genotype dependent, as the prevalence of specific bacteria genera (e.g., *Bacteroides*, *Roseburia*) known as critical systemic metabolism modulators whose abundance is associated with weight loss and improved glucose control were altered differently by VSG *Fxr* knockout mice. In addition to FXR signaling, another bile-acid regulated receptor TGR5 is activated after RYGB, which potentiates GLP-1 secretion from enteroendocrine L cells. GLP-1 is a major incretin hormone to promote glucose metabolism, insulin sensitivity and energy expenditure to achieve glycaemia and energy control, which is rapidly increased after RYGB in plasma (419, 420). Gastric bypass alternative procedure VSG induced elevation in energy expenditure was reported to be TGR5 independent in mice. However, *Tgr5* deficiency attenuated improved glucose tolerance, insulin signaling and metabolism in bile acid profiles after VSG, suggesting TGR5 signaling contributes to the postsurgery glucoregulatory benefits by promoting metabolically favorable shifts in gut microbial and circulating bile acid profiles (421). Notably, the inconsistency in post-prandial bile acid changes after RYGB, VSG, and LAGB might suggest different enterohepatic bile acid signaling, while the concrete mechanism of each surgical type remains to be elucidated. The variability in the composition of the bile acid pool among independent studies indicates the analytical

limitation and unreliability of bile acid quantitation protocols with inconsistent sampling timing, analytical technique, statistical analysis, and reporting (422).

Dietary Control

Dietary factors have both direct modulatory effect on SCFAs/bile acids kinetics and indirect effects through shaping the gut microbiome and remodeling the microbiome-metabolite-host interactions. The SCFAs concentration depends on the type and the quantity of fiber consumed with a non-linear pattern. It has been observed that elevated cecal SCFAs levels with 10% of dietary wheat starch replaced by inulin, while decreased when replaced by 20% inulin (423). Additionally, inulin shifted SCFAs composition from acetate to beneficial propionate and butyrate (424). A recent human study suggested a fiber-rich diet like the typical Mediterranean diet is linked to an elevated level of health promoting SCFAs and an expansion of SCFAs- producing bacteria including *Lachnospira* and *Prevotella* (425). Dietary factors directly affect bile acid metabolism and kinetics through regulating the rate of gallbladder emptying, the gut transit time, the fractional turnover rate, and bile acid pool size in response to a meal. Dietary fat content and composition have been shown to influence the response of CYP7A1 to dietary cholesterol during *de novo* bile acid synthesis thus affecting bile acid metabolism in animal models, though human studies showed less consistent links between dietary fat intake and bile acid kinetics (426). Dietary factors indirectly modulate bile acid composition and signaling by reshaping the microbial community structure and selectively favoring or inhibiting species involved in bile acid synthesis, regulation, and biotransformation. The dynamic interplay between gut microbiome and bile acids/SCFAs

which could be modified by dietary components leading to host metabolic alterations, supports the notion that dietary therapeutic solutions for metabolic disease can be explored.

Probiotics

Probiotics of the genera *Lactobacillus* and *Bifidobacterium* have been widely used as food ingredients and over-the-counter supplements for gut microbiota homeostasis, general health improvement, and medical condition treatment including diarrhea and hypercholesterolemia (427). According to a recent meta-analysis of randomized controlled trails including a total of 1971 patients from public database dating from 2007 to 2017, probiotics administration has been shown to significantly reduce total cholesterol levels in serum between 9.8 to 16.74% with 95% confidential interval in the random-effect model analysis (428). Evidence suggests that probiotics exert their metabolic and immunological benefits through modifying bile acid composition as probiotic stains with BSH activity generate various bile acid species with different signaling functions (427). A recent study reported the probiotic cocktail formulation VSL#3 caused significant microbial composition shift towards Firmicutes and Actinobacteria at the expense of Bacteroidetes and Proteobacteria, along with enhanced ileal bile acid deconjugation and fecal excretion corresponding with increased fecal BSH activity, as well as upregulated Cyp7a1 and Cyp8b expression and consequently enhanced hepatic bile acid synthesis via FXR-Fgf15 suppression dependent pathway (429). In a 2,4,6-trinitrobenzenesulfonic acid-induced colitis rodent model, VSL#3 administration corrected the inflammation-driven metabolic dysfunction through bile acid-regulated nuclear receptors FXR, PXR as

well as PPARγ (430). Despite the growing body of health- promoting evidence for BSH-positive probiotic strain supplementation, safety concerns may arise knowing microbial BSH could be potentially detrimental as BSH catalyzed deconjugation is the prerequisite for generation of toxic secondary bile acids via microbial-mediated 7α/β-dehydroxylation. Therefore, a better understanding of the role of BSH and attentive selection of specific strain that is incapable of further modifying unconjugated bile salts, or is unlikely to produce harmful products of BSH deconjugation are necessary to address the medical concerns about the possible side effects associated with BSH-positive probiotic supplementation (431).

Prebiotics

Prebiotic refers to a substrate that is selectively utilized by host microorganisms conferring a health benefit (432). Prebiotics are reported to improve gastrointestinal disorders (e.g., irritable bowel syndrome) and metabolic disorders (e.g., hypercholesterolaemia), prevent carcinogenesis and lower tumor incidence (433). Saccharolytic fermentation by bacteria lead to SCFAs production that are recognized as preferred energy substrates for colonic epithelium to maintain gut barrier function and positive metabolic and immunological modulators. Prebiotics like inulin-type fructans selectively favor growth of specific microbial genera like *Bifidobacteria* and *Lactobacilli*, which have relatively lower xenobiotic-metabolizing enzymes, might beneficially reduce carcinogen, pre-cancerous lesions and tumor formation (433). A recent study using apolipoprotein E knockout (*Apoe*−/−) mice model with endothelial dysfunction in mesenteric arteries has shown inulin-type fructans supplementation upregulated gene

expression involved in bile acid metabolism including *Cyp7a1, Slc10a2, Fabp6, Slc51a/b*, and modulated the plasma and cecal BA profiles with an increase in primary bile acids (CA, CDCA), MAC and UDCA, but a decrease in secondary bile acids (DCA) and tauro-conjugated bile acids, which are correlated with marked decrease of Ruminococcaceae and Lachnospiraceae families and expended Bifidobacteriaceae and Erysipelotrichaceae families and *Akkermansia* genus. The expended NO-producing bacteria, elevated circulating bile acids, increased L cells density and promoted glucagon-like peptide 1 production might co-contribute to the improvement of enteric vascular dysfunction through activation of the endothelial NOS–nitric oxide pathway (434).

Xenobiotic/Drug Targeting of Microbial-Derived Signaling

Increased understanding of microbial-derived signaling routes and effects covering physiological, metabolic and immunological functions, have drawn vast interest in the development of novel therapeutic approaches by targeting gut microbiome-metabolite-receptors axis for metabolic and inflammatory diseases treatment. One most popular strategy is therapeutically targeting FXR signaling. A 6-α ethyl derivative of CDCA (6-ECDCA), also knowns as OCA, a semi-synthetic steroidal dual FXR/TGR5 agonist with a 100-fold greater FXR selectivity compared to CDCA (435), has been used as a first-in-class selective FXR agonist under double-blinded, placebo-controlled clinical phase 2 trails in the treatment of NAFLD and NASH. Other FXR agonists including WAY-362450 (FXR-450), PX-102, PX-104, LJN452, GS-9674, are already completed or under active clinical trials ranging from phase 1 to 2 (436). Other developed FXR agonists like GW4064 or INT-767 have shown promising effect for the improvement of

insulin resistance, steatosis, and fibrosis in diet-induced diabetic and NASH animal models (271, 437). Follow-up clinical trials are currently underway but no convincing efficacy data as of yet has been reported.

Interestingly, gut-restricted FXR agonism might offer a safer therapeutic alternative in the treatment of metabolic syndrome with beneficial systemic efficacy and minimum systemic toxicity. A gut-restricted drug fexaramine, which is administered orally while poorly absorbed into the circulation, counters obesity and metabolic syndrome, promotes energy expenditure and fat browning, and improves insulin response in diet-induced obesity mice, likely through FXR-Fgf15 signaling and alterations in bile acid composition (297). The role of selective FXR agonism/antagonism in metabolic disorders is controversial and complicated, as the comparative analysis of liver-specific and intestine-specific *Fxr* knockout mice revealed distinct metabolic outcomes in diet-induced or genetic obese/diabetic mice models (267, 272, 360, 438, 439). Emerging evidence revealed the intestinal-specific FXR antagonism attenuated HFD-induced hepatic steatosis and ameliorated HFD-induced hyperglycemia, suggesting the potential therapeutic strategy of tissue specific FXR inhibition for obesity-related metabolic disorders (267, 360). The antioxidant tempol which has anti-obesity and metabolic beneficial effects in mice (181, 440), increases FXR antagonist levels, specifically TβMCA in the intestinal bile acid pool by inhibiting BSH producing *Lactobacillus*. By knocking out BSH, tempol inhibits the deconjugation process (hydrolysis of tauro-conjugated bile acid to free bile acid) to upregulate TβMCA and intestinal FXR inhibition. Another new orally available, synthesized bile acid analog glycine-β-muricholic acid (GMCA) was developed as a more potent intestine-specific FXR

inhibitor as it is not hydrolyzed by BSH. GMCA induced intestine-specific FXR inhibition prevents diet-induced and genetic obesity and hepatic steatosis in mice through intestinal FXR-ceramide axis, whereby intestinal FXR regulated-ceramides enter circulation and regulate hepatic *de novo* fatty acid synthesis via the Srebp1-c/Cidea signaling pathway (441). A newly discovered BSH inhibitor CAPE reverses hyperglycemia in HFD fed mice by selectively suppressing intestinal FXR-ceramides signaling (267). Additional pre-clinical and clinical experiments need to be done to fully determine if FXR antagonism can be therapeutically exploited in the treatment of metabolic syndrome in human.

The antidiabetic, anti-inflammatory and energy expenditure effects of TGR5 uncovers a therapeutic avenue through TGR5 agonism to conquer type 2 diabetes, atherosclerosis and other obesity-related metabolic disorders (62, 293). Mice studies have revealed TGR activation by administering synthetic TGR5 agonist like INT-777 and TRC210258 addresses the multiple metabolic and immunological abnormalities related to obesity and diabetes, including dyslipidemia, hyperglycemia, diabetic nephropathy, renal damage and kidney disease (442, 443). However, controversial results and potential risk of TGR5 agonism have been reported (444-447), indicating the challenges for pharmaceutical application of TGR5 agonist-based therapy.

Although animal studies have identified the great therapeutic potential by manipulating microbial-derived signals in the treatment of enterohepatic and metabolic disorders, including cholestasis, nonalcoholic liver disease (NAFLD and NASH) and diabetes (448-450), the clinically available therapies targeting microbial-derived signaling (SCFAs and bile acids) are limited, and promising drug candidates are still

under development phase and early clinical trials. More fundamental and translational investigations will be needed to elucidate microbial-derived signaling and xenobiotics-microbiome-host interactions to fully exploit the therapeutic potential of microbial-derived metabolites and their signaling in the treatment of metabolic and immunological disorders.

Research Objectives

The central hypothesis is metabolomics in addition with other informative techniques enables the comprehensive and complementary understanding of the mechanistic interplay between xenobiotic and host-associated microbiome. By testing the hypothesis, this dissertation explores the application of MS- and NMR-based metabolomics combined with molecular biology, biochemistry, flow cytometry and other elegant approaches to quantify bacterial-derived metabolites, characterize the xenobiotic induced-microbial modulation of host metabolic profiles, evaluate impact of xenobiotic on microbiome function and host metabolism, and discover xenobiotics-microbiome-host interactions for potential therapeutic application. In chapter 2, reliable and dependable metabolomics methods for SCFAs quantitation were investigated. Different SCFAs quantitation methods using two independent metabolomics platform GC-MS and ^{1}H NMR were compared, optimized and combined for accurate quantitation, feasibility validation and extensive application. In chapter 3, the metabolic functional roles of gut microbiome and how to target microbiome therapeutically to achieve metabolic improvement on host was elucidated by investigating anti-obesity mechanism of a xenobiotic tempol. The effect of tempol on microbial fermentation and host metabolic

profiles and energy homeostasis were fully investigated with the global and targeted metabolomics methods developed. A xenobiotic-microbiome-host interaction was established for microbiome-targeting therapeutic strategy development. In chapter 4, a novel approach combining in vitro bacterial incubation, single-cell flow cytometry, and global metabolomics tools was developed to characterize microbiome viability, physiology, and metabolic activity following direct xenobiotic tempol exposure, aiming to understand the direct impact of xenobiotic/toxicants on microbiome toxicity for better inform risk assessment and drug screening. Chapter 5 thoroughly discussed the key findings of the work and future directions with the powerful metabolomics tools to uncover xenobiotic-microbiome-host interactions, the role of the gut microbiome in the context of human diseases and the best ways to manipulate the microbiome therapeutically to achievement health benefits in host.

REFERENCE

1. Guinane CM, and Cotter PD. Role of the gut microbiota in health and chronic gastrointestinal disease: understanding a hidden metabolic organ. *Therapeutic Advances in Gastroenterology.* 2013;6(4):295-308.
2. Conlon MA, and Bird AR. The Impact of Diet and Lifestyle on Gut Microbiota and Human Health. *Nutrients.* 2015;7(1):17-44.
3. Clemente Jose C, Ursell Luke K, Parfrey Laura W, and Knight R. The Impact of the Gut Microbiota on Human Health: An Integrative View. *Cell.* 2012;148(6):1258-70.
4. Claus SP, Guillou H, and Ellero-Simatos S. The gut microbiota: a major player in the toxicity of environmental pollutants? *Npj Biofilms And Microbiomes.* 2016;2(16003.
5. Davis C. *Chapter 6: Normal Flora. Medical Microbiology. 4th edition.* . Galveston (TX): University of Texas Medical Branch at Galveston; 1996.
6. Rajilic-Stojanovic M, and de Vos WM. The first 1000 cultured species of the human gastrointestinal microbiota. *FEMS Microbiol Rev.* 2014;38(5):996-1047.
7. Hayashi H, Sakamoto M, and Benno Y. Phylogenetic analysis of the human gut microbiota using 16S rDNA clone libraries and strictly anaerobic culture-based methods. *Microbiology and immunology.* 2002;46(8):535-48.
8. Thursby E, and Juge N. Introduction to the human gut microbiota. *Biochemical Journal.* 2017;474(11):1823-36.
9. Jandhyala SM, Talukdar R, Subramanyam C, Vuyyuru H, Sasikala M, and Reddy DN. Role of the normal gut microbiota. *World Journal of Gastroenterology : WJG.* 2015;21(29):8787-803.
10. Rodríguez JM, Murphy K, Stanton C, Ross RP, Kober OI, Juge N, Avershina E, Rudi K, Narbad A, Jenmalm MC, et al. The composition of the gut microbiota throughout life, with an emphasis on early life. *Microbial Ecology in Health and Disease.* 2015;26(10.3402/mehd.v26.26050.
11. Cox LM, Yamanishi S, Sohn J, Alekseyenko AV, Leung JM, Cho I, Kim SG, Li H, Gao Z, Mahana D, et al. Altering the intestinal microbiota during a critical developmental window has lasting metabolic consequences. *Cell.* 2014;158(4):705-21.
12. Gu S, Chen D, Zhang JN, Lv X, Wang K, Duan LP, Nie Y, and Wu XL. Bacterial community mapping of the mouse gastrointestinal tract. *PloS one.* 2013;8(10):e74957.
13. Swidsinski A, Sydora BC, Doerffel Y, Loening-Baucke V, Vaneechoutte M, Lupicki M, Scholze J, Lochs H, and Dieleman LA. Viscosity gradient within the mucus layer determines the mucosal barrier function and the spatial organization of the intestinal microbiota. *Inflammatory bowel diseases.* 2007;13(8):963-70.
14. Pedron T, Mulet C, Dauga C, Frangeul L, Chervaux C, Grompone G, and Sansonetti PJ. A crypt-specific core microbiota resides in the mouse colon. *MBio.* 2012;3(3).
15. Swidsinski A, Weber J, Loening-Baucke V, Hale LP, and Lochs H. Spatial organization and composition of the mucosal flora in patients with inflammatory bowel disease. *Journal of clinical microbiology.* 2005;43(7):3380-9.
16. Eckburg PB, Bik EM, Bernstein CN, Purdom E, Dethlefsen L, Sargent M, Gill SR, Nelson KE, and Relman DA. Diversity of the human intestinal microbial flora. *Science.* 2005;308(5728):1635-8.
17. Malmuthuge N, Griebel PJ, and Guan le L. Taxonomic identification of commensal bacteria associated with the mucosa and digesta throughout the gastrointestinal tracts of preweaned calves. *Appl Environ Microbiol.* 2014;80(6):2021-8.
18. Koh JH, and Kim W-U. Dysregulation of gut microbiota and chronic inflammatory disease: from epithelial defense to host immunity. *Experimental & Molecular Medicine.* 2017;49(5):e337.

19. Jandhyala SM, Talukdar R, Subramanyam C, Vuyyuru H, Sasikala M, and Nageshwar Reddy D. Role of the normal gut microbiota. *World journal of gastroenterology.* 2015;21(29):8787-803.
20. Wostmann BS, Larkin C, Moriarty A, and Bruckner-Kardoss E. Dietary intake, energy metabolism, and excretory losses of adult male germfree Wistar rats. *Laboratory animal science.* 1983;33(1):46-50.
21. Mcneil NI. The Contribution of the Large-Intestine to Energy Supplies in Man. *Am J Clin Nutr.* 1984;39(2):338-42.
22. Zambell KL, Fitch MD, and Fleming SE. Acetate and butyrate are the major substrates for de novo lipogenesis in rat colonic epithelial cells. *The Journal of nutrition.* 2003;133(11):3509-15.
23. Kasubuchi M, Hasegawa S, Hiramatsu T, Ichimura A, and Kimura I. Dietary Gut Microbial Metabolites, Short-chain Fatty Acids, and Host Metabolic Regulation. *Nutrients.* 2015;7(4):2839-49.
24. Sun M, Wu W, Liu Z, and Cong Y. Microbiota metabolite short chain fatty acids, GPCR, and inflammatory bowel diseases. *Journal of Gastroenterology.* 2017;52(1):1-8.
25. Brown AJ, Goldsworthy SM, Barnes AA, Eilert MM, Tcheang L, Daniels D, Muir AI, Wigglesworth MJ, Kinghorn I, Fraser NJ, et al. The Orphan G protein-coupled receptors GPR41 and GPR43 are activated by propionate and other short chain carboxylic acids. *J Biol Chem.* 2003;278(13):11312-9.
26. Turnbaugh PJ, Ley RE, Mahowald MA, Magrini V, Mardis ER, and Gordon JI. An obesity-associated gut microbiome with increased capacity for energy harvest. *Nature.* 2006;444(1027.
27. Thomas CM, Hong T, van Pijkeren JP, Hemarajata P, Trinh DV, Hu W, Britton RA, Kalkum M, and Versalovic J. Histamine derived from probiotic Lactobacillus reuteri suppresses TNF via modulation of PKA and ERK signaling. *PloS one.* 2012;7(2):e31951.
28. De Biase D, and Pennacchietti E. Glutamate decarboxylase-dependent acid resistance in orally acquired bacteria: function, distribution and biomedical implications of the gadBC operon. *Molecular microbiology.* 2012;86(4):770-86.
29. Smith EA, and Macfarlane GT. Enumeration of amino acid fermenting bacteria in the human large intestine: effects of pH and starch on peptide metabolism and dissimilation of amino acids. *FEMS microbiology ecology.* 1998;25(4):355-68.
30. Dai ZL, Wu G, and Zhu WY. Amino acid metabolism in intestinal bacteria: links between gut ecology and host health. *Frontiers in bioscience (Landmark edition).* 2011;16(1768-86.
31. Atasoglu C, Valdes C, Walker ND, Newbold CJ, and Wallace RJ. De novo synthesis of amino acids by the ruminal bacteria Prevotella bryantii B14, Selenomonas ruminantium HD4, and Streptococcus bovis ES1. *Appl Environ Microbiol.* 1998;64(8):2836-43.
32. Gill SR, Pop M, Deboy RT, Eckburg PB, Turnbaugh PJ, Samuel BS, Gordon JI, Relman DA, Fraser-Liggett CM, and Nelson KE. Metagenomic analysis of the human distal gut microbiome. *Science.* 2006;312(5778):1355-9.
33. Hill MJ. Intestinal flora and endogenous vitamin synthesis. *European journal of cancer prevention : the official journal of the European Cancer Prevention Organisation (ECP).* 1997;6 Suppl 1(S43-5.
34. Ramakrishna BS. Role of the gut microbiota in human nutrition and metabolism. *Journal of gastroenterology and hepatology.* 2013;28 Suppl 4(9-17.
35. LeBlanc JG, Milani C, de Giori GS, Sesma F, van Sinderen D, and Ventura M. Bacteria as vitamin suppliers to their host: a gut microbiota perspective. *Current opinion in biotechnology.* 2013;24(2):160-8.
36. Yamada K. In: Sigel A, Sigel H, and Sigel RKO eds. *Interrelations between Essential Metal Ions and Human Diseases*. Dordrecht: Springer Netherlands; 2013:295-320.

37. Decroos K, Vanhemmens S, Cattoir S, Boon N, and Verstraete W. Isolation and characterisation of an equol-producing mixed microbial culture from a human faecal sample and its activity under gastrointestinal conditions. *Archives of Microbiology.* 2005;183(1):45-55.
38. Marín L, Miguélez EM, Villar CJ, and Lombó F. Bioavailability of Dietary Polyphenols and Gut Microbiota Metabolism: Antimicrobial Properties. *BioMed research international.* 2015;2015(905215.
39. Haiser HJ, and Turnbaugh PJ. Developing a metagenomic view of xenobiotic metabolism. *Pharmacological research : the official journal of the Italian Pharmacological Society.* 2013;69(1):21-31.
40. Spanogiannopoulos P, Bess EN, Carmody RN, and Turnbaugh PJ. The microbial pharmacists within us: a metagenomic view of xenobiotic metabolism. *Nature Reviews Microbiology.* 2016;14(273.
41. Haiser HJ, Gootenberg DB, Chatman K, Sirasani G, Balskus EP, and Turnbaugh PJ. Predicting and manipulating cardiac drug inactivation by the human gut bacterium Eggerthella lenta(). *Science (New York, NY).* 2013;341(6143):295-8.
42. Bjorkholm B, Bok CM, Lundin A, Rafter J, Hibberd ML, and Pettersson S. Intestinal microbiota regulate xenobiotic metabolism in the liver. *PLoS One.* 2009;4(9):e6958.
43. Selwyn FP, Cui JY, and Klaassen CD. RNA-Seq Quantification of Hepatic Drug Processing Genes in Germ-Free Mice. *Drug metabolism and disposition: the biological fate of chemicals.* 2015;43(10):1572-80.
44. Clayton TA, Baker D, Lindon JC, Everett JR, and Nicholson JK. Pharmacometabonomic identification of a significant host-microbiome metabolic interaction affecting human drug metabolism. *Proc Natl Acad Sci U S A.* 2009;106(34):14728-33.
45. Wu H-J, and Wu E. The role of gut microbiota in immune homeostasis and autoimmunity. *Gut Microbes.* 2012;3(1):4-14.
46. Smith K, McCoy KD, and Macpherson AJ. Use of axenic animals in studying the adaptation of mammals to their commensal intestinal microbiota. *Seminars in immunology.* 2007;19(2):59-69.
47. Iwasaki A, and Kelsall BL. Freshly isolated Peyer's patch, but not spleen, dendritic cells produce interleukin 10 and induce the differentiation of T helper type 2 cells. *The Journal of experimental medicine.* 1999;190(2):229-39.
48. Smythies LE, Shen R, Bimczok D, Novak L, Clements RH, Eckhoff DE, Bouchard P, George MD, Hu WK, Dandekar S, et al. Inflammation anergy in human intestinal macrophages is due to Smad-induced IkappaBalpha expression and NF-kappaB inactivation. *The Journal of biological chemistry.* 2010;285(25):19593-604.
49. Olszak T, An D, Zeissig S, Vera MP, Richter J, Franke A, Glickman JN, Siebert R, Baron RM, Kasper DL, et al. Microbial exposure during early life has persistent effects on natural killer T cell function. *Science.* 2012;336(6080):489-93.
50. An D, Oh SF, Olszak T, Neves JF, Avci F, Erturk-Hasdemir D, Lu X, Zeissig S, Blumberg RS, and Kasper DL. Sphingolipids from a symbiotic microbe regulate homeostasis of host intestinal natural killer T cells. *Cell.* 2014;156(0):123-33.
51. Mazmanian SK, Liu CH, Tzianabos AO, and Kasper DL. An immunomodulatory molecule of symbiotic bacteria directs maturation of the host immune system. *Cell.* 2005;122(1):107-18.
52. Belkaid Y, and Hand T. Role of the Microbiota in Immunity and inflammation. *Cell.* 2014;157(1):121-41.
53. Mazmanian SK, Liu CH, Tzianabos AO, and Kasper DL. An Immunomodulatory Molecule of Symbiotic Bacteria Directs Maturation of the Host Immune System. *Cell.* 2005;122(1):107-18.

54. Gaboriau-Routhiau V, Rakotobe S, Lécuyer E, Mulder I, Lan A, Bridonneau C, Rochet V, Pisi A, De Paepe M, Brandi G, et al. The Key Role of Segmented Filamentous Bacteria in the Coordinated Maturation of Gut Helper T Cell Responses. *Immunity.* 2009;31(4):677-89.
55. Lecuyer E, Rakotobe S, Lengline-Garnier H, Lebreton C, Picard M, Juste C, Fritzen R, Eberl G, McCoy KD, Macpherson AJ, et al. Segmented filamentous bacterium uses secondary and tertiary lymphoid tissues to induce gut IgA and specific T helper 17 cell responses. *Immunity.* 2014;40(4):608-20.
56. Atarashi K, Tanoue T, Shima T, Imaoka A, Kuwahara T, Momose Y, Cheng G, Yamasaki S, Saito T, Ohba Y, et al. Induction of Colonic Regulatory T Cells by Indigenous Clostridium Species. *Science (New York, NY).* 2011;331(6015):337-41.
57. Fiorucci S, and Distrutti E. Bile Acid-Activated Receptors, Intestinal Microbiota, and the Treatment of Metabolic Disorders. *Trends in molecular medicine.* 2015;21(11):702-14.
58. Qi Y, Jiang C, Cheng J, Krausz KW, Li T, Ferrell JM, Gonzalez FJ, and Chiang JY. Bile acid signaling in lipid metabolism: metabolomic and lipidomic analysis of lipid and bile acid markers linked to anti-obesity and anti-diabetes in mice. *Biochimica et biophysica acta.* 2015;1851(1):19-29.
59. Claudel T, Staels B, and Kuipers F. The Farnesoid X receptor: a molecular link between bile acid and lipid and glucose metabolism. *Arteriosclerosis, thrombosis, and vascular biology.* 2005;25(10):2020-30.
60. Fiorucci S, Rizzo G, Donini A, Distrutti E, and Santucci L. Targeting farnesoid X receptor for liver and metabolic disorders. *Trends in molecular medicine.* 2007;13(7):298-309.
61. Jiang Y, Jin J, Iakova P, Hernandez JC, Jawanmardi N, Sullivan E, Guo GL, Timchenko NA, and Darlington GJ. Farnesoid X receptor directly regulates xenobiotic detoxification genes in the long-lived Little mice. *Mechanisms of ageing and development.* 2013;134(9):407-15.
62. Watanabe M, Houten SM, Mataki C, Christoffolete MA, Kim BW, Sato H, Messaddeq N, Harney JW, Ezaki O, Kodama T, et al. Bile acids induce energy expenditure by promoting intracellular thyroid hormone activation. *Nature.* 2006;439(484.
63. Gropper SS, and Smith JL. *Advanced nutrition and human metabolism.* Belmont, OH: Cengage Learning; 2012.
64. Ridlon JM, Kang D-J, and Hylemon PB. Isolation and characterization of a bile acid inducible 7α-dehydroxylating operon in Clostridium hylemonae TN271. *Anaerobe.* 2010;16(2):137-46.
65. Macdonald IA, Bokkenheuser VD, Winter J, McLernon AM, and Mosbach EH. Degradation of steroids in the human gut. *J Lipid Res.* 1983;24(6):675-700.
66. Ridlon JM, Kang DJ, and Hylemon PB. Bile salt biotransformations by human intestinal bacteria. *J Lipid Res.* 2006;47(2):241-59.
67. Ruppin H, Bar-Meir S, Soergel KH, Wood CM, and Schmitt MG, Jr. Absorption of short-chain fatty acids by the colon. *Gastroenterology.* 1980;78(6):1500-7.
68. Wong JM, de Souza R, Kendall CW, Emam A, and Jenkins DJ. Colonic health: fermentation and short chain fatty acids. *Journal of clinical gastroenterology.* 2006;40(3):235-43.
69. Wolever TMS. Short-Chain Fatty-Acids and Carbohydrate-Metabolism. *Falk Symp.* 1994;73(251-9.
70. Frost G, Sleeth ML, Sahuri-Arisoylu M, Lizarbe B, Cerdan S, Brody L, Anastasovska J, Ghourab S, Hankir M, Zhang S, et al. The short-chain fatty acid acetate reduces appetite via a central homeostatic mechanism. *Nature Communications.* 2014;5(3611.

71. Byrne CS, Chambers ES, Morrison DJ, and Frost G. The role of short chain fatty acids in appetite regulation and energy homeostasis. *International journal of obesity.* 2015;39(1331.
72. Chambers ES, Viardot A, Psichas A, Morrison DJ, Murphy KG, Zac-Varghese SE, MacDougall K, Preston T, Tedford C, Finlayson GS, et al. Effects of targeted delivery of propionate to the human colon on appetite regulation, body weight maintenance and adiposity in overweight adults. *Gut.* 2015;64(11):1744-54.
73. Weitkunat K, Schumann S, Nickel D, Kappo KA, Petzke KJ, Kipp AP, Blaut M, and Klaus S. Importance of propionate for the repression of hepatic lipogenesis and improvement of insulin sensitivity in high-fat diet-induced obesity. *Mol Nutr Food Res.* 2016.
74. Anderson JW, and Siesel AE. Hypocholesterolemic effects of oat products. *Advances in experimental medicine and biology.* 1990;270(17-36.
75. Hosseini E, Grootaert C, Verstraete W, and Van de Wiele T. Propionate as a health-promoting microbial metabolite in the human gut. *Nutr Rev.* 2011;69(5):245-58.
76. Tong LC, Wang Y, Wang ZB, Liu WY, Sun S, Li L, Su DF, and Zhang LC. Propionate Ameliorates Dextran Sodium Sulfate-Induced Colitis by Improving Intestinal Barrier Function and Reducing Inflammation and Oxidative Stress. *Front Pharmacol.* 2016;7(253.
77. Bindels LB, Porporato P, Dewulf EM, Verrax J, Neyrinck AM, Martin JC, Scott KP, Buc Calderon P, Feron O, Muccioli GG, et al. Gut microbiota-derived propionate reduces cancer cell proliferation in the liver. *Br J Cancer.* 2012;107(8):1337-44.
78. Roediger WE. Utilization of nutrients by isolated epithelial cells of the rat colon. *Gastroenterology.* 1982;83(2):424-9.
79. Velazquez OC, Lederer HM, and Rombeau JL. Butyrate and the colonocyte. Production, absorption, metabolism, and therapeutic implications. *Advances in experimental medicine and biology.* 1997;427(123-34.
80. Frankel W, Lew J, Su B, Bain A, Klurfeld D, Einhorn E, MacDermott RP, and Rombeau J. Butyrate increases colonocyte protein synthesis in ulcerative colitis. *J Surg Res.* 1994;57(1):210-4.
81. Qiao Y, Qian J, Lu Q, Tian Y, Chen Q, and Zhang Y. Protective effects of butyrate on intestinal ischemia-reperfusion injury in rats. *J Surg Res.* 2015;197(2):324-30.
82. Cushing K, Alvarado DM, and Ciorba MA. Butyrate and Mucosal Inflammation: New Scientific Evidence Supports Clinical Observation. *Clin Transl Gastroenterol.* 2015;6(e108.
83. Scharlau D, Borowicki A, Habermann N, Hofmann T, Klenow S, Miene C, Munjal U, Stein K, and Glei M. Mechanisms of primary cancer prevention by butyrate and other products formed during gut flora-mediated fermentation of dietary fibre. *Mutat Res.* 2009;682(1):39-53.
84. Blouin JM, Penot G, Collinet M, Nacfer M, Forest C, Laurent-Puig P, Coumoul X, Barouki R, Benelli C, and Bortoli S. Butyrate elicits a metabolic switch in human colon cancer cells by targeting the pyruvate dehydrogenase complex. *Int J Cancer.* 2011;128(11):2591-601.
85. Pouillart PR. Role of butyric acid and its derivatives in the treatment of colorectal cancer and hemoglobinopathies. *Life Sci.* 1998;63(20):1739-60.
86. McNeil NI. The contribution of the large intestine to energy supplies in man. *Am J Clin Nutr.* 1984;39(2):338-42.
87. Donohoe DR, Garge N, Zhang X, Sun W, O'Connell TM, Bunger MK, and Bultman SJ. The microbiome and butyrate regulate energy metabolism and autophagy in the mammalian colon. *Cell metabolism.* 2011;13(5):517-26.

88. Donohoe DR, Garge N, Zhang X, Sun W, O'Connell TM, Bunger MK, and Bultman SJ. The Microbiome and Butyrate Regulate Energy Metabolism and Autophagy in the Mammalian Colon. *Cell metabolism.* 2011;13(5):517-26.
89. Roediger WE. The starved colon--diminished mucosal nutrition, diminished absorption, and colitis. *Diseases of the colon and rectum.* 1990;33(10):858-62.
90. Peng L, Li Z-R, Green RS, Holzman IR, and Lin J. Butyrate Enhances the Intestinal Barrier by Facilitating Tight Junction Assembly via Activation of AMP-Activated Protein Kinase in Caco-2 Cell Monolayers. *The Journal of Nutrition.* 2009;139(9):1619-25.
91. VanHook AM. Butyrate benefits the intestinal barrier. *Science Signaling.* 2015;8(378):ec135-ec.
92. Groschwitz KR, and Hogan SP. Intestinal Barrier Function: Molecular Regulation and Disease Pathogenesis. *The Journal of allergy and clinical immunology.* 2009;124(1):3-22.
93. Knowles SE, Jarrett IG, Filsell OH, and Ballard FJ. Production and utilization of acetate in mammals. *Biochemical Journal.* 1974;142(2):401-11.
94. Bloemen JG, Venema K, van de Poll MC, Olde Damink SW, Buurman WA, and Dejong CH. Short chain fatty acids exchange across the gut and liver in humans measured at surgery. *Clin Nutr.* 2009;28(6):657-61.
95. Roy CC, Kien CL, Bouthillier L, and Levy E. Short-chain fatty acids: ready for prime time? *Nutr Clin Pract.* 2006;21(4):351-66.
96. Aschenbach JR, Kristensen NB, Donkin SS, Hammon HM, and Penner GB. Gluconeogenesis in Dairy Cows: The Secret of Making Sweet Milk from Sour Dough. *Iubmb Life.* 2010;62(12):869-77.
97. Singh V, Chassaing B, Zhang L, Yeoh BS, Xiao X, Kumar M, Baker MT, Cai J, Walker R, Borkowski K, et al. Microbiota-Dependent Hepatic Lipogenesis Mediated by Stearoyl CoA Desaturase 1 (SCD1) Promotes Metabolic Syndrome in TLR5-Deficient Mice. *Cell metabolism.* 2015;22(6):983-96.
98. Pluznick J. A novel SCFA receptor, the microbiota, and blood pressure regulation. *Gut Microbes.* 2014;5(2):202-7.
99. Layden BT, Angueira AR, Brodsky M, Durai V, and Lowe WL, Jr. Short chain fatty acids and their receptors: new metabolic targets. *Translational research : the journal of laboratory and clinical medicine.* 2013;161(3):131-40.
100. Le Poul E, Loison C, Struyf S, Springael JY, Lannoy V, Decobecq ME, Brezillon S, Dupriez V, Vassart G, Van Damme J, et al. Functional characterization of human receptors for short chain fatty acids and their role in polymorphonuclear cell activation. *J Biol Chem.* 2003;278(28):25481-9.
101. Senga T, Iwamoto S, Yoshida T, Yokota T, Adachi K, Azuma E, Hamaguchi M, and Iwamoto T. LSSIG is a novel murine leukocyte-specific GPCR that is induced by the activation of STAT3. *Blood.* 2003;101(3):1185-7.
102. Xiong Y, Miyamoto N, Shibata K, Valasek MA, Motoike T, Kedzierski RM, and Yanagisawa M. Short-chain fatty acids stimulate leptin production in adipocytes through the G protein-coupled receptor GPR41. *Proceedings of the National Academy of Sciences of the United States of America.* 2004;101(4):1045-50.
103. Thangaraju M, Cresci GA, Liu K, Ananth S, Gnanaprakasam JP, Browning DD, Mellinger JD, Smith SB, Digby GJ, Lambert NA, et al. GPR109A is a G-protein-coupled receptor for the bacterial fermentation product butyrate and functions as a tumor suppressor in colon. *Cancer research.* 2009;69(7):2826-32.
104. Pluznick JL, Protzko RJ, Gevorgyan H, Peterlin Z, Sipos A, Han J, Brunet I, Wan LX, Rey F, Wang T, et al. Olfactory receptor responding to gut microbiota-derived signals plays a role in renin secretion and blood pressure regulation. *Proc Natl Acad Sci U S A.* 2013;110(11):4410-5.

105. Nishina PM, and Freedland RA. Effects of propionate on lipid biosynthesis in isolated rat hepatocytes. *J Nutr.* 1990;120(7):668-73.
106. Demigne C, Morand C, Levrat MA, Besson C, Moundras C, and Remesy C. Effect of propionate on fatty acid and cholesterol synthesis and on acetate metabolism in isolated rat hepatocytes. *The British journal of nutrition.* 1995;74(2):209-19.
107. Weitkunat K, Schumann S, Nickel D, Kappo KA, Petzke KJ, Kipp AP, Blaut M, and Klaus S. Importance of propionate for the repression of hepatic lipogenesis and improvement of insulin sensitivity in high-fat diet-induced obesity. *Molecular nutrition & food research.* 2016;60(12):2611-21.
108. Rodwell VW, Nordstrom JL, and Mitschelen JJ. Regulation of HMG-CoA reductase. *Advances in lipid research.* 1976;14(1-74.
109. Bush RS, and Milligan LP. Study of the mechanism of inhibition of ketogenesis by propionate in bovine liver. *Can J Anim Sci.* 1971;51(1):121-7.
110. Zaibi MS, Stocker CJ, O'Dowd J, Davies A, Bellahcene M, Cawthorne MA, Brown AJ, Smith DM, and Arch JR. Roles of GPR41 and GPR43 in leptin secretory responses of murine adipocytes to short chain fatty acids. *FEBS Lett.* 2010;584(11):2381-6.
111. Hong YH, Nishimura Y, Hishikawa D, Tsuzuki H, Miyahara H, Gotoh C, Choi KC, Feng DD, Chen C, Lee HG, et al. Acetate and propionate short chain fatty acids stimulate adipogenesis via GPCR43. *Endocrinology.* 2005;146(12):5092-9.
112. Ge H, Li X, Weiszmann J, Wang P, Baribault H, Chen JL, Tian H, and Li Y. Activation of G protein-coupled receptor 43 in adipocytes leads to inhibition of lipolysis and suppression of plasma free fatty acids. *Endocrinology.* 2008;149(9):4519-26.
113. Kimura I, Ozawa K, Inoue D, Imamura T, Kimura K, Maeda T, Terasawa K, Kashihara D, Hirano K, Tani T, et al. The gut microbiota suppresses insulin-mediated fat accumulation via the short-chain fatty acid receptor GPR43. *Nature communications.* 2013;4(1829.
114. Xiong Y, Miyamoto N, Shibata K, Valasek MA, Motoike T, Kedzierski RM, and Yanagisawa M. Short-chain fatty acids stimulate leptin production in adipocytes through the G protein-coupled receptor GPR41. *Proc Natl Acad Sci U S A.* 2004;101(4):1045-50.
115. Boillot J, Alamowitch C, Berger AM, Luo J, Bruzzo F, Bornet FR, and Slama G. Effects of dietary propionate on hepatic glucose production, whole-body glucose utilization, carbohydrate and lipid metabolism in normal rats. *The British journal of nutrition.* 1995;73(2):241-51.
116. Heimann E, Nyman M, and Degerman E. Propionic acid and butyric acid inhibit lipolysis and de novo lipogenesis and increase insulin-stimulated glucose uptake in primary rat adipocytes. *Adipocyte.* 2015;4(2):81-8.
117. Berggren AM, Nyman EM, Lundquist I, and Bjorck IM. Influence of orally and rectally administered propionate on cholesterol and glucose metabolism in obese rats. *The British journal of nutrition.* 1996;76(2):287-94.
118. Todesco T, Rao AV, Bosello O, and Jenkins DJ. Propionate lowers blood glucose and alters lipid metabolism in healthy subjects. *Am J Clin Nutr.* 1991;54(5):860-5.
119. Wolever TM, Spadafora P, and Eshuis H. Interaction between colonic acetate and propionate in humans. *Am J Clin Nutr.* 1991;53(3):681-7.
120. Pingitore A, Chambers ES, Hill T, Maldonado IR, Liu B, Bewick G, Morrison DJ, Preston T, Wallis GA, Tedford C, et al. The diet-derived short chain fatty acid propionate improves beta-cell function in humans and stimulates insulin secretion from human islets in vitro. *Diabetes Obes Metab.* 2017;19(2):257-65.
121. den Besten G, Bleeker A, Gerding A, van Eunen K, Havinga R, van Dijk TH, Oosterveer MH, Jonker JW, Groen AK, Reijngoud DJ, et al. Short-Chain Fatty Acids Protect Against High-Fat Diet-Induced Obesity via a PPARgamma-Dependent Switch From Lipogenesis to Fat Oxidation. *Diabetes.* 2015;64(7):2398-408.

122. Psichas A, Sleeth ML, Murphy KG, Brooks L, Bewick GA, Hanyaloglu AC, Ghatei MA, Bloom SR, and Frost G. The short chain fatty acid propionate stimulates GLP-1 and PYY secretion via free fatty acid receptor 2 in rodents. *International Journal of Obesity (2005).* 2015;39(3):424-9.
123. Drucker DJ. The biology of incretin hormones. *Cell metabolism.* 2006;3(3):153-65.
124. van den Hoek AM, Heijboer AC, Corssmit EP, Voshol PJ, Romijn JA, Havekes LM, and Pijl H. PYY3-36 reinforces insulin action on glucose disposal in mice fed a high-fat diet. *Diabetes.* 2004;53(8):1949-52.
125. Cherbut C, Ferrier L, Roze C, Anini Y, Blottiere H, Lecannu G, and Galmiche JP. Short-chain fatty acids modify colonic motility through nerves and polypeptide YY release in the rat. *Am J Physiol.* 1998;275(6 Pt 1):G1415-22.
126. Zhou J, Martin RJ, Tulley RT, Raggio AM, McCutcheon KL, Shen L, Danna SC, Tripathy S, Hegsted M, and Keenan MJ. Dietary resistant starch upregulates total GLP-1 and PYY in a sustained day-long manner through fermentation in rodents. *American Journal of Physiology - Endocrinology and Metabolism.* 2008;295(5):E1160-E6.
127. Freeland KR, and Wolever TM. Acute effects of intravenous and rectal acetate on glucagon-like peptide-1, peptide YY, ghrelin, adiponectin and tumour necrosis factor-alpha. *The British journal of nutrition.* 2010;103(3):460-6.
128. Priyadarshini M, Wicksteed B, Schiltz GE, Gilchrist A, and Layden BT. SCFA Receptors in Pancreatic β Cells: Novel Diabetes Targets? *Trends in Endocrinology & Metabolism.* 2016;27(9):653-64.
129. De Vadder F, Kovatcheva-Datchary P, Goncalves D, Vinera J, Zitoun C, Duchampt A, Bäckhed F, and Mithieux G. Microbiota-Generated Metabolites Promote Metabolic Benefits via Gut-Brain Neural Circuits. *Cell.* 2014;156(1):84-96.
130. Soty M, Penhoat A, Amigo-Correig M, Vinera J, Sardella A, Vullin-Bouilloux F, Zitoun C, Houberdon I, and Mithieux G. A gut–brain neural circuit controlled by intestinal gluconeogenesis is crucial in metabolic health. *Molecular Metabolism.* 2015;4(2):106-17.
131. Brennan AM, and Mantzoros CS. Drug Insight: the role of leptin in human physiology and pathophysiology--emerging clinical applications. *Nature clinical practice Endocrinology & metabolism.* 2006;2(6):318-27.
132. Minokoshi Y, Kim YB, Peroni OD, Fryer LG, Muller C, Carling D, and Kahn BB. Leptin stimulates fatty-acid oxidation by activating AMP-activated protein kinase. *Nature.* 2002;415(6869):339-43.
133. Yu X, McCorkle S, Wang M, Lee Y, Li J, Saha AK, Unger RH, and Ruderman NB. Leptinomimetic effects of the AMP kinase activator AICAR in leptin-resistant rats: prevention of diabetes and ectopic lipid deposition. *Diabetologia.* 2004;47(11):2012-21.
134. Gao Z, Yin J, Zhang J, Ward RE, Martin RJ, Lefevre M, Cefalu WT, and Ye J. Butyrate Improves Insulin Sensitivity and Increases Energy Expenditure in Mice. *Diabetes.* 2009;58(7):1509-17.
135. Hu GX, Chen GR, Xu H, Ge RS, and Lin J. Activation of the AMP activated protein kinase by short-chain fatty acids is the main mechanism underlying the beneficial effect of a high fiber diet on the metabolic syndrome. *Medical hypotheses.* 2010;74(1):123-6.
136. Lin J, Handschin C, and Spiegelman BM. Metabolic control through the PGC-1 family of transcription coactivators. *Cell Metab.* 2005;1(6):361-70.
137. Winder WW, and Hardie DG. AMP-activated protein kinase, a metabolic master switch: possible roles in type 2 diabetes. *Am J Physiol.* 1999;277(1 Pt 1):E1-10.
138. Kondo T, Kishi M, Fushimi T, and Kaga T. Acetic acid upregulates the expression of genes for fatty acid oxidation enzymes in liver to suppress body fat accumulation. *J Agric Food Chem.* 2009;57(13):5982-6.

139. Harig JM, Soergel KH, Komorowski RA, and Wood CM. Treatment of diversion colitis with short-chain-fatty acid irrigation. *The New England journal of medicine.* 1989;320(1):23-8.
140. Jiminez JA, Uwiera TC, Abbott DW, Uwiera RRE, and Inglis GD. Butyrate Supplementation at High Concentrations Alters Enteric Bacterial Communities and Reduces Intestinal Inflammation in Mice Infected with Citrobacter rodentium. *mSphere.* 2017;2(4).
141. Chang PV, Hao L, Offermanns S, and Medzhitov R. The microbial metabolite butyrate regulates intestinal macrophage function via histone deacetylase inhibition. *Proc Natl Acad Sci U S A.* 2014;111(6):2247-52.
142. Place RF, Noonan EJ, and Giardina C. HDAC inhibition prevents NF-kappa B activation by suppressing proteasome activity: down-regulation of proteasome subunit expression stabilizes I kappa B alpha. *Biochem Pharmacol.* 2005;70(3):394-406.
143. Meijer K, de Vos P, and Priebe MG. Butyrate and other short-chain fatty acids as modulators of immunity: what relevance for health? *Curr Opin Clin Nutr Metab Care.* 2010;13(6):715-21.
144. Sina C, Gavrilova O, Forster M, Till A, Derer S, Hildebrand F, Raabe B, Chalaris A, Scheller J, Rehmann A, et al. G protein-coupled receptor 43 is essential for neutrophil recruitment during intestinal inflammation. *Journal of immunology.* 2009;183(11):7514-22.
145. Maslowski KM, Vieira AT, Ng A, Kranich J, Sierro F, Yu D, Schilter HC, Rolph MS, Mackay F, Artis D, et al. Regulation of inflammatory responses by gut microbiota and chemoattractant receptor GPR43. *Nature.* 2009;461(7268):1282-6.
146. Vinolo MA, Rodrigues HG, Hatanaka E, Sato FT, Sampaio SC, and Curi R. Suppressive effect of short-chain fatty acids on production of proinflammatory mediators by neutrophils. *The Journal of nutritional biochemistry.* 2011;22(9):849-55.
147. Nastasi C, Candela M, Bonefeld CM, Geisler C, Hansen M, Krejsgaard T, Biagi E, Andersen MH, Brigidi P, Ødum N, et al. The effect of short-chain fatty acids on human monocyte-derived dendritic cells. *Scientific reports.* 2015;5(16148.
148. Millard AL, Mertes PM, Ittelet D, Villard F, Jeannesson P, and Bernard J. Butyrate affects differentiation, maturation and function of human monocyte-derived dendritic cells and macrophages. *Clinical and Experimental Immunology.* 2002;130(2):245-55.
149. Gurav A, Sivaprakasam S, Bhutia YD, Boettger T, Singh N, and Ganapathy V. Slc5a8, a Na(+)-coupled high-affinity transporter for short-chain fatty acids, is a conditional tumor suppressor in colon that protects against colitis and colon cancer under low-fiber dietary conditions. *The Biochemical journal.* 2015;469(2):267-78.
150. Haghikia A, Jörg S, Duscha A, Berg J, Manzel A, Waschbisch A, Hammer A, Lee D-H, May C, Wilck N, et al. Dietary Fatty Acids Directly Impact Central Nervous System Autoimmunity via the Small Intestine. *Immunity.* 2015;43(4):817-29.
151. Furusawa Y, Obata Y, Fukuda S, Endo TA, Nakato G, Takahashi D, Nakanishi Y, Uetake C, Kato K, Kato T, et al. Commensal microbe-derived butyrate induces the differentiation of colonic regulatory T cells. *Nature.* 2013;504(446.
152. Zaiss MM, Rapin A, Lebon L, Dubey LK, Mosconi I, Sarter K, Piersigilli A, Menin L, Walker AW, Rougemont J, et al. The Intestinal Microbiota Contributes to the Ability of Helminths to Modulate Allergic Inflammation. *Immunity.* 2015;43(5):998-1010.
153. Gonçalves P, Araújo JR, Pinho MJ, and Martel F. In Vitro Studies on the Inhibition of Colon Cancer by Butyrate and Polyphenolic Compounds. *Nutrition and cancer.* 2011;63(2):282-94.
154. McIntyre A, Gibson PR, and Young GP. Butyrate production from dietary fibre and protection against large bowel cancer in a rat model. *Gut.* 1993;34(3):386-91.

155. Gonçalves P, and Martel F. Regulation of colonic epithelial butyrate transport: Focus on colorectal cancer. *Porto Biomedical Journal.* 2016;1(3):83-91.
156. Tang Y, Chen Y, Jiang H, Robbins GT, and Nie D. G-protein-coupled receptor for short-chain fatty acids suppresses colon cancer. *International Journal of Cancer.* 2011;128(4):847-56.
157. Arellano M, Jomard P, El Kaddouri S, Roques C, Nepveu F, and Couderc F. Routine analysis of short-chain fatty acids for anaerobic bacteria identification using capillary electrophoresis and indirect ultraviolet detection. *Journal of Chromatography B.* 2000;741(1):89-100.
158. Arellano M, ElKaddouri S, Roques C, Couderc F, and Puig P. Capillary electrophoresis and indirect UV detection as a fast and simple analytical tool for bacterial taxonomy. *J Chromatogr A.* 1997;781(1-2):497-501.
159. Stein J, Kulemeier J, Lembcke B, and Caspary WF. Simple and rapid method for determination of short-chain fatty acids in biological materials by high-performance liquid chromatography with ultraviolet detection. *J Chromatogr.* 1992;576(1):53-61.
160. de Sa LRV, de Oliveira MAL, Cammarota MC, Matos A, and Ferreira-Leitao VS. Simultaneous analysis of carbohydrates and volatile fatty acids by HPLC for monitoring fermentative biohydrogen production. *Int J Hydrogen Energ.* 2011;36(23):15177-86.
161. Han J, Lin K, Sequeira C, and Borchers CH. An isotope-labeled chemical derivatization method for the quantitation of short-chain fatty acids in human feces by liquid chromatography-tandem mass spectrometry. *Anal Chim Acta.* 2015;854(86-94.
162. Bachmann C, Colombo JP, and Beruter J. Short chain fatty acids in plasma and brain: quantitative determination by gas chromatography. *Clin Chim Acta.* 1979;92(2):153-9.
163. Murase M, Kimura Y, and Nagata Y. Determination of portal short-chain fatty acids in rats fed various dietary fibers by capillary gas chromatography. *J Chromatogr B Biomed Appl.* 1995;664(2):415-20.
164. Lewandowski ED, Chari MV, Roberts R, and Johnston DL. NMR studies of beta-oxidation and short-chain fatty acid metabolism during recovery of reperfused hearts. *The American journal of physiology.* 1991;261(2 Pt 2):H354-63.
165. Jensen PR, Peitersen T, Karlsson M, In 't Zandt R, Gisselsson A, Hansson G, Meier S, and Lerche MH. Tissue-specific short chain fatty acid metabolism and slow metabolic recovery after ischemia from hyperpolarized NMR in vivo. *The Journal of biological chemistry.* 2009;284(52):36077-82.
166. Zhao G, Nyman M, and Jonsson JA. Rapid determination of short-chain fatty acids in colonic contents and faeces of humans and rats by acidified water-extraction and direct-injection gas chromatography. *Biomed Chromatogr.* 2006;20(8):674-82.
167. Hillman RE. Simple, rapid method for determination of propionic acid and other short-chain fatty acids in serum. *Clin Chem.* 1978;24(5):800-3.
168. Garcia-Villalba R, Gimenez-Bastida JA, Garcia-Conesa MT, Tomas-Barberan FA, Carlos Espin J, and Larrosa M. Alternative method for gas chromatography-mass spectrometry analysis of short-chain fatty acids in faecal samples. *J Sep Sci.* 2012;35(15):1906-13.
169. Bjork JT, Soergel KH, and Wood CM. Composition of Free Stool Water. *Gastroenterology.* 1976;70(5):864-.
170. Vernia P, Breuer RI, Gnaedinger A, Latella G, and Santoro ML. Composition of fecal water. Comparison of "in vitro" dialysis with ultrafiltration. *Gastroenterology.* 1984;86(6):1557-61.
171. Innocente N, Moret S, Corradini C, and Conte LS. A rapid method for the quantitative determination of short-chain free volatile fatty acids from cheese. *Journal of agricultural and food chemistry.* 2000;48(8):3321-3.

172. Dejong C, and Badings HT. Determination of Free Fatty-Acids in Milk and Cheese - Procedures for Extraction, Clean up, and Capillary Gas-Chromatographic Analysis. *Hrc-J High Res Chrom.* 1990;13(2):94-8.
173. Ren YP, Wang JJ, Li XF, and Wang XH. Reactive Extraction of Short-Chain Fatty Acids from Synthetic Acidic Fermentation Broth of Organic Solid Wastes and Their Stripping. *J Chem Eng Data.* 2012;57(1):46-51.
174. Boswell CE. Fast and efficient volatile compound analysis by purge-and-trap GC-MS. *Lc Gc N Am.* 2000;18(7):726-+.
175. Heikes DL, Jensen SR, and Flemingjones ME. Purge-and-Trap Extraction with Gc-Ms Determination of Volatile Organic-Compounds in Table-Ready Foods. *Journal of agricultural and food chemistry.* 1995;43(11):2869-75.
176. Chen Y, Li Y, Xiong Y, Fang C, and Wang X. An effective pre-treatment method for the determination of short-chain fatty acids in a complex matrix by derivatization coupled with headspace single-drop microextraction. *J Chromatogr A.* 2014;1325(49-55.
177. Henningsson AM, Nyman EMGL, and Bjorck IME. Short-chain fatty acid content in the hindgut of rats fed various composite foods and commercial dietary fibre fractions from similar sources. *J Sci Food Agr.* 2002;82(4):385-93.
178. Zheng X, Qiu Y, Zhong W, Baxter S, Su M, Li Q, Xie G, Ore BM, Qiao S, Spencer MD, et al. A targeted metabolomic protocol for short-chain fatty acids and branched-chain amino acids. *Metabolomics.* 2013;9(4):818-27.
179. Savorani F, Rasmussen MA, Mikkelsen MS, and Engelsen SB. A primer to nutritional metabolomics by NMR spectroscopy and chemometrics. *Food Res Int.* 2013;54(1):1131-45.
180. Jacobs DM, Deltimple N, van Velzen E, van Dorsten FA, Bingham M, Vaughan EE, and van Duynhoven J. H-1 NMR metabolite profiling of feces as a tool to assess the impact of nutrition on the human microbiome. *Nmr Biomed.* 2008;21(6):615-26.
181. Cai J, Zhang L, Jones RA, Correll JB, Hatzakis E, Smith PB, Gonzalez FJ, and Patterson AD. Antioxidant Drug Tempol Promotes Functional Metabolic Changes in the Gut Microbiota. *J Proteome Res.* 2016;15(2):563-71.
182. Cai J, Zhang J, Tian Y, Zhang L, Hatzakis E, Krausz KW, Smith PB, Gonzalez FJ, and Patterson AD. Orthogonal Comparison of GC–MS and 1H NMR Spectroscopy for Short Chain Fatty Acid Quantitation. *Analytical Chemistry.* 2017;89(15):7900-6.
183. Myant NB, and Mitropoulos KA. Cholesterol 7 alpha-hydroxylase. *J Lipid Res.* 1977;18(2):135-53.
184. Bjorkhem I. Mechanism of degradation of the steroid side chain in the formation of bile acids. *J Lipid Res.* 1992;33(4):455-71.
185. Chiang JY. Bile acid metabolism and signaling. *Comprehensive Physiology.* 2013;3(3):1191-212.
186. Zwicker BL, and Agellon LB. Transport and biological activities of bile acids. *The international journal of biochemistry & cell biology.* 2013;45(7):1389-98.
187. Sayin SI, Wahlstrom A, Felin J, Jantti S, Marschall HU, Bamberg K, Angelin B, Hyotylainen T, Oresic M, and Backhed F. Gut microbiota regulates bile acid metabolism by reducing the levels of tauro-beta-muricholic acid, a naturally occurring FXR antagonist. *Cell metabolism.* 2013;17(2):225-35.
188. Chiang JY. Negative feedback regulation of bile acid metabolism: impact on liver metabolism and diseases. *Hepatology.* 2015;62(4):1315-7.
189. Jones SA. Physiology of FGF15/19. *Adv Exp Med Biol.* 2012;728(171-82.
190. Elliott WH. In: Danielsson H, and Sjövall J eds. *New Comprehensive Biochemistry*. Elsevier; 1985:303-29.
191. Chiang JYL. Bile acid metabolism and signaling in liver disease and therapy. *Liver research.* 2017;1(1):3-9.

192. Basu KP, and S. C. Chakravarty. Action of B. coli on conjugated bile acids. *Indian J Mpd Res.* 1934;21(691-4

193. Shimada K, Bricknell KS, and Finegold SM. Deconjugation of bile acids by intestinal bacteria: review of literature and additional studies. *The Journal of infectious diseases.* 1969;119(3):273-81.
194. Tannock GW, Dashkevicz MP, and Feighner SD. Lactobacilli and bile salt hydrolase in the murine intestinal tract. *Appl Environ Microbiol.* 1989;55(7):1848-51.
195. Tanaka H, Doesburg K, Iwasaki T, and Mierau I. Screening of lactic acid bacteria for bile salt hydrolase activity. *J Dairy Sci.* 1999;82(12):2530-5.
196. Jones BV, Begley M, Hill C, Gahan CG, and Marchesi JR. Functional and comparative metagenomic analysis of bile salt hydrolase activity in the human gut microbiome. *Proc Natl Acad Sci U S A.* 2008;105(36):13580-5.
197. Kawamoto K, Horibe I, and Uchida K. Purification and characterization of a new hydrolase for conjugated bile acids, chenodeoxycholyltaurine hydrolase, from Bacteroides vulgatus. *Journal of biochemistry.* 1989;106(6):1049-53.
198. Stellwag EJ, and Hylemon PB. Purification and characterization of bile salt hydrolase from Bacteroides fragilis subsp. fragilis. *Biochim Biophys Acta.* 1976;452(1):165-76.
199. Grill J, Schneider F, Crociani J, and Ballongue J. Purification and Characterization of Conjugated Bile Salt Hydrolase from Bifidobacterium longum BB536. *Appl Environ Microbiol.* 1995;61(7):2577-82.
200. Maddox RHACS. Hydrolysis of bile acid conjugates by Clostridium bifermentans. *Eur J Appl Microbiol.* 1982;14(1):41-5.
201. Coleman JP, and Hudson LL. Cloning and characterization of a conjugated bile acid hydrolase gene from Clostridium perfringens. *Applied and environmental microbiology.* 1995;61(7):2514-20.
202. Dussurget O, Cabanes D, Dehoux P, Lecuit M, Buchrieser C, Glaser P, Cossart P, and European Listeria Genome C. Listeria monocytogenes bile salt hydrolase is a PrfA-regulated virulence factor involved in the intestinal and hepatic phases of listeriosis. *Molecular microbiology.* 2002;45(4):1095-106.
203. Begley M, Sleator RD, Gahan CG, and Hill C. Contribution of three bile-associated loci, bsh, pva, and btlB, to gastrointestinal persistence and bile tolerance of Listeria monocytogenes. *Infect Immun.* 2005;73(2):894-904.
204. Norman A, and Grubb R. Hydrolysis of conjugated bile acids by Clostridia and enterococci; bile acids and steroids 25. *Acta pathologica et microbiologica Scandinavica.* 1955;36(6):537-47.
205. Franz CM, Specht I, Haberer P, and Holzapfel WH. Bile salt hydrolase activity of Enterococci isolated from food: screening and quantitative determination. *Journal of food protection.* 2001;64(5):725-9.
206. Chand D, Ramasamy S, and Suresh CG. A highly active bile salt hydrolase from Enterococcus faecalis shows positive cooperative kinetics. *Process Biochemistry.* 2016;51(2):263-9.
207. Lorenzo-Zuniga V, Bartoli R, Planas R, Hofmann AF, Vinado B, Hagey LR, Hernandez JM, Mane J, Alvarez MA, Ausina V, et al. Oral bile acids reduce bacterial overgrowth, bacterial translocation, and endotoxemia in cirrhotic rats. *Hepatology.* 2003;37(3):551-7.
208. Hofmann AF, and Eckmann L. How bile acids confer gut mucosal protection against bacteria. *Proc Natl Acad Sci U S A.* 2006;103(12):4333-4.
209. Kitahara M, Takamine F, Imamura T, and Benno Y. Clostridium hiranonis sp. nov., a human intestinal bacterium with bile acid 7alpha-dehydroxylating activity. *International journal of systematic and evolutionary microbiology.* 2001;51(Pt 1):39-44.

210. Takamine F, and Imamura T. Isolation and characterization of bile acid 7-dehydroxylating bacteria from human feces. *Microbiology and immunology.* 1995;39(1):11-8.
211. Mallonee DH, White WB, and Hylemon PB. Cloning and sequencing of a bile acid-inducible operon from Eubacterium sp. strain VPI 12708. *Journal of bacteriology.* 1990;172(12):7011-9.
212. Doerner KC, Takamine F, LaVoie CP, Mallonee DH, and Hylemon PB. Assessment of fecal bacteria with bile acid 7 alpha-dehydroxylating activity for the presence of bai-like genes. *Appl Environ Microb.* 1997;63(3):1185-8.
213. Lei S, Huang F, Zhao A, Chen T, Chen W, Xie G, Zheng X, Zhang Y, Yu H, Zhang P, et al. The ratio of dihomo-gamma-linolenic acid to deoxycholic acid species is a potential biomarker for the metabolic abnormalities in obesity. *FASEB journal : official publication of the Federation of American Societies for Experimental Biology.* 2017;31(9):3904-12.
214. Berr F, Pratschke E, Fischer S, and Paumgartner G. Disorders of bile acid metabolism in cholesterol gallstone disease. *The Journal of clinical investigation.* 1992;90(3):859-68.
215. Mamianetti A, Garrido D, Carducci CN, and Vescina MC. Fecal bile acid excretion profile in gallstone patients. *Medicina (B Aires).* 1999;59(3):269-73.
216. Yoshimoto S, Loo TM, Atarashi K, Kanda H, Sato S, Oyadomari S, Iwakura Y, Oshima K, Morita H, Hattori M, et al. Obesity-induced gut microbial metabolite promotes liver cancer through senescence secretome. *Nature.* 2013;499(7456):97-101.
217. Milovic V, Teller IC, Murphy GM, Caspary WF, and Stein J. Deoxycholic acid stimulates migration in colon cancer cells. *European journal of gastroenterology & hepatology.* 2001;13(8):945-9.
218. Pai R, Tarnawski AS, and Tran T. Deoxycholic acid activates beta-catenin signaling pathway and increases colon cell cancer growth and invasiveness. *Molecular biology of the cell.* 2004;15(5):2156-63.
219. Baijal PK, Fitzpatrick DW, and Bird RP. Comparative effects of secondary bile acids, deoxycholic and lithocholic acids, on aberrant crypt foci growth in the postinitiation phases of colon carcinogenesis. *Nutrition and cancer.* 1998;31(2):81-9.
220. Ajouz H, Mukherji D, and Shamseddine A. Secondary bile acids: an underrecognized cause of colon cancer. *World journal of surgical oncology.* 2014;12(164.
221. Gerard P. Metabolism of cholesterol and bile acids by the gut microbiota. *Pathogens.* 2013;3(1):14-24.
222. Kisiela M, Skarka A, Ebert B, and Maser E. Hydroxysteroid dehydrogenases (HSDs) in bacteria: a bioinformatic perspective. *The Journal of steroid biochemistry and molecular biology.* 2012;129(1-2):31-46.
223. Edenharder R, and Mielek K. Epimerization, oxidation and reduction of bile acids by Eubacterium lentum. *Systematic and Applied Microbiology.* 1984;5(3):287-98.
224. Devlin AS, and Fischbach MA. A biosynthetic pathway for a prominent class of microbiota-derived bile acids. *Nature chemical biology.* 2015;11(9):685-90.
225. Ridlon JM, Harris SC, Bhowmik S, Kang DJ, and Hylemon PB. Consequences of bile salt biotransformations by intestinal bacteria. *Gut microbes.* 2016;7(1):22-39.
226. Ley RE, Backhed F, Turnbaugh P, Lozupone CA, Knight RD, and Gordon JI. Obesity alters gut microbial ecology. *Proc Natl Acad Sci U S A.* 2005;102(31):11070-5.
227. Turnbaugh PJ, Ley RE, Mahowald MA, Magrini V, Mardis ER, and Gordon JI. An obesity-associated gut microbiome with increased capacity for energy harvest. *Nature.* 2006;444(7122):1027-31.
228. Rodrigues CM, Fan G, Ma X, Kren BT, and Steer CJ. A novel role for ursodeoxycholic acid in inhibiting apoptosis by modulating mitochondrial membrane perturbation. *The Journal of clinical investigation.* 1998;101(12):2790-9.

229. Im E, and Martinez JD. Ursodeoxycholic acid (UDCA) can inhibit deoxycholic acid (DCA)-induced apoptosis via modulation of EGFR/Raf-1/ERK signaling in human colon cancer cells. *J Nutr.* 2004;134(2):483-6.
230. Kardorff R, Melter M, Rodeck B, and Brodehl J. [Long-term ursodeoxycholic acid treatment of cholestatic liver diseases in childhood--clinical and biochemical effects]. *Klinische Padiatrie.* 1996;208(3):118-22.
231. Festi D, Montagnani M, Azzaroli F, Lodato F, Mazzella G, Roda A, Di Biase AR, Roda E, Simoni P, and Colecchia A. Clinical efficacy and effectiveness of ursodeoxycholic acid in cholestatic liver diseases. *Current clinical pharmacology.* 2007;2(2):155-77.
232. Marschall HU, Oppermann UC, Svensson S, Nordling E, Persson B, Hoog JO, and Jornvall H. Human liver class I alcohol dehydrogenase gammagamma isozyme: the sole cytosolic 3beta-hydroxysteroid dehydrogenase of iso bile acids. *Hepatology.* 2000;31(4):990-6.
233. Edenharder R, and Hammann R. Deoxycholic Acid Methyl Ester — a Novel Bacterial Metabolite of Cholic Acid. *Systematic and Applied Microbiology.* 1985;6(1):18-22.
234. Kelsey MI, and Thompson RJ. The biosynthesis of ethyl lithocholate by fecal microorganisms. *Journal of Steroid Biochemistry.* 1976;7(2):117-24.
235. Robben J, Van Eldere J, and Eyssen H. In: De Clercq E ed. *Frontiers in Microbiology: From Antibiotics to AIDS.* Dordrecht: Springer Netherlands; 1987:241-3.
236. Robben J, Janssen G, Merckx R, and Eyssen H. Formation of delta 2- and delta 3-cholenoic acids from bile acid 3-sulfates by a human intestinal Fusobacterium strain. *Appl Environ Microbiol.* 1989;55(11):2954-9.
237. Tazuke Y, Matsuda K, Adachi K, and Tsukada Y. Purification and properties of a novel sulfatase from Pseudomonas testosteroni that hydrolyzed 3 beta-hydroxy-5-cholenoic acid 3-sulfate. *Bioscience, biotechnology, and biochemistry.* 1998;62(9):1739-44.
238. Eyssen H, van Eldere J, Parmentier G, Huijghebaert S, and Mertens J. Influence of microbial bile salt desulfation upon the fecal excretion of bile salts in gnotobiotic rats. *Journal of Steroid Biochemistry.* 1985;22(4):547-54.
239. Alnouti Y. Bile Acid sulfation: a pathway of bile acid elimination and detoxification. *Toxicological sciences : an official journal of the Society of Toxicology.* 2009;108(2):225-46.
240. Goddard P, and Hill MJ. Degradation of steroids by intestinal bacteria: IV. The aromatisation of ring A. *Biochimica et Biophysica Acta (BBA) - Lipids and Lipid Metabolism.* 1972;280(2):336-42.
241. Aries VC, and Hill MJ. The formation of unsaturated bile acids by intestinal bacteria. *Biochemical Journal.* 1970;119(5):37P-8P.
242. Chiang JYL. Negative feedback regulation of bile acid metabolism: impact on liver metabolism and diseases. *Hepatology (Baltimore, Md).* 2015;62(4):1315-7.
243. Russell DW. The enzymes, regulation, and genetics of bile acid synthesis. *Annual review of biochemistry.* 2003;72(137-74.
244. Eloranta JJ, and Kullak-Ublick GA. Coordinate transcriptional regulation of bile acid homeostasis and drug metabolism. *Archives of biochemistry and biophysics.* 2005;433(2):397-412.
245. Arrese M, and Ananthanarayanan M. The bile salt export pump: molecular properties, function and regulation. *Pflügers Archiv.* 2004;449(2):123-31.
246. Kast HR, Goodwin B, Tarr PT, Jones SA, Anisfeld AM, Stoltz CM, Tontonoz P, Kliewer S, Willson TM, and Edwards PA. Regulation of multidrug resistance-associated protein 2 (ABCC2) by the nuclear receptors pregnane X receptor, farnesoid X-activated receptor, and constitutive androstane receptor. *J Biol Chem.* 2002;277(4):2908-15.
247. Boyer JL, Trauner M, Mennone A, Soroka CJ, Cai S-Y, Moustafa T, Zollner G, Lee JY, and Ballatori N. Upregulation of a basolateral FXR-dependent bile acid efflux transporter

OSTα-OSTβ in cholestasis in humans and rodents. *American Journal of Physiology-Gastrointestinal and Liver Physiology.* 2006;290(6):G1124-G30.
248. Denson LA, Sturm E, Echevarria W, Zimmerman TL, Makishima M, Mangelsdorf DJ, and Karpen SJ. The Orphan Nuclear Receptor, shp, Mediates Bile Acid-Induced Inhibition of the Rat Bile Acid Transporter, ntcp. *Gastroenterology.* 2001;121(1):140-7.
249. Zollner G, Wagner M, Fickert P, Geier A, Fuchsbichler A, Silbert D, Gumhold J, Zatloukal K, Kaser A, Tilg H, et al. Role of nuclear receptors and hepatocyte-enriched transcription factors for Ntcp repression in biliary obstruction in mouse liver. *American Journal of Physiology-Gastrointestinal and Liver Physiology.* 2005;289(5):G798-G805.
250. Jung D, Podvinec M, Meyer UA, Mangelsdorf DJ, Fried M, Meier PJ, and Kullak–Ublick GA. Human organic anion transporting polypeptide 8 promoter is transactivated by the farnesoid X receptor/bile acid receptor. *Gastroenterology.* 2002;122(7):1954-66.
251. Shneider BL. Intestinal bile acid transport: biology, physiology, and pathophysiology. *Journal of pediatric gastroenterology and nutrition.* 2001;32(4):407-17.
252. Coppola CP, Gosche JR, Arrese M, Ancowitz B, Madsen J, Vanderhoof J, and Shneider BL. Molecular analysis of the adaptive response of intestinal bile acid transport after ileal resection in the rat. *Gastroenterology.* 1998;115(5):1172-8.
253. Holt JA, Luo G, Billin AN, Bisi J, McNeill YY, Kozarsky KF, Donahee M, Wang DY, Mansfield TA, Kliewer SA, et al. Definition of a novel growth factor-dependent signal cascade for the suppression of bile acid biosynthesis. *Genes & Development.* 2003;17(13):1581-91.
254. Song KH, Li T, Owsley E, Strom S, and Chiang JY. Bile acids activate fibroblast growth factor 19 signaling in human hepatocytes to inhibit cholesterol 7alpha-hydroxylase gene expression. *Hepatology.* 2009;49(1):297-305.
255. Potthoff MJ, Boney-Montoya J, Choi M, He T, Sunny NE, Satapati S, Suino-Powell K, Xu HE, Gerard RD, Finck BN, et al. FGF15/19 regulates hepatic glucose metabolism by inhibiting the CREB-PGC-1alpha pathway. *Cell Metab.* 2011;13(6):729-38.
256. Morton GJ, Matsen ME, Bracy DP, Meek TH, Nguyen HT, Stefanovski D, Bergman RN, Wasserman DH, and Schwartz MW. FGF19 action in the brain induces insulin-independent glucose lowering. *The Journal of clinical investigation.* 2013;123(11):4799-808.
257. Zhang F, Yu L, Lin X, Cheng P, He L, Li X, Lu X, Tan Y, Yang H, Cai L, et al. Minireview: Roles of Fibroblast Growth Factors 19 and 21 in Metabolic Regulation and Chronic Diseases. *Molecular endocrinology.* 2015;29(10):1400-13.
258. Sinal CJ, Tohkin M, Miyata M, Ward JM, Lambert G, and Gonzalez FJ. Targeted Disruption of the Nuclear Receptor FXR/BAR Impairs Bile Acid and Lipid Homeostasis. *Cell.* 2000;102(6):731-44.
259. Tomlinson E, Fu L, John L, Hultgren B, Huang X, Renz M, Stephan JP, Tsai SP, Powell-Braxton L, French D, et al. Transgenic Mice Expressing Human Fibroblast Growth Factor-19 Display Increased Metabolic Rate and Decreased Adiposity. *Endocrinology.* 2002;143(5):1741-7.
260. Miyata M, Sakaida Y, Matsuzawa H, Yoshinari K, and Yamazoe Y. Fibroblast Growth Factor 19 Treatment Ameliorates Disruption of Hepatic Lipid Metabolism in Farnesoid X Receptor (Fxr)-Null Mice. *Biological and Pharmaceutical Bulletin.* 2011;34(12):1885-9.
261. Parks DJ, Blanchard SG, Bledsoe RK, Chandra G, Consler TG, Kliewer SA, Stimmel JB, Willson TM, Zavacki AM, Moore DD, et al. Bile acids: Natural ligands for an orphan nuclear receptor. *Science.* 1999;284(5418):1365-8.
262. Makishima M, Okamoto AY, Repa JJ, Tu H, Learned RM, Luk A, Hull MV, Lustig KD, Mangelsdorf DJ, and Shan B. Identification of a Nuclear Receptor for Bile Acids. *Science.* 1999;284(5418):1362-5.

263. Li Y, Jadhav K, and Zhang Y. Bile acid receptors in non-alcoholic fatty liver disease. *Biochemical Pharmacology.* 2013;86(11):1517-24.
264. Li F, Jiang C, Krausz KW, Li Y, Albert I, Hao H, Fabre KM, Mitchell JB, Patterson AD, and Gonzalez FJ. Microbiome remodelling leads to inhibition of intestinal farnesoid X receptor signalling and decreased obesity. *Nature communications.* 2013;4(2384.
265. Miyata M, Takamatsu Y, Kuribayashi H, and Yamazoe Y. Administration of ampicillin elevates hepatic primary bile acid synthesis through suppression of ileal fibroblast growth factor 15 expression. *J Pharmacol Exp Ther.* 2009;331(3):1079-85.
266. Swann JR, Want EJ, Geier FM, Spagou K, Wilson ID, Sidaway JE, Nicholson JK, and Holmes E. Systemic gut microbial modulation of bile acid metabolism in host tissue compartments. *Proc Natl Acad Sci U S A.* 2011;108 Suppl 1(4523-30.
267. Xie C, Jiang C, Shi J, Gao X, Sun D, Sun L, Wang T, Takahashi S, Anitha M, Krausz KW, et al. An Intestinal Farnesoid X Receptor–Ceramide Signaling Axis Modulates Hepatic Gluconeogenesis in Mice. *Diabetes.* 2017;66(3):613-26.
268. Shyng S-L. Targeting the Gut Microbiota–FXR Signaling Axis for Glycemic Control: Does a Dietary Supplement Work Magic? *Diabetes.* 2017;66(3):571-3.
269. Russell DW. The Enzymes, Regulation, and Genetics of Bile Acid Synthesis. *Annual review of biochemistry.* 2003;72(1):137-74.
270. Yamagata K, Daitoku H, Shimamoto Y, Matsuzaki H, Hirota K, Ishida J, and Fukamizu A. Bile acids regulate gluconeogenic gene expression via small heterodimer partner-mediated repression of hepatocyte nuclear factor 4 and Foxo1. *The Journal of biological chemistry.* 2004;279(22):23158-65.
271. Ma Y, Huang Y, Yan L, Gao M, and Liu D. Synthetic FXR agonist GW4064 prevents diet-induced hepatic steatosis and insulin resistance. *Pharmaceutical research.* 2013;30(5):1447-57.
272. Zhang Y, Lee FY, Barrera G, Lee H, Vales C, Gonzalez FJ, Willson TM, and Edwards PA. Activation of the nuclear receptor FXR improves hyperglycemia and hyperlipidemia in diabetic mice. *Proceedings of the National Academy of Sciences of the United States of America.* 2006;103(4):1006-11.
273. Zhang HM, Wang X, Wu ZH, Liu HL, Chen W, Zhang ZZ, Chen D, and Zeng TS. Beneficial effect of farnesoid X receptor activation on metabolism in a diabetic rat model. *Molecular medicine reports.* 2016;13(3):2135-42.
274. Renga B, Mencarelli A, Vavassori P, Brancaleone V, and Fiorucci S. The bile acid sensor FXR regulates insulin transcription and secretion. *Biochimica et Biophysica Acta (BBA) - Molecular Basis of Disease.* 2010;1802(3):363-72.
275. Shen H, Zhang Y, Ding H, Wang X, Chen L, Jiang H, and Shen X. Farnesoid X receptor induces GLUT4 expression through FXR response element in the GLUT4 promoter. *Cellular physiology and biochemistry : international journal of experimental cellular physiology, biochemistry, and pharmacology.* 2008;22(1-4):1-14.
276. Trabelsi M-S, Daoudi M, Prawitt J, Ducastel S, Touche V, Sayin SI, Perino A, Brighton CA, Sebti Y, Kluza J, et al. Farnesoid X Receptor Inhibits Glucagon-Like Peptide-1 Production by Enteroendocrine L-cells. *Nature communications.* 2015;6(7629-.
277. Sinal CJ, Tohkin M, Miyata M, Ward JM, Lambert G, and Gonzalez FJ. Targeted disruption of the nuclear receptor FXR/BAR impairs bile acid and lipid homeostasis. *Cell.* 2000;102(6):731-44.
278. Watanabe M, Houten SM, Wang L, Moschetta A, Mangelsdorf DJ, Heyman RA, Moore DD, and Auwerx J. Bile acids lower triglyceride levels via a pathway involving FXR, SHP, and SREBP-1c. *The Journal of clinical investigation.* 2004;113(10):1408-18.
279. Claudel T, Inoue Y, Barbier O, Duran-Sandoval D, Kosykh V, Fruchart J, Fruchart JC, Gonzalez FJ, and Staels B. Farnesoid X receptor agonists suppress hepatic apolipoprotein CIII expression. *Gastroenterology.* 2003;125(2):544-55.

280. Kast HR, Nguyen CM, Sinal CJ, Jones SA, Laffitte BA, Reue K, Gonzalez FJ, Willson TM, and Edwards PA. Farnesoid X-Activated Receptor Induces Apolipoprotein C-II Transcription: a Molecular Mechanism Linking Plasma Triglyceride Levels to Bile Acids. *Molecular endocrinology.* 2001;15(10):1720-8.
281. Prieur X, Coste H, and Rodríguez JC. The Human Apolipoprotein AV Gene Is Regulated by Peroxisome Proliferator-activated Receptor-α and Contains a Novel Farnesoid X-activated Receptor Response Element. *J Biol Chem.* 2003;278(28):25468-80.
282. Sirvent A, Claudel T, Martin G, Brozek J, Kosykh V, Darteil R, Hum DW, Fruchart J-C, and Staels B. The farnesoid X receptor induces very low density lipoprotein receptor gene expression. *FEBS Letters.* 2004;566(1):173-7.
283. Anisfeld AM, Kast-Woelbern HR, Meyer ME, Jones SA, Zhang Y, Williams KJ, Willson T, and Edwards PA. Syndecan-1 expression is regulated in an isoform-specific manner by the farnesoid-X receptor. *J Biol Chem.* 2003;278(22):20420-8.
284. Chennamsetty I, Claudel T, Kostner KM, Baghdasaryan A, Kratky D, Levak-Frank S, Frank S, Gonzalez FJ, Trauner M, and Kostner GM. Farnesoid X receptor represses hepatic human APOA gene expression. *The Journal of clinical investigation.* 2011;121(9):3724-34.
285. Claudel T, Sturm E, Duez H, Torra IP, Sirvent A, Kosykh V, Fruchart J-C, Dallongeville J, Hum DW, Kuipers F, et al. Bile acid-activated nuclear receptor FXR suppresses apolipoprotein A-I transcription via a negative FXR response element. *The Journal of clinical investigation.* 2002;109(7):961-71.
286. Lefebvre P, Cariou B, Lien F, Kuipers F, and Staels B. Role of bile acids and bile acid receptors in metabolic regulation. *Physiological reviews.* 2009;89(1):147-91.
287. Lambert G, Amar MJA, Guo G, Brewer HB, Gonzalez FJ, and Sinal CJ. The Farnesoid X-receptor Is an Essential Regulator of Cholesterol Homeostasis. *J Biol Chem.* 2003;278(4):2563-70.
288. Li T, Matozel M, Boehme S, Kong B, Nilsson LM, Guo G, Ellis E, and Chiang JY. Overexpression of cholesterol 7alpha-hydroxylase promotes hepatic bile acid synthesis and secretion and maintains cholesterol homeostasis. *Hepatology.* 2011;53(3):996-1006.
289. Repa JJ, Berge KE, Pomajzl C, Richardson JA, Hobbs H, and Mangelsdorf DJ. Regulation of ATP-binding cassette sterol transporters ABCG5 and ABCG8 by the liver X receptors alpha and beta. *J Biol Chem.* 2002;277(21):18793-800.
290. Xu Y, Li F, Zalzala M, Xu J, Gonzalez FJ, Adorini L, Lee Y-K, Yin L, and Zhang Y. FXR Activation Increases Reverse Cholesterol Transport by Modulating Bile Acid Composition and Cholesterol Absorption. *Hepatology (Baltimore, Md).* 2016;64(4):1072-85.
291. Gnerre C, Blattler S, Kaufmann MR, Looser R, and Meyer UA. Regulation of CYP3A4 by the bile acid receptor FXR: evidence for functional binding sites in the CYP3A4 gene. *Pharmacogenetics.* 2004;14(10):635-45.
292. Song CS, Echchgadda I, Baek BS, Ahn SC, Oh T, Roy AK, and Chatterjee B. Dehydroepiandrosterone sulfotransferase gene induction by bile acid activated farnesoid X receptor. *J Biol Chem.* 2001;276(45):42549-56.
293. Erichsen TJ, Aehlen A, Ehmer U, Kalthoff S, Manns MP, and Strassburg CP. Regulation of the human bile acid UDP-glucuronosyltransferase 1A3 by the farnesoid X receptor and bile acids. *Journal of Hepatology.* 2010;52(4):570-8.
294. Barbier O, Torra IP, Sirvent A, Claudel T, Blanquart C, Duran-Sandoval D, Kuipers F, Kosykh V, Fruchart JC, and Staels B. FXR induces the UGT2B4 enzyme in hepatocytes: a potential mechanism of negative feedback control of FXR activity. *Gastroenterology.* 2003;124(7):1926-40.

295. Cai J, Zhang L, Jones RA, Correll JB, Hatzakis E, Smith PB, Gonzalez FJ, and Patterson AD. Antioxidant Drug Tempol Promotes Functional Metabolic Changes in the Gut Microbiota. *J Proteome Res.* 2016.
296. Cariou B, Bouchaert E, Abdelkarim M, Dumont J, Caron S, Fruchart JC, Burcelin R, Kuipers F, and Staels B. FXR-deficiency confers increased susceptibility to torpor. *FEBS Lett.* 2007;581(27):5191-8.
297. Fang S, Suh JM, Reilly SM, Yu E, Osborn O, Lackey D, Yoshihara E, Perino A, Jacinto S, Lukasheva Y, et al. Intestinal FXR agonism promotes adipose tissue browning and reduces obesity and insulin resistance. *Nature medicine.* 2015;21(2):159-65.
298. Fu L, John LM, Adams SH, Yu XX, Tomlinson E, Renz M, Williams PM, Soriano R, Corpuz R, Moffat B, et al. Fibroblast growth factor 19 increases metabolic rate and reverses dietary and leptin-deficient diabetes. *Endocrinology.* 2004;145(6):2594-603.
299. Tomlinson E, Fu L, John L, Hultgren B, Huang X, Renz M, Stephan JP, Tsai SP, Powell-Braxton L, French D, et al. Transgenic mice expressing human fibroblast growth factor-19 display increased metabolic rate and decreased adiposity. *Endocrinology.* 2002;143(5):1741-7.
300. Lee CG, Kim YW, Kim EH, Meng Z, Huang W, Hwang SJ, and Kim SG. Farnesoid X Receptor Protects Hepatocytes From Injury by Repressing miR-199a-3p, Which Increases Levels of LKB1. *Gastroenterology.* 2012;142(5):1206-17.e7.
301. Noh K, Kim YM, Kim YW, and Kim SG. Farnesoid X receptor activation by chenodeoxycholic acid induces detoxifying enzymes through AMP-activated protein kinase and extracellular signal-regulated kinase 1/2-mediated phosphorylation of CCAAT/enhancer binding protein beta. *Drug metabolism and disposition: the biological fate of chemicals.* 2011;39(8):1451-9.
302. Alasmael N, Mohan R, Meira LB, Swales KE, and Plant NJ. Activation of the Farnesoid X-receptor in breast cancer cell lines results in cytotoxicity but not increased migration potential. *Cancer letters.* 2016;370(2):250-9.
303. Pu J, Yuan A, Shan P, Gao E, Wang X, Wang Y, Lau WB, Koch W, Ma XL, and He B. Cardiomyocyte-expressed farnesoid-X-receptor is a novel apoptosis mediator and contributes to myocardial ischaemia/reperfusion injury. *European heart journal.* 2013;34(24):1834-45.
304. Duboc H, Taché Y, and Hofmann AF. The bile acid TGR5 membrane receptor: From basic research to clinical application. *Digestive and Liver Disease.* 2014;46(4):302-12.
305. Poole DP, Godfrey C, Cattaruzza F, Cottrell GS, Kirkland JG, Pelayo JC, Bunnett NW, and Corvera CU. Expression and function of the bile acid receptor GpBAR1 (TGR5) in the murine enteric nervous system. *Neurogastroenterology & Motility.* 2010;22(7):814-e228.
306. Thomas C, Gioiello A, Noriega L, Strehle A, Oury J, Rizzo G, Macchiarulo A, Yamamoto H, Mataki C, Pruzanski M, et al. TGR5-Mediated Bile Acid Sensing Controls Glucose Homeostasis. *Cell metabolism.* 2009;10(3):167-77.
307. Keitel V, Reinehr R, Gatsios P, Rupprecht C, Görg B, Selbach O, Häussinger D, and Kubitz R. The G-protein coupled bile salt receptor TGR5 is expressed in liver sinusoidal endothelial cells. *Hepatology.* 2007;45(3):695-704.
308. Broeders EP, Nascimento EB, Havekes B, Brans B, Roumans KH, Tailleux A, Schaart G, Kouach M, Charton J, Deprez B, et al. The Bile Acid Chenodeoxycholic Acid Increases Human Brown Adipose Tissue Activity. *Cell Metab.* 2015;22(3):418-26.
309. Thomas C, Auwerx J, and Schoonjans K. Bile acids and the membrane bile acid receptor TGR5--connecting nutrition and metabolism. *Thyroid : official journal of the American Thyroid Association.* 2008;18(2):167-74.

310. Reinehr R, Becker S, Keitel V, Eberle A, Grether–Beck S, and Häussinger D. Bile Salt–Induced Apoptosis Involves NADPH Oxidase Isoform Activation. *Gastroenterology.* 2005;129(6):2009-31.
311. Cipriani S, Mencarelli A, Chini MG, Distrutti E, Renga B, Bifulco G, Baldelli F, Donini A, and Fiorucci S. The Bile Acid Receptor GPBAR-1 (TGR5) Modulates Integrity of Intestinal Barrier and Immune Response to Experimental Colitis. *PloS one.* 2011;6(10):e25637.
312. Wang Y-D, Chen W-D, Yu D, Forman BM, and Huang W. The G-Protein-coupled bile acid receptor, Gpbar1 (TGR5), negatively regulates hepatic inflammatory response through antagonizing nuclear factor kappa light-chain enhancer of activated B cells (NF-κB) in mice. *Hepatology.* 2011;54(4):1421-32.
313. MacDonald PE, El-kholy W, Riedel MJ, Salapatek AMF, Light PE, and Wheeler MB. The Multiple Actions of GLP-1 on the Process of Glucose-Stimulated Insulin Secretion. *Diabetes.* 2002;51(suppl 3):S434-S42.
314. Tong J, and D'Alessio D. Give the Receptor a Brake: Slowing Gastric Emptying by GLP-1. *Diabetes.* 2014;63(2):407-9.
315. Hansen M, Scheltema MJ, Sonne DP, Hansen JS, Sperling M, Rehfeld JF, Holst JJ, Vilsboll T, and Knop FK. Effect of chenodeoxycholic acid and the bile acid sequestrant colesevelam on glucagon-like peptide-1 secretion. *Diabetes Obes Metab.* 2016;18(6):571-80.
316. Tolhurst G, Heffron H, Lam YS, Parker HE, Habib AM, Diakogiannaki E, Cameron J, Grosse J, Reimann F, and Gribble FM. Short-chain fatty acids stimulate glucagon-like peptide-1 secretion via the G-protein-coupled receptor FFAR2. *Diabetes.* 2012;61(2):364-71.
317. Hansen KB, Rosenkilde MM, Knop FK, Wellner N, Diep TA, Rehfeld JF, Andersen UB, Holst JJ, and Hansen HS. 2-Oleoyl glycerol is a GPR119 agonist and signals GLP-1 release in humans. *J Clin Endocrinol Metab.* 2011;96(9):E1409-17.
318. Everard A, Belzer C, Geurts L, Ouwerkerk JP, Druart C, Bindels LB, Guiot Y, Derrien M, Muccioli GG, Delzenne NM, et al. Cross-talk between Akkermansia muciniphila and intestinal epithelium controls diet-induced obesity. *Proceedings of the National Academy of Sciences.* 2013;110(22):9066-71.
319. Wang J, Dai S, Guo Y, Xie W, and Zhai Y. Biology of PXR: role in drug-hormone interactions. *EXCLI J.* 2014;13(728-39.
320. Staudinger JL, Goodwin B, Jones SA, Hawkins-Brown D, MacKenzie KI, LaTour A, Liu Y, Klaassen CD, Brown KK, Reinhard J, et al. The nuclear receptor PXR is a lithocholic acid sensor that protects against liver toxicity. *Proceedings of the National Academy of Sciences.* 2001;98(6):3369-74.
321. Xu C, Li CY-T, and Kong A-NT. Induction of phase I, II and III drug metabolism/transport by xenobiotics. *Archives of Pharmacal Research.* 2005;28(3):249.
322. Hoekstra M, Lammers B, Out R, Li Z, Van Eck M, and Van Berkel TJC. Activation of the Nuclear Receptor PXR Decreases Plasma LDL-Cholesterol Levels and Induces Hepatic Steatosis in LDL Receptor Knockout Mice. *Molecular pharmaceutics.* 2009;6(1):182-9.
323. Ihunnah CA, Jiang M, and Xie W. Nuclear receptor PXR, transcriptional circuits and metabolic relevance. *Biochimica et Biophysica Acta (BBA) - Molecular Basis of Disease.* 2011;1812(8):956-63.
324. Li T, and Chiang JY. Mechanism of rifampicin and pregnane X receptor inhibition of human cholesterol 7 alpha-hydroxylase gene transcription. *Am J Physiol Gastrointest Liver Physiol.* 2005;288(1):G74-84.

325. Wistuba W, Gnewuch C, Liebisch G, Schmitz G, and Langmann T. Lithocholic acid induction of the FGF19 promoter in intestinal cells is mediated by PXR. *World journal of gastroenterology.* 2007;13(31):4230-5.
326. Ma Y, and Liu D. Activation of Pregnane X Receptor by Pregnenolone 16 α-carbonitrile Prevents High-Fat Diet-Induced Obesity in AKR/J Mice. *PloS one.* 2012;7(6):e38734.
327. Makishima M, Lu TT, Xie W, Whitfield GK, Domoto H, Evans RM, Haussler MR, and Mangelsdorf DJ. Vitamin D Receptor As an Intestinal Bile Acid Sensor. *Science.* 2002;296(5571):1313-6.
328. Drocourt L, Ourlin J-C, Pascussi J-M, Maurel P, and Vilarem M-J. Expression of CYP3A4, CYP2B6, andCYP2C9 Is Regulated by the Vitamin D Receptor Pathway in Primary Human Hepatocytes. *J Biol Chem.* 2002;277(28):25125-32.
329. Echchgadda I, Song CS, Roy AK, and Chatterjee B. Dehydroepiandrosterone Sulfotransferase Is a Target for Transcriptional Induction by the Vitamin D Receptor. *Molecular pharmacology.* 2004;65(3):720-9.
330. Saeki M, Kurose K, Tohkin M, and Hasegawa R. Identification of the functional vitamin D response elements in the human MDR1 gene. *Biochem Pharmacol.* 2008;76(4):531-42.
331. McCarthy TC, Li X, and Sinal CJ. Vitamin D receptor-dependent regulation of colon multidrug resistance-associated protein 3 gene expression by bile acids. *J Biol Chem.* 2005;280(24):23232-42.
332. Han S, and Chiang JYL. Mechanism of Vitamin D Receptor Inhibition of Cholesterol 7α-Hydroxylase Gene Transcription in Human Hepatocytes. *Drug Metabolism and Disposition.* 2009;37(3):469-78.
333. Nehring JA, Zierold C, and DeLuca HF. Lithocholic acid can carry out in vivo functions of vitamin D. *Proceedings of the National Academy of Sciences of the United States of America.* 2007;104(24):10006-9.
334. van de Kerkhof PC. Reduction of epidermal abnormalities and inflammatory changes in psoriatic plaques during treatment with vitamin D3 analogs. *The journal of investigative dermatology Symposium proceedings.* 1996;1(1):78-81.
335. Hashimoto K, Matsumoto K, Higashiyama M, Nishida Y, and Yoshikawa K. Growth-inhibitory effects of 1,25-dihydroxyvitamin D3 on normal and psoriatic keratinocytes. *The British journal of dermatology.* 1990;123(1):93-8.
336. Kozoni V, Tsioulias G, Shiff S, and Rigas B. The effect of lithocholic acid on proliferation and apoptosis during the early stages of colon carcinogenesis: differential effect on apoptosis in the presence of a colon carcinogen. *Carcinogenesis.* 2000;21(5):999-1005.
337. Mathiasen IS, Lademann U, and Jaattela M. Apoptosis induced by vitamin D compounds in breast cancer cells is inhibited by Bcl-2 but does not involve known caspases or p53. *Cancer research.* 1999;59(19):4848-56.
338. Boonstra A, Barrat FJ, Crain C, Heath VL, Savelkoul HF, and O'Garra A. 1alpha,25-Dihydroxyvitamin d3 has a direct effect on naive CD4(+) T cells to enhance the development of Th2 cells. *Journal of immunology.* 2001;167(9):4974-80.
339. Vojinovic J. Vitamin D receptor agonists' anti-inflammatory properties. *Annals of the New York Academy of Sciences.* 2014;1317(1):47-56.
340. Adorini L, and Penna G. Control of autoimmune diseases by the vitamin D endocrine system. *Nature clinical practice Rheumatology.* 2008;4(8):404-12.
341. Rowley WR, Bezold C, Arikan Y, Byrne E, and Krohe S. Diabetes 2030: Insights from Yesterday, Today, and Future Trends. *Population Health Management.* 2017;20(1):6-12.
342. Finkelstein EA, Khavjou OA, Thompson H, Trogdon JG, Pan L, Sherry B, and Dietz W. Obesity and Severe Obesity Forecasts Through 2030. *American Journal of Preventive Medicine.* 2012;42(6):563-70.

343. Grice EA, and Segre JA. The Human Microbiome: Our Second Genome. *Annual review of genomics and human genetics.* 2012;13(151-70.
344. Wang B, Yao M, Lv L, Ling Z, and Li L. The Human Microbiota in Health and Disease. *Engineering.* 2017;3(1):71-82.
345. Vincent RP, Omar S, Ghozlan S, Taylor DR, Cross G, Sherwood RA, Fandriks L, Olbers T, Werling M, Alaghband-Zadeh J, et al. Higher circulating bile acid concentrations in obese patients with type 2 diabetes. *Annals of Clinical Biochemistry.* 2013;50(4):360-4.
346. Herrema H, Meissner M, van Dijk TH, Brufau G, Boverhof R, Oosterveer MH, Reijngoud DJ, Muller M, Stellaard F, Groen AK, et al. Bile salt sequestration induces hepatic de novo lipogenesis through farnesoid X receptor- and liver X receptor alpha-controlled metabolic pathways in mice. *Hepatology.* 2010;51(3):806-16.
347. Ridaura VK, Faith JJ, Rey FE, Cheng J, Duncan AE, Kau AL, Griffin NW, Lombard V, Henrissat B, Bain JR, et al. Gut Microbiota from Twins Discordant for Obesity Modulate Metabolism in Mice. *Science.* 2013;341(6150).
348. Begley M, Gahan CGM, and Hill C. The interaction between bacteria and bile. *FEMS Microbiology Reviews.* 2005;29(4):625-51.
349. Islam KBMS, Fukiya S, Hagio M, Fujii N, Ishizuka S, Ooka T, Ogura Y, Hayashi T, and Yokota A. Bile Acid Is a Host Factor That Regulates the Composition of the Cecal Microbiota in Rats. *Gastroenterology.* 2011;141(5):1773-81.
350. Silhavy TJ, Kahne D, and Walker S. The Bacterial Cell Envelope. *Cold Spring Harbor Perspectives in Biology.* 2010;2(5):a000414.
351. Ridlon JM, Alves JM, Hylemon PB, and Bajaj JS. Cirrhosis, bile acids and gut microbiota: Unraveling a complex relationship. *Gut Microbes.* 2013;4(5):382-7.
352. Mekhjian HS, and Phillips SF. Perfusion of the canine colon with unconjugated bile acids. Effect on water and electrolyte transport, morphology, and bile acid absorption. *Gastroenterology.* 1970;59(1):120-9.
353. Fickert P, Fuchsbichler A, Marschall H-U, Wagner M, Zollner G, Krause R, Zatloukal K, Jaeschke H, Denk H, and Trauner M. Lithocholic Acid Feeding Induces Segmental Bile Duct Obstruction and Destructive Cholangitis in Mice. *The American Journal of Pathology.* 2006;168(2):410-22.
354. Bernstein H, Payne CM, Bernstein C, Schneider J, Beard SE, and Crowley CL. Activation of the promoters of genes associated with DNA damage, oxidative stress, ER stress and protein malfolding by the bile salt, deoxycholate. *Toxicol Lett.* 1999;108(1):37-46.
355. Zhu Y, Liu H, Zhang M, and Guo GL. Fatty liver diseases, bile acids, and FXR. *Acta Pharmaceutica Sinica B.* 2016;6(5):409-12.
356. Estes C, Razavi H, Loomba R, Younossi Z, and Sanyal AJ. Modeling the epidemic of nonalcoholic fatty liver disease demonstrates an exponential increase in burden of disease. *Hepatology.* 2018;67(1):123-33.
357. Tolman KG, and Dalpiaz AS. Treatment of non-alcoholic fatty liver disease. *Therapeutics and Clinical Risk Management.* 2007;3(6):1153-63.
358. Sattar N, Forrest E, and Preiss D. Non-alcoholic fatty liver disease. *BMJ : British Medical Journal.* 2014;349(
359. Carr RM, and Reid AE. FXR Agonists as Therapeutic Agents for Non-alcoholic Fatty Liver Disease. *Current Atherosclerosis Reports.* 2015;17(4):16.
360. Jiang C, Xie C, Li F, Zhang L, Nichols RG, Krausz KW, Cai J, Qi Y, Fang ZZ, Takahashi S, et al. Intestinal farnesoid X receptor signaling promotes nonalcoholic fatty liver disease. *The Journal of clinical investigation.* 2015;125(1):386-402.
361. Pols Thijs WH, Nomura M, Harach T, Lo Sasso G, Oosterveer Maaike H, Thomas C, Rizzo G, Gioiello A, Adorini L, Pellicciari R, et al. TGR5 Activation Inhibits

Atherosclerosis by Reducing Macrophage Inflammation and Lipid Loading. *Cell Metabolism.* 2011;14(6):747-57.
362. Okushin K, Tsutsumi T, Enooku K, Fujinaga H, Kado A, Shibahara J, Fukayama M, Moriya K, Yotsuyanagi H, and Koike K. The intrahepatic expression levels of bile acid transporters are inversely correlated with the histological progression of nonalcoholic fatty liver disease. *Journal of Gastroenterology.* 2016;51(8):808-18.
363. Lionarons DA, Heger M, van Golen RF, Alles LK, van der Mark VA, Kloek JJ, de Waart DR, Marsman HA, Rusch H, Verheij J, et al. Simple steatosis sensitizes cholestatic rats to liver injury and dysregulates bile salt synthesis and transport. *Scientific reports.* 2016;6(31829.
364. Rao A, Kosters A, Mells JE, Zhang W, Setchell KDR, Amanso AM, Wynn GM, Xu T, Keller BT, Yin H, et al. Inhibition of Ileal Bile Acid Uptake Protects Against Non-alcoholic Fatty Liver Disease in High Fat Diet-fed Mice. *Science translational medicine.* 2016;8(357):357ra122-357ra122.
365. Rodríguez-Garay EA. Cholestasis: human disease and experimental animal models. *Ann Hepatol.* 2003;2(4):150-8.
366. Fisk NM, and Bruce Storey GN. Fetal outcome in obstetric cholestasis. *BJOG: An International Journal of Obstetrics & Gynaecology.* 1988;95(11):1137-43.
367. Geenes V, and Williamson C. Intrahepatic cholestasis of pregnancy. *World Journal of Gastroenterology : WJG.* 2009;15(17):2049-66.
368. Xie W, Radominska-Pandya A, Shi Y, Simon CM, Nelson MC, Ong ES, Waxman DJ, and Evans RM. An essential role for nuclear receptors SXR/PXR in detoxification of cholestatic bile acids. *Proceedings of the National Academy of Sciences.* 2001;98(6):3375-80.
369. Li T, and Apte U. Bile acid metabolism and signaling in cholestasis, inflammation and cancer. *Advances in pharmacology (San Diego, Calif).* 2015;74(263-302.
370. Pullinger CR, Eng C, Salen G, Shefer S, Batta AK, Erickson SK, Verhagen A, Rivera CR, Mulvihill SJ, Malloy MJ, et al. Human cholesterol 7alpha-hydroxylase (CYP7A1) deficiency has a hypercholesterolemic phenotype. *The Journal of clinical investigation.* 2002;110(1):109-17.
371. Xie Y, Blanc V, Kerr TA, Kennedy S, Luo J, Newberry EP, and Davidson NO. Decreased expression of cholesterol 7alpha-hydroxylase and altered bile acid metabolism in Apobec-1-/- mice lead to increased gallstone susceptibility. *J Biol Chem.* 2009;284(25):16860-71.
372. Bertolotti M, Gabbi C, Anzivino C, Carulli L, and Carulli N. Changes in bile acid synthesis in gallstone disease: Cause, consequence, or neither? *Hepatology.* 2007;46(5):1664-.
373. Marcus SN, and Heaton KW. Deoxycholic acid and the pathogenesis of gall stones. *Gut.* 1988;29(4):522-33.
374. Wang J, Gåfvels M, Rudling M, Murphy C, Björkhem I, Einarsson C, and Eggertsen G. Critical role of cholic acid for development of hypercholesterolemia and gallstones in diabetic mice. *Biochemical and Biophysical Research Communications.* 2006;342(4):1382-8.
375. Vassileva G, Golovko A, Markowitz L, Abbondanzo SJ, Zeng M, Yang S, Hoos L, Tetzloff G, Levitan D, Murgolo NJ, et al. Targeted deletion of Gpbar1 protects mice from cholesterol gallstone formation. *The Biochemical journal.* 2006;398(3):423-30.
376. Li T, Holmstrom SR, Kir S, Umetani M, Schmidt DR, Kliewer SA, and Mangelsdorf DJ. The G Protein-Coupled Bile Acid Receptor, TGR5, Stimulates Gallbladder Filling. *Molecular endocrinology.* 2011;25(6):1066-71.

377. Duboc H, Rajca S, Rainteau D, Benarous D, Maubert MA, Quervain E, Thomas G, Barbu V, Humbert L, Despras G, et al. Connecting dysbiosis, bile-acid dysmetabolism and gut inflammation in inflammatory bowel diseases. *Gut.* 2013;62(4):531-9.
378. Herman-Edelstein M, Weinstein T, and Levi M. Bile acid receptors and the kidney. *Current opinion in nephrology and hypertension.* 2018;27(1):56-62.
379. Zhu C, Fuchs CD, Halilbasic E, and Trauner M. Bile acids in regulation of inflammation and immunity: friend or foe? *Clin Exp Rheumatol.* 2016;34(4 Suppl 98):25-31.
380. Kim ND, Moon J-OK, Slitt AL, and Copple BL. Early Growth Response Factor-1 Is Critical for Cholestatic Liver Injury. *Toxicological Sciences.* 2006;90(2):586-95.
381. O'Brien KM, Allen KM, Rockwell CE, Towery K, Luyendyk JP, and Copple BL. IL-17A Synergistically Enhances Bile Acid–Induced Inflammation during Obstructive Cholestasis. *The American Journal of Pathology.* 2013;183(5):1498-507.
382. Shaik FB, Prasad DVR, and Narala VR. Role of farnesoid X receptor in inflammation and resolution. *Inflammation Research.* 2015;64(1):9-20.
383. Jiang T, Wang XX, Scherzer P, Wilson P, Tallman J, Takahashi H, Li J, Iwahashi M, Sutherland E, Arend L, et al. Farnesoid X receptor modulates renal lipid metabolism, fibrosis, and diabetic nephropathy. *Diabetes.* 2007;56(10):2485-93.
384. Walker IA, Nelson-Piercy C, and Williamson C. Role of bile acid measurement in pregnancy. *Annals of Clinical Biochemistry.* 2002;39(2):105-13.
385. Skrede S, Solberg HE, Blomhoff JP, and Gjone E. Bile acids measured in serum during fasting as a test for liver disease. *Clinical Chemistry.* 1978;24(7):1095-9.
386. Morita T, Matsuyama Y, Fujimoto T, Higuchi M, Tsujii T, and Matsuoka Y. Clinical significance of serum bile acid measurement in liver diseases. *Gastroenterologia Japonica.* 1978;13(6):491-502.
387. Sarafian MH, Lewis MR, Pechlivanis A, Ralphs S, McPhail MJW, Patel VC, Dumas M-E, Holmes E, and Nicholson JK. Bile Acid Profiling and Quantification in Biofluids Using Ultra-Performance Liquid Chromatography Tandem Mass Spectrometry. *Analytical Chemistry.* 2015;87(19):9662-70.
388. Zhang G-H, Cong A-R, Xu G-B, Li C-B, Yang R-F, and Xia T-A. An enzymatic cycling method for the determination of serum total bile acids with recombinant 3α-hydroxysteroid dehydrogenase. *Biochemical and Biophysical Research Communications.* 2004;326(1):87-92.
389. Mashige F, Tanaka N, Maki A, Kamei S, and Yamanaka M. Direct spectrophotometry of total bile acids in serum. *Clinical Chemistry.* 1981;27(8):1352-6.
390. Niu XY, Xu Y, Yang QL, Tang XW, Yang L, and Wang ZT. Analytical methods for characterization of bile acids and its application in quality control of cow-bezoar and bear bile powder *American Journal of Applied Chemistry.* 2014;2(6):96-104.
391. Street JM, and Setchell KDR. Chromatographic methods for bile acid analysis. *Biomedical Chromatography.* 1987;2(6):229-41.
392. Robb TA, Davidson GP, and Kirubakaran C. Conjugated bile acids in serum and secretions in response to cholecystokinin/secretin stimulation in children with cystic fibrosis. *Gut.* 1985;26(11):1246-56.
393. Robb TA, and Davidson GP. Analysis of Individual Bile Acids and Their Glycine/Taurine Conjugates by High-Performance Thin-Layer Chromatography and Densitometry. *Annals of Clinical Biochemistry.* 1984;21(2):137-40.
394. Onishi S, Itoh S, and Ishida Y. Assay of free and glycine- and taurine-conjugated bile acids in serum by high-pressure liquid chromatography by using post-column reaction after group separation. *Biochemical Journal.* 1982;204(1):135-9.
395. Hernanz A, and Codoceo R. An improved high-performance liquid-chromatographic determination of conjugated bile acids in serum using paired-ion chromatography. *Clinica Chimica Acta.* 1985;145(2):197-203.

396. VandenHeuvel WJA, Sweeley CC, and Horning EC. Microanalytical separations by gas chromatography in the sex hormone and bile acid series. *Biochemical and Biophysical Research Communications.* 1960;3(1):33-6.
397. Batta AK, and Salen G. Gas chromatography of bile acids. *Journal of Chromatography B: Biomedical Sciences and Applications.* 1999;723(1):1-16.
398. Roda A, Piazza F, and Baraldini M. Separation techniques for bile salts analysis. *Journal of Chromatography B: Biomedical Sciences and Applications.* 1998;717(1):263-78.
399. Humbert L, Maubert MA, Wolf C, Duboc H, Mahé M, Farabos D, Seksik P, Mallet JM, Trugnan G, Masliah J, et al. Bile acid profiling in human biological samples: Comparison of extraction procedures and application to normal and cholestatic patients. *Journal of Chromatography B.* 2012;899(135-45.
400. Nezami Ranjbar MR, Luo Y, Di Poto C, Varghese RS, Ferrarini A, Zhang C, Sarhan NI, Soliman H, Tadesse MG, Ziada DH, et al. GC-MS Based Plasma Metabolomics for Identification of Candidate Biomarkers for Hepatocellular Carcinoma in Egyptian Cohort. *PloS one.* 2015;10(6):e0127299.
401. Kakiyama G, Muto A, Takei H, Nittono H, Murai T, Kurosawa T, Hofmann AF, Pandak WM, and Bajaj JS. A simple and accurate HPLC method for fecal bile acid profile in healthy and cirrhotic subjects: validation by GC-MS and LC-MS. *J Lipid Res.* 2014;55(5):978-90.
402. Griffiths WJ, and Sjövall J. Bile acids: analysis in biological fluids and tissues. *J Lipid Res.* 2010;51(1):23-41.
403. Griffiths WJ, and Sjovall J. Bile acids: analysis in biological fluids and tissues. *Journal of lipid research.* 2010;51(1):23-41.
404. Perwaiz S, Tuchweber B, Mignault D, Gilat T, and Yousef IM. Determination of bile acids in biological fluids by liquid chromatography-electrospray tandem mass spectrometry. *J Lipid Res.* 2001;42(1):114-9.
405. Suzuki Y, Kaneko R, Nomura M, Naito H, Kitamori K, Nakajima T, Ogawa T, Hattori H, Seno H, and Ishii A. Simple and rapid quantitation of 21 bile acids in rat serum and liver by UPLC-MS-MS: effect of high fat diet on glycine conjugates of rat bile acids. *Nagoya journal of medical science.* 2013;75(1-2):57-71.
406. Nagana Gowda GA, Shanaiah N, Cooper A, Maluccio M, and Raftery D. Bile Acids Conjugation in Human Bile Is Not Random: New Insights from 1H-NMR Spectroscopy at 800 MHz. *Lipids.* 2009;44(6):527-35.
407. Ijare OB, Somashekar BS, Gowda GA, Sharma A, Kapoor VK, and Khetrapal CL. Quantification of glycine and taurine conjugated bile acids in human bile using 1H NMR spectroscopy. *Magnetic resonance in medicine.* 2005;53(6):1441-6.
408. Jain AK, Roux CW, Puri P, Tavakkoli A, Gletsu-Miller N, Laferrère B, Kellermayer R, DiBaise JK, Martindale RG, and Wolfe BM. Proceedings of the 2017 ASPEN Research Workshop—Gastric Bypass: Role of the Gut. *Journal of Parenteral and Enteral Nutrition.* 2018;42(2):279-95.
409. Noel OF, Still CD, Argyropoulos G, Edwards M, and Gerhard GS. Bile Acids, FXR, and Metabolic Effects of Bariatric Surgery. *Journal of Obesity.* 2016;2016(8.
410. Kohli R, Bradley D, Setchell KD, Eagon JC, Abumrad N, and Klein S. Weight Loss Induced by Roux-en-Y Gastric Bypass But Not Laparoscopic Adjustable Gastric Banding Increases Circulating Bile Acids. *The Journal of Clinical Endocrinology & Metabolism.* 2013;98(4):E708-E12.
411. Furet JP, Kong LC, Tap J, Poitou C, Basdevant A, Bouillot JL, Mariat D, Corthier G, Dore J, Henegar C, et al. Differential adaptation of human gut microbiota to bariatric surgery-induced weight loss: links with metabolic and low-grade inflammation markers. *Diabetes.* 2010;59(12):3049-57.

412. Liou AP, Paziuk M, Luevano J-M, Machineni S, Turnbaugh PJ, and Kaplan LM. Conserved Shifts in the Gut Microbiota Due to Gastric Bypass Reduce Host Weight and Adiposity. *Science translational medicine.* 2013;5(178):178ra41-ra41.
413. Liou AP, Paziuk M, Luevano JM, Jr., Machineni S, Turnbaugh PJ, and Kaplan LM. Conserved shifts in the gut microbiota due to gastric bypass reduce host weight and adiposity. *Sci Transl Med.* 2013;5(178):178ra41.
414. Myronovych A, Kirby M, Ryan KK, Zhang W, Jha P, Setchell KD, Dexheimer PJ, Aronow B, Seeley RJ, and Kohli R. Vertical sleeve gastrectomy reduces hepatic steatosis while increasing serum bile acids in a weight-loss-independent manner. *Obesity.* 2014;22(2):390-400.
415. Li JV, Ashrafian H, Bueter M, Kinross J, Sands C, le Roux CW, Bloom SR, Darzi A, Athanasiou T, Marchesi JR, et al. Metabolic surgery profoundly influences gut microbial–host metabolic cross-talk. *Gut.* 2011;60(9):1214-23.
416. Zhang H, DiBaise JK, Zuccolo A, Kudrna D, Braidotti M, Yu Y, Parameswaran P, Crowell MD, Wing R, Rittmann BE, et al. Human gut microbiota in obesity and after gastric bypass. *P Natl Acad Sci USA.* 2009;106(7):2365-70.
417. Jansen PL, van Werven J, Aarts E, Berends F, Janssen I, Stoker J, and Schaap FG. Alterations of hormonally active fibroblast growth factors after Roux-en-Y gastric bypass surgery. *Digestive diseases (Basel, Switzerland).* 2011;29(1):48-51.
418. Ryan KK, Tremaroli V, Clemmensen C, Kovatcheva-Datchary P, Myronovych A, Karns R, Wilson-Perez HE, Sandoval DA, Kohli R, Backhed F, et al. FXR is a molecular target for the effects of vertical sleeve gastrectomy. *Nature.* 2014;509(7499):183-8.
419. Korner J, Bessler M, Inabnet W, Taveras C, and Holst JJ. Exaggerated glucagon-like peptide-1 and blunted glucose-dependent insulinotropic peptide secretion are associated with Roux-en-Y gastric bypass but not adjustable gastric banding. *Surgery for obesity and related diseases : official journal of the American Society for Bariatric Surgery.* 2007;3(6):597-601.
420. Laferrère B, Heshka S, Wang K, Khan Y, McGinty J, Teixeira J, Hart AB, and Olivan B. Incretin Levels and Effect Are Markedly Enhanced 1 Month After Roux-en-Y Gastric Bypass Surgery in Obese Patients With Type 2 Diabetes. *Diabetes Care.* 2007;30(7):1709-16.
421. McGavigan AK, Garibay D, Henseler ZM, Chen J, Bettaieb A, Haj FG, Ley RE, Chouinard ML, and Cummings BP. TGR5 contributes to glucoregulatory improvements after vertical sleeve gastrectomy in mice. *Gut.* 2016.
422. Cole AJ, Teigen LM, Jahansouz C, Earthman CP, and Sibley SD. The Influence of Bariatric Surgery on Serum Bile Acids in Humans and Potential Metabolic and Hormonal Implications: a Systematic Review. *Current Obesity Reports.* 2015;4(4):441-50.
423. Levrat MA, Remesy C, and Demigne C. High propionic acid fermentations and mineral accumulation in the cecum of rats adapted to different levels of inulin. *J Nutr.* 1991;121(11):1730-7.
424. Hedemann MS, Theil PK, and Bach Knudsen KE. The thickness of the intestinal mucous layer in the colon of rats fed various sources of non-digestible carbohydrates is positively correlated with the pool of SCFA but negatively correlated with the proportion of butyric acid in digesta. *The British journal of nutrition.* 2009;102(1):117-25.
425. De Filippis F, Pellegrini N, Vannini L, Jeffery IB, La Storia A, Laghi L, Serrazanetti DI, Di Cagno R, Ferrocino I, Lazzi C, et al. High-level adherence to a Mediterranean diet beneficially impacts the gut microbiota and associated metabolome. *Gut.* 2016;65(11):1812-21.
426. Bisschop PH, Bandsma RHJ, Stellaard F, ter Harmsel A, Meijer AJ, Sauerwein HP, Kuipers F, and Romijn JA. Low-fat, high-carbohydrate and high-fat, low-carbohydrate

diets decrease primary bile acid synthesis in humans. *The American Journal of Clinical Nutrition.* 2004;79(4):570-6.
427. Pavlović N, Stankov K, and Mikov M. Probiotics—Interactions with Bile Acids and Impact on Cholesterol Metabolism. *Applied Biochemistry and Biotechnology.* 2012;168(7):1880-95.
428. Wang L, Guo MJ, Gao Q, Yang JF, Yang L, Pang XL, and Jiang XJ. The effects of probiotics on total cholesterol: A meta-analysis of randomized controlled trials. *Medicine.* 2018;97(5):e9679.
429. Degirolamo C, Rainaldi S, Bovenga F, Murzilli S, and Moschetta A. Microbiota Modification with Probiotics Induces Hepatic Bile Acid Synthesis via Downregulation of the Fxr-Fgf15 Axis in Mice. *Cell Reports.* 2014;7(1):12-8.
430. Mencarelli A, Distrutti E, Renga B, D'Amore C, Cipriani S, Palladino G, Donini A, Ricci P, and Fiorucci S. Probiotics Modulate Intestinal Expression of Nuclear Receptor and Provide Counter-Regulatory Signals to Inflammation-Driven Adipose Tissue Activation. *PloS one.* 2011;6(7):e22978.
431. Begley M, Hill C, and Gahan CG. Bile salt hydrolase activity in probiotics. *Appl Environ Microbiol.* 2006;72(3):1729-38.
432. Gibson GR, Hutkins R, Sanders ME, Prescott SL, Reimer RA, Salminen SJ, Scott K, Stanton C, Swanson KS, Cani PD, et al. Expert consensus document: The International Scientific Association for Probiotics and Prebiotics (ISAPP) consensus statement on the definition and scope of prebiotics. *Nature Reviews Gastroenterology &Amp; Hepatology.* 2017;14(491.
433. Roberfroid M, Gibson GR, Hoyles L, McCartney AL, Rastall R, Rowland I, Wolvers D, Watzl B, Szajewska H, Stahl B, et al. Prebiotic effects: metabolic and health benefits. *British Journal of Nutrition.* 2010;104(S2):S1-S63.
434. Catry E, Bindels LB, Tailleux A, Lestavel S, Neyrinck AM, Goossens J-F, Lobysheva I, Plovier H, Essaghir A, Demoulin J-B, et al. Targeting the gut microbiota with inulin-type fructans: preclinical demonstration of a novel approach in the management of endothelial dysfunction. *Gut.* 2018;67(2):271-83.
435. Pellicciari R, Costantino G, Camaioni E, Sadeghpour BM, Entrena A, Willson TM, Fiorucci S, Clerici C, and Gioiello A. Bile acid derivatives as ligands of the farnesoid X receptor. Synthesis, evaluation, and structure-activity relationship of a series of body and side chain modified analogues of chenodeoxycholic acid. *Journal of medicinal chemistry.* 2004;47(18):4559-69.
436. Arab JP, Karpen SJ, Dawson PA, Arrese M, and Trauner M. Bile acids and nonalcoholic fatty liver disease: Molecular insights and therapeutic perspectives. *Hepatology.* 2017;65(1):350-62.
437. Roth JD, Feigh M, Veidal SS, Fensholdt LKD, Rigbolt KT, Hansen HH, Chen LC, Petitjean M, Friley W, Vrang N, et al. INT-767 improves histopathological features in a diet-induced ob/ob mouse model of biopsy-confirmed non-alcoholic steatohepatitis. *World journal of gastroenterology.* 2018;24(2):195-210.
438. Prawitt J, Abdelkarim M, Stroeve JHM, Popescu I, Duez H, Velagapudi VR, Dumont J, Bouchaert E, Van Dijk TH, Lucas A, et al. Farnesoid x receptor deficiency improves glucose homeostasis in mouse models of obesity. *Diabetes.* 2011;60(7):1861-71.
439. Cariou B, van Harmelen K, Duran-Sandoval D, van Dijk TH, Grefhorst A, Abdelkarim M, Caron S, Torpier G, Fruchart J-C, Gonzalez FJ, et al. The Farnesoid X Receptor Modulates Adiposity and Peripheral Insulin Sensitivity in Mice. *J Biol Chem.* 2006;281(16):11039-49.
440. Li F, Jiang C, Krausz KW, Li Y, Albert I, Hao H, Fabre KM, Mitchell JB, Patterson AD, and Gonzalez FJ. Microbiome remodelling leads to inhibition of intestinal farnesoid X receptor signalling and decreased obesity. *Nature communications.* 2013;4(2384.

441. Jiang C, Xie C, Lv Y, Li J, Krausz KW, Shi J, Brocker CN, Desai D, Amin SG, Bisson WH, et al. Intestine-selective farnesoid X receptor inhibition improves obesity-related metabolic dysfunction. *Nature communications.* 2015;6(10166.
442. Wang XX, Edelstein MH, Gafter U, Qiu L, Luo Y, Dobrinskikh E, Lucia S, Adorini L, D'Agati VD, Levi J, et al. G Protein-Coupled Bile Acid Receptor TGR5 Activation Inhibits Kidney Disease in Obesity and Diabetes. *Journal of the American Society of Nephrology : JASN.* 2016;27(5):1362-78.
443. Zambad SP, Tuli D, Mathur A, Ghalsasi SA, Chaudhary AR, Deshpande S, Gupta RC, Chauthaiwale V, and Dutt C. TRC210258, a novel TGR5 agonist, reduces glycemic and dyslipidemic cardiovascular risk in animal models of diabesity. *Diabetes, metabolic syndrome and obesity : targets and therapy.* 2013;7(1-14.
444. Perides G, Laukkarinen JM, Vassileva G, and Steer ML. Biliary Acute Pancreatitis in Mice is Mediated by the G-Protein−Coupled Cell Surface Bile Acid Receptor Gpbar1. *Gastroenterology.* 2010;138(2):715-25.
445. Vassileva G, Golovko A, Markowitz L, Abbondanzo Susan J, Zeng M, Yang S, Hoos L, Tetzloff G, Levitan D, Murgolo Nicholas J, et al. Targeted deletion of Gpbar1 protects mice from cholesterol gallstone formation. *Biochemical Journal.* 2006;398(3):423-30.
446. Li T, Holmstrom SR, Kir S, Umetani M, Schmidt DR, Kliewer SA, and Mangelsdorf DJ. The G protein-coupled bile acid receptor, TGR5, stimulates gallbladder filling. *Molecular endocrinology.* 2011;25(6):1066-71.
447. Briere DA, Ruan X, Cheng CC, Siesky AM, Fitch TE, Dominguez C, Sanfeliciano SG, Montero C, Suen CS, Xu Y, et al. Novel Small Molecule Agonist of TGR5 Possesses Anti-Diabetic Effects but Causes Gallbladder Filling in Mice. *PloS one.* 2015;10(8):e0136873.
448. Schaap FG, Trauner M, and Jansen PLM. Bile acid receptors as targets for drug development. *Nature Reviews Gastroenterology &Amp; Hepatology.* 2013;11(55.
449. Sepe V, Distrutti E, Limongelli V, Fiorucci S, and Zampella A. Steroidal scaffolds as FXR and GPBAR1 ligands: from chemistry to therapeutical application. *Future Medicinal Chemistry.* 2015;7(9):1109-35.
450. Finamore C, Festa C, Renga B, Sepe V, Carino A, Masullo D, Biagioli M, Marchianò S, Capolupo A, Monti MC, et al. Navigation in bile acid chemical space: discovery of novel FXR and GPBAR1 ligands. *Scientific reports.* 2016;6(29320.

Figure 1-1

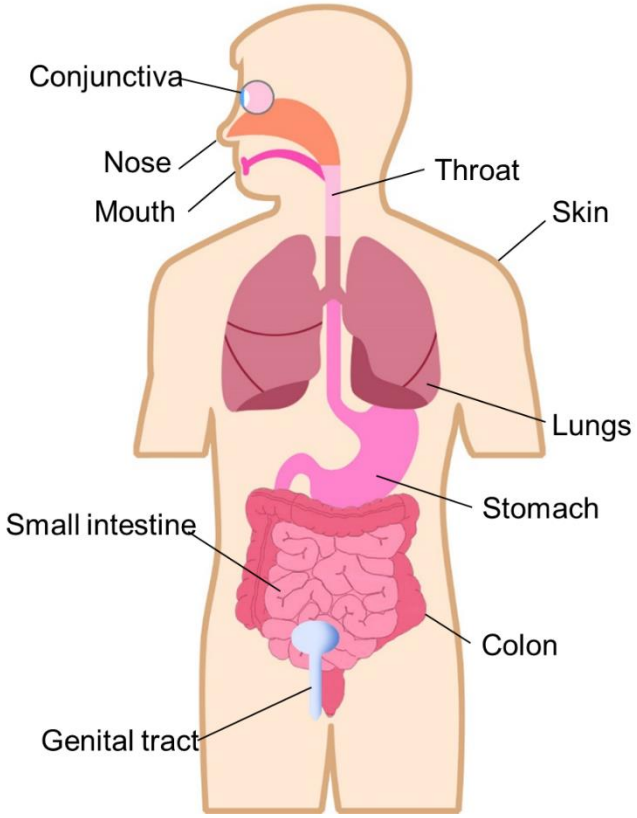

Figure 1-1. Dynamic Distribution of Normal Microbiota. Normal microbiota refers to a stable, regular microorganism community acquired during birth, newborn handling and feeding after birth. The microbiome remains throughout life and participates in the health maintenance without causing disease under normal circumstance. In the healthy human body, the microbiome inhabits at mucous membrane (conjunctiva), surface tissues like skin, digestive tract (mouth, stomach and intestinal tract), respiratory tract (nose primarily and lung) and genital tract (urinary and vaginal tract). The internal tissues like brain, circulation system (blood, heart), and muscles are considered microorganism-free. Normal microbiome is characterized with body region-specific, life stage-, pH- and hormonal level- dependent microbial inhabitants.

Figure 1-2. SCFAs involved in metabolic and immunological functional pathways

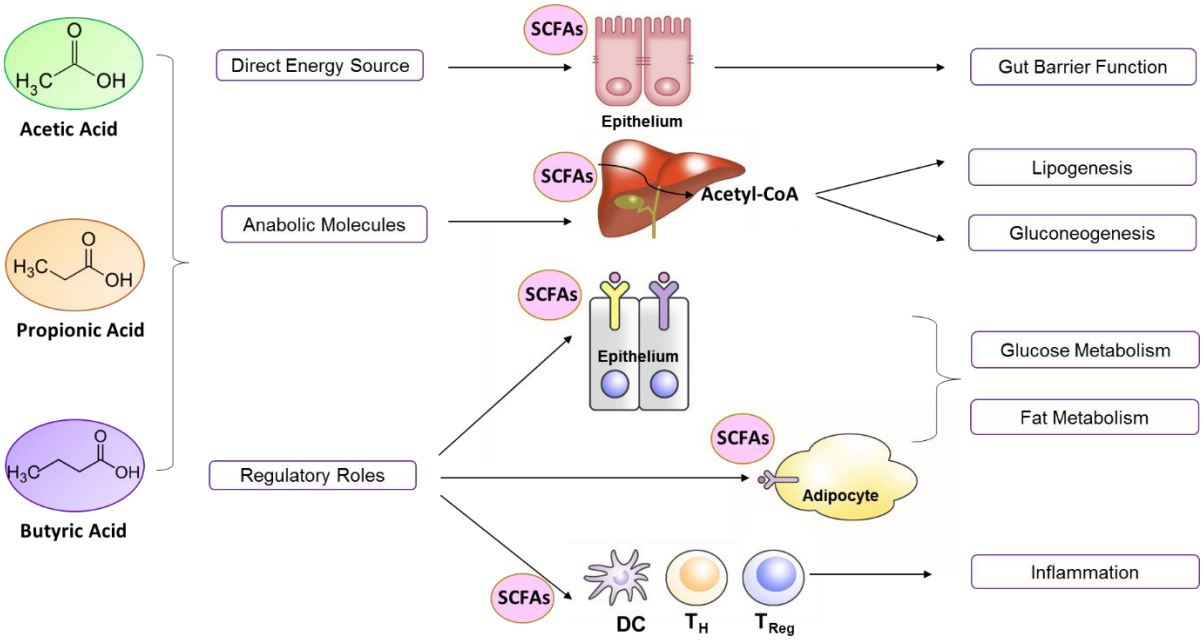

Figure 1-2. SCFAs Involved in Metabolic and Immunological Functional Pathways. The primary fermentation-derived SCFAs acetic acid (C2), propionic acid (C3) and butyric acid (C4) are utilized by the colon epicedium as energy source to maintain gut barrier function. SCFAs serve as anabolic substrates or precursors for biogenic synthesis in the liver including lipogenesis and gluconeogenesis. SCFAs also function as signaling molecules to activate GPRs/FFARs for metabolic and immunological regulation.

Figure 1-3

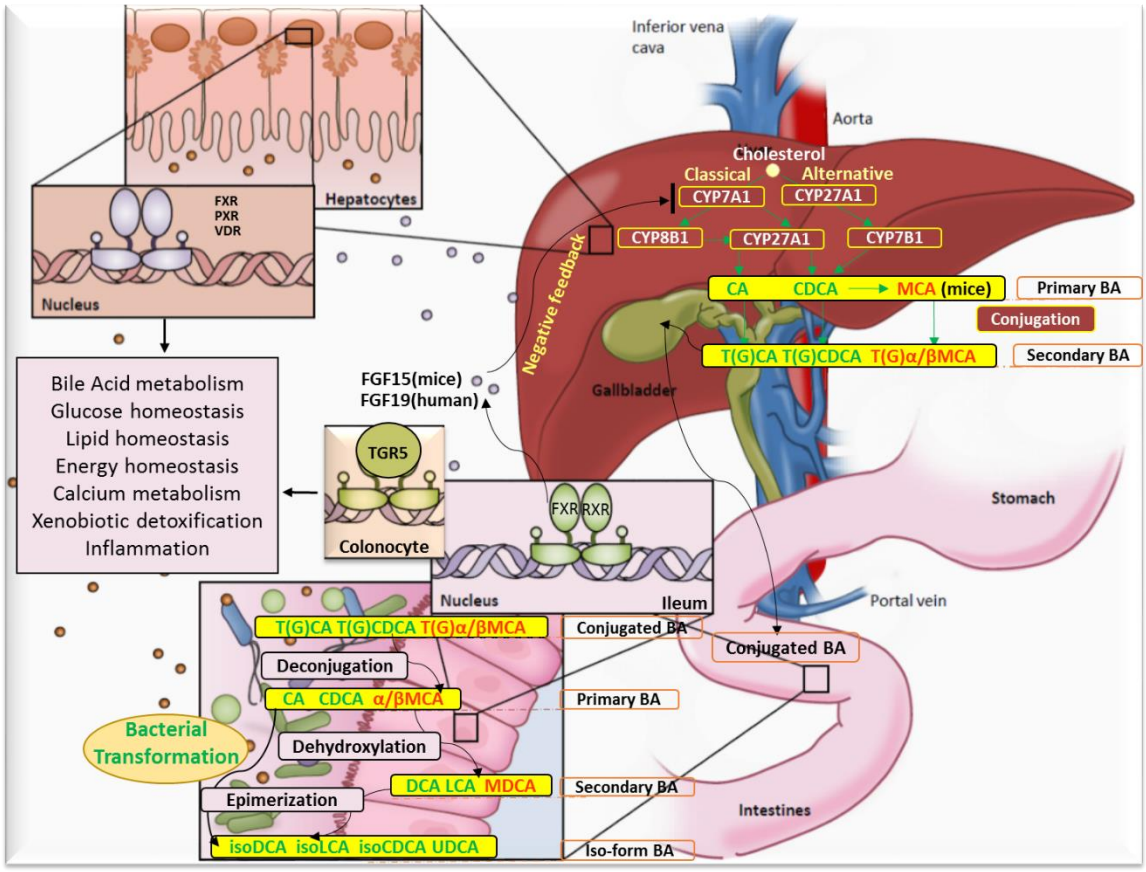

Figure 1-3. Bile Acid Synthesis, Biotransformation and Regulation. Primary Bile acids CA and CDCA are initially synthesized from cholesterol in the liver, and undergo extensively bacterial transformation as moving along the intestinal tract, eventually form a bile acid pool with great diversity. Bacterial-transformed bile acids activate different bile acid receptors FXR, TGR5, PXR and VDR to regulate signaling pathways with a broad coverage of complex symbiotic metabolism networks, including lipid metabolism, glucose metabolism, xenobiotics metabolism, energy homeostasis and inflammation.

Table 1-1. Bacterial Transformation of Bile Acids

Main Bacteria Genera	Transformation and enzyme regulated*/produced by bacteria	Initial metabolite	End metabolites	Location
	bile acid *de novo* synthesis CYP7A1*,CYP7B1*, CYP8B1*,CYP27A1*	Cholesterol	**Primary bile acid** CA,CDCA (in human) CA,CDCA, UDCA,MCA (murine)	Liver
Clostridum XIVa, *Clostridum* XI *Eubacterium*	bile acid dehydroxylation 7α-dehydroxylase	**Primary bile acid** CA,CDCA (human) CA,CDCA UDCA,MCA (murine)	**Secondary bile acid** DCA,LCA (human) DCA,LCA,MDCA (murine)	Intestine
Lactobacillus, Bacteroides, Bifidobacterium, Clostridium, Listeria, Enterococcus, Brevibacillus	Bile acid deconjugation Bile salt hydrolases (BSH)	**Conjugated bile acid** T(G)CA,T(G)CDCA, T(G)DCA,T(G)UDCA Tα/β/ωMCA (murine)	**Free bile acid** CA,LCA,DCA UDCA α/β/ωMCA (murine)	Intestine
Bacteroides, Clostridium, Eubacterium, Peptostreptococcus, Ruminococcus, Bifidobacterium, Egghertella, Enterobacter, Escherichia	Bile acid oxidation and epimerization hydroxysteroid dehydrogenase (HSDH)	**α-Hydroxyl bile acid** DCA, LCA, UDCA, CDCA	**β-hydroxyl (Iso) bile acid** isoDCA, isoLCA, isoUDCA isoCDCA UDCA (7β isomer of CDCA)	Intestine
Clostridium, Fusobacterium, Peptococcus, Pseudomonas	Bile acid desulfatation bile salt sulfatases	**Bile acid sulfate ester**	**Unsulfated bile acid**	Colon
Bacteroides, Eubacterium, Lactobacillus, Citrobacter, Peptostreptococcus	Bile acid esterification	**Unesterfied bile acid**	**Fatty acid ethyl esterified bile acid**	In vitro
Pseudomonas, Clostridium	Bile acid unsaturation of the steroid ring A Nuclear dehydrogenase (NDH)	**Saturated bile acid**	**Unsaturated bile acid**	In vitro

Table 1-2. Bile Acid Receptors and Signaling Pathways.

Receptor	Ligand potency	Signaling pathway	Transcriptional regulation	Physiological and metabolic effect	Metabolism regulated
FXR	CDCA>LCA=DCA>CA TβMCA (antagonist)	FXR/SHP/LRH-1/LXRα FXR/FGF19(15)/FGF-R4	CYP7A1↓, CYP8B1↓, BSEP↑, MRP2↑, MDR3↑, OST α and β↑, I-BABP↓ NTCP↓, OATP1B1↓, OATP1B3↓, ASBT↓,	Inhibited *de novo* bile acid synthesis Enhanced bile acid export Decreased of Bile acid influx	Bile acid
		FXR/Shp/Hnf4 and Foxo1 PI3K/Akt/Gsk3β FXR deficiency	G6pase↓, Pepck↓, Gsk3β phosphorylation↑ Glut2↑, Glut4↑ Proglulcagon↑	Decreased gluconeogenesis Increased glycogenesis Improved insulin transcription and secretion Improved glycaemia	Hepatic Glucose
		FXR/SHP/Srebp-1c FXR/RXR FXR depletion	Fas↓ ApoC-II↑, APOA(human)↑ VLDL-R↑, syndecan-1↑, ApoC-III↓, PPARα↑, Abcg5↑, Abcg8↑, Ceh↑, Scp↑, SrbI↑ Cyp7a1↑	Decreased serum TG Promoted VLDL and chylomicrons clearance Promoted fat oxidation Enhanced cholesterol reverse transportation and clearance Stimulated cholesterol *de novo* synthesis	Lipid, Cholesterol
		FXR	Human: CYP3A4↑, SULT2A1↑, UGT1A3↑, UGT2B4↑ Mouse: Abcb1↑, Fmo3↑,Gsta2↑	Promoted Phase I and II detoxification	Drugs and xenobiotic
		FXR/FGF19(15)/FGF-R4 AMPK-ERK1/2-C/EBPβ	Pfk-1↑, Acly↑, Scd↑, Acc2↓, Pgc1α ↑, Pgc1β ↑, Ucp1↑, Fabp1↑,Esrrg↑, Glut4↑,Aox↑,DIO2↑ Lkb1↑, AMPK↑ GCS↑, MnSOD↑, UGT1A↑, HO-1↑, GSTA2↑, Mrp2↑	Increased metabolic rate Enhanced thermogenesis, mitochondrial biogenesis and fatty acid oxidation Reduced adiposity Ameliorated hyperglycemia	Energy metabolism
TGR5	LCA≥DCA>CDCA>CA	TGR5-cAMP-PKA	DIO2↑, PGC-1α↑, PGC-1β↑, UCP-1↑, UCP-3↑, ACO↑,mCPT-I↑	Enhanced thermogenesis and energy expenditure	Energy metabolism
		TGR5-cAMP-NF-kB	IL-1α↓, IL-1β↓, IL-6↓, TNF-α↓, IFN-γ↓	Attenuated inflammation	inflammation
		TGR-5/cAMP/Ca^{2+}	Proglulcagon↑,	promoted insulin secretion inhibited gastric empty and acid secretion delayed intestinal transit reduced food intake, enhanced satiety	Glucose

Table 1-2. Continued

Receptor	Ligand potency	Signaling pathway	Transcriptional regulation	Physiological and metabolic effect	Metabolism regulated
PXR	3-keto-LCA > LCA > DCA = CA	PXR/HNF4α/PGC1α PXR/FGF19	CYP7A1↓ OATPs↑ (OATP1B1, OATP1B3, OATP2), MRPs↑(MRP2, MRP3, MRP4, and MRP5), MDR1↑ CYPs↑(CYP3A, CYP2B,CYP2C, CYP1A) UGTs↑ (UGT1A1, UGT1A6, UGT1A3, UGT1A4), SULTs↑(SULT2A1), GSTs↑(GSTA1,GSTA2,GSTM1)	Inhibited *de novo* bile acid synthesis Enhanced xenobiotics and bile acid transport Promoted Phase I and II detoxification	Xenobiotics and bile acid detoxification
		PXR/Creb and Foxo1 PXR/Hnf4α/Pgc1α	G6pase↓, Pepck↓,	Decreased gluconeogenesis	Hepatic Glucose
		PXR PXR/Foxa2 PXR	Cd36↑,Pparγ2↑, Scd1↑ Cpt1a↓, Hmgcs2↓ Cyp27a1↑, Abca1↑, Abcg1↑, ApoA1↑	Promoted lipogenesis Suppressed β-oxidation and ketogenesis Enhanced cholesterol detoxification	Lipid, Cholesterol
			Dio2, Pgc-1α, Pgc-1β, Cidea, and Ucp-3	Increased energy expenditure	Energy metabolism
VDR	LCA>DCA>CA	VDR/RXR VDR/HNF4α	CYP2↑, CYP3A↑, SULT2A1↑ MDR1↑, MRP3↑ CYP7A1↓	Promoted Phase I and II detoxification Promoted xenobiotics transportation Inhibited of *de novo* bile acid synthesis	Xenobiotics and bile acid detoxification
			Calbindin D_{9K}, Ca^{2+}ATPase, TRPV6, CYP24	Elevated serum calcium originating from enhanced intestinal absorption and bone mobilization	Calcium metabolism
			IFN-γ↓, IL-2↓, IL-17↓, IL-23↓, IL-10↑	Attenuated inflammation	inflammation
			EGF-R, c-MYC, K16	Induced apoptosis Inhibited proliferation	Proliferation

Chapter 2

Orthogonal Comparison of GC-MS and ^{1}H NMR Spectroscopy for Short Chain Fatty Acid Quantitation

Published in the Analytical Chemistry

Anal. Chem., 2017, 89 (15), pp 7900–7906

DOI: 10.1021/acs.analchem.7b00848

Jingwei Cai[1], Jingtao Zhang[1], Yuan Tian[1,2], Limin Zhang[2], Emmanuel Hatzakis[4], Kristopher W. Krausz[5], Philip B. Smith[3], Frank J. Gonzalez[5], Andrew D. Patterson[1]

Affiliations: [1]Center for Molecular Toxicology and Carcinogenesis, Department of Veterinary and Biomedical Sciences, Pennsylvania State University, University Park, State College, Pennsylvania, 16802, USA; [2]CAS Key Laboratory of Magnetic Resonance in Biological Systems, State Key Laboratory of Magnetic Resonance and Atomic and Molecular Physics, National Centre for Magnetic Resonance in Wuhan, Wuhan Institute of Physics and Mathematics, Chinese Academy of Sciences (CAS), Wuhan 430071, China; [3]Metabolomics Facility, Huck Institutes of Life Sciences, Pennsylvania State University, University Park, State College, Pennsylvania, 16802, USA; [4]Department of Chemistry, Pennsylvania State University, University Park, Pennsylvania, 16802, USA; [5]Laboratory of Metabolism, National Cancer Institute, NIH, Bethesda, Maryland, 20892, USA

Contributions: JC and ADP conceived and coordinated the study and wrote the manuscript. JC designed, performed, and analyzed the data of SCFAs method comparison with GC-MS and NMR shown in Figure 2-1 to 2-10, Table 2-1 to 2-3. JZ, YT, LZ, EH contributed to the NMR data interpretation and technical support shown in Figure 2-4, 2-5 and 2-8. PBS provided technical assistance with GC-MS analysis. KWK and FJG contributed to the data interpretation and preparation of the manuscript. All authors reviewed the results and approved the final version of the manuscript.

ABSTRACT

Short chain fatty acids (SCFAs) are important regulators of host physiology and metabolism and may contribute to obesity and associated metabolic diseases. Interest in SCFAs has increased in part due to the recognized importance of how production of SCFAs by the microbiota may signal to the host. Therefore, reliable, reproducible, and affordable methods for SCFA profiling are required for accurate identification and quantitation. In the current study, four different methods for SCFA (acetic acid, propionic acid, and butyric acid) extraction and quantitation were compared using two independent platforms including gas chromatography coupled with mass spectrometry (GC-MS) and ^{1}H nuclear magnetic resonance (NMR) spectroscopy. Sensitivity, recovery, repeatability, matrix effect, and validation using mouse fecal samples were determined across all methods. The GC-MS propyl esterification method exhibited superior sensitivity for acetic acid and butyric acid measurement (LOD<0.01 μg mL^{-1}, LOQ<0.1 μg mL^{-1}) and recovery accuracy (99.4%-108.3% recovery rate for 100 μg mL^{-1} SCFA mixed standard spike in and 97.8%-101.8% recovery rate for 250 μg mL^{-1} SCFAs mixed standard spike in). NMR methods by either quantitation relative to an internal standard or quantitation using a calibration curve, yielded better repeatability and minimal matrix effects compared to GC-MS methods. All methods generated good calibration curve linearity (R^2>0.99) and comparable measurement of fecal SCFA concentration. Lastly, these methods were used to quantitate fecal SCFAs obtained from conventionally-raised (CONV-R) and germ free (GF) mice. Results from global metabolomic analysis of feces generated by ^{1}H NMR and bomb calorimetry were used to further validate these approaches.

INTRODUCTION

It is generally appreciated that compositional and functional changes in the gut microbiota promote or modify metabolic diseases (1, 2). The gut microbiota impact host metabolism by producing or catabolizing metabolites (e.g., short chain fatty acids, SCFA), generating a barrier against pathogens (3, 4), and altering the physiological activity of the host (5, 6). An important activity of the gut microbiota is fermentation of non-digestible dietary fibers to produce SCFAs. SCFAs are fatty acids with an aliphatic tail less than six carbons and the primary fermentation-derived SCFAs are acetic acid (C2), propionic acid (C3) and butyric acid (C4). Ninety percent of SCFAs derived by bacterial fermentation are reabsorbed rapidly in the colon (7), utilized by the host as an energy source (8), and serve as anabolic substrates or precursors for biogenic synthesis (9). Acetate is the most abundant SCFA in colon where it is transported to the liver and transformed into acetyl-CoA, a precursor for lipogenesis (9) and gluconeogenesis (10). Further, acetic acid was reported to be involved in central appetite regulation for energy intake control (11, 12). Propionic acid provides beneficial effects including anti-gluconeogenic (13, 14), anti-lipogenic (14, 15), anti-cholesterogenic (15, 16), anti-inflammatory (17, 18) and anti-carcinogenic (17, 19) activity. Butyric acid serves as a preferred nutrient for colonocytes (20, 21) and is implicated in colonic mucosa proliferation, intestinal lining integrity maintenance (21, 22), colonic inflammation attenuation (23, 24), and colonic cancer prevention (23, 25) and treatment (26, 27). The discovery of the metabolic, immunological, and physiological implications of SCFAs has strengthened the demand for effective and precise quantitation approaches.

Given the biological significance of SCFAs, MS- and NMR-based metabolomics are utilized for SCFAs measurement in the past decades. A basic analytical question is therefore raised regarding the complementarity and reproducibility of quantitation methods. Or to what extent can current techniques (GC-MS or NMR) be combined to increase the analytical confidence and minimize irreproducible measurements. To compare the quantitative performance of GC-MS-based and NMR-based techniques for SCFAs measurement in biological samples, four common SCFA quantitation methods were assessed including GC-MS-based propyl esterification method (28), GC-MS-based acidified water extraction method (29, 30), ^{1}H NMR-based quantitation relative to the reference compound sodium 3-trimethylsilyl [2,2,3,3-d4] propionate (TSP-d4), and ^{1}H NMR based quantitation with calibration curve **(Figure 2-1)**. Validation indices including sensitivity, recovery accuracy, repeatability, matrix effect, and biological concentrations were compared and evaluated across all methods. The methods were also applied to a comparison of conventional and germ-free mouse feces and further validated by NMR metabolic fingerprinting profiling and bomb calorimetry.

MATERIALS AND METHODS

Chemical and Reagents

Acetic acid, propionic acid and butyric acid, 1- ^{13}C acetate, 1-^{13}C propionate, 1-^{13}C butyrate, 1-propanol, pyridine sodium chloride, K_2HPO_4, and NaH_2PO_4 were purchased from Sigma-Aldrich Chemical Co. Ltd. (St. Louis, MO). Hexane and methanol were purchased from EMD Chemicals Inc (Gibbstown, NJ). Internal standard hexanoic acid-6,6,6-d_3 was obtained from C/D/N Isotopes Inc (Pointe-Claire, Quebec, Canada).

Sodium 3-trimethylsilyl [2,2,3,3-d_4], propionate (TSP-d_4) and D_2O (99.9% in D) were purchased from Cambridge Isotope Laboratories (Miami, FL). Standard benzoic acid pellets were obtained from Parr Instrument Company (Moline, IL). All compounds were of the highest grade available.

Animal Samples

For the method assessment experiment, feces obtained from conventionally-raised C57BL/6J wild-type male mice (Jackson Laboratory, Bar Harbor, Maine) were pooled and measured. For method validation experiments, fresh feces were obtained from conventionally- raised mice and germ free mice (The Pennsylvania State University Gnotobiotic Facility).

Gas Chromatography–Mass Spectrometry (GC-MS) Analysis Procedure

Preparation of Standard SCFAs and Calibration for GC-MS Methods

Acetic acid, propionic acid and butyric acid stock solutions at 10 mg mL^{-1} and internal standard hexanoic acid-6,6,6-d_3 solution at 100 µg mL^{-1} were prepared by dissolving individual SCFAs or internal standard in the calculated amount of HPLC water based on the initial stock density of each compound. The three 10 mg mL^{-1} SCFAs solutions and the 100 µg mL^{-1} internal standard solution were pooled together then to generate a final concentration 500 µg mL^{-1} of each SCFAs containing 10 µg mL^{-1} internal standard. Pooled solution was further diluted by 10 µg mL^{-1} internal standard solution to obtain 500 µg mL^{-1}, 250 µg mL^{-1}, 100 µg mL^{-1}, 50 µg mL^{-1}, 25 µg mL^{-1}, 10 µg mL^{-1}, 5 µg mL^{-1}, 1 µg mL^{-1}, 0.5 µg mL^{-1} 0.1 µg mL^{-1} SCFAs containing 10 µg mL^{-1} internal

standard. The calibration curve was constructed by plotting relative peak area of each SCFA (peak area of SCFA was normalized to peak area of internal standard) to the corresponding concentration of SCFA standard. By normalizing the peak area to that of the internal standard, the potential variabilities in the instrument conditions, injection volumes and mass spectrometer response would expected be corrected.

GC-MS Sample Preparation

Fresh feces collected randomly from wild type mice was pooled and spiked with 1-^{13}C SCFAs at different concentration levels (250 µg mL^{-1}, 100 µg mL^{-1}, 10 µg mL^{-1}). For the propyl esterification method (28), 50 mg of 1-^{13}C SCFAs spiked feces were mixed with 1 mL of 0.005 M NaOH (containing 10 µg mL^{-1} internal standard hexanoic acid-6,6,6-d3), homogenized (Bertin Technologies, Rockville, MD) at 6500 rpm, 1 cycle, 60s with 1.0 mm diameter Zirconia/Silica beads (BioSpec, Bartlesville, OK) added and then centrifuged (Eppendorf, Hamburg, Germany) at 13,200 x g, 4 °C, 20 min. The supernatant was collected and mixed with an aliquot of 500 µL of 1-propanol/pyridine (v/v=3:2) mixture. 100 µL of propyl chloroformate subsequently was added following a brief vortex for 1 minute. Samples were derivatized in an incubator (Thermo Scientific, Marietta OH) at 60 °C for an hour. The derivatized samples were extracted with a two-step hexane extraction (300 µL + 200 µL). A total 500 µL volume of extracts were obtained and stored at -20 °C for GC-MS quantitation. For the acidified water-extraction method, 50 mg of 1-^{13}C SCFAs spiked fecal samples were mixed with 1 mL HPLC water containing 10 µg mL^{-1} internal standard hexanoic acid-6,6,6-d3. The mixture then was homogenized and the pH of the suspension was adjusted to 2-3 by adding 12 M HCl (29).

The suspension was kept at room temperature for 10 min with occasional shaking then centrifuged at 13200 x g, 4 °C, 20 min. The supernatant was transferred to autosampler and stored at 4°C for GC-MS analysis.

Experimental Condition for GC-MS Methods

SCFAs were quantified with an Agilent 7890A gas chromatograph coupled with an Agilent 5975 mass spectrometer (Agilent Technologies Santa Clara, CA). The experimental conditions of propyl esterification method and acidified water extraction method are as previously described (28, 30).

For propyl esterification method, a HP-5 ms (5%-Phenyl-methylpolysiloxane) capillary GC column (30 m x 250 μm i.d. 0.25 μm film thickness, Agilent Technologies) was employed with helium as the carrier gas at a constant flow rate of 1 mL/min. samples (0.5 uL) were injected using a pressure pulsed split mode (10 psi) with a split ratio of 10:1. The initial column oven temperature was 50ºC for 2 min and then increased to 70ºC at a rate of 10ºC /min, and then increased to 85ºC at a rate of 3 ºC/min, then increased to 110ºC at a rate of 5ºC /min, and then increased at a rate of 30ºC/min to a final temperature of 290ºC where it was held for 5 min. The temperatures of the front inlet, transfer line and mass source were set at 260ºC, 290ºC, and 230ºC, respectively. The total run time was 25 min and the mass spectral data was collected in full scan mode with a mass range 30-300 m/z.

For the acidified water extraction method2, a NUKOL (cross-linked and bonded acid-modified polyethylene glycol) capillary GC column, (30m × 250μm × 0.25μm, Supelco, Bellefonte, PA) was employed, with helium as carrier gas at a constant flow rate

of 1 mL/min. Samples (0.5 μL) were injected using a pressure pulsed split mode (10 psi) with a split ration of 10:1. The initial column oven temperature was 100 ºC for 1min, and then increased to 120 ºC at a rate of 10ºC/min and held for 5 min, then increased to a final temperature of 220 ºC at a rate of 30ºC/min and held for 3 min. The total run time was 14.3 min and all the data was collected in full scan mode with a mass range of 40-300 m/z.

GC-MS Spectra Data Processing

All data were processed with Enhanced Chemstation (Agilent MSD chemstation). The peak area of extracted ions and retention time of each peak signal were calculated by the ion integration tools in Enhanced Chemstation. Standard SCFAs were identified by matching mass spectra in NIST 2011 Library with a match index over 90 and further confirmed by comparing spectra and retention time with reference (28) (**Figure 2-2**). Sample SCFAs were identified by comparing spectra retention time with standard SCFAs. The following extracted ions and retention time were used for determining the concentration of unlabeled and 1-^{13}C labeled of SCFAs (**Figure 2-3**). For the propyl esterification method (**Figure 2-3 A-C**), *m/z* 43 at 2.73 min for unlabeled acetic acid, *m/z* 44 at 2.73 min for [1-^{13}C acetic acid]; *m/z* 57 at 4.01 min for unlabeled propionic acid, *m/z* 58 at 4.01 min for [1-^{13}C propionic acid]; and, *m/z* 71 at 5.66 min for unlabeled butyric acid, *m/z* 72 at 5.66 min for [1-^{13}C butyric acid]. For the acidified water extraction method (**Figure 2-3 D-F**), *m/z* 43 at 5.62 min for unlabeled acetic acid, *m/z* 44 at 5.66 min for [1-^{13}C acetic acid]; *m/z* 74 at 7.40 min for unlabeled propionic acid, *m/z* 75 at 7.47 min for [1-^{13}C propionic acid]; and *m/z* 60 at 9.27 min for unlabeled butyric acid,

m/z 61 at 9.31 min for [1-^{13}C butyric acid];. The integrated areas for all SCFAs were normalized with the internal standard and quantified with standard curve constructed.

GC Method Validation

Sensitivity

Sensitivity is expressed by three indexes; limit of detection (LOD), limit of quantitation (LOQ), and linear range (LR). LOD represents the lowest detectable concentration of an individual SCFA in a sample with a signal-to-noise ratio greater than three. LOQ is the lowest concentration of SCFA in a sample which can be quantitatively determined with a signal-to-noise ratio above ten (31). LR is defined as the concentration range where the calibration curve displays linearity with correlation coefficient R^2 >0.99.

Precision

Precision was expressed as recovery rate determined at three concentrations (250 µg mL^{-1}, 100 µg mL^{-1}, 10 µg mL^{-1}). Six fecal samples spiked with 1-^{13}C SCFAs were analyzed. The fecal suspension without adding the SCFA standards was also analyzed to determine the initial amount of targeted compound present in the sample. Recovery rate was calculated by comparing calculated 1-^{13}C standards concentration with the nominal concentration. Specifically, percent recovery (%R) was calculated using the following equation: %R = (quantified 1-^{13}C SCFAs standards spiked in fecal sample-initial amount of 1-^{13}C SCFAs present in the fecal samples)/ nominal standards conc.× 100.

Repeatability

Repeatability was expressed by intra-day and inter-day relative standard deviation (%RSD). Intra-day repeatability was determined by running the same standard samples five times a day within a 24 hour interval. Inter-day precision measurement was performed on the same samples on five different days. Mean and standard deviation of peak area of extracted ions for each injection were obtained. %RSD = standard deviation/ mean × 100.

Matrix Effect

Matrix effect was evaluated by comparing the response of the pure SCFA standards dissolved in extract solvent with the response of the SCFAs in the fecal matrix. Different concentrations of pure 1-^{13}C SCFAs standards were spiked in either fecal suspensions or extract solvent. Unspiked samples were also analyzed to substrate the initial amount of SCFAs present in the samples out. The percent Matrix Effect (%ME) = (Normalized area of SCFA in spiked fecal samples - normalized area of SCFAs of the unspiked fecal samples)/ normalized area of SCFA in extract solvent.

Nuclear Magnetic Resonance (NMR) Spectroscopy

SCFA Standard and Sample Preparation

Fecal samples (50-60 mg) were extracted with 1 mL of phosphate buffer (K_2HPO_4/NaH_2PO_4, 0.1 M, pH 7.4, 50% v/v D_2O) containing 145.1 µM TSP-d4 as a chemical shift reference (δ 0.00). The samples were freeze-thawed three times with liquid nitrogen then homogenized (6500 rpm, 1 cycle, 60s) and centrifuged (11,180 x g, 4°C, 10 min). The supernatants were transferred to a new tube, and another 600 µL of PBS was

added to the pellets followed by the same procedure described above. Fecal supernatants were combined and centrifuged (max speed, 4°C, 10 min), then spiked with the SCFA standards at three final concentrations (250 μg mL^{-1}, 100 μg mL^{-1}, 10 μg mL^{-1}), and 600 μL of spiked fecal extract was transferred to a 5 mm NMR tube (Norell, Morganton, NC). Unspiked fecal supernatants were also analyzed to determine the initial amount of each SCFA presented in the sample.

^{1}H NMR Spectra Acquisition

In detail, All of the ^{1}H NMR spectra were recorded at 298 K on a Bruker NMR spectrometer (600 MHz for ^{1}H) equipped with a 5-mm inverse cryogenic probe as previously described (32). A standard one-dimensional pulse sequence noesypr1d (recycle delay-90°-t1-90°-tm-90°-acquisition) was used with a 90 pulse length of approximately 10 μs (-9.6 dbW). 64 transients were collected into 65,536 data points for each spectrum, with a spectral width of 9.6 KHz. Receive gain was automatically set to 12. Water suppression was achieved with a weak irradiation during the recycle delay (4 s) and mixing time (50 ms). The spectra were acquired without spinning the NMR tube in order to avoid artifacts, such as spinning side bands of the first or higher order. Chemical shifts are reported in ppm from TSP (δ = 0.00). For quantitation purpose, a repetition time ≥ 5T1 are typically used to ensure quantitative results. The total repetition time (relaxation delay of 5s, recycle delay of 4s, and acquisition time of 3.4 s) is 12.4 s (5 × the longest relaxation time of 2.4s T1 of acetic acid) was therefore used here. For the resonance assignment, two-dimensional ^{1}H–^{1}H total correlation spectroscopy (TOCSY) NMR spectroscopy (**Figure 2-4**) and ^{1}H-^{13}C heteronuclear single quantum correlation

(HSQC) NMR spectroscopy (**Figure 2-5**) spectra were acquired. In TOSCY experiment, pulse sequence dipsi2phpr was used with the mixing time of 60 ms. 64 transients were collected into 2K data points for each of the 256 increments, and the spectral widths were 6009 Hz for both ^{1}H dimensions. In HSQC experiment, a Bruker standard pulse sequence hsqcetgpsisp2.2 was employed. Globally alternating optimized rectangular pulses was employed for ^{13}C-decoupling during the acquisition period, 360 transients for each of 150 increments were collected into 2K data points with spectral width of 6009 in F2 dimension (^{1}H) and 26409 HZ in the F1 dimension (^{13}C).

^{1}H NMR Quantitation Analysis

Quantitation relative to TSP-d_4 reference Due to the basic NMR theory that the integrated area of a given ^{1}H NMR signal is proportional to the proton number, the concentration of target metabolites can be measured by equating the integral areas of the target metabolites and a reference compound with known proton number and concentration (33). TSP-d_4 area of one sharp singlet (Regions δ 0.00) formed by three methyl groups (9H) of TSP-d_4 were chosen as a reference for quantitation. Acetate, propionate and butyrate were identified with 2D ^{1}H-^{1}H TOCSY NMR spectroscopy (**Figure 2-4**) and 2D ^{1}H-^{13}C HSQC NMR spectroscopy (**Figure 2-5**). Regions of δ 1.91 (acetate-methyl group, 3H), δ 1.06 (fully resolved left peak of propionate-methyl group triplet, which account for ¼ of the total area of the methyl-group, 3H), δ 0.90 (butyrate-methyl group, 3H) were integrated. Concentration of acetate, propionate and butyrate were calculated using the following formula based on the basic NMR quantitation equation previously described (33)

Molarity of acetate or butyrate= (9 × Molarity of TSP-d_4 × Area of acetate or butyrate)/ (3× Area of TSP-d_4);

Molarity of propionate=4 × (9 × Molarity of TSP-d_4 × Area of propionate)/ (3 × Area of TSP-d_4)

Quantitation with calibration curve A stock solution containing the mixture of SCFAs standards in 0.1 M phosphate buffer containing 145.1 µM TSP-d4 was diluted to obtain a calibration curve ranging from 250 µg mL^{-1} to 1 µg mL^{-1}. Peak area of each SCFAs was calculated with represented regions described above. All integrated area was normalized to the signal area of TSP-d_4 (δ 0.00). The calibration curve was constructed by plotting the normalized peak area versus concentration of individual SCFAs. The relative peak area of the SCFAs in fecal extract was integrated and the concentration of SCFAs in fecal extract was calculated by the calibration curve.

^{1}H NMR Spectra processing and Multivariate Data Analysis

Quality of all ^{1}H NMR Spectra were improved by manually adjusting phase and baseline using Topspin 3.0 (Bruker Biospin, Germany). The chemical shift was referenced to the TSP-d_4 (δ 0.0 The spectra were bucketed into 0.004 ppm bins by AMIX 3.9.14 software (Bruker Biospin, Germany). The residual water signal (region δ 4.2-5.2) was removed prior to normalization. The binned spectral data were normalized to the sum of total intensity of the spectrum to compensate for the overall concentration differences. Multivariate data analysis was performed with SIMCA 13 (Umetrics, Sweden). Orthogonal Projection to Latent Structures with Discriminant Analysis (OPLS-DA) were used to process NMR data. To perform OPLS-DA, a binary variable for Y is created and

assigned when defining a class (in this case, conventionally raised mice group is 0, germ-free mice group is 1) before importing to SIMCA. After importing the data in SIMCA, OPLS-DA was selected for modelling with UV scaling. A 7-fold cross validation method was employed to validate the OPLS-DA models and the R^2X and Q^2 values generated from the method represent the predictive power and validity of the models, respectively. The validation of the OPLS-DA model was further confirmed by ANOVA of the cross-validated residuals (CV-ANOVA) analysis (implemented in SIMCA 13) (34).To facilitate interpretation of the results, color-coded loading plots were generated from the OPLS-DA to facilitate result interpretation as previously described (32).

Bomb Calorimetry

Bomb calorimetry was performed on a 6200 isoperibol calorimeter (Parr Instrument Company, Moline, IL). Fecal samples (100 mg) were weighed and ground in a clean mortar and pestle. Ground samples were pressed into ¼ inch diameter pellets (Parr 2812 Pellet Press, Moline, IL). Extra moisture content was removed from pellet using speedvac concentrator (Thermo Fish Scientific, Marietta, OH). ¼ inch diameter benzoic acid pellets were used for standardization. Samples were placed in a tared fuel capsule (208AC) in the 1109A semi-micro oxygen bombs (Parr Instrument Company, Moline, IL) and fixed by a coiled 10 cm of NiCr fuse wire (PN 45C10). A minimum 99.5% purity oxygen was provided with 420 psig pressure to the bomb. Prepared Semi-micro bomb was set on a ring support in the A604DD twin-chambered calorimeter bucket. Gross heat of samples was determined by temperature change recorded by

calorimeter resulting from energy released by the combustion, expressed as calories/gram feces. Each gross heat was averaged from duplications.

Method Validation and Application

^{1}H NMR-based SCFAs quantitation methods based on TSP-d_4 as a reference or on the calibration curve were validated by measurement of accuracy, repeatability, sensitivity, and matrix effect. Further, the methods described were applied to investigate the SCFAs level and metabolic status differences between CONV-R and GF mice combined with bomb calorimetry technique.

Statistical Analysis

Graphical illustrations and statistical analyses were performed using Prism version 6. All data values were expressed as mean ± SEM. Statistical significance was defined as $p<0.05$.

RESULTS AND DISCUSSION

Linearity and Sensitivity of GC-MS-Based and NMR-Based Methods

The linearity (i.e., the correlation between numerical points), calibration range, LOD, LOQ, and calibration curve are extremely critical to assess the sensitivity and application of an analytical method. As summarized in **Table 2-1**, all calibration curves generated from four orders of magnitude of SCFA standard mixture demonstrated satisfactory linearity ($R^2>0.99$) thus indicating that these methods could be employed extensively for quantifying SCFAs in biological samples with a wide range of

concentrations. The GC-MS propyl esterification method yielded the lowest LOD and LOQ for acetic acid (LOD = 0.002 μg mL^{-1}, LOQ = 0.02 μg mL^{-1}) and butyric acid (LOD = 0.01 μg mL^{-1}, LOQ = 0.09 μg mL^{-1}). Propionate LOD/LOQ was not calculated as it could be detected in the background due to impurity in the derivatization solvent (28), whereas the GC-MS acidified water method (non-derivatization) showed a relatively high LOD and LOQ for acetic acid (LOD = 0.5 μg mL^{-1}, LOQ = 5 μg mL^{-1}), propionic acid (LOD = 0.8 μg mL^{-1}, LOQ = 3 μg mL^{-1}) and butyric acid (LOD = 0.2 μg mL^{-1}, LOQ = 1 μg mL^{-1}). LOD and LOQ detected were comparable with previous studies using the acidified water extraction method (29, 30). Comparison of LOD and LOQ between derivatization and non-derivatization methods suggested that the improved volatility with derivatization increased the sensitivity compared to the non-derivatization method. Due to the high sensitivity of the derivatization approach, concentrations above 250 μg mL^{-1} saturated the detector thus compromising linearity. However, the acidified water method could quantify higher concentrations due to the relatively low sensitivity. Detectable SCFAs concentrations for the NMR method are approximately 2 μg mL^{-1}, 100 fold less sensitive than GC-MS methods, which ranged from 0.002-0.01 μg mL^{-1}. Quantifiable SCFAs levels by the NMR method started from 4 μg mL^{-1}, significantly higher than GC-MS propyl esterification method which started from 0.02 μg mL^{-1}.

Recovery and Matrix Effect of Measurement Based on Spiked Sample Matrix

Recovery assessment was done by measuring a known amount of SCFA spiked into the biological matrix. Recovery is an informative indicator of whether the method presents satisfactory precision with interference from the biological matrix and bias

created during sample preparation and analysis. In the current study, 250 μg mL^{-1}, 100 μg mL^{-1}, and 10 μg mL^{-1} of 1-^{13}C SCFAs mixture was spiked in pooled fecal extracts and recovery was investigated by comparing the SCFA levels quantified by different methods and the expected concentration. GC-MS propyl esterification method was superior as almost 100% of 100 μg mL^{-1} and 250 μg mL^{-1} spiked concentration were recovered for all three SCFAs (**Table 2-2**). The GC-MS acidified water method showed better recovery at higher concentrations, ranging from 87.6% to 118.9%; however it was inferior to the GC-MS propyl esterification method at lower concentrations. The two NMR-based methods showed very similar recovery, demonstrating the stability of the NMR-based technique. However, the recovery rate is inferior to the GC-MS propyl esterification method. The matrix effect is defined as the difference between the response of standards in solvents and those in a biological matrix which is known to interfere with the chromatographic efficiency and introduce error in the mass spectroscopy-based technique (35, 36). Specific to the GC-MS based technique, matrix components may cause enhancement (37) or suppression (38) of the analyte signal thus severely affecting quantitative analysis. Numerous factors might contribute to the matrix effect including matrix components, extraction reagents, the procedure itself, the purity of the reference standards, analyte physico-chemical properties (stability, mass, charge, concentration), column used, and myriad other factors. To minimize matrix effect, both GC-MS based methods used reagents and standards of the highest grade available and the use of an internal standard to eliminate possible instrumentation errors. As shown in **Table 2-2**, the signal is suppressed by the matrix with GC-MS-based methods with a signal loss up to 24%, suggesting the accumulation of non-volatile matrix components from fecal extracts

like phospholipids and protein in the injection liner and column. The matrix effect introduced in NMR is usually due to pH, temperature, ionic strength, and protein content, resulting in peak position shifts and line width variations (39). The NMR quantitation method has reduced matrix effect compared to the GC-MS quantitation method, most likely due to the fact that it is less sensitive to matrix constituents and solvents and due to the simple extraction procedure (typically only requires dilution using phosphate buffer solution). In the present study, the NMR-based method demonstrated signal enhancement up to 18%, the majority of matrix effects are around 10% signal enhancement, except 10 μg mL^{-1} spiked in butyric acid, which exhibited significant matrix effect (36% signal suppression), likely due to interference signals from the branched chain amino acids (valine, leucine, isoleucine) with a resonance located δ 0.9, and compromised sensitivity in the low concentration range for the NMR-based quantitation method.

Intraday and Interday Repeatability Revealed Reliability of Different Methods

Repeatability assessment is a critical aspect of investigating alternative analytical methods for reliable and robust quantitation. High repeatability also increases quantitative accuracy and efficiency by minimizing experimental replicates. Repeatability is assessed for each measurement method separately from replicated measurement on the same set of samples and described by within-subject relative standard deviation (RSD). In the current study, replicated measurements of different concentrations of SCFAs standard mixture were performed five times either within the same day (intraday) or on five different days (interday) by the four different measurement methods (**Table 2-3**). Generally, the NMR-based techniques generated the smallest intraday and interday RSD

ranging from 0.3% to 6.7%, with 80% of the RSD below 3%. The GC-MS propyl esterification method presented better intraday and interday repeatability compared to GC-MS acidified water method, except for propionic acid. Due to introduction of propionate to the background with the GC-MS propyl esterification solvent (28), propionic acid measurement was inconsistent at the lowest concentration 10 μg mL^{-1}. The RSD for intraday and interday measurement reached 12.2% and 21.3%, respectively. Aside from the reduced impact from the matrix, the most attractive feature for NMR-based analytical techniques is the high repeatability. It is partially due to the unbiased detection nature of the NMR technique where the peak integrals relate directly to the chemical structure of the compound (number of protons giving rise to the peak in ^{1}H NMR), thus less interference from instrumentation and other external environmental factors would be introduced during intraday and interday repeated measurement. Further, the simple extraction process, non-volatile extraction solution, and non-destructive detection platform maintain the maximum level of integrity and stability of the samples, contributing to the high repeatability especially during interday measurement. Conversely, MS-based methods are highly dependent on instrumentation (injector, column, inlet, liner) and chromatographic conditions (40), sample preparation and storage (especially for highly volatile samples after derivatization), which raise issues with data repeatability and reproducibility between different research groups and research facilities (41). In the current study, GC-MS repeatability was improved (intraday and interday RSD of propyl esterification method ranging from 1.2% to 21.3% with 71% of the RSD below 7%, intraday and interday RSD of acidified water extraction method ranging from 2.4% to 12.6% with 67% of the RSD below 7%) through optimization of the instrument

parameters, chromatographic conditions, normalization with internal standards as well as the addition of multiple washes pre and post injection and blank samples run between injections to eliminate carryover. However extra attention for low level of propionic acid measurement using GC-MS propyl esterification methods is warranted (12.2% and 21.3% for intraday and interday RSD at 10 μg mL^{-1}, respectively), additional replicates or blank samples are requisite to minimize and/or understand background interference.

Application and Validation of SCFAs Quantitative Methods in CONV-R and GF Mice Feces Study

The SCFAs methods were used to quantify SCFAs levels in feces obtained from CONV-R and GF mice. SCFAs were measurable but significantly lower in GF mice feces compared to CONV-R mice feces ($p<0.001$, **Figure 2-6**), consistent with the level and proportion of SCFAs in GF mice previously reported. For example, Hoverstad et al (42) reported the following concentrations using the GC-MS acidified water method with additional steps including vacuum distillation, alkalization, evaporation, and dissolution: acetic acid=990±380 μmol/kg (equivalent to 59.4±22.8 μg/g), propionic acid=17±5.8 μmol/kg (equivalent to 1.3±0.4 μg/g), and butyric acid=7.1±3.6 μmol/kg (equivalent to 0.6±0.3 μg/g). For CONV-R mice, as shown in **Figure 2-7**, biological concentration of SCFAs determined with GC-MS and NMR techniques were not significantly different, providing further validation for the applicability of the methods compared in the current study. The GC-MS acidified water method captured the broadest range of the biological concentration for all three SCFAs measured, indicating the greatest variation and least stability. The SCFAs concentrations quantified with different methods in this study

(**Figure 2-7**) were in good agreement with reported proportion and quantity of three primary SCFAs in fecal samples measured with other methods. For example, Lu et al (43) reported mouse fecal SCFAs concentrations using modified GC-MS acidified water direct injection method as: acetic acid=1468±299 μg/g, propionic acid=285±94 μg/g, butyric acid=192±55 μg/g; García-Villalba et al (44) reported the following SCFAs concentrations in rat fecal samples extracted with ethyl acetate: acetic acid=2818.3 ± 720.7 μg/g, propionic acid= 268.5 ± 73.6 μg/g, butyric acid ranging from 1387.8 ± 613.3 μg/g. In addition, the global metabolic profile between CONV-R and GF mice feces generated by ^{1}H NMR (**Figure 2-8**) also revealed significant differences based on discriminant analysis (OPLS-DA, described by $R^2X=0.58$, $Q^2=0.976$) and CV-ANOVA test ($p<0.0001$), supporting a dramatically different metabolic status imparted by the gut microbiota. Moreover, PLS-DA using only the SCFAs regions (the chemical shift [ppm] at 1.92 [acetate], 1.06 [propionate] and 0.9 [butyrate]) obtained via the ^{1}H NMR approach were performed (**Figure 2-9**). The groups are clearly and significantly separated by only SCFAs ($R^2X=0.859$, $Q^2=0.972$, CV-ANOVA $p<0.0001$), suggesting SCFAs themselves are sufficient to distinguish CONV-R and GF mice. GF mice showed a significantly lower level of fermentation end products SCFAs (acetate, propionate, butyrate), branched chain amino acids (valine, leucine, isoleucine) and bacterial-associated metabolites like taurine (45). Moreover, reduced glucose, phenylalanine, tyrosine, tryptophan, urocanate, hypoxanthine, inosine, uracil, and increased histidine were seen in feces of GF mice comparing to CONV-R mice, indicating altered glucose, amino acid, and nucleotide metabolism due to lack of microbial activity. Further, fermentation substrates like raffinose, stachyose and many oligosaccharides were excreted in significantly higher

levels into feces for GF mice, demonstrating the reduced metabolism of those substrates due to the absence of gut microbiota. Fecal energy quantitation was conducted with bomb calorimetry to further investigate the metabolic status in GF and CONV-R mice feces. The gross heat of feces from GF mice was 4110±38.2 calorie per gram feces, approximately 140 calorie per gram higher than the gross heat of feces from CONV-R mice, which was 3970±12.2 calorie per gram (**Figure 2-10**). Excessive fecal energy excretion in GF mice is consistent with high level of fecal dietary fibers determined by ^{1}H NMR global metabolites profile. Because of the absence of bacterial fermentation in GF mice, host energy harvest capability and metabolic efficiency is reduced. Dietary fibers as potential energy sources are no longer accessible in the germ free gut and are excreted intact. The results are in good agreement with the previous studies from lean and obesity-resistant GF mice (46, 47), suggesting the feasibility of the described methods for metabolic studies.

CONCLUSION

High-throughput metabolite profiling approaches including GC-MS and ^{1}H NMR provide excellent platforms for quantitative detection of SCFAs in complex biological matrices. While MS-based methods, especially after derivatization, have incomparable sensitivity and precision, they can be influenced by matrix interference thus impacting repeatability. In practical applications, GC-MS propyl esterification method is highly recommended for trace/ultratrace detection of SCFAs in biological fluid(48) (plasma and urine) or intracellular SCFAs in cell culture and intestinal tissue. Because of the easier sample preparation procedure and short run time, GC-MS acidified water method is most

suitable for studies with large quantity, including samples from biodigesters or large-scale human studies. Alternatively, NMR-based methods, while exhibiting relatively low sensitivity, exhibit high repeatability and low matrix effect due to the nondestructive and noninvasive sample preparation and measurement technique. Additionally, NMR spectroscopy provides informative metabolic profiles of the overall metabolic characteristics, thus it is best suited to measure cecal or fecal samples (higher SCFA concentration). In the CONV-R and GF mice feces study, the combination of GC-MS and NMR provided comprehensive and complementary views of SCFAs status and overall metabolic profile. Bomb calorimetry further confirmed the compromised energy harvesting capability of GF mice. Three mutually independent methods, GC-MS, NMR, and bomb calorimetry led to consistent results, demonstrating the feasibility of the techniques used in metabolomics studies and the critical function that gut microbiota play in host energy balance and metabolic status.

REFERENCE

1. Ley RE, Backhed F, Turnbaugh P, Lozupone CA, Knight RD, and Gordon JI. Obesity alters gut microbial ecology. *Proc Natl Acad Sci U S A.* 2005;102(31):11070-5.
2. Serino M, Luche E, Gres S, Baylac A, Berge M, Cenac C, Waget A, Klopp P, Iacovoni J, Klopp C, et al. Metabolic adaptation to a high-fat diet is associated with a change in the gut microbiota. *Gut.* 2012;61(4):543-53.
3. Natividad JM, and Verdu EF. Modulation of intestinal barrier by intestinal microbiota: pathological and therapeutic implications. *Pharmacol Res.* 2013;69(1):42-51.
4. Sharma R, Young C, and Neu J. Molecular modulation of intestinal epithelial barrier: contribution of microbiota. *J Biomed Biotechnol.* 2010;2010(305879.
5. Blumberg R, and Powrie F. Microbiota, disease, and back to health: a metastable journey. *Sci Transl Med.* 2012;4(137):137rv7.
6. Hooper LV, Wong MH, Thelin A, Hansson L, Falk PG, and Gordon JI. Molecular analysis of commensal host-microbial relationships in the intestine. *Science.* 2001;291(5505):881-4.
7. Ruppin H, Bar-Meir S, Soergel KH, Wood CM, and Schmitt MG, Jr. Absorption of short-chain fatty acids by the colon. *Gastroenterology.* 1980;78(6):1500-7.
8. Mcneil NI. The Contribution of the Large-Intestine to Energy Supplies in Man. *Am J Clin Nutr.* 1984;39(2):338-42.
9. Zambell KL, Fitch MD, and Fleming SE. Acetate and butyrate are the major substrates for de novo lipogenesis in rat colonic epithelial cells. *J Nutr.* 2003;133(11):3509-15.
10. Wolever TMS. Short-Chain Fatty-Acids and Carbohydrate-Metabolism. *Falk Symp.* 1994;73(251-9.
11. Byrne CS, Chambers ES, Morrison DJ, and Frost G. The role of short chain fatty acids in appetite regulation and energy homeostasis. *Int J Obesity.* 2015;39(9):1331-8.
12. Frost G, Sleeth ML, Sahuri-Arisoylu M, Lizarbe B, Cerdan S, Brody L, Anastasovska J, Ghourab S, Hankir M, Zhang S, et al. The short-chain fatty acid acetate reduces appetite via a central homeostatic mechanism. *Nat Commun.* 2014;5(
13. Ximenes HM, Hirata AE, Rocha MS, Curi R, and Carpinelli AR. Propionate inhibits glucose-induced insulin secretion in isolated rat pancreatic islets. *Cell Biochem Funct.* 2007;25(2):173-8.
14. Chambers ES, Viardot A, Psichas A, Morrison DJ, Murphy KG, Zac-Varghese SE, MacDougall K, Preston T, Tedford C, Finlayson GS, et al. Effects of targeted delivery of propionate to the human colon on appetite regulation, body weight maintenance and adiposity in overweight adults. *Gut.* 2015;64(11):1744-54.
15. Weitkunat K, Schumann S, Nickel D, Kappo KA, Petzke KJ, Kipp AP, Blaut M, and Klaus S. Importance of propionate for the repression of hepatic lipogenesis and improvement of insulin sensitivity in high-fat diet-induced obesity. *Mol Nutr Food Res.* 2016.
16. Anderson JW, and Siesel AE. Hypocholesterolemic effects of oat products. *Adv Exp Med Biol.* 1990;270(17-36.
17. Hosseini E, Grootaert C, Verstraete W, and Van de Wiele T. Propionate as a health-promoting microbial metabolite in the human gut. *Nutr Rev.* 2011;69(5):245-58.
18. Tong LC, Wang Y, Wang ZB, Liu WY, Sun S, Li L, Su DF, and Zhang LC. Propionate Ameliorates Dextran Sodium Sulfate-Induced Colitis by Improving Intestinal Barrier Function and Reducing Inflammation and Oxidative Stress. *Front Pharmacol.* 2016;7(253.
19. Bindels LB, Porporato P, Dewulf EM, Verrax J, Neyrinck AM, Martin JC, Scott KP, Buc Calderon P, Feron O, Muccioli GG, et al. Gut microbiota-derived propionate reduces cancer cell proliferation in the liver. *Br J Cancer.* 2012;107(8):1337-44.

20. Roediger WE. Utilization of nutrients by isolated epithelial cells of the rat colon. *Gastroenterology.* 1982;83(2):424-9.
21. Velazquez OC, Lederer HM, and Rombeau JL. Butyrate and the colonocyte. Production, absorption, metabolism, and therapeutic implications. *Adv Exp Med Biol.* 1997;427(123-34.
22. Frankel W, Lew J, Su B, Bain A, Klurfeld D, Einhorn E, MacDermott RP, and Rombeau J. Butyrate increases colonocyte protein synthesis in ulcerative colitis. *J Surg Res.* 1994;57(1):210-4.
23. Qiao Y, Qian J, Lu Q, Tian Y, Chen Q, and Zhang Y. Protective effects of butyrate on intestinal ischemia-reperfusion injury in rats. *J Surg Res.* 2015;197(2):324-30.
24. Cushing K, Alvarado DM, and Ciorba MA. Butyrate and Mucosal Inflammation: New Scientific Evidence Supports Clinical Observation. *Clin Transl Gastroenterol.* 2015;6(e108.
25. Scharlau D, Borowicki A, Habermann N, Hofmann T, Klenow S, Miene C, Munjal U, Stein K, and Glei M. Mechanisms of primary cancer prevention by butyrate and other products formed during gut flora-mediated fermentation of dietary fibre. *Mutat Res.* 2009;682(1):39-53.
26. Blouin JM, Penot G, Collinet M, Nacfer M, Forest C, Laurent-Puig P, Coumoul X, Barouki R, Benelli C, and Bortoli S. Butyrate elicits a metabolic switch in human colon cancer cells by targeting the pyruvate dehydrogenase complex. *Int J Cancer.* 2011;128(11):2591-601.
27. Pouillart PR. Role of butyric acid and its derivatives in the treatment of colorectal cancer and hemoglobinopathies. *Life Sci.* 1998;63(20):1739-60.
28. Zheng X, Qiu Y, Zhong W, Baxter S, Su M, Li Q, Xie G, Ore BM, Qiao S, Spencer MD, et al. A targeted metabolomic protocol for short-chain fatty acids and branched-chain amino acids. *Metabolomics.* 2013;9(4):818-27.
29. Zhao G, Nyman M, and Jonsson JA. Rapid determination of short-chain fatty acids in colonic contents and faeces of humans and rats by acidified water-extraction and direct-injection gas chromatography. *Biomed Chromatogr.* 2006;20(8):674-82.
30. Mulat DG, and Feilberg A. GC/MS method for determining carbon isotope enrichment and concentration of underivatized short-chain fatty acids by direct aqueous solution injection of biogas digester samples. *Talanta.* 2015;143(56-63.
31. Currie LA. Nomenclature in Evaluation of Analytical Methods Including Detection and Quantification Capabilities (Iupac Recommendations 1995). *Pure Appl Chem.* 1995;67(10):1699-723.
32. Zhang L, Nichols RG, Correll J, Murray IA, Tanaka N, Smith PB, Hubbard TD, Sebastian A, Albert I, Hatzakis E, et al. Persistent Organic Pollutants Modify Gut Microbiota-Host Metabolic Homeostasis in Mice Through Aryl Hydrocarbon Receptor Activation. *Environ Health Perspect.* 2015;123(7):679-88.
33. Dai H, Xiao C, Liu H, and Tang H. Combined NMR and LC-MS analysis reveals the metabonomic changes in Salvia miltiorrhiza Bunge induced by water depletion. *J Proteome Res.* 2010;9(3):1460-75.
34. Eriksson L, Trygg J, and Wold S. CV-ANOVA for significance testing of PLS and OPLS (R) models. *J Chemometr.* 2008;22(11-12):594-600.
35. Rogatsky E, and Stein D. Evaluation of matrix effect and chromatography efficiency: new parameters for validation of method development. *J Am Soc Mass Spectrom.* 2005;16(11):1757-9.
36. Luigi Silvestro ITaSRS. Matrix Effects in Mass Spectrometry Combined with Separation Methods — Comparison HPLC, GC and Discussion on Methods to Control these Effects, Tandem Mass Spectrometry - Molecular Characterization,Dr. Ana Varela Coelho (Ed.). *InTech.* 2013.

37. Hajslova J, Holadova K, Kocourek V, Poustka J, Godula M, Cuhra P, and Kempny M. Matrix-induced effects: a critical point in the gas chromatographic analysis of pesticide residues. *J Chromatogr A.* 1998;800(2):283-95.
38. Hajslova J, and Zrostlikova J. Matrix effects in (ultra)trace analysis of pesticide residues in food and biotic matrices. *J Chromatogr A.* 2003;1000(1-2):181-97.
39. Weljie AM, Newton J, Mercier P, Carlson E, and Slupsky CM. Targeted profiling: quantitative analysis of 1H NMR metabolomics data. *Anal Chem.* 2006;78(13):4430-42.
40. Barwick VJ. Sources of uncertainty in gas chromatography and high-performance liquid chromatography. *J Chromatogr A.* 1999;849(1):13-33.
41. Biber A, Scherer G, Hoepfner I, Adlkofer F, Heller WD, Haddow JE, and Knight GJ. Determination of nicotine and cotinine in human serum and urine: an interlaboratory study. *Toxicol Lett.* 1987;35(1):45-52.
42. Hoverstad T, and Midtvedt T. Short-chain fatty acids in germfree mice and rats. *J Nutr.* 1986;116(9):1772-6.
43. Lu Y, Fan C, Li P, Lu Y, Chang X, and Qi K. Short Chain Fatty Acids Prevent High-fat-diet-induced Obesity in Mice by Regulating G Protein-coupled Receptors and Gut Microbiota. *Sci Rep.* 2016;6(37589.
44. Garcia-Villalba R, Gimenez-Bastida JA, Garcia-Conesa MT, Tomas-Barberan FA, Carlos Espin J, and Larrosa M. Alternative method for gas chromatography-mass spectrometry analysis of short-chain fatty acids in faecal samples. *J Sep Sci.* 2012;35(15):1906-13.
45. Cook AM, and Denger K. Metabolism of taurine in microorganisms: a primer in molecular biodiversity? *Adv Exp Med Biol.* 2006;583(3-13.
46. Gordon HA, and Pesti L. The gnotobiotic animal as a tool in the study of host microbial relationships. *Bacteriol Rev.* 1971;35(4):390-429.
47. Backhed F, Manchester JK, Semenkovich CF, and Gordon JI. Mechanisms underlying the resistance to diet-induced obesity in germ-free mice. *P Natl Acad Sci USA.* 2007;104(3):979-84.
48. Singh V, Chassaing B, Zhang L, San Yeoh B, Xiao X, Kumar M, Baker MT, Cai J, Walker R, Borkowski K, et al. Microbiota-Dependent Hepatic Lipogenesis Mediated by Stearoyl CoA Desaturase 1 (SCD1) Promotes Metabolic Syndrome in TLR5-Deficient Mice. *Cell Metab.* 2015;22(6):983-96.

Figure 2-1

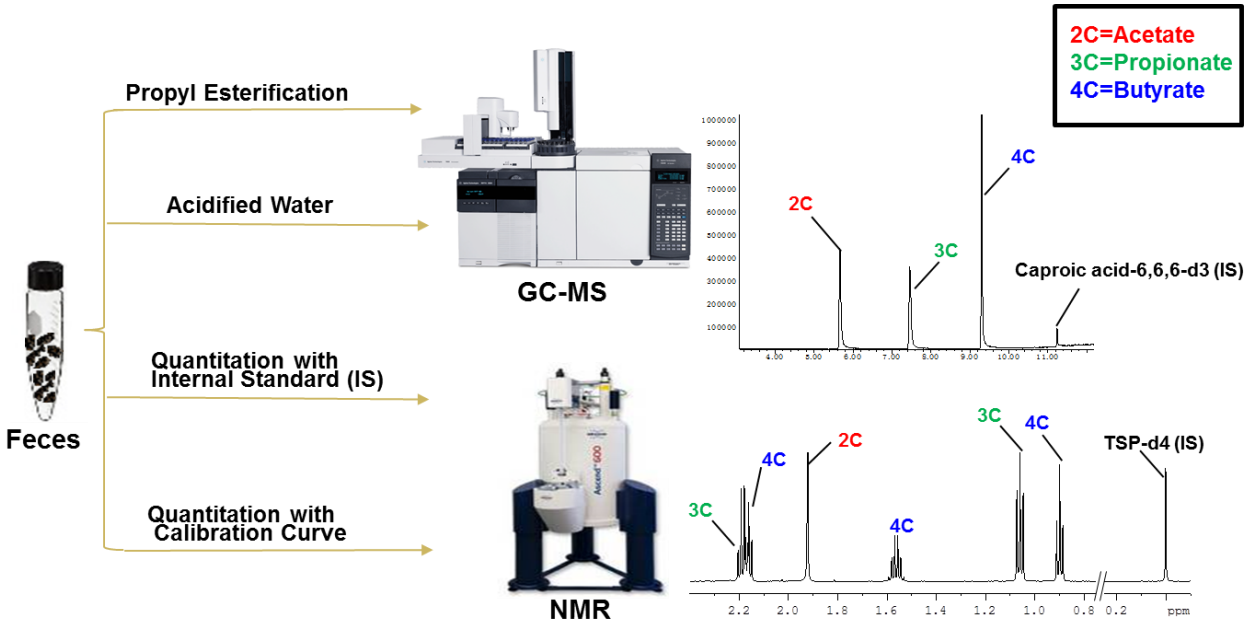

Figure 2-1. Experimental Scheme for Orthogonal Comparison of SCFA Quantitation Methods

Figure 2-2

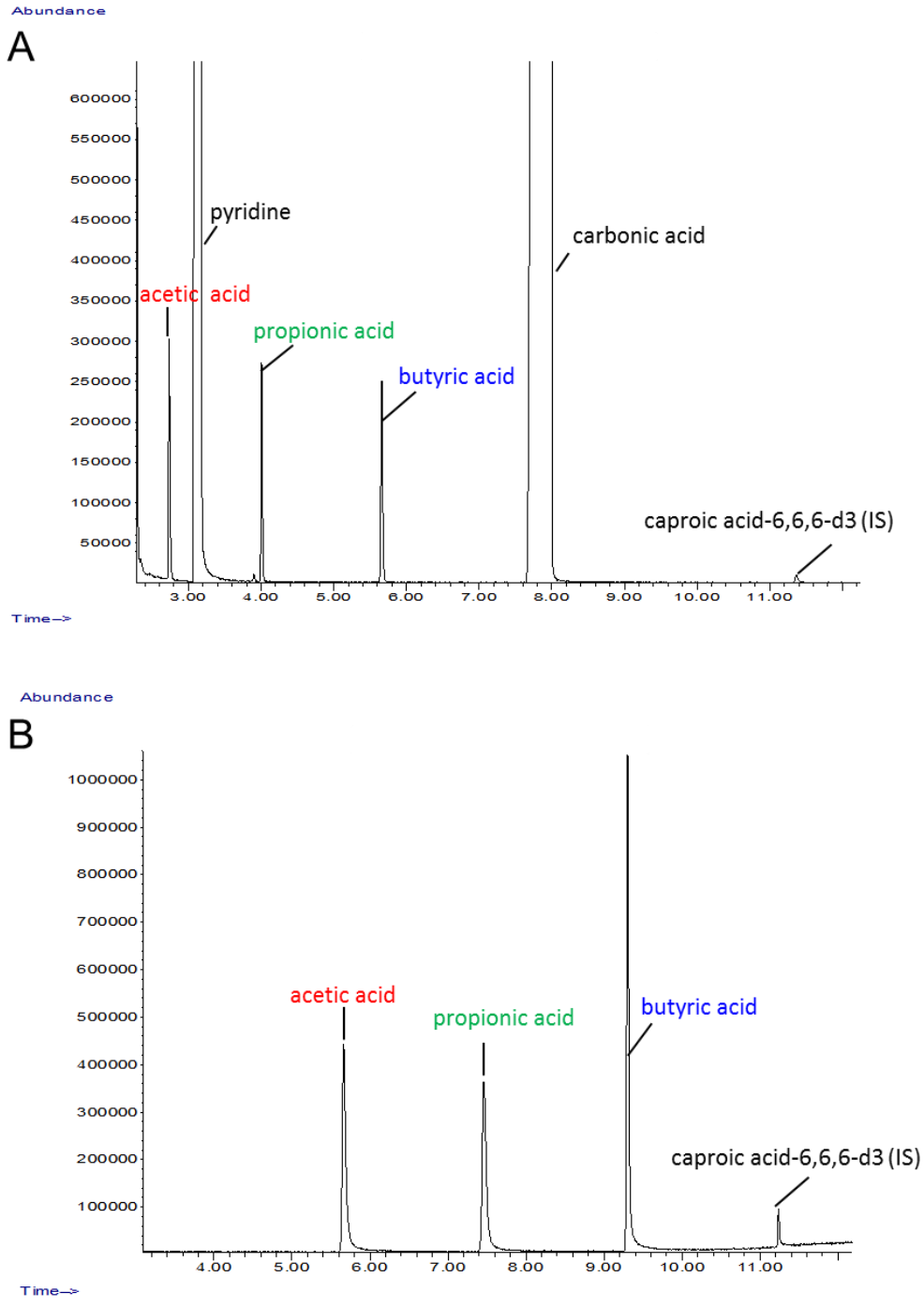

Figure 2-2. Total Ion Chromatogram of SCFAs Standard Mixture (100 µg/mL) with Caproic Acid-6,6,6-d3 as Internal Standard (IS) (10 µg/ml). (A) propyl esterification method and (B) acidified water method

Figure 2-3

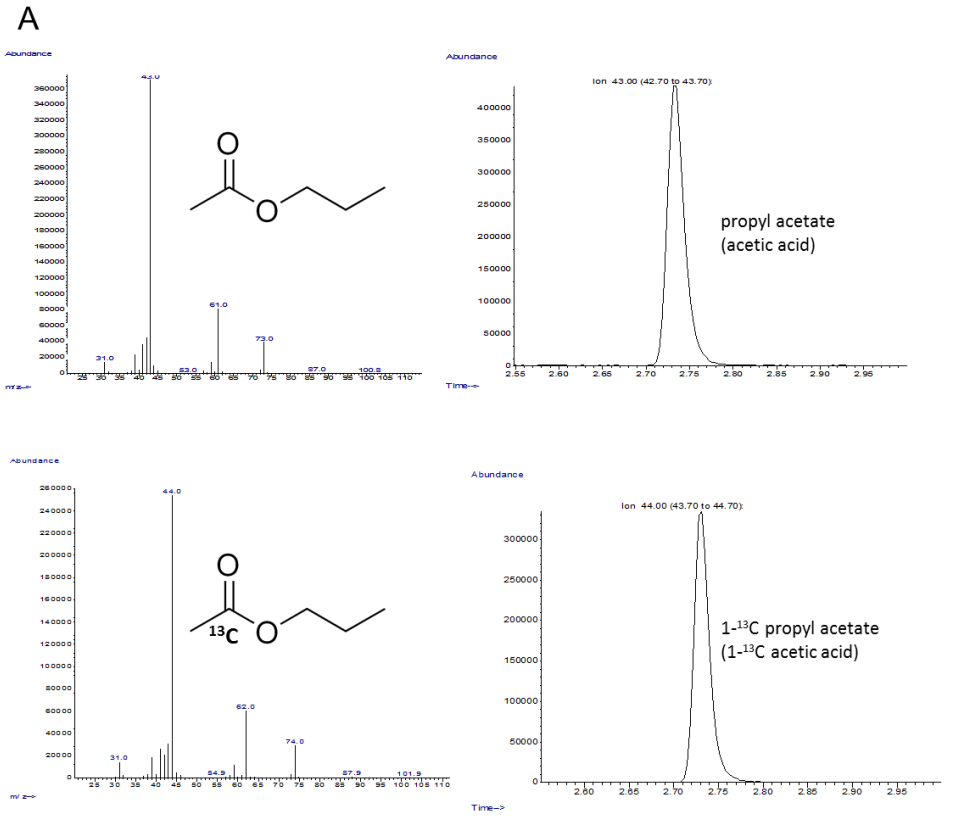
A
Abundance
m/z-->
Abundance
Ion 43.00 (42.70 to 43.70):
propyl acetate
(acetic acid)
Time-->
Abundance
m/z-->
Abundance
Ion 44.00 (43.70 to 44.70):
1-13C propyl acetate
(1-13C acetic acid)
Time-->

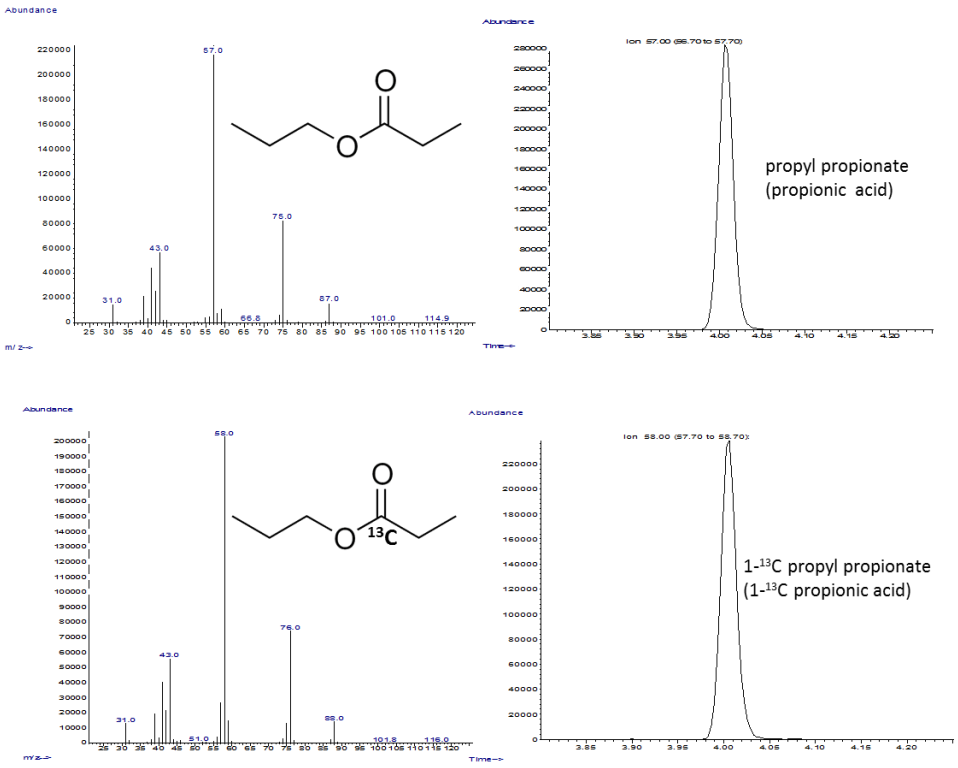
B
Abundance
m/z-->
Abundance
Ion 57.00 (56.70 to 57.70):
propyl propionate
(propionic acid)
Time-->
Abundance
m/z-->
Abundance
Ion 58.00 (57.70 to 58.70):
1-13C propyl propionate
(1-13C propionic acid)
Time-->

Figure 2-3. Continued

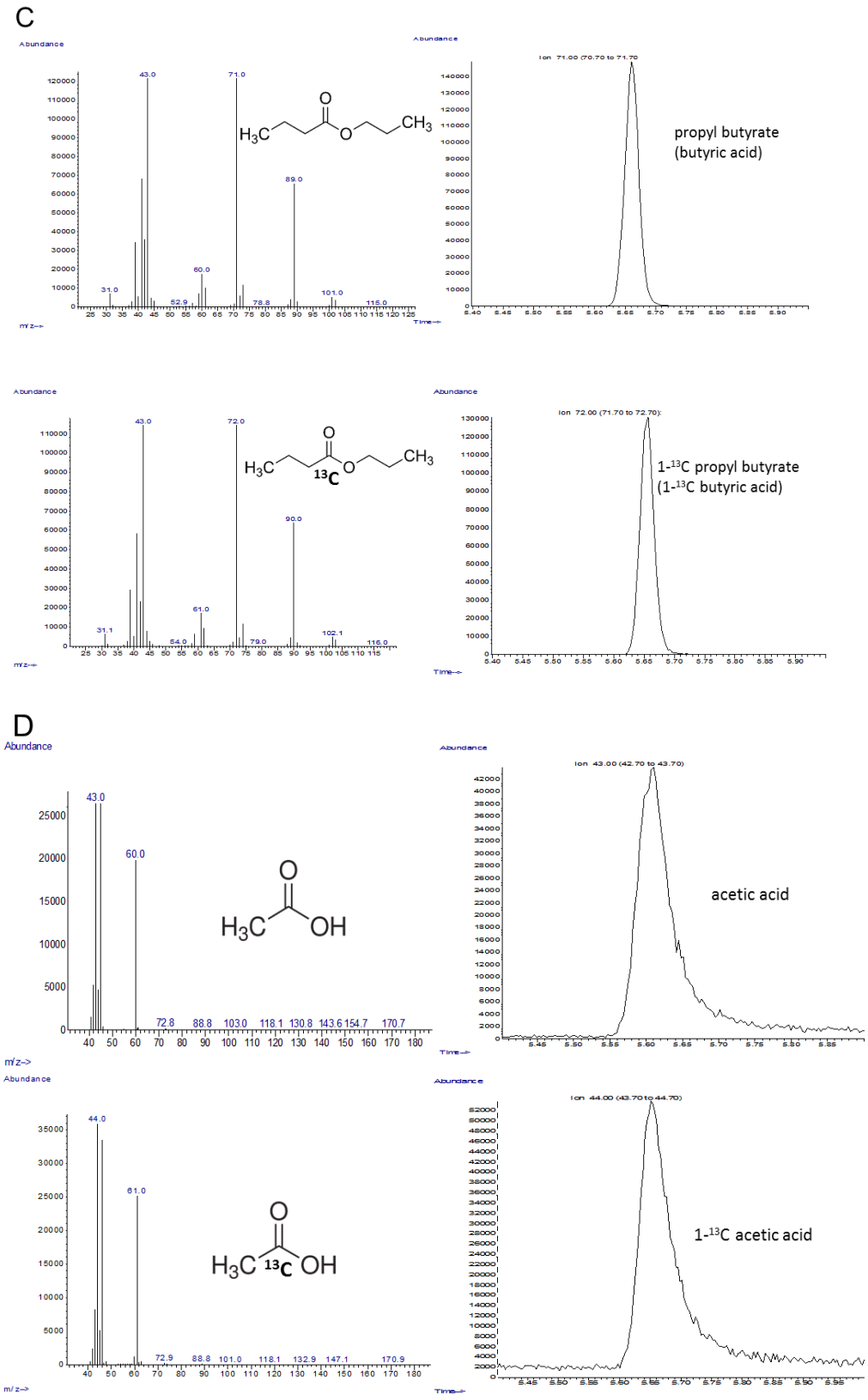

Figure 2-3. Continued

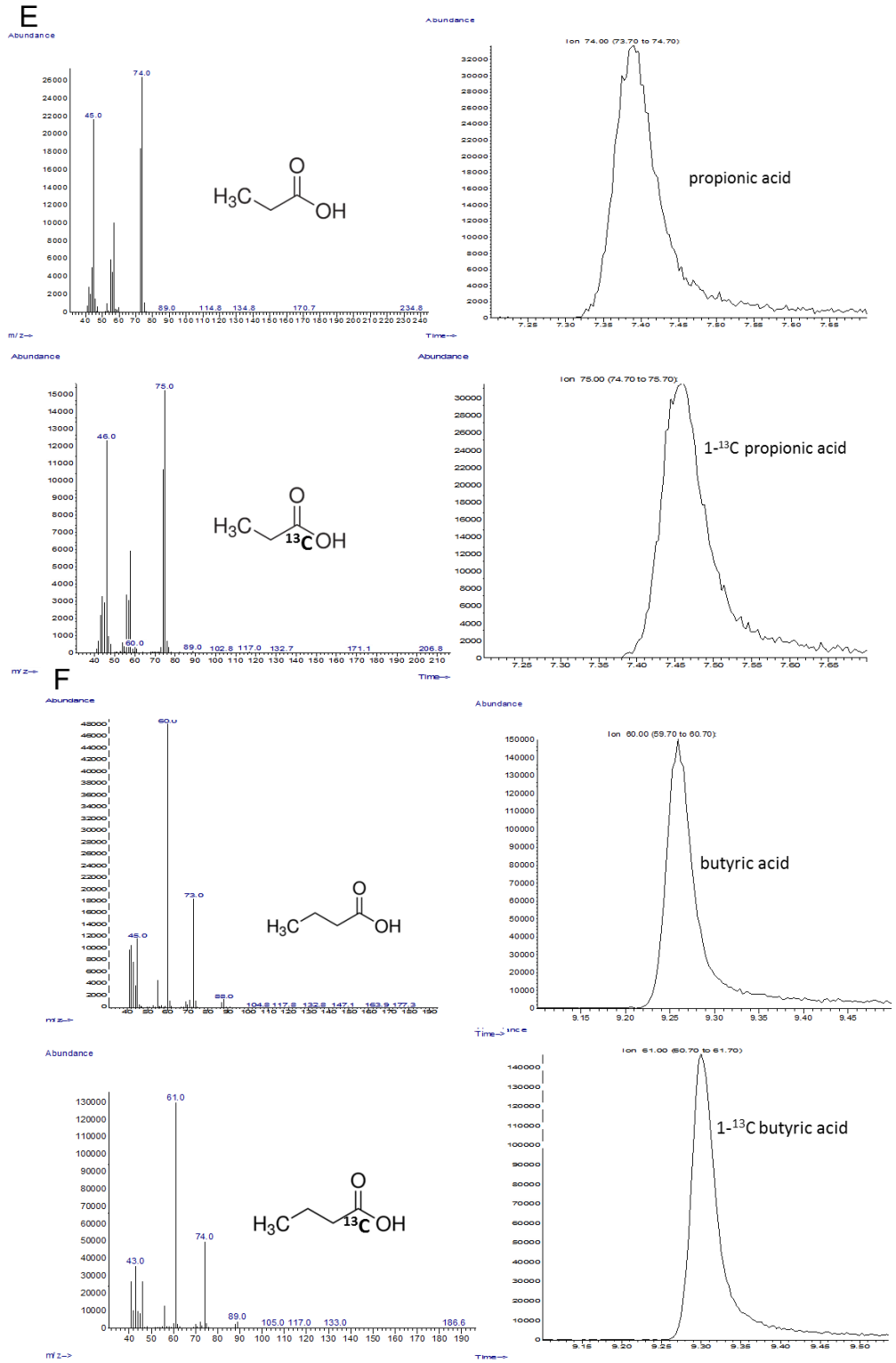

Figure 2-3. Fragmentation Pattern and Extract Ion Chromatogram for Unlabeled and 1-^{13}C Labeled SCFAs Standard. (A-C) propyl esterification method and (D-F) acidified water method.

Figure 2-4

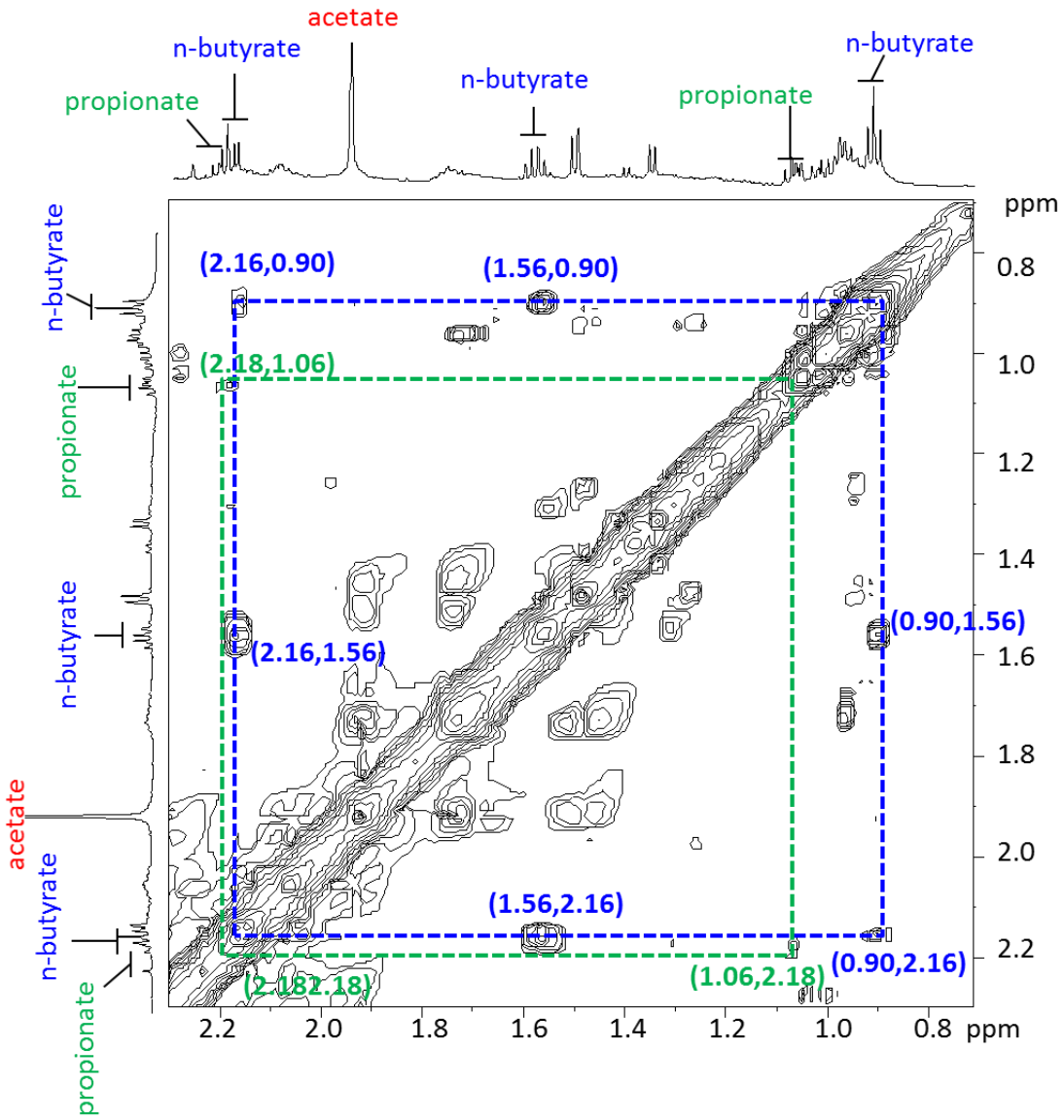

Figure 2-4. 2D ^{1}H-^{1}H TOCSY NMR Spectroscopy of Mice Feces.

Figure 2-5

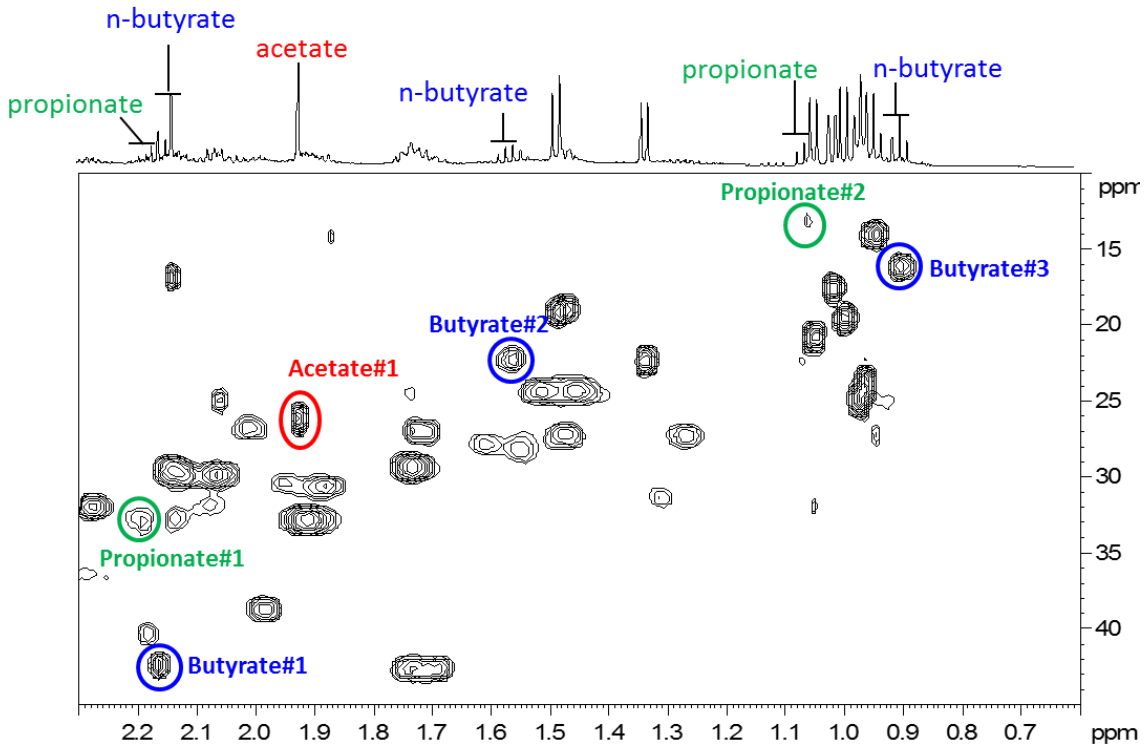

Metabolites	Structure	Position	F2 (ppm)	F1 (ppm)
Acetate		#1	1.91	26.15
Propionate		#1	2.18	32.97
		#2	1.06	13.05
Butyrate		#1	2.16	42.49
		#2	1.56	22.23
		#3	0.90	16.10

Figure 2-5. 2D ^{1}H-13C HSQC NMR Spectroscopy of Mice Feces. Reference spectra were obtained from Human Metabolome Database (HMDB). Acetate (HMDB00042), Propionate (HMDB00237) and Butyrate (HMDB00039).

Figure 2-6

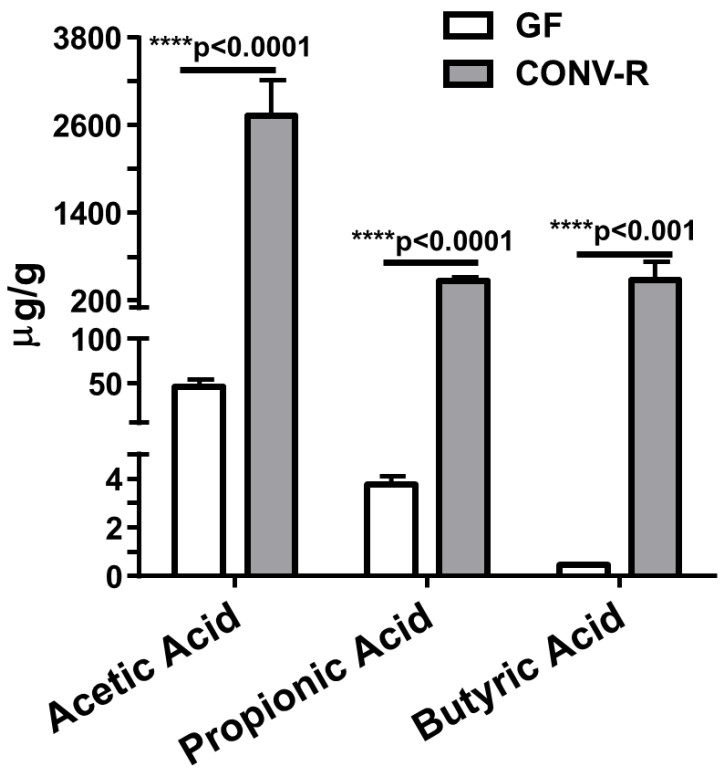

Figure 2-6. Biological Concentrations of SCFAs in Germ Free (GF) and Conventionally Raised (CONV-R) Fecal Samples Measured by GC-MS Propyl Esterification Method. Values are expressed as the mean ± sd. (n=5). Significance was determined using a two-tailed Student t-test.

Figure 2-7

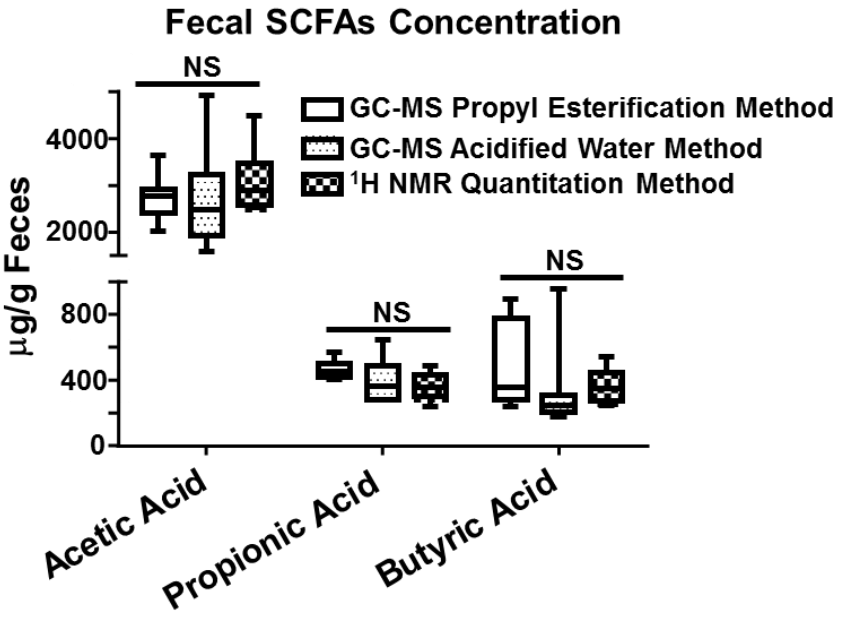

Figure 2-7. Biological Concentrations of Fecal SCFAs in CONV-R Mice (n=10 per group) Measured by GC-MS Propyl Esterification Method, GC-MS Acidified Water method, and ^{1}H NMR Quantitation Method. Values are expressed as the mean ± 95% CI. Data was analyzed using ANOVA with Bonferroni's correction. Biological concentrations measured by different methods were not significantly different.

Figure 2-8

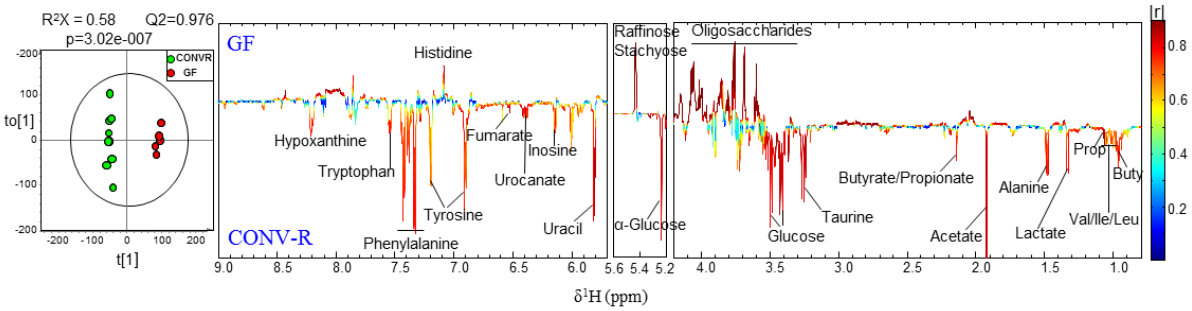

Figure 2-8. Global Metabolic Profiling of Feces from Germ Free (GF) and Conventionally Raised (CONV-R) Mice Determined by ^{1}H NMR. OPLS-DA scores represent indicative power of models, p-value (CV-ANOVA) demonstrates the significance testing of OPLS model. Correlation coefficient-coded loadings plots for the models (right) from NMR spectra fecal extracts displaying changes and significance. The upward-pointed peak indicates the metabolite that peak represents (metabolite labeled) presented in higher level in GF mice. Peak pointing downward represents the metabolite presented more in CONV-R mice. The color-coded correlation coefficient indicates the significance of that change, the significance increases, as color gets warmer. A cutoff value of $|r| > 0.754$ ($r > 0.754$ and $r < -0.754$) is chosen for correlation coefficient as significant based on the discrimination significance ($p \leq 0.05$).

Figure 2-9

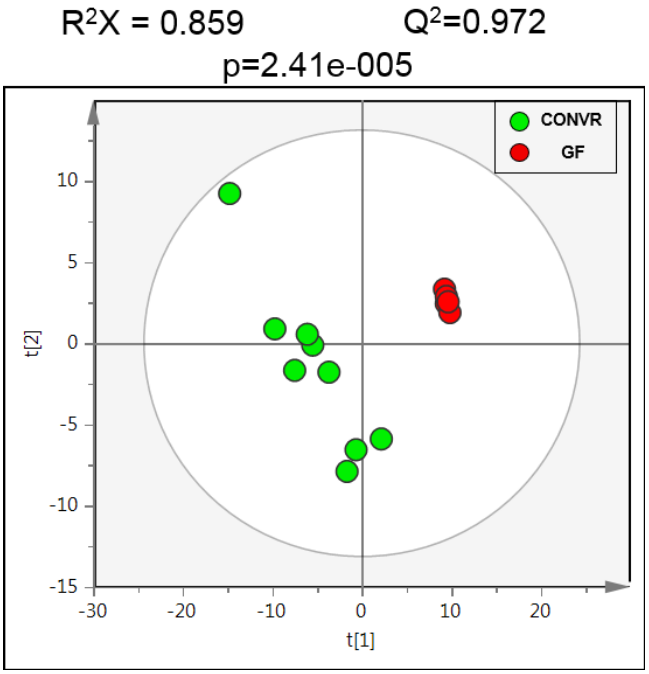

Figure 2-9. PLS-DA of Fecal SCFAs Profiling from Germ Free (GF) and Conventionally Raised (CONV-R) mice determined by ^{1}H NMR.

Figure 2-10

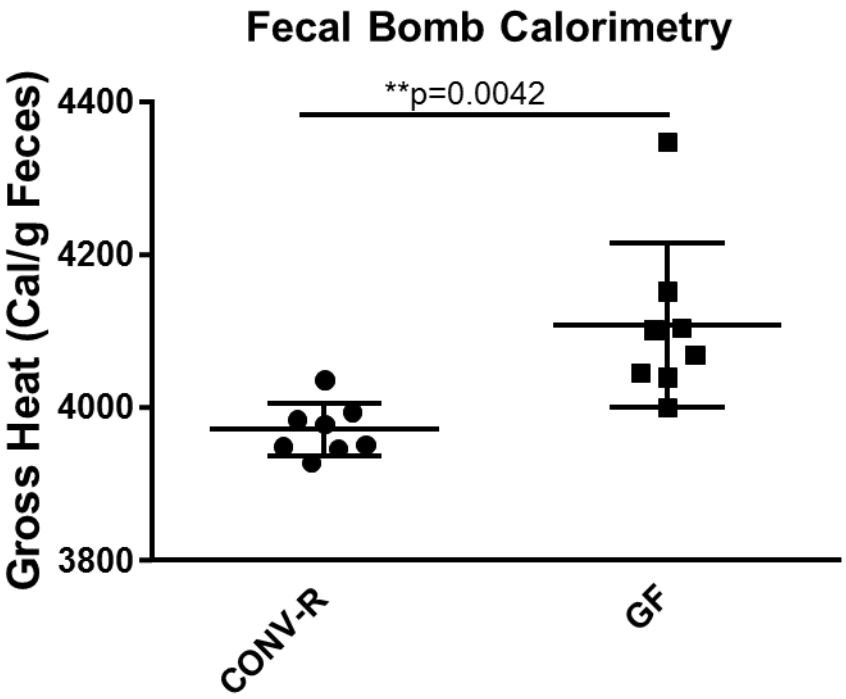

Figure 2-10. Quantitation of Gross Heat of Feces from Conventionally Raised (CONV-R) and Germ Free (GF) Mice by Bomb Calorimetry (n=8 mice per group). Data was analyzed using a two-tailed Student t-test. $P<0.05$ was considered significant.

Table 2-1. Linearity and Sensitivity of Different Methods. Calibration curve: x=concentration µg/ml, y=target peak area relative to internal standards. Linear range (LR), limit of detection (LOD) and limit of quantitation (LOQ) expressed as µg/ml.

GC-MS Propyl Esterification Method						
Compounds	Target ion	Calibration curve	R^2	LR (µg/ml)	LOD (µg/ml)	LOQ (µg/ml)
Acetic Acid	43	y = 0.4588x - 1.1311	0.9946	LOQ-250	0.002	0.02
Propionic Acid	57	y = 0.3324x + 1.042	0.9937	LOQ-250	*	*
Butyric Acid	71	y = 0.2704x - 1.654	0.9913	LOQ-250	0.01	0.09
GC-MS Acidified Water Method						
Compounds	Target ion	Calibration curve	R^2	LR (µg/ml)	LOD (µg/ml)	LOQ (µg/ml)
Acetic Acid	43	y = 0.0503x - 0.0295	0.9992	LOQ-500	0.5	5
Propionic Acid	74	y = 0.0287x - 0.059	0.9998	LOQ-500	0.8	3
Butyric Acid	60	y = 0.0849x - 0.4245	0.9992	LOQ-500	0.2	1
^{1}H NMR Quantitation Method						
Compounds	Chemical shift (ppm)	Calibration curve	R^2	LR (µg/ml)	LOD (µg/ml)	LOQ (µg/ml)
Acetic Acid	1.91 (CH_3)	y = 0.0374x - 0.1722	0.9949	LOQ-250	2	4
Propionic Acid	1.06 (CH_3)	y = 0.0098x - 0.0613	0.9916	LOQ-250	2	4
Butyric Acid	0.90 (CH_3)	y = 0.0261x - 0.1549	0.9916	LOQ-250	3	4

*LOD and LOQ of propionic acid were not calculated in GC-MS propyl esterification method as propyl propionate could be detected in background which is introduced by impurity of derivatization solvents.

Table 2-2. Recovery and Matrix Effect of SCFAs from Fecal Extracts Spiked with Different Concentration of SCFAs Standards by Different Quantitation Methods. Values are expressed as mean ± SD. n=6 per group.

GC-MS Propyl Esterification Method					
Compounds	Spiked amount (µg/ml)	Amount recovered (µg/ml)	%Recovery	%RSD	%Matrix effect
Acetic Acid	10	6.7±1.0	66.9	14.9	76.3
	100	108.3±15.0	108.3	13.9	94.4
	250	254.5±16.3	101.8	5.9	92.7
Propionic Acid	10	7.2±1.2	72.3	16.9	74.2
	100	100.2±17.6	100.2	17.5	84.2
	250	244.5±36.6	97.8	15.0	92.7
Butytic Acid	10	6.7±1.1	67.0	11.2	77.7
	100	99.4±20.4	99.4	20.6	88.2
	250	249.7±38.1	99.8	15.3	97.4
GC-MS Acidified Water Method					
Compounds	Spiked amount (µg/ml)	Amount recovered (µg/ml)	%Recovery	%RSD	%Matrix effect
Acetic Acid	10	7.5±1.9	74.8	25.1	116.8
	100	108.7±14.9	108.7	13.7	95.7
	250	226.1±19.2	90.4	8.5	76.2
Propionic Acid	10	7.5±1.2	75.4	16.0	95.1
	100	106.3±10.7	106.3	10.1	80.3
	250	297.2±23.1	118.9	7.8	76.2
Butyric Acid	10	5.2±0.4	52.2	6.8	89.6
	100	87.6±17.0	87.6	20.6	76.2
	250	291.7±24.3	116.7	8.3	79.7
^{1}H NMR Quantitation Relative to TSP Method					
Compounds	Spiked amount (µg/ml)	Amount recovered (µg/ml)	%Recovery	%RSD	%Matrix effect
Acetic Acid	10	8.4±0.4	83.7	4.2	90.6
	100	97.7±4.3	97.7	4.4	118.5
	250	271.7±16.0	108.7	5.9	111.7
Propionic Acid	10	10.1±0.6	101.4	6.0	107.2
	100	116.6±5.5	116.6	4.7	116.1
	250	332.1±15.3	132.8	4.6	104.8
Butyric Acid	10	5.4±0.8	54.2	14.7	64.1
	100	92.9±4.6	92.9	5.0	118.1
	250	263.2±14.7	105.3	5.6	106.8
^{1}H NMR Quantitation with Calibration Curve Method					
Compounds	Spiked amount (µg/ml)	Amount recovered (µg/ml)	%Recovery	%RSD	
Acetic Acid	10	8.6±0.4	85.6	4.2	
	100	98.7±5.1	98.7	5.2	
	250	277.9±16.3	111.2	5.9	
Propionic Acid	10	8.0±0.48	80.2	6.0	
	100	91.4±4.6	91.4	5.0	
	250	262.7±12.1	105.1	4.6	
Butyric Acid	10	5.4±0.8	54.1	14.7	
	100	92.0±4.7	92.0	5.1	
	250	263.0±14.7	105.2	5.6	

Table 2-3. Intraday and Interday Repeatability of Standard SCFAs Samples (10, 25, 100, 250 µg/ml) by Different Quantitation Methods. Expressed as the relative standard deviation (%RSD).

GC-MS Propyl Esterification Method									
Compounds	No. of injections	Intraday				Interday			
		10 µg/ml	25 µg/ml	100 µg/ml	250µg/ml	10 µg/ml	25 µg/ml	100 µg/ml	250 µg/ml
Acetic Acid	1	11.4	24.5	101.0	251.0	10.4	22.9	91.1	253.0
	2	10.9	24.4	85.4	252.4	11.8	21.7	74.0	259.9
	3	10.1	23.7	99.2	257.8	11.3	21.5	70.3	245.9
	4	11.0	24.6	91.7	244.7	10.6	20.7	72.7	244.7
	5	10.4	22.9	91.1	267.3	11.1	21.1	72.4	267.3
	Mean	10.7	24.0	93.7	254.7	11.0	21.6	76.1	254.1
	SD	0.5	0.6	5.7	7.6	0.5	0.7	7.6	8.5
	%RSD	4.3	2.7	6.1	3.0	4.5	3.5	10.0	3.4
Propionic Acid	1	11.0	23.5	109.8	248.1	9.5	22.4	95.3	263.1
	2	12.2	24.2	89.1	240.0	16.7	25.3	80.5	250.1
	3	8.7	25.3	105.2	253.1	11.8	21.3	70.9	218.0
	4	11.5	26.4	94.6	236.7	11.3	22.2	76.3	232.3
	5	9.5	22.4	95.3	276.5	15.9	21.2	71.8	276.5
	Mean	10.6	24.4	98.8	250.9	13.0	22.5	79.0	248.0
	SD	1.3	1.4	7.6	14.0	2.8	1.5	8.9	20.9
	%RSD	12.2	5.7	7.7	5.6	21.3	6.5	11.2	8.4
Butyric Acid	1	13.7	24.2	98.8	252.1	13.6	25.0	89.7	281.6
	2	14.0	26.0	84.9	247.0	16.3	27.7	84.7	240.5
	3	13.8	26.3	97.3	254.0	14.5	24.2	77.9	233.2
	4	14.0	26.7	88.5	239.4	15.1	27.1	86.2	256.3
	5	13.6	25.0	89.7	266.8	16.8	25.4	83.0	266.8
	Mean	13.8	25.6	91.9	251.9	15.3	25.9	84.3	255.7
	SD	0.2	0.9	5.3	9.0	1.2	1.3	3.9	17.5
	%RSD	1.2	3.5	5.8	3.6	7.7	5.1	4.6	6.9
GC-MS Acidified Water Method									
Compounds	No. of injections	Intraday				Interday			
		10 µg/ml	25 µg/ml	100 µg/ml	250µg/ml	10 µg/ml	25 µg/ml	100 µg/ml	250 µg/ml
Acetic Acid	1	9.6	24.0	89.1	247.2	9.6	24.0	89.1	247.2
	2	11.3	25.3	89.9	227.1	11.9	22.7	89.4	224.3
	3	13.8	28.4	100.5	247.7	9.5	20.7	91.9	240.8
	4	13.3	28.8	98.3	262.0	10.5	20.9	95.5	212.3
	5	12.7	26.3	99.0	246.6	9.1	21.3	80.2	230.7
	Mean	12.1	26.6	95.4	246.1	10.1	21.9	89.2	231.1
	SD	1.5	1.8	4.9	11.1	1.0	1.2	5.1	12.3
	%RSD	12.6	6.8	5.1	4.5	9.8	5.6	5.7	5.3
Propionic Acid	1	9.9	23.2	95.3	248.2	9.3	23.1	96.0	249.7
	2	11.4	29.1	101.7	252.6	11.0	23.7	105.3	275.3
	3	11.6	26.3	109.4	273.5	11.7	23.2	118.4	284.4
	4	11.6	25.8	105.2	287.9	12.2	25.4	118.9	303.5
	5	10.4	26.9	108.0	262.1	11.6	28.3	109.5	313.9
	Mean	11.0	26.3	103.9	264.9	11.2	24.7	109.6	285.4
	SD	0.7	1.9	5.1	14.4	1.0	1.9	8.6	22.4
	%RSD	6.4	7.2	4.9	5.4	8.9	7.9	7.8	7.9
Butyric Acid	1	11.1	23.5	92.8	242.8	11.1	23.5	92.8	242.8
	2	11.5	25.5	99.0	246.7	12.3	22.4	93.7	260.2
	3	11.0	25.1	106.9	267.9	11.4	20.8	102.1	259.2
	4	11.2	22.8	105.4	280.9	11.0	23.3	105.4	298.3
	5	10.6	24.8	102.6	254.0	10.8	25.3	107.4	290.4
	Mean	11.1	24.4	101.3	258.5	11.3	23.1	100.3	270.2
	SD	0.3	1.0	5.1	14.1	0.5	1.5	6.0	20.8
	%RSD	2.4	4.2	5.0	5.5	4.7	6.4	6.0	7.7

Table 2-3. Continued

^{1}H NMR Quantitation Relative to TSP									
Compounds	No. of injections	Intraday				Interday			
		10 µg/ml	25 µg/ml	100 µg/ml	250 µg/ml	10 µg/ml	25 µg/ml	100 µg/ml	250 µg/ml
Acetic Acid	1	6.8	17.1	81.7	245.7	6.8	17.1	81.7	245.7
	2	7.2	16.7	81.8	235.3	6.9	19.7	81.8	243.5
	3	7.1	16.6	82.2	242.4	6.5	19.9	82.2	243.7
	4	7.0	16.9	82.4	249.2	7.0	19.4	82.4	241.6
	5	7.1	15.0	82.3	243.5	6.9	19.2	82.3	242.0
	Mean	7.1	16.5	82.1	243.2	6.8	19.0	82.1	243.3
	SD	0.1	0.8	0.3	4.6	0.2	1.0	0.3	1.4
	%RSD	1.7	4.6	0.3	1.9	2.6	5.3	0.3	0.6
Propionic Acid	1	7.9	19.6	99.8	319.2	7.9	19.6	99.8	319.2
	2	8.4	19.2	95.1	303.9	7.8	20.8	95.8	308.9
	3	8.1	19.4	100.7	312.6	7.7	20.1	97.1	308.0
	4	8.8	19.5	102.3	330.8	7.6	21.0	97.0	302.1
	5	8.1	19.7	99.4	318.4	7.9	20.2	97.0	303.0
	Mean	8.2	19.5	99.5	317.0	7.8	20.3	97.3	308.2
	SD	0.3	0.2	2.4	8.8	0.1	0.5	1.3	6.1
	%RSD	3.8	0.9	2.4	2.8	1.4	2.4	1.4	2.0
Butyric Acid	1	7.5	16.0	79.0	251.5	7.5	16.0	79.0	251.5
	2	6.7	16.2	76.0	240.0	6.7	17.0	78.8	237.1
	3	6.7	15.8	78.0	240.0	6.7	17.0	80.2	235.7
	4	7.1	16.5	79.0	249.8	7.1	16.1	79.7	257.1
	5	7.0	14.4	77.8	250.7	6.7	16.6	78.7	259.5
	Mean	7.0	15.8	78.0	246.4	6.9	16.5	79.3	248.2
	SD	0.3	0.7	1.1	5.3	0.3	0.4	0.6	10.0
	%RSD	4.3	4.5	1.4	2.1	4.5	2.6	0.7	4.0
^{1}H NMR Quantitation with Calibration Curve									
Compounds	No. of injections	Intraday				Interday			
		10 µg/ml	25 µg/ml	100 µg/ml	250 µg/ml	10 µg/ml	25 µg/ml	100 µg/ml	250 µg/ml
Acetic Acid	1	11.6	22.1	88.2	255.9	11.6	22.1	88.2	255.9
	2	12.0	21.7	85.2	245.3	11.7	24.7	88.3	253.6
	3	11.8	21.6	88.3	252.5	11.2	25.0	88.7	253.9
	4	11.8	21.8	89.9	259.5	11.7	24.4	88.9	251.8
	5	11.9	18.3	87.8	253.7	11.7	24.3	88.8	252.2
	Mean	11.8	21.1	87.9	253.4	11.6	24.1	88.6	253.5
	SD	0.1	1.4	1.5	4.7	0.2	1.0	0.3	1.5
	%RSD	1.1	6.7	1.7	1.8	1.6	4.3	0.3	0.6
Propionic Acid	1	12.5	21.8	85.2	258.7	12.5	21.8	85.2	258.7
	2	12.9	21.4	81.5	246.7	12.5	22.7	82.0	250.6
	3	12.6	21.6	86.0	253.6	12.4	22.2	83.1	249.9
	4	13.2	21.7	87.2	267.9	12.3	22.9	83.0	245.2
	5	12.7	21.8	84.9	258.1	12.5	22.2	83.0	245.9
	Mean	12.8	21.7	84.9	257.0	12.4	22.4	83.3	250.1
	SD	0.3	0.1	1.9	7.0	0.1	0.4	1.0	4.8
	%RSD	2.0	0.7	2.3	2.7	0.7	1.7	1.3	1.9
Butyric Acid	1	13.4	21.9	84.9	257.1	13.4	21.9	84.9	257.1
	2	12.6	22.1	81.9	245.7	12.6	22.9	84.7	242.8
	3	12.6	21.7	83.8	245.6	12.6	22.9	86.1	241.4
	4	13.0	22.4	84.8	255.5	13.0	22.0	85.6	262.8
	5	12.9	20.3	83.7	256.4	12.6	22.5	84.6	265.1
	Mean	12.9	21.7	83.8	252.1	12.8	22.4	85.2	253.8
	SD	0.3	0.7	1.1	5.2	0.3	0.4	0.6	10.0
	%RSD	2.3	3.2	1.3	2.1	2.4	1.9	0.7	3.9

Chapter 3

The Anti-Oxidant Drug Tempol Promotes Functional Metabolic Changes in the Gut Microbiota

Published in the Journal of Proteome Research

J Proteome Res 2016,15(2),563-71.

DOI:10.1021/acs.jproteome.5b00957

Jingwei Cai[1], Limin Zhang[1,2], Richard A. Jones[1], Jared B. Correll[1], Emmanuel Hatzakis[4], Philip B. Smith[3], Frank J. Gonzalez[5], Andrew D. Patterson[1]

Affiliations: [1]Center for Molecular Toxicology and Carcinogenesis, Department of Veterinary and Biomedical Sciences, Pennsylvania State University, University Park, State College, Pennsylvania, 16802, USA; [2]CAS Key Laboratory of Magnetic Resonance in Biological Systems, State Key Laboratory of Magnetic Resonance and Atomic and Molecular Physics, National Centre for Magnetic Resonance in Wuhan, Wuhan Institute of Physics and Mathematics, Chinese Academy of Sciences (CAS), Wuhan 430071, China; [3]Metabolomics Facility, Huck Institutes of Life Sciences, Pennsylvania State University, University Park, State College, Pennsylvania, 16802, USA; [4]Department of Chemistry, Pennsylvania State University, University Park, Pennsylvania, 16802, USA; [5]Laboratory of Metabolism, National Cancer Institute, NIH, Bethesda, Maryland, 20892, USA

Contributions: JC and ADP conceived and coordinated the study and wrote the manuscript. JC designed, performed, and analyzed the data of physiology and histology, GC-MS, bomb calorimetry and qPCR shown in Figures 3-1, 3-2, 3-3, 3-6, 3-9, 3-10. LZ and EH contributed to the NMR technical support and data interpretation in Figures 3-1, 3-3, 3-5, 3-7, 3-8. RAJ contributed to bomb calorimetry analysis shown in Figure 3-6, JBC helped with mice experiment and sample collection. PBS provided technical assistance with GC-MS analysis. FJG contributed to the data interpretation and preparation of the manuscript. All authors reviewed the results and approved the final version of the manuscript.

ABSTRACT

Recent studies have identified the important role of the gut microbiota in the pathogenesis and progression of obesity and related metabolic disorders. The antioxidant tempol was shown to prevent or reduce weight gain and modulate the gut microbiota community in mice; however, the mechanism by which tempol modulates weight gain/loss with respect to the host and gut microbiota has not been clearly established. Here we show that tempol (0, 1, 10, and 50 mg/kg p.o. for 5 days) decreased cecal bacterial fermentation and increased fecal energy excretion in a dose-dependent manner. Liver ^{1}H NMR-based metabolomics identified a dose-dependent decrease in glycogen and glucose, enhanced glucogenic and ketogenic activity (tyrosine and phenylalanine), and increased activation of the glycolysis pathway. Serum ^{1}H NMR-based metabolomics indicated that tempol promotes enhanced glucose catabolism. Hepatic gene expression was significantly altered as demonstrated by an increase in *Pepck and G6pase* and a decrease in *Hnf4a*, *ChREBP*, *Fabp1*, and *Cd36* mRNAs. No significant change in the liver and serum metabolomic profiles were observed in germ-free mice thus establishing a significant role for the gut microbiota in mediating the beneficial metabolic effects of tempol. These results demonstrate that tempol modulates the gut microbial community and its function resulting in reduced host energy availability and a significant shift in liver metabolism towards a more catabolic state.

INTRODUCTION

Obesity and related metabolic disorders are major public health concerns. Previous studies identified the gut microbiota as an important factor involved in

metabolic homeostasis due to their role in extracting energy from the diet (1), interfering with metabolic signaling (2), and modulating gut inflammation (3). The population and functions of the gut microbiota can be manipulated by xenobiotics (e.g., antibiotics) (4, 5), pathogens (e.g., diarrhea-causing organisms) (6), drugs (7), and host genetic factors (8). Additionally, the gut microbiota has been identified as a promising target for therapeutic intervention to treat metabolic disorders including obesity (9).

Tempol (4-hydroxy-2,2,6,6-tetramethylpiperidine-N-oxyl) is a water soluble nitroxide, stable free radical, which has been reported to be an effective antioxidant in detoxifying reactive oxygen species in cell culture and animal studies (10, 11) . Tempol was reported to inhibit body weight gain in mice (12) and can dramatically influence non-alcoholic fatty liver disease (NAFLD) through alterations in signaling between the gut microbiota and the farnesoid X receptor (FXR) (13). The protective effects of tempol against NAFLD were found to be mediated specifically through changes in the composition of the gut microbiota, attenuated FXR signaling, and inhibition of hepatic SREBP1C and *de novo* lipogenesis (14). Based on these previous studies, the anti-obesity effect of tempol is strongly associated with alterations in the gut microbiota and host signaling axis.

The gut microbiota has been implicated in host metabolic status mainly through its control of energy availability by fermenting non-digestible dietary fiber into available, absorbable, and transportable short chain fatty acids (SCFAs). SCFAs are saturated fatty acid with aliphatic tails with less than six carbons, among which acetate (C2), propionate (C3), butyrate (C4) are primary ones with most abundance (15). Acetate is the most abundant SCFAs in the gut compare to propionate and butyrate (16). Bacterial-

fermentation-origin SCFAs account for about 5-10% of daily energy intake of the host (17). Overall the host reabsorbs and utilizes SCFAs as an energy source or as anabolic substrates for processes including de novo lipogenesis (18).

In the current study, modulation of host energy metabolism by tempol through changes in gut microbiota fermentation was explored. To test the hypothesis, cecal and fecal SCFA concentrations, fecal energy excretion, liver and serum metabolite profiles were investigated via combined ^{1}H NMR-based metabolomics, targeted GC-MS profiling, bomb calorimetry, and hepatic gene expression was measured in mice after 5 day intragastric administration of tempol. Notably, a dose-dependent decrease in bacterial fermentation was found in tempol-treated mice along with significant changes in liver metabolism. Metabolic changes were found to be microbial dependent. This study provides an additional mechanism for the anti-obesity effect of tempol mediated by the gut microbiota.

MATERIALS AND METHODS

Chemicals

Tempol, short chain fatty acids, 1-propanol, propyl chloroformate, pyridine, sodium chloride, K_2HPO_4, and NaH_2PO_4 were purchased from Sigma-Aldrich Chemical Co. Ltd. (St. Louis, MO). Hexane and methanol were purchased from EMD Chemicals Inc (Gibbstown, NJ). The internal standard hexanoic acid-6,6,6-d_3 was obtained from C/D/N Isotopes Inc (Pointe-Claire, Quebec, Canada). Sodium 3-trimethylsilyl [2,2,3,3-d_4] propionate (TSP-d_4) and D_2O (99.9% in D) were purchased from Cambridge Isotope Laboratories (Miami, FL). Standard benzoic acid pellets were purchased from Parr

Instrument Company (Moline, IL). All compounds were of the highest analytical grade possible.

Tempol Treatment and Sample Collection

C57BL/6J wild-type male mice (4-week-old) were purchased from the Jackson Laboratory (Bar Harbor, Maine). The mice were housed in polypropylene cages with corncob bedding in a well-controlled environment (temperature, 65-75°F; relative humidity, 30%-70%; photoperiod, 12 h light/dark cycle). Water and regular chow were supplied *ad libitum*. Mice were randomly grouped after one-week acclimatization before treatment. Tempol (dissolved in 0.9% saline) was administered in the morning by gavage for 5 consecutive days. The control group was administered an equivalent amount of 0.9% saline. Mice were transferred to nalgene metabolic cage systems (Tecniplast, USA) and housed individually for 24 hours during the acclimatization period and treatment period every other day for fecal sample collection. Mice were weighed in the mornings and killed on day 6. Liver, cecum, and serum samples were collected immediately following CO_2 asphyxiation. All samples were quickly placed in liquid nitrogen then stored at -80 °C for future analysis. All procedures were performed in accordance with the Institute of Laboratory Animal Resources guidelines and approved by the Pennsylvania State University Institutional Animal Care and Use Committee. Germ free mice wild-type C57Bl/6J mice were bred and maintained by the Pennsylvania State University Gnotobiotic Facility, housed in germ free isolators, and fed an autoclaved diet. All materials and supplies were sterilized before transfer into the isolators. Germ free status was monitored continuously and confirmed through a series of culture based assays.

Gas Chromatography–Mass Spectrometry (GC-MS) Analysis

SCFAs level in tissues were measured with a targeted metabolomics protocol as described previously (19). 50 mg of cecal content/ feces were mixed with 1 mL of 0.005 M aqueous NaOH containing internal standard hexanoic acid-6,6,6-d_3 (5 µg/mL), homogenized (Bertin Technologies, Rockville, MD) at 6500 rpm,1 cycle, 60s and then centrifuged (Eppendorf, Hamburg, Germany) at 13,200 x g at 4 °C for 15 min. The supernatant was collected and an aliquot of 500 µL of a solvent mixture of 1-propanol /pyridine (3/2, v/v) and 100 µL of propyl chloroformate was subsequently added into supernatant and briefly vortexed. Samples were heated (Thermo Scientific, Marietta, OH) at 60 °C for 1 hour. The derivatized samples were extracted with a two-step hexane extraction. 300 µL of hexane was added to the sample, vortexed for 30 s, and then centrifuged (2000 x g, 4 °C for 5 min). 300 µL of the upper layer was transferred to a glass auto sampler vial for GC-MS analysis. Another 200 µL of hexane was added to the sample and the extraction repeated. Samples were analyzed using a 7890A gas chromatograph coupled with an Agilent 5975C mass selective detector (Agilent Technologies, Santa Clara, CA). A HP-5-MS (5 %-diphenyl 95%-methylpolysiloxane) capillary GC column (30 m x 250 µm i.d. 2.5µm film thickness, Agilent Technologies) was used with helium as the carrier gas at a constant flow rate of 1 mL/min. 0.5 µL sample was injected onto the column using a pressure pulsed split (10 psi, split ratio 10/1) The initial column temperature was set at 55 ºC for 0.5 min and then increased to 70 ºC at a rate of 10 ºC /min, increased to 85 ºC at a rate of 3 ºC /min, increased to 110 ºC at a rate of 5 ºC /min, increased to a final temperature of 290 ºC at a rate of 30 ºC/ min which was held for 5 minutes. The temperatures of the front inlet, transfer line and mass source were

set at 260 ºC, 290 ºC, 230 ºC. Mass spectral data was collected in a full scan mode over the a mass range 35-500 *m/z* with an electron energy of 70eV. All raw data were processed with Enhanced Chemstation (Agilent Technologies) for mass spectral visualization, identification, and quantitation. The integrated areas of the SCFAs were normalized to the internal standard and quantified with a standard curve constructed from serial dilutions (2500 µM, 1250 µM, 625 µM, 315 µM, 156.25 µM, 78.125 µM, 0) of SCFAs .

Nuclear Magnetic Resonance (NMR) Spectroscopy Sample Preparation

Cecal content or fecal samples (50 mg-100 mg) was mixed with 800 µL of phosphate buffer (K_2HPO4/NaH_2PO4, 0.1 M, pH 7.4, 50% v/v D_2O) containing 0.005% TSP-d4 as a chemical shift reference (δ 0.00 ppm). The sample was freeze/thawed three times with liquid nitrogen then homogenized (Precellys 24, Bertin Technologies, Rockville, MD) and centrifuged (13,200 x g, 4 °C) for 10 min. The supernatant was transferred to a new microcentrifuge tube and another 400 µL of PBS was added to the pellets and the above procedure repeated. The supernatants were combined, centrifuged (13,200 x g, 4 °C, 10 min), and 550 µL was transferred to NMR tubes. Liver tissues (50 mg) were extracted three times with 600 µL of precooled methanol-water mixture (2/1, v/v) using the Precellys tissue homogenizer (Bertin Technologies). After homogenization and centrifugation (13,200 x g, 4 °C, 10 min), the combined supernatants were dried and reconstituted in 600 µL phosphate buffer (K2HPO4/NaH2PO4, 0.1M, pH 7.4, containing 50% D_2O and 0.005% TSP-d_4). After centrifugation (13,200 x g, 4 °C, 10 min), 550 µL of each extract was transferred into an NMR tube for analysis. Serum samples (200 µL)

were combined with 400 µL of phosphate buffer (K_2HPO4/NaH_2PO4, 45mM, pH 7.4, 50% v/v D_2O containing 0.9% NaCl) and centrifuged (13,200 x g, 4 °C, 10 min). 550 µL of supernatant was transferred into NMR tubes for analysis.

^{1}H NMR Spectroscopy, Spectral Data Processing, and Multivariate Data Analysis

^{1}H NMR-based metabolomic analysis was performed as previously described (20). Color-coded loading plots were generated from the OPLS-DA models using a script for MATLAB (The Mathworks Inc.; Natick, MA). OPLS-DA scores represent the model power and the color-coded correlation coefficient indicates the significance of the metabolite contribution to the class separation, with a "hot" color (e.g., red) being more significant than a "cold" color (e.g., blue). In this study, a cutoff value of $|r| > 0.707$ ($r > 0.707$ and $r < -0.707$) was chosen for correlation coefficient as significant based on the discrimination significance ($p \leq 0.05$). SCFAs in cecal content and feces were assigned with two dimensional ^{1}H-^{1}H total correlation spectroscopy (TOCSY) NMR (**Figure 3-1**). Relative content of each SCFA is determined by NMR peak area of SCFA relative to internal standard (TSP-d_4).

Bomb Calorimetry

Bomb calorimetry was performed using a 6200 isoperibol calorimeter (Parr Instrument Company, Moline, IL). Dried fecal samples (100 mg) were weighed and ground in a clean mortar and pestle. Ground samples were pressed into ¼ inch diameter pellets (Parr 2812 Pellet Press, Moline, IL). The remaining moisture content was removed from the fecal pellet using a speedvac concentrator (Thermo Fisher Scientific,

Marietta, OH). Benzoic acid pellets were used for standardization and optimization of the bomb calorimeter. Samples were placed in a tared fuel capsule (208AC) in the 1109A semi-micro oxygen bombs (Parr Instrument Company, Moline, IL) and fixed by a coiled 10 cm of NiCr fuse wire (PN 45C10). A minimum 99.5% purity oxygen was provided with 420 psi pressure to the bomb. Prepared semi-micro bomb were set on a ring support in the A604DD twin-chambered calorimeter bucket. Gross heat of samples were determined by the temperature change recorded during combustion and expressed as calories/gram feces.

Quantitative PCR analysis

RNA of liver (50mg) were extracted using TRIzol reagent (Invitrogen, Carlsbad, CA). DNA concentration was determined by Nanodrop. cDNA was synthesized from 1 μg of total RNA using qScript cDNA SuperMix (Quanta Biosciences, Gaithersburg, MD) and then were diluted to 1μg/μL before subjected to quantitative PCR. QPCR was performed using SYBR green QPCR master mix on an ABI Prism 7900HT Fast Real-Time PCR sequence detection system (Applied Biosystems, Foster City, CA). QPCR conditions were 95°C for 20 s; 95 °C for 0.01 s; 60 °C for 20 s; 95 °C for 15 s; 60 °C for 15 s and 95 °C for 15 s, 40 cycles. The reactions were analyzed according to the ΔΔCT method. All targeted mRNA were normalized to the GADPH mRNA as an internal control. Primer sequences for qPCR analysis of genes were listed in **Table 3-1**.

Statistical Analysis

Graphical illustrations and statistical analysis were performed using Prism GraphPad version 6. All data values were expressed as mean ± SEM. $p<0.05$ was considered significant.

RESULTS

Tempol Influences Weight Gain and Preserves Liver Function in a Dose-Dependent Manner

To determine if the observed anti-obesity effect of tempol is dose-dependent, mice were treated with tempol (0, 1, 10, 50 mg/kg) by gavage for 5 consecutive days. The control group and 1 mg/kg tempol group mice showed a 1.5% increase in body weight per day over the treatment period (**Figure 3-2A**). However, the body weight gain for 10 mg/kg tempol treated mice showed a similar rate (1.5% per day) for the first two days, and then decreased to 0.47% per day from day 2 to day 5. The 50 mg/kg tempol-treated mice showed significant weight loss over the entire study (1.65% per day). This data demonstrates that the body weight gain is inversely associated with the tempol dose. Change in body weights were not due to toxicity, as no change in wet liver weight to body weight ratio was observed (**Figure 3-2B**). Additionally, liver histology (**Figure 3-2C**) showed no morphological difference between control and tempol treated groups, further indicating that tempol treatment did not cause substantial physiological and histological abnormalities.

Tempol Modulates SCFAs Availability in Gut

It was reported that fecal SCFA concentrations are significantly higher in obese than lean counterparts (21, 22). In agreement with this finding, decreased cecal SCFAs

were found in 100 mg/kg, tempol-treated mice (**Figure 3-3**), suggesting that tempol inhibits bacterial fermentation and decreases SCFAs availability in the lower gut. To determine whether the SCFAs inhibition effect of tempol is dose-dependent, SCFA levels were measured in mice treated with different doses of tempol by global ^{1}H NMR metabolomics and targeted GC-MS metabolomic analysis. As shown in **Figure 3-4**, a dose-dependent decrease of SCFAs was observed in extracts from the cecal and feces upon tempol with the most significant decrease observed in the 50 mg/kg dose group. Specifically, when compared with control, the 50 mg/kg group exhibited a 41%, 25% and 39% decrease in cecal acetate, propionate, and butyrate, respectively, as identified by ^{1}H NMR. These changes were confirmed by GC-MS revealing a 28%, 63% and 37% decrease in cecal acetate, propionate and butyrate, respectively. In feces, a 50%, 36%, 21% decrease of acetate, propionate and butyrate and a 42%, 41%, 33% decrease of acetate, propionate and butyrate were identified by ^{1}H NMR and GC-MS, respectively. In general, higher amount of SCFAs were measured in the cecal contents than from feces by GC-MS quantification, indicating the SCFAs reabsorption and utilization occurred as the cecal contents passed through the colon. Interestingly, in the 50 mg/kg tempol group, an increase of amino acids (tyrosine and phenylalanine), nitrogenous bases (uracil) and the nitrogenous base derivative (hypoxanthine) were identified as being significantly changed in the cecum (**Figure 3-5A**) suggesting further alterations in amino acid and nucleotide metabolism in the small intestine.

Tempol-Treated Mice Excrete More Energy

Analysis of fecal metabolites revealed a dose-dependent increase of glucose and oligosaccharides in tempol-treated groups (**Figure 3-4C**) which are substrates for

microbial fermentation. This observation suggests decreased microbial fermentation ability of tempol-treated mice. To further validate these findings, bomb calorimetry was performed to determine the energy loss into feces (**Figure 3-6**). The feces collected from metabolic cages after the final dosing with tempol was used for gross heat measurements. The results demonstrated that as the tempol dose increased, there was a proportional increase in the total gross heat measured in the fecal pellets. Specifically, one gram of feces from the 50 mg/kg tempol treated mice contains, on average, 139 more calories compared to control mice. The increased fecal energy excretion is consistent with the decreased energy availability revealed by lower SCFA production after tempol treatment.

Tempol-Mediated Metabolic Changes in Liver Are Microbiota Dependent

To further determine the impact of tempol on energy metabolism, the liver metabolome was measured by ^{1}H NMR. No hepatic metabolite differences were identified for the 1 mg/kg dose (**Figure 3-7A**). However, at the 50 mg/kg dose, reduced glycogen, sugars and amino acids were identified and indicative of increased hepatic energy storage mobilization. The glucogenic and ketogenic amino acids phenylalanine and tyrosine, which promote catabolism for energy availability (23) were increased. Additionally, uridine, a nucleoside involved in glycolysis was upregulated in the 50 mg/kg tempol group compared to control. Another immunoprotective and neuroprotective nucleoside, inosine (24), was upregulated. These results suggest that the overall liver metabolism balance shifted from energy storage to energy generation.

Although observations in the current and previous studies suggested that tempol changes the gut microbiota and causes metabolic alterations in the liver, it is unclear whether these changes are a direct effect of tempol administration or are microbiota-

mediated. The germ-free mouse liver metabolome was not changed by 50 mg/kg tempol treatment as observed in conventionally-raised mice (**Figure 3-7B**), indicating the microbiota play a vital role in directing metabolic alterations with tempol.

Tempol-Altered Microbiota Result in Altered Serum Metabolites

Similar to the ^{1}H NMR metabolomics profiles of the liver, a significant dose-dependent effect was identified in the serum of conventionally-raised mice (**Figure 3-8A**). No significant changes were seen in the 1 mg/kg tempol treated mice, while a variety of metabolites were altered in the 10 mg/kg and 50 mg/kg groups. Specifically, pyruvate, lactate, and citrate were increased while glucose was markedly decreased, indicating upregulation of glycolysis. However, the germ free mouse serum profile was not significantly changed compared to control (**Figure 3-8B**), again demonstrating that the induced metabolic shifts by tempol are microbiota-dependent.

Tempol Alters Hepatic Gene Expression Involved in Glucose and Lipid Metabolism

To further investigate the molecular mechanisms associated with the observed metabolic changes, the expression of genes associated with glucose and lipid metabolic pathway were analyzed by QPCR. The 50 mg/kg tempol treatment group had significantly increased hepatic expression of *Pepck and G6pase* mRNA by one to two fold in conventionally-raised mice (**Figure 3-9A**), indicating upregulation of gluconeogenesis and glycolysis. Moreover, an overall decrease or decreased trend of hepatic expression of *Hnf4a*, *ChREBP*, *Fabp1*, *Fabp2*, *Fabp5*, and *Cd36* mRNAs encoding adipogenic transcription factors and proteins were detected in the conventional 50 mg/kg tempol treated mice (**Figure 3-9B**). These results suggest upregulation of *de*

novo lipogenesis and improvement of lipid metabolism, consistent with the adiposity-resistant phenotype observed with tempol. No significant changes in the expression of these genes were identified in germ-free tempol-treated mice, again demonstrating the effects of tempol are highly dependent on the gut microbiota.

DISSCUSION

Here we have proposed that tempol restricts energy availability in the host through inhibition of microbial SCFA production. Other studies reported greater colonic SCFA production in overweight and obese individuals compared to lean counterparts in humans independent of dietary intake (21, 22, 25) . These observations indicate SCFA metabolism plays a significant role in obesity. Consistently, the anti-obesity compound tempol decreases cecal and fecal acetate, propionate, and butyrate levels in a dose-dependent manner. Moreover, the substrates for microbial fermentation, glucose and oligosaccharides, were excreted in greater quantities into feces in tempol treated mice. Thus it is likely that the reduced energy-harvesting potential of tempol-altered gut microbiota contributes to the metabolic improvements observed in models of diet-induced obesity (2, 26).

In addition to the restriction in energy availability, tempol profoundly impacts the overall metabolism of the host. SCFAs are not only direct energy substrates for tissues but also substrates for gluconeogenesis (e.g., propionate) (27, 28) and lipogenesis (18). For gluconeogenesis, propionate acts as a precursor (29, 30) which is first converted to propionyl-CoA and then to succinyl-CoA. Succinyl-CoA enters the citrate cycle to generate oxaloacetate, the direct precursor for gluconeogenesis. Therefore, a restricted

SCFAs availability would be expected to lead to downregulated glucose anabolism and decreased anabolic product like glycogen and glucose. As expected, with tempol treatment, an overall decrease in glycogen, sugars, and amino acid reserves in were observed in liver, suggesting decreased glucose anabolism and increased glucose catabolism, consistent with a lean phenotype and the previously described insulin sensitivity improvement effect of tempol (31). Moreover, elevated hepatic acetate levels suggest increased fatty acid catabolism, as acetate is an end product of fatty acid oxidation in liver peroxisomes (32, 33). The glucogenic and ketogenic essential amino acids phenylalanine and tyrosine are important for energy generation and they are also precursors of thyroid hormone and catecholamines (e.g., dopamine, epinephrine, norepinephrine) that act on adipose tissue to modulate lipolysis and thermogenesis (23). An upregulation of phenylalanine and tyrosine in tempol treated mice might indicate an alteration in energy production and lipid metabolism. Previous mouse studies suggested the serum glucose levels were decreased by restricting calories (34, 35). Serum glucose levels are also positively correlated with body mass index (BMI) observed in human studies (36, 37). Tempol serum metabolite profiles identified decreased glucose and amino acids levels consistent with the decreased hepatic glucose and amino acid reserves, improved insulin sensitivity, and lean phenotype. Lactate is derived from anaerobic glycolysis and subcutaneous fat (38, 39), which is also a major precursor for gluconeogenesis. Elevated lactate is consistent with upregulated glucose utilization and fat mobilization.

Alterations in the expression of key hepatic genes associated with glucose and lipid metabolic pathways further confirmed the metabolic changes revealed by

metabolomics. PEPCK is a rate-controlling enzyme in gluconeogenesis and its mRNA was upregulated in the 50 mg/kg tempol treated livers of conventional mice. mRNA encoding *G6Pase*, the key enzyme in gluconeogenesis and glycogenolysis that hydrolyzes glucose-6-phosphate to free glucose that can then enter circulation (40), was increased in the 50 mg/kg tempol group. Glycogenolysis and gluconeogenesis are two pathways to generate glucose from either glycogen or non-carbohydrate precursors. Both pathways are upregulated in tempol-treated group likely due to an adaptive response of liver in attempt to restore glucose level. As glucose utilization is accelerated with tempol treatment, hepatic glucose are deprived. Since glycolysis is upregulated, glucose is utilized quicker, and hepatic glucose is depleted. In order to keep up with the demand for glucose utilization, liver mobilizes both glucogenic pathways. Primarily, glycogenolysis is upregulated to free glucose from glycogen. Secondarily, gluconeogenesis is activated to generate more glucose from non-carbohydrate substrates. The upregulated glycogenolysis and gluconeogenesis indicated by hepatic gene expression with tempol treatment are consistent with the decreased hepatic glycogen reserves and increased hepatic gluconeogenic precursors (phenylalanine and tyrosine) revealed by ^{1}H NMR-based liver metabolites profiling. There was an increasing trend of *Glut*2 mRNA as well, typically increased with improved insulin sensitivity as seen in type II diabetes (41). Besides glucose metabolism related genes, mRNAs encoding transcription factors *Hnf4a and ChREBP*, and lipogenic proteins *Fabp1 and Cd36* were downregulated. The downregulation of genes involved in lipid metabolism in conventional tempol treated mice reveals inhibition of *de novo* lipogenesis by tempol which also explains the observed adiposity-resistant phenotype of conventional tempol treated mice.

Metabolic profiling of conventional tempol-treated mice suggests an energy balance shift from energy storage to substrate breakdown and energy generation, including glycogen catabolism, upregulating lipolysis, glycolysis for energy expenditure to compensate SCFAs restriction. It is likely that the combined effects of these pathways all contribute to the observed anti-obesity phenotyped in tempol-treated mice. Furthermore, these effects were highly dependent on the gut microbiota as germ free mice treated with tempol had no significant changes in their serum or liver metabolomics profile.

Obese microbiota profiling generated from mice and human studies were characterized as an elevated Firmicutes to Bacteriodetes ratio (26, 42-44) indicative of better fermentability with greater energy harvesting potential from the microbial community. Consistent with previous studies (13), a decreased Firmicutes to Bacteriodetes ratio was observed in the 50 mg/kg tempol group on a normal chow diet (**Figure 3-10B**). Other microbial changes reported with tempol treatment including decreasing abundance of β-Proteobacteria and *Lactobacillus* spp, were also confirmed in this study (**Figure 3-10C, 3-10D**). Overall, tempol helps modulate a more obesity resistant microbial community which provides a better gut environment for energy restriction and metabolic regulation.

CONCLUSION

The anti-obesity effects of tempol have been associated with its anti-oxidative stress properties (31, 45). Here, by comparing conventionally-raised and germ-free mice, the current studies demonstrated that tempol exerts its anti-obesity effect through

interactions with the gut microbiota and the host. Further, the tempol-altered microbiota is sufficient to promote the obesity resistant phenotype by causing metabolic changes from energy storage to expenditure.

REFERENCE

1. Wichmann A, Allahyar A, Greiner TU, Plovier H, Lunden GO, Larsson T, Drucker DJ, Delzenne NM, Cani PD, and Backhed F. Microbial modulation of energy availability in the colon regulates intestinal transit. *Cell host & microbe.* 2013;14(5):582-90.
2. Turnbaugh PJ, Ley RE, Mahowald MA, Magrini V, Mardis ER, and Gordon JI. An obesity-associated gut microbiome with increased capacity for energy harvest. *Nature.* 2006;444(7122):1027-31.
3. Guarner F, and Malagelada JR. Gut flora in health and disease. *Lancet.* 2003;361(9356):512-9.
4. Jernberg C, Lofmark S, Edlund C, and Jansson JK. Long-term ecological impacts of antibiotic administration on the human intestinal microbiota. *ISME J.* 2007;1(1):56-66.
5. Jakobsson HE, Jernberg C, Andersson AF, Sjolund-Karlsson M, Jansson JK, and Engstrand L. Short-term antibiotic treatment has differing long-term impacts on the human throat and gut microbiome. *PloS one.* 2010;5(3):e9836.
6. Pop M, Walker AW, Paulson J, Lindsay B, Antonio M, Hossain MA, Oundo J, Tamboura B, Mai V, Astrovskaya I, et al. Diarrhea in young children from low-income countries leads to large-scale alterations in intestinal microbiota composition. *Genome Biol.* 2014;15(6):R76.
7. Touw K, Wang YW, Leone V, Nadimpalli A, Nathaniel H, Gianricol F, Kashyap P, and Chang E. Drug-induced constipation alters gut microbiota stability leading to physiological changes in the host. *Faseb Journal.* 2014;28(1).
8. Benson AK, Kelly SA, Legge R, Ma F, Low SJ, Kim J, Zhang M, Oh PL, Nehrenberg D, Hua K, et al. Individuality in gut microbiota composition is a complex polygenic trait shaped by multiple environmental and host genetic factors. *Proc Natl Acad Sci U S A.* 2010;107(44):18933-8.
9. Jia W, Li H, Zhao L, and Nicholson JK. Gut microbiota: a potential new territory for drug targeting. *Nature reviews Drug discovery.* 2008;7(2):123-9.
10. Wilcox CS. Effects of tempol and redox-cycling nitroxides in models of oxidative stress. *Pharmacology & therapeutics.* 2010;126(2):119-45.
11. Francischetti IM, Gordon E, Bizzarro B, Gera N, Andrade BB, Oliveira F, Ma D, Assumpcao TC, Ribeiro JM, Pena M, et al. Tempol, an intracellular antioxidant, inhibits tissue factor expression, attenuates dendritic cell function, and is partially protective in a murine model of cerebral malaria. *PloS one.* 2014;9(2):e87140.
12. Kim CH, Mitchell JB, Bursill CA, Sowers AL, Thetford A, Cook JA, van Reyk DM, and Davies MJ. The nitroxide radical TEMPOL prevents obesity, hyperlipidaemia, elevation of inflammatory cytokines, and modulates atherosclerotic plaque composition in apoE-/- mice. *Atherosclerosis.* 2015;240(1):234-41.
13. Li F, Jiang C, Krausz KW, Li Y, Albert I, Hao H, Fabre KM, Mitchell JB, Patterson AD, and Gonzalez FJ. Microbiome remodelling leads to inhibition of intestinal farnesoid X receptor signalling and decreased obesity. *Nature communications.* 2013;4(2384.
14. Jiang C, Xie C, Li F, Zhang L, Nichols RG, Krausz KW, Cai J, Qi Y, Fang ZZ, Takahashi S, et al. Intestinal farnesoid X receptor signaling promotes nonalcoholic fatty liver disease. *The Journal of clinical investigation.* 2015;125(1):386-402.
15. Cummings JH. Short chain fatty acids in the human colon. *Gut.* 1981;22(9):763-79.
16. Hijova E, and Chmelarova A. Short chain fatty acids and colonic health. *Bratisl Med J.* 2007;108(8):354-8.
17. McNeil NI. The contribution of the large intestine to energy supplies in man. *Am J Clin Nutr.* 1984;39(2):338-42.
18. Zambell KL, Fitch MD, and Fleming SE. Acetate and butyrate are the major substrates for de novo lipogenesis in rat colonic epithelial cells. *J Nutr.* 2003;133(11):3509-15.

19. Zheng X, Qiu Y, Zhong W, Baxter S, Su M, Li Q, Xie G, Ore BM, Qiao S, Spencer MD, et al. A targeted metabolomic protocol for short-chain fatty acids and branched-chain amino acids. *Metabolomics : Official journal of the Metabolomic Society.* 2013;9(4):818-27.
20. Zhang L, Nichols RG, Correll J, Murray IA, Tanaka N, Smith PB, Hubbard TD, Sebastian A, Albert I, Hatzakis E, et al. Persistent Organic Pollutants Modify Gut Microbiota-Host Metabolic Homeostasis in Mice Through Aryl Hydrocarbon Receptor Activation. *Environ Health Perspect.* 2015;123(7):679-88.
21. Schwiertz A, Taras D, Schafer K, Beijer S, Bos NA, Donus C, and Hardt PD. Microbiota and SCFA in lean and overweight healthy subjects. *Obesity.* 2010;18(1):190-5.
22. Teixeira TF, Grzeskowiak L, Franceschini SC, Bressan J, Ferreira CL, and Peluzio MC. Higher level of faecal SCFA in women correlates with metabolic syndrome risk factors. *The British journal of nutrition.* 2013;109(5):914-9.
23. Pan YH, Zhang Y, Cui J, Liu Y, McAllan BM, Liao CC, and Zhang S. Adaptation of phenylalanine and tyrosine catabolic pathway to hibernation in bats. *PloS one.* 2013;8(4):e62039.
24. Guinzberg R, Cortes D, Diaz-Cruz A, Riveros-Rosas H, Villalobos-Molina R, and Pina E. Inosine released after hypoxia activates hepatic glucose liberation through A3 adenosine receptors. *American journal of physiology Endocrinology and metabolism.* 2006;290(5):E940-51.
25. Fernandes J, Su W, Rahat-Rozenbloom S, Wolever TMS, and Comelli EM. Adiposity, gut microbiota and faecal short chain fatty acids are linked in adult humans. *Nutr Diabetes.* 2014;4(
26. Ley RE, Backhed F, Turnbaugh P, Lozupone CA, Knight RD, and Gordon JI. Obesity alters gut microbial ecology. *P Natl Acad Sci USA.* 2005;102(31):11070-5.
27. Anderson JW, and Bridges SR. Short-chain fatty acid fermentation products of plant fiber affect glucose metabolism of isolated rat hepatocytes. *Proceedings of the Society for Experimental Biology and Medicine Society for Experimental Biology and Medicine.* 1984;177(2):372-6.
28. Reilly KJ, and Rombeau JL. Metabolism and Potential Clinical-Applications of Short-Chain Fatty-Acids. *Clin Nutr.* 1993;12(97-105.
29. Roy CC, Kien CL, Bouthillier L, and Levy E. Short-chain fatty acids: ready for prime time? *Nutr Clin Pract.* 2006;21(4):351-66.
30. Aschenbach JR, Kristensen NB, Donkin SS, Hammon HM, and Penner GB. Gluconeogenesis in Dairy Cows: The Secret of Making Sweet Milk from Sour Dough. *Iubmb Life.* 2010;62(12):869-77.
31. Banday AA, Marwaha A, Tallam LS, and Lokhandwala MF. Tempol reduces oxidative stress, improves insulin sensitivity, decreases renal dopamine D1 receptor hyperphosphorylation, and restores D1 receptor-G-protein coupling and function in obese Zucker rats. *Diabetes.* 2005;54(7):2219-26.
32. Leighton F, Bergseth S, Rortveit T, Christiansen EN, and Bremer J. Free Acetate Production by Rat Hepatocytes during Peroxisomal Fatty-Acid and Dicarboxylic-Acid Oxidation. *J Biol Chem.* 1989;264(18):10347-50.
33. Hovik R, Brodal B, Bartlett K, and Osmundsen H. Metabolism of Acetyl-Coa by Isolated Peroxisomal Fractions - Formation of Acetate and Acetoacetyl-Coa. *J Lipid Res.* 1991;32(6):993-9.
34. Mohamad-Shahi M, Karandish M, Haidari F, Omidian K, Fatemi-Tabatabayei SR, and Rafiei H. Effect of daidzein-low-calorie diet on body weight, serum levels of glucose, resistin, and high sensitive C-reactive protein in high fat, high calorie diet induced rats. *Saudi medical journal.* 2012;33(1):70-5.
35. Yamada KA. Calorie restriction and glucose regulation. *Epilepsia.* 2008;49(94-6.

36. Mehdad S, Hamrani A, El Kari K, El Hamdouchi A, Barakat A, El Mzibri M, Mokhtar N, and Aguenaou H. Body mass index, waist circumference, body fat, fasting blood glucose in a sample of moroccan adolescents aged 11-17 years. *Journal of nutrition and metabolism.* 2012;2012(510458.
37. Bakari AG, Onyemelukwe C, Sani BG, Aliyu S, Hassan SS, and Aliyu TM. Relationship between casual blood sugar and body mass index in a suburban northern Nigerian population: a short communication. *Nigerian journal of medicine : journal of the National Association of Resident Doctors of Nigeria.* 2007;16(1):77-8.
38. Gladden LB. Lactate metabolism: a new paradigm for the third millennium. *The Journal of physiology.* 2004;558(Pt 1):5-30.
39. DiGirolamo M, Newby FD, and Lovejoy J. Lactate production in adipose tissue: a regulated function with extra-adipose implications. *FASEB journal : official publication of the Federation of American Societies for Experimental Biology.* 1992;6(7):2405-12.
40. Beaufay H, and De Duve C. [The hexosephosphatase system. IV. Specificity of glucose-6-phosphatase]. *Bulletin de la Societe de chimie biologique.* 1954;36(11-12):1525-37.
41. Ren ZQ, Zhang PB, Zhang XZ, Chen SK, Zhang H, Lv DT, Zhuang BQ, Wen YQ, Hu HH, Ding WC, et al. Duodenal-jejunal exclusion improves insulin resistance in type 2 diabetic rats by upregulating the hepatic insulin signaling pathway. *Nutrition.* 2015;31(5):733-9.
42. Ley RE, Turnbaugh PJ, Klein S, and Gordon JI. Microbial ecology: human gut microbes associated with obesity. *Nature.* 2006;444(7122):1022-3.
43. Turnbaugh PJ, Backhed F, Fulton L, and Gordon JI. Diet-induced obesity is linked to marked but reversible alterations in the mouse distal gut microbiome. *Cell host & microbe.* 2008;3(4):213-23.
44. Furet JP, Kong LC, Tap J, Poitou C, Basdevant A, Bouillot JL, Mariat D, Corthier G, Dore J, Henegar C, et al. Differential adaptation of human gut microbiota to bariatric surgery-induced weight loss: links with metabolic and low-grade inflammation markers. *Diabetes.* 2010;59(12):3049-57.
45. Mitchell JB, Xavier S, DeLuca AM, Sowers AL, Cook JA, Krishna MC, Hahn SM, and Russo A. A low molecular weight antioxidant decreases weight and lowers tumor incidence. *Free radical biology & medicine.* 2003;34(1):93-102.

Figure 3-1

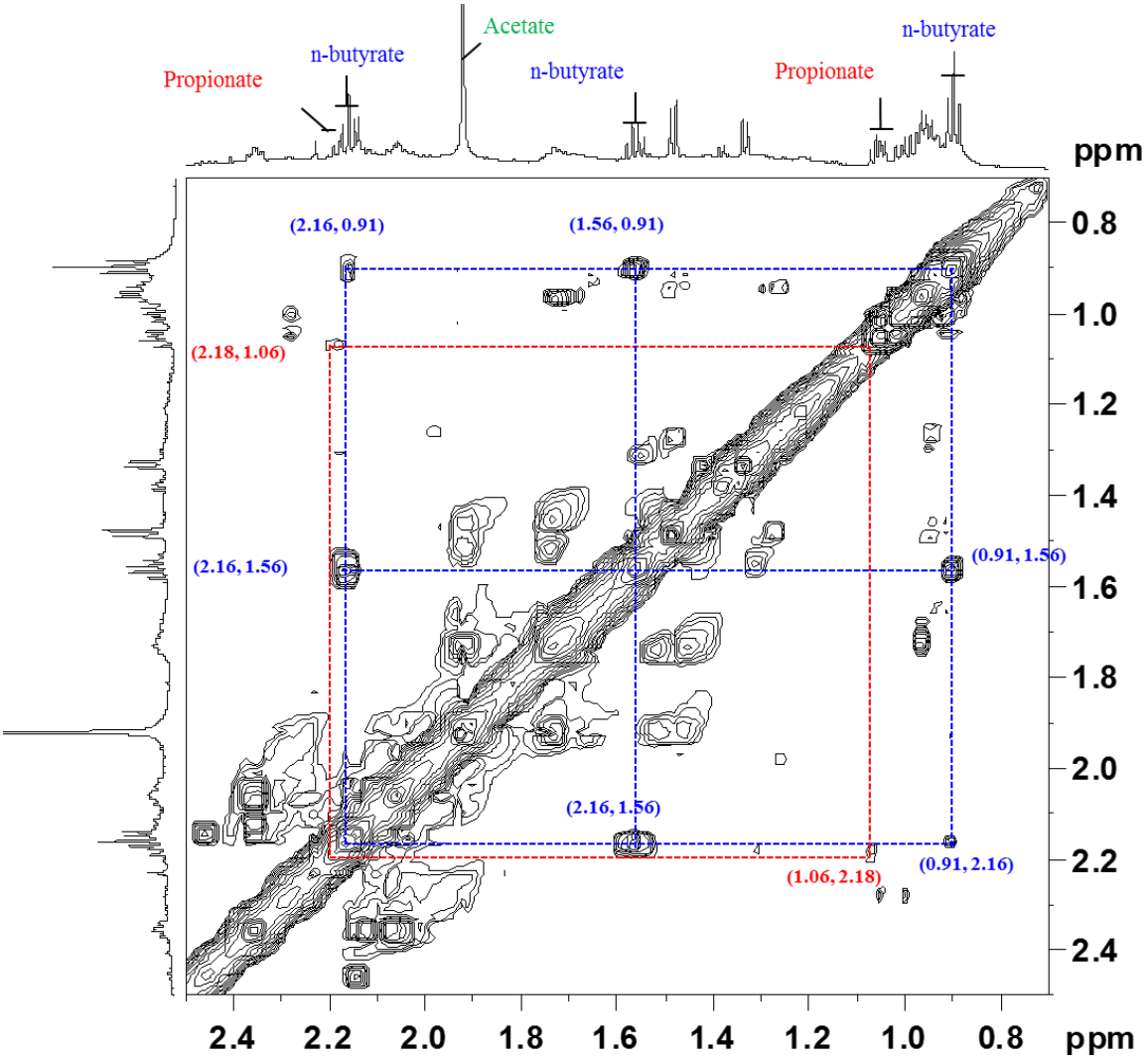

Figure 3-1. Two Dimensional ^{1}H-^{1}H Total Correlation Spectroscopy (TOCSY) NMR for SCFAs Identification. The cross peaks of propionate and n-butyrate are highlighted with red and blue dotted lines, respectively.

Figure 3-2

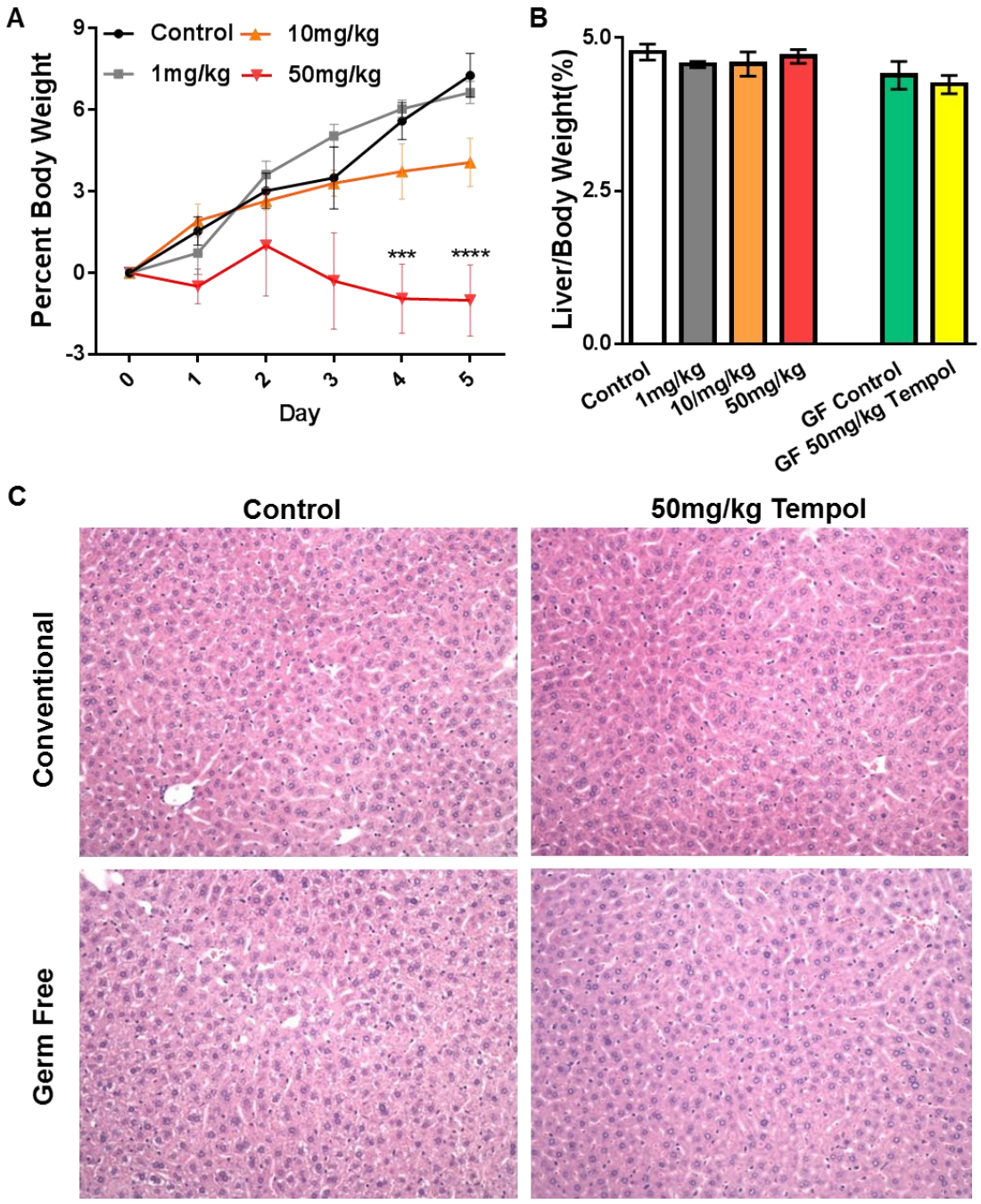

Figure 3-2. Tempol-Associated Weight Loss is Not Associated with Any Gross Histological Changes in the Liver. (A) Body weight change over 5 day tempol treatment (0.9% saline, 1 mg/kg, 10 mg/kg, 50 mg/kg) on a normal chow diet (n=5 mice per group). (B) Liver to body weight ratios in mice after gavage with tempol (n=5 mice per group). (C) Hepatic histology of representative hematoxylin and eosin-stained liver sections. All data are presented as mean ± SEM and analyzed using one-way ANOVA with Tukey's correction or two-tailed student's t-test. ***p<0.001, ****p<0.0001.

Figure 3-3

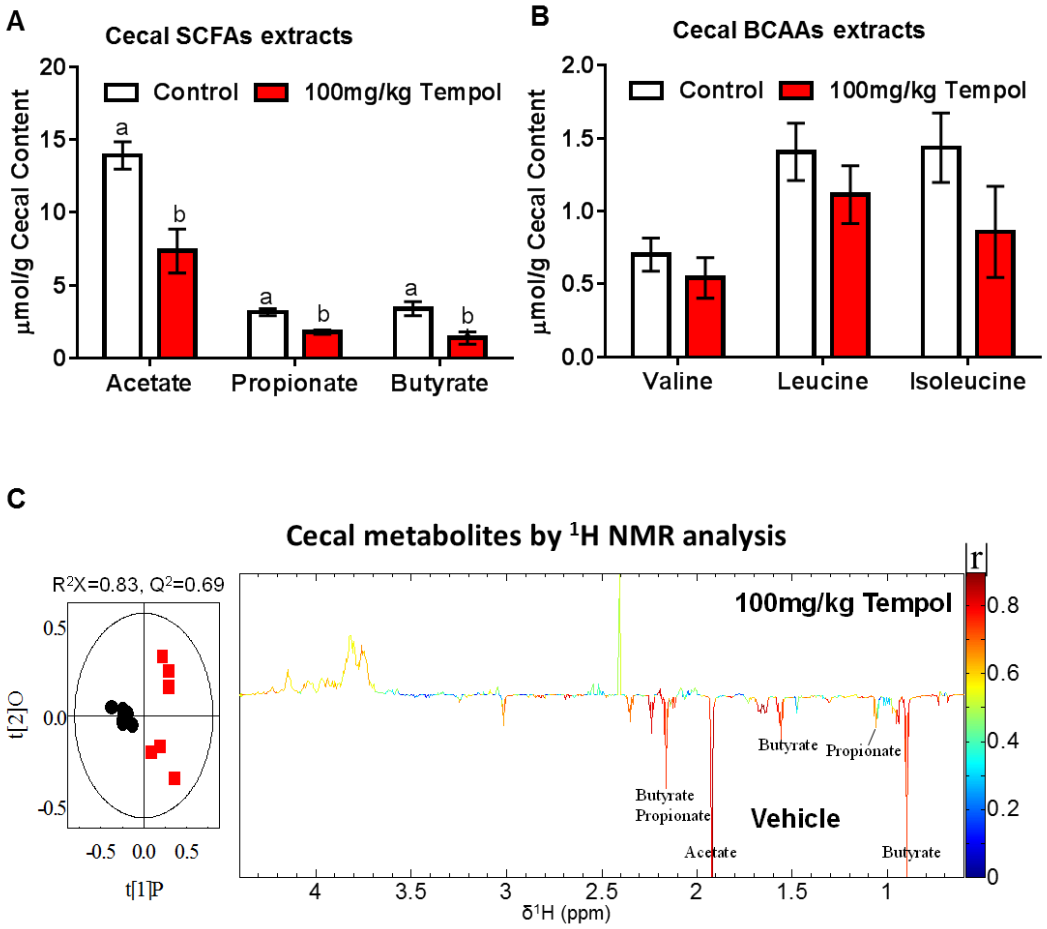

Figure 3-3. Tempol Causes Pronounced Changes in Bacteria Fermentation. (A-B) GC-MS quantification of cecal SCFAs and BCAAs in mice gavaged with 100 mg/kg tempol for 5 days (n=6 mice per group). Mann-Whitney test. Groups with different letters are significantly different ($p<0.05$). All data are presented as mean ± SEM. (C) Cecal metabolites change determined by ^{1}H NMR. OPLS-DA scores (left) represent indicative power of models and correlation coefficient-coded loadings plots for the models (right) from NMR spectra displaying changes and significance (n=6 mice per group).

Figure 3-4

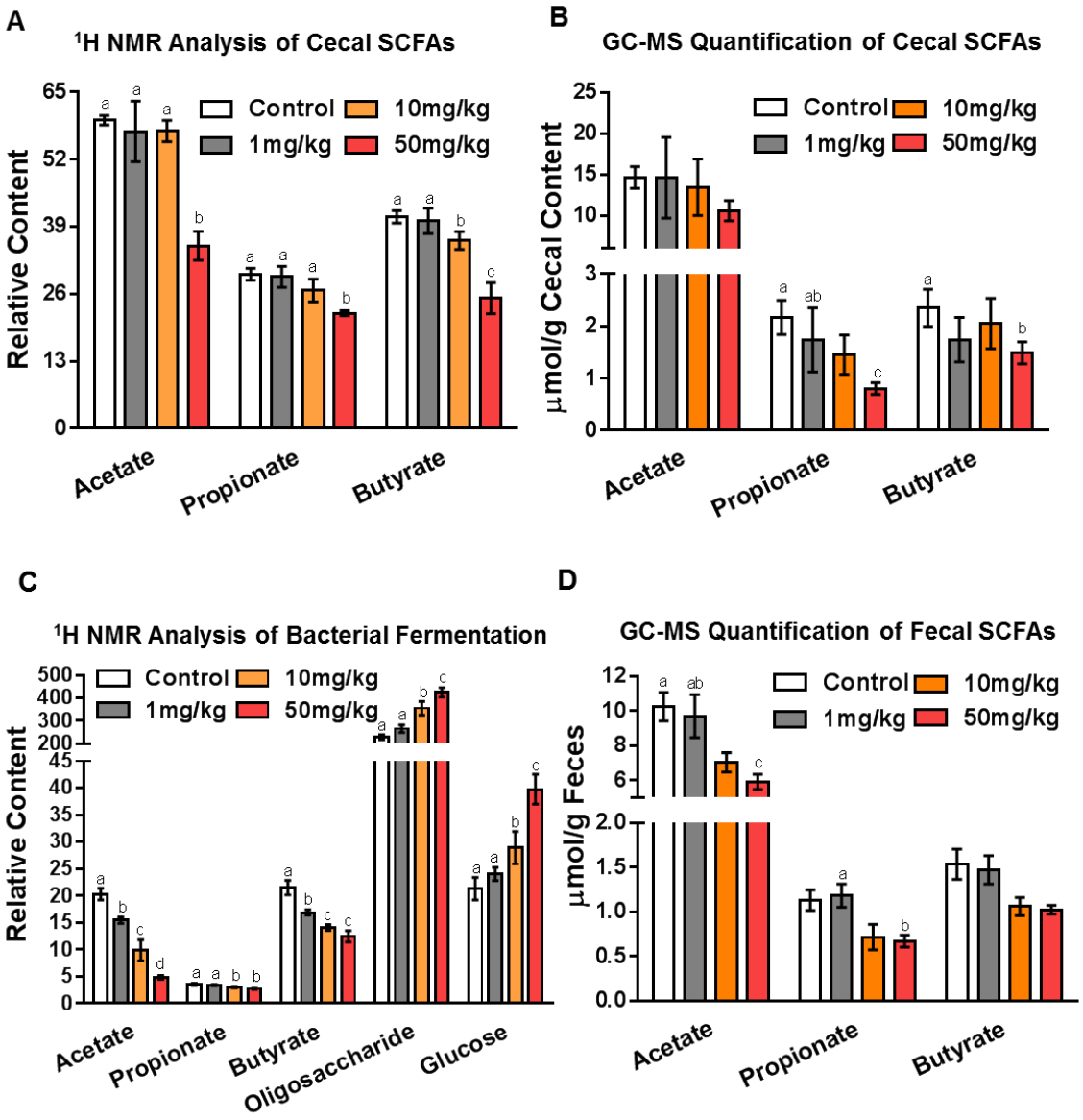

Figure 3-4. Tempol Inhibits Bacteria Fermentation in a Dose-Dependent Manner. (A and C) Cecal and fecal metabolites changes were determined by ^{1}H NMR. Relative content of metabolites were determined by NMR peak integration compared to the internal standard TSP in the cecal content and feces. Groups labeled with different letters are statistically significant ($p<0.05$), while groups sharing at least one letter are not significantly different. Groups without labels are not significantly different from other groups. (B and D) Quantification of SCFAs by GC-MS analysis was performed to validate results obtained via ^{1}H NMR. All data are presented as mean ± SEM. (n=5 mice per group) and analyzed using one-way ANOVA with Tukey's correction.

Figure 3-5

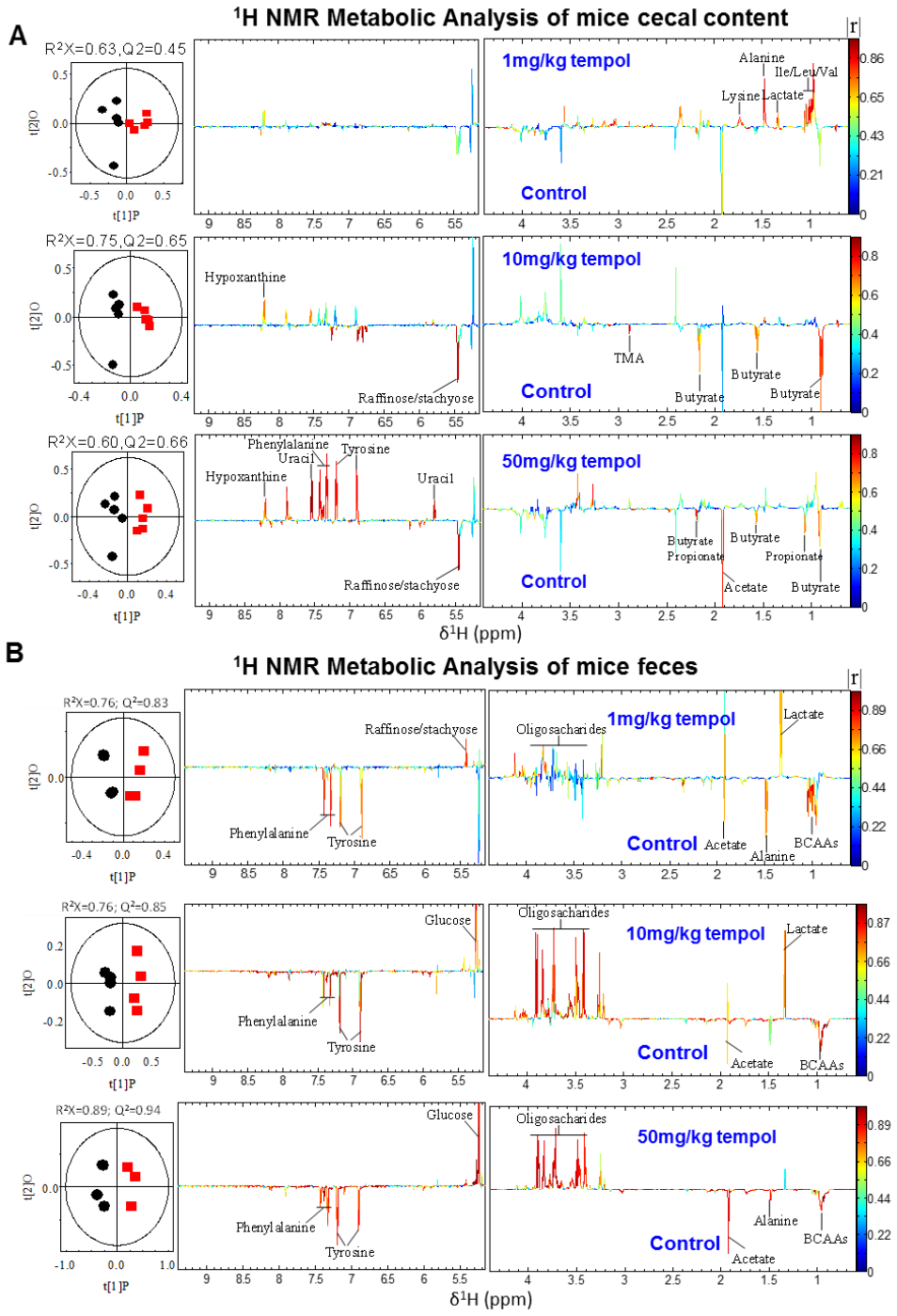

Figure 3-5. Tempol Causes Pronounced Changes in Cecal and Fecal Metabolites Determined by ^{1}H NMR. OPLS-DA scores (left) and correlation coefficient-coded loadings plots for the models (right) from NMR spectra of (A) cecal content, (B) feces obtained from different dose of tempol treated mice, displaying changes of metabolites between control group (black circles) and tempol treated group (red squares). (n=5 mice per group).

Figure 3-6

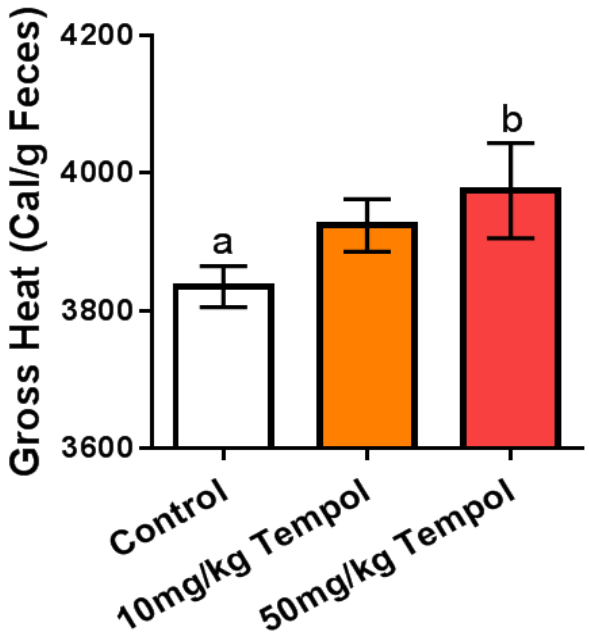

Figure 3-6. Quantification of Gross Heat of Feces by Bomb Calorimetry. Each Gross heat was averaged from duplications (n=5 mice per group). Groups with different letters are significantly different ($p<0.05$). Groups without labels are not significantly different from the other groups. One-way ANOVA with Tukey's correction. All Data are presented as mean ± SEM.

Figure 3-7

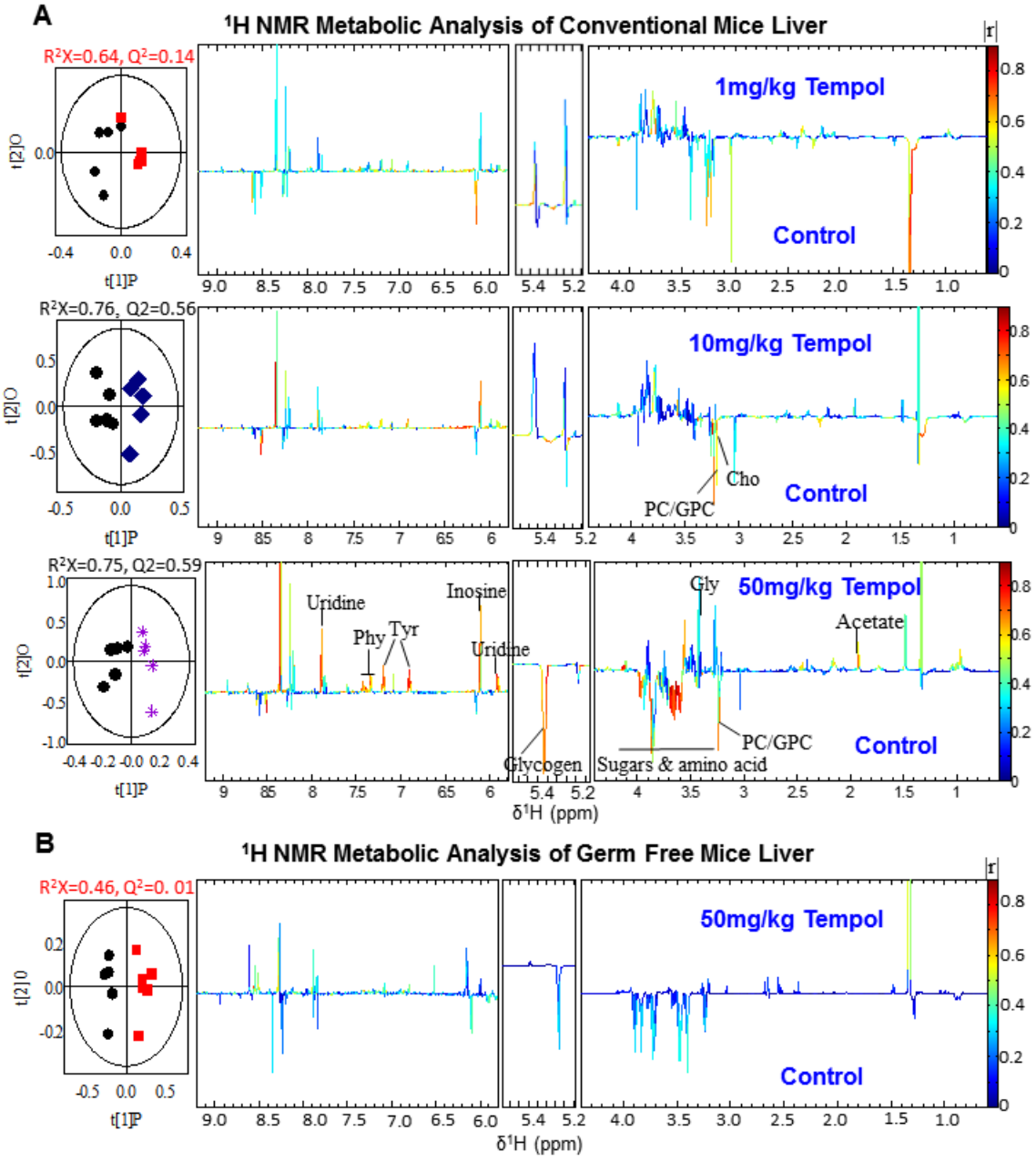

Figure 3-7. Liver Metabolism Shifts to a More Catabolic State in Conventionally Raised (CONV-R) Mice Treated with Increasing Doses of Tempol. (A) Conventionally-raised mouse liver metabolic profiles of control group (black circles) and 1 mg/kg (red squares), 10 mg/kg (blue squares), and 50 mg/kg (purple asterisks) tempol groups determined by ^{1}H NMR. OPLS-DA scores (left) and coefficient-coded loadings plots (right) for the models obtained from the ^{1}H NMR liver spectra (n=5 mice per group). (B) Comparison of germ-free mice liver metabolites between control group (back circles) and 50 mg/kg tempol group (red squares) determined by ^{1}H NMR (n=5 mice per group).

Figure 3-8

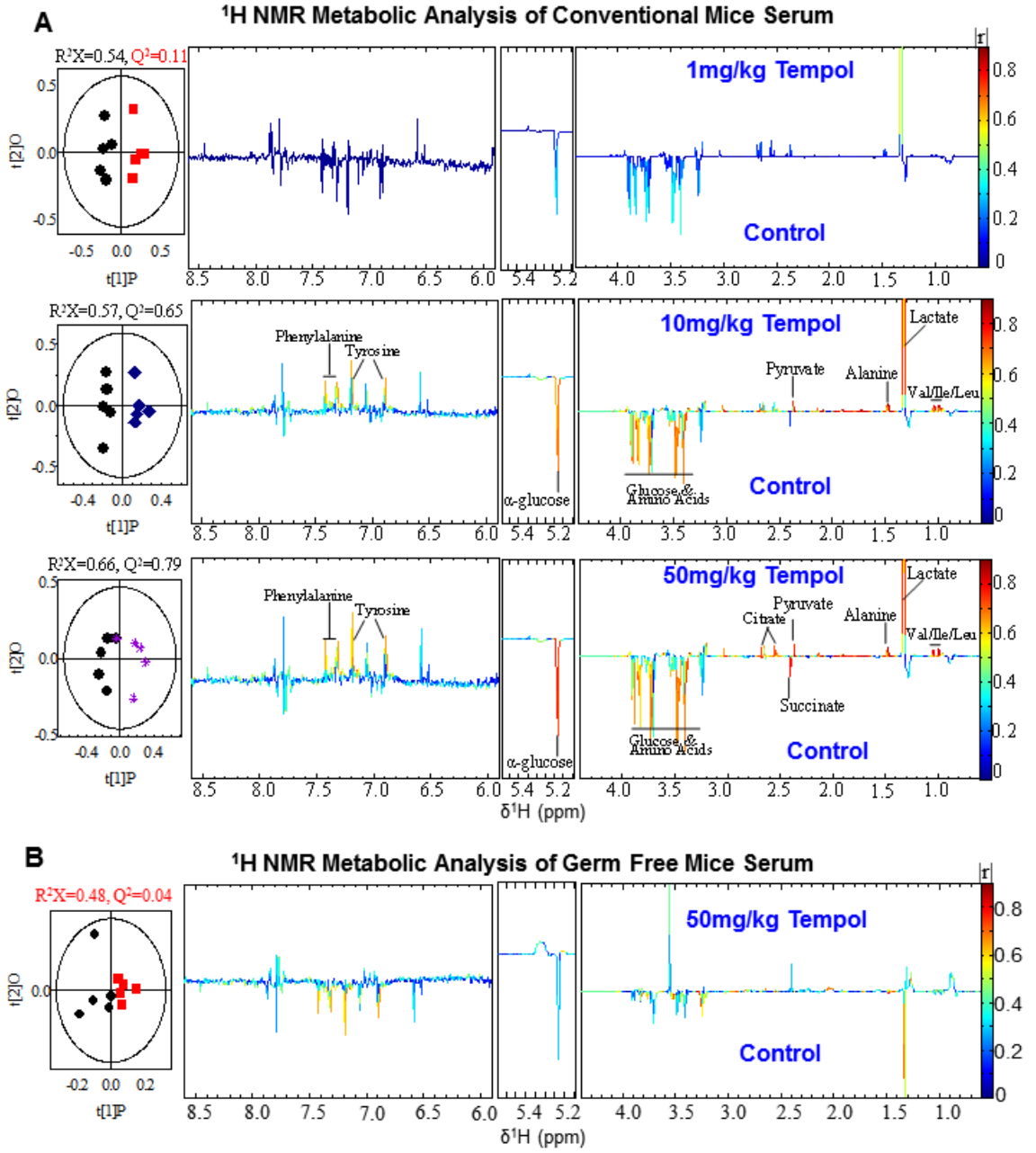

Figure 3-8. Serum Metabolites are Associated with Increased Glycolysis in Conventionally Raised (CONV-R) Mice Treated with Increasing Doses of Tempol. (A) Comparison of serum metabolic profiles of conventionally-raised mice between control group (black circles) and 1 mg/kg (red squares), 10 mg/kg (blue squares), and 50 mg/kg (purple asterisks) tempol groups determined by ^{1}H NMR. OPLS-DA scores (left) and the coefficient-coded loadings plots (right) for the models obtained from the NMR spectra of serum extracts (n=5 mice per group). (B) Comparison of serum metabolites between control group (black circles) and 50 mg/kg tempol group (red squares) determined by ^{1}H NMR in germ-free mice (n=5 mice per group).

Figure 3-9

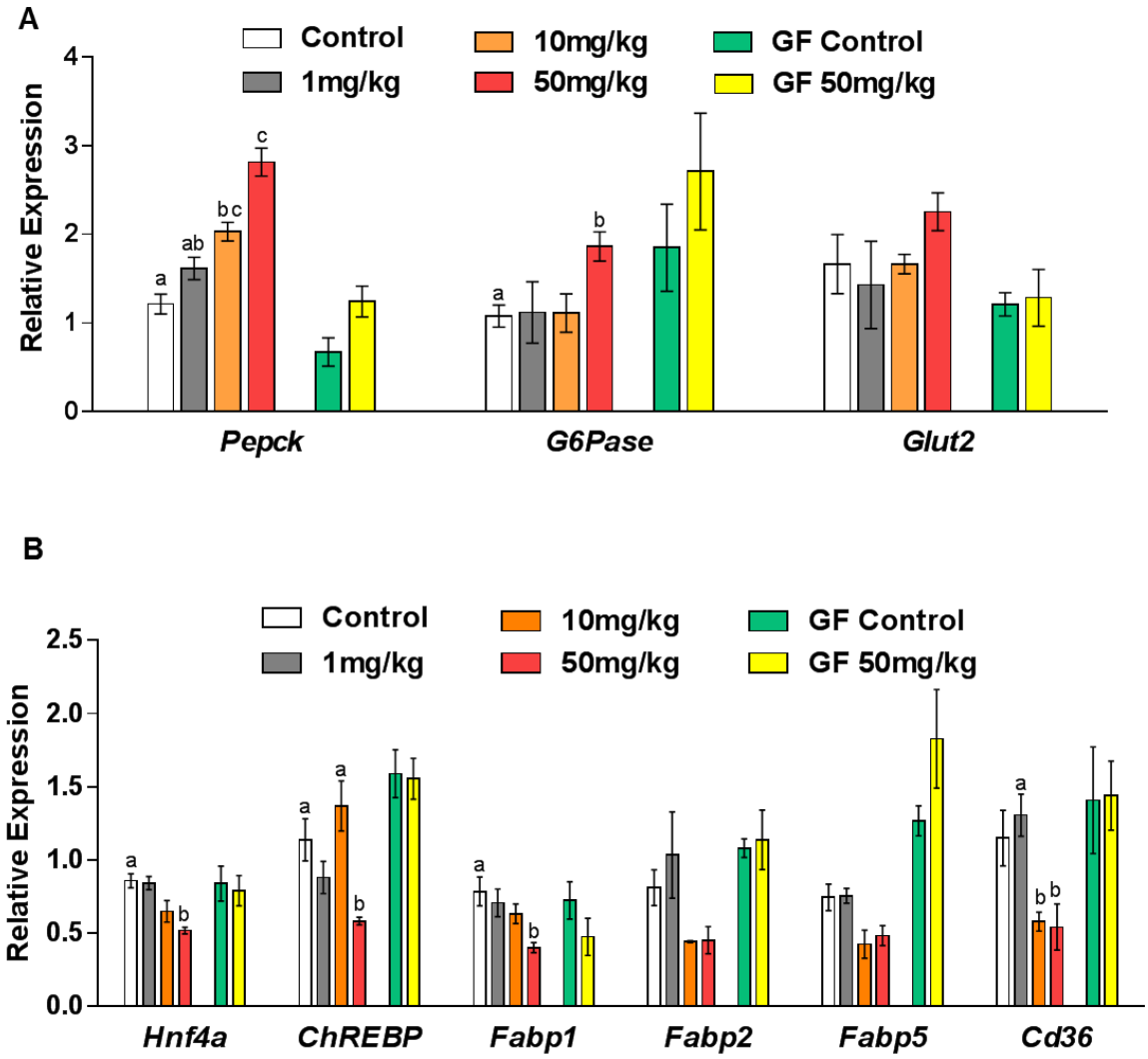

Figure 3-9. Tempol Altered Hepatic Expression of Genes Involved in Glucose and Lipid Metabolism. QPCR analysis of hepatic mRNA levels of (A) glucose metabolism related genes, (B) lipid metabolism related genes in conventionally-raised and germ-free mice after 5-day tempol treatment. Groups with different letters are significantly different ($p<0.05$). Groups without labels are not significantly different from other groups. All data are presented as mean ± SEM (n=5 mice per group) and analyzed using one-way ANOVA with Tukey's correction, or two-tailed Student's t-test.

Figure 3-10

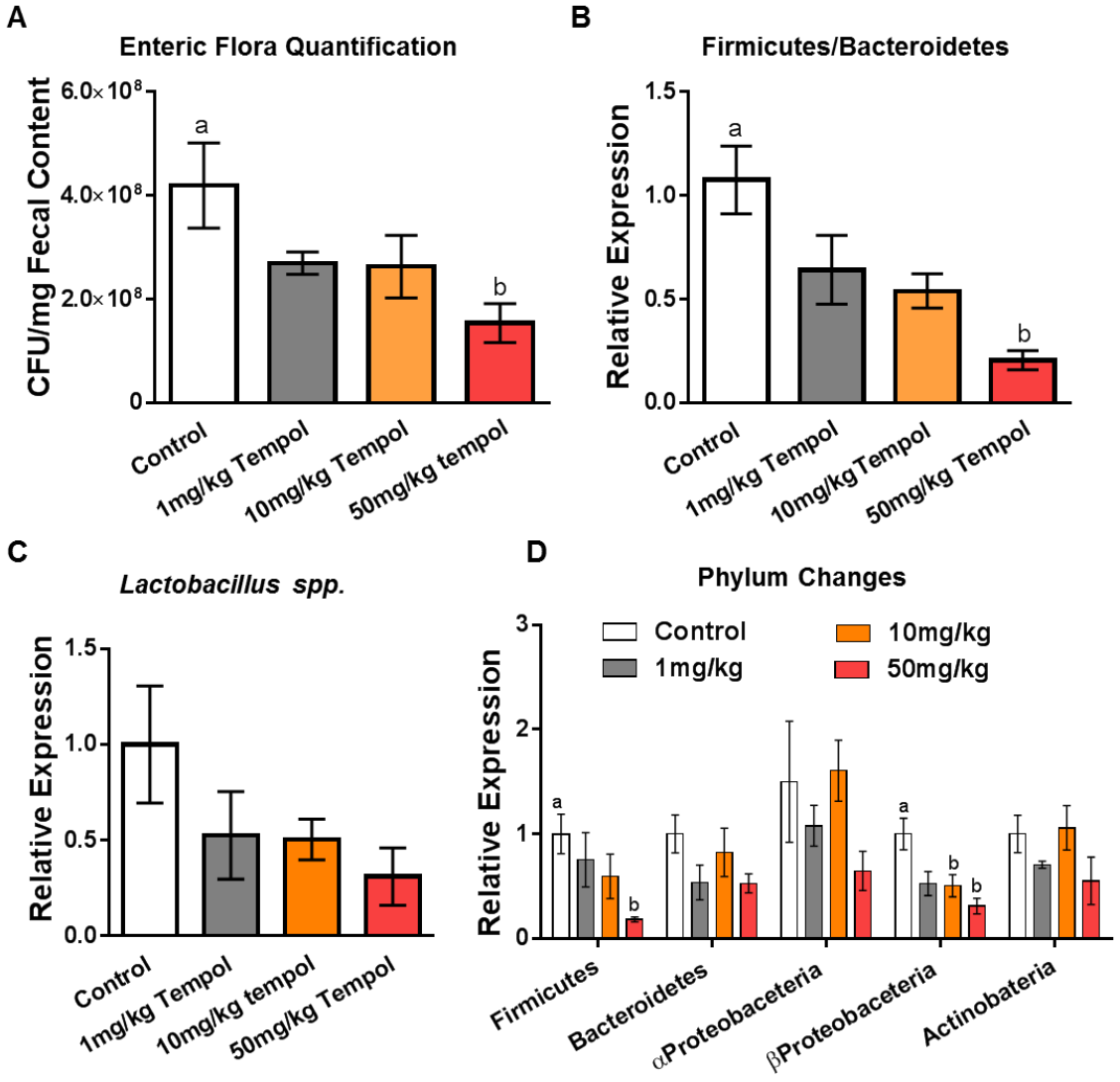

Figure 3-10. Tempol Modulates Bacterial Community Quantitatively and Compositionally (A) Quantitative PCR analysis of universal 16s rRNA gene of fecal microbiome using universal primers after 5-day tempol treatment at gradient dose (n=5 per group). Groups with different superscript letters were different with statistic significance ($p<0.05$). One-way ANOVA with Tukey's correction. All data are presented as mean ± SEM. (B-D) qPCR quantification of targeted 16s rRNA genes using specific primers after 5-day gradient tempol treatment (n=5 per group). Groups with different superscript letters were different with statistic significance ($p<0.05$). Group without label is not significantly different from other groups. One-way ANOVA with Tukey's correction. All data are presented as mean ± SEM.

Table 3-1. Primer Sequences for QPCR Analysis of (A) genes associated with glucose and lipid metabolic pathway, related to Figure 3-9. (B) Bacterial primer sequences, related to Figure 3-10.

A

species	gene name	sequence 5'-3'	sequence 3'-5'
mouse	*GADPH*	CCTCGTCCCGTAGACAAAATG	TGAAGGGGTCGTTGATGGC
mouse	*G6Pase*	CCATGCAAAGGACTAGGAACAA	TACCAGGGCCGATGTCAAC
mouse	*Pepck*	CCACAGCTGGTGCAGAACA	GAAGGGTCGATGGCAAA
mouse	*Glut2*	GTCCAGAAAGCCCCAGATACC	GTGACATCCTCAGTTCCTCTTAG
mouse	*Hnf4a*	TGAGCACCTGCTGCTTGGA	TCGAGGATGCGAATGGACAC
mouse	*ChREBP*	CTGGGGACCTAAACAGGAGC	GAAGCCACCCTATAGCTCCC
mouse	*Fabp1*	TCAAGCTGGAAGGTGACAATAA	GTCTCCATTGAGTTCAGTCACG
mouse	*Fabp2*	TCGGTTCCTGAGGATACAAGAT	TTTGATGACTGTGGGATTGAAG
mouse	*Fabp5*	ACAGGGTTTTTGCATTCCTG	TTGGTTCTTTCGAACCTTG
mouse	*Cd36*	TGGCCTTACTTGGGATTGG	CCAGTGTATATGTAGGCTCATCCA
mouse	*IL-1β*	TCGCTCAGGGTCACAAGAAA	CATCAGAGGCAAGGAGGAAAA
mouse	*Lcn-2*	ATTTCCCAGAGTGAACTGGC	AATGTCACCTCCATCCTGGT
mouse	*TNF-α*	AGGCTGCCCCGACTACGT	GACTTTCTCCTGGTATGAGATAGCAAA
mouse	*IFN-γ*	CAGCAACAGCAAGGCGAA	CTGGACCTGTGGGTTGTTGAC
mouse	*cyp1a1*	GGTTAACCATGACCGGGAACT	TGCCCAAACCAAAGAGAGTGA

B

target group	forward primer	reverse primer
All bacteria	AGAGTTTGATCCTGGCTCAG (8F)	CTGCTGCCTCCCGTAGGAGT (338R)
Lactobacillus.spp	AGCAGTAGGGAATCTTCCA (LabF362)	CACCGCTACACATGGAG (LabR677)
Firmicutes	GCAGTAGGGAATCTTCCG (Lgc353)	ATTACCGCGGCTGCTGG (Eub518)
Bacteroidetes	GTACTGAGACACGGACCA(Cfb319)	ATTACCGCGGCTGCTGG (Eub518)
αProteobacteria	ACTCCTACGGGAGGCAGCAG (Eub338)	TCTACGRATTTCACCYCTAC (Alf685)
βProteobacteria	ACTCCTACGGGAGGCAGCAG (Eub338)	TCACTGCTACACGYG (Bet680)
Actinobacteria	CGCGGCCTATCAGCTTGTTG (Actino235)	ATTACCGCGGCTGCTGG (Eub518)

Chapter 4

Multi-Platform Physiological and Metabolic Phenotyping Reveals Microbial Toxicity

Jingwei Cai[1], Robert G. Nichols [1], Imhoi Koo[1], Zachary A. Kalikow[1], Yuan Tian[1,2], Jingtao Zhang[1], Philip B. Smith[3], Andrew D. Patterson[1]

Affiliations: [1]Center for Molecular Toxicology and Carcinogenesis, Department of Veterinary and Biomedical Sciences, Pennsylvania State University, University Park, State College, Pennsylvania, 16802, USA; [2]CAS Key Laboratory of Magnetic Resonance in Biological Systems, State Key Laboratory of Magnetic Resonance and Atomic and Molecular Physics, National Centre for Magnetic Resonance in Wuhan, Wuhan Institute of Physics and Mathematics, Chinese Academy of Sciences (CAS), Wuhan 430071, China; [3]Metabolomics Facility, Huck Institutes of Life Sciences, Pennsylvania State University, University Park, State College, Pennsylvania, 16802, USA

Contributions: JC and ADP conceived and coordinated the study and wrote the manuscript. JC and ADP designed the experiment scheme shown in Figure 4-1 and 4-2 performed. JC performed the flow cytometry and metabolomics analysis and analyzed the data shown in Figure 4-3 to 4-9 and Table 4-1. RGN contributed to microbial sample preparation and data correlation analysis shown in Figure 4-5 and 4-8. IK contributed to LCMS data shown in Figure 4-9 and Table 4-1. YT, JZ, PBS contributed to the

metabolomics data interpretation and technical support shown in Figure 4-4, 4-6, 4-8 and 4-9. ZAK contributed to the animal model establish and sample preparation for flow cytometry and metabolomics analysis.

ABSTRACT

The gut microbiome can be considered an environmental and dietary sensor as it is extremely susceptible to modulation by environmental stimuli. Recent evidence suggests that xenobiotics can disrupt the intimate relationship between the microbiome and host. Here, we describe a novel approach that combines in vitro microbial incubation (isolated cecal contents from mice), flow cytometry, mass spectrometry- and ^{1}H NMR-based metabolomics to evaluate the effect of xenobiotics on microbial toxicity. A typical xenobiotic tempol known to remodel the microbial structure in vivo and improve host metabolism with unclear mechanism was assessed. The microbial cells were isolated from mouse cecal content and exposed to tempol for 4h under strict anaerobic condition in vitro. The flow cytometry data suggested DiBAC+ and PI+ cells were significantly increased with tempol exposure, indicating excessive membrane depolarization and loss of membrane integrity. CFDA+ cells were significantly decreased with tempol exposure, indicating compromised metabolic activity. NMR metabolic profiling revealed a unique, strong and direct correlation of microbial physiology and microbial metabolites, including short chain fatty acids, branched chain amino acids, amino acids, glucose and oligosaccharides, suggesting the disrupted microbial metabolic activity is strongly correlated with the microbial membrane damage by direct xenobiotic exposure. Orbitrap-LC-MS analysis identified over 40 significantly changed microbial metabolites with a broad coverage of metabolic pathways, providing additional biomarkers for microbial membrane damage and metabolism disruption following xenobiotic exposure. In addition, an in vivo mouse study with tempol (5 days gavage) showed similar microbial physiological and metabolic phenotypes, indicating the translational application of the in

vitro approach. Our results, through phenotypic evaluation of microbial viability, physiology and metabolism, and comparison of in vitro and in vivo exposures with representative xenobiotics like tempol, suggests this novel multi-platform physiological and metabolic phenotyping provides unique insight into gut microbiome toxicity to better inform risk assessment and drug screening.

INTRODUCTION

Trillions of microbes reside in the gastrointestinal tract and can significantly influence host health, by producing metabolites or molecules that function as available energy sources (e.g., short-chain fatty acid (SCFA)) (1, 2), metabolic signals (e.g., bile acid) (3, 4) and immune signals (e.g., lipopolysaccharides (LPS))(5, 6). The gut microbiota is also profoundly involved in xenobiotic metabolism (drug, environmental toxicants), through altering xenobiotic-metabolizing enzymes levels (7, 8), regulating the activation of nuclear receptors like the aryl hydrocarbon receptor (AHR) (9, 10), or executing direct microbial biotransformation (11). Emerging metagenomic and taxonomic tools like long read sequencing with the Pacific Biosciences Sequel system (12), online user interfaces like Microbiome Analysist (13), and machine learning prediction algorithms (14) have enabled the exploration of the diverse and complex microbial community structure. Additionally, metabolomics approaches, including MS- and NMR-based techniques provide valuable data to inspect the metabolic fingerprints and investigate the correlations between the metabolic profile and physiological or metabolic phenotype. Despite metagenomics and metabolomics have revealed a critical xenobiotic-microbiome-host axis (9), direct microbial toxicity caused by xenobiotic

exposure remains unexplored. Microbial toxicity assessment is important to understand the potential for drugs and other xenobiotics to influence the microbiome directly. This is especially true for pharmaceutical chemicals whose metabolic fate and risk are not fully elucidated (e.g., tempol (4-hydroxy-2,2,6,6-tetramethylpiperidin-1-oxyl)).

Single-cell techniques, including flow cytometry opens the door for investigating physical and chemical characteristics of microbial communities on a cellular level. Flow cytometric analysis has been employed to study biochemical activity of a microbial population within environmental systems including waste water (15, 16) and aquatic ecosystems (17, 18), characterize the physiological structure of the gut microbiota (19, 20), and assess the microbial response to xenobiotic (21-23) and physical stress (24-26). Physiological and metabolic status can be characterized with different fluorescent dyes **(Figure 4-1).** One critical physiological parameter is nucleic acid content. Generally, cells with high nucleic acid content indicate more rapid transcriptional and metabolic activity and higher growth rate than cells with low nucleic acid content (27, 28). Nucleic acid-labeling with the fluorescent dye like SYBR Green stains single and double stranded nucleic acids with relatively high affinity regardless of cell membrane status. The microbial membrane status is a vital physiological indicator of cellular damage, as the loss of membrane integrity and polarity resulting in compromised selective permeability and functionality. Propidium iodide (PI) is the most commonly used red nucleic acid dye to determine viability of cell (29, 30), as it cannot penetrate intact cell membrane due to its biochemical properties unless the membrane is severely damaged and unable to prevent the dye from leaking in and staining the nucleic acid. Oxonol dyes like Bis-(1,3-Dibutylbarbituric Acid) Trimethine Oxonol (DiBAC) can be used to assess loss of

membrane polarity (31, 32), another indicator of moderate cell damage. Typically, DiBAC is excluded from the cell as both the dye and phospholipid membrane are negatively charged. Once the membrane is depolarized and loses membrane potential, DiBAC enters and binds to the cellular lipid-containing component. Another indicative physiological feature of bacteria is metabolic activity, which can be measured by fluorogenic esterase substrates like carboxyfluorescein diacetate (CFDA) (15, 33, 34) and carboxyfluorescein diacetate succinimidyl ester (CFSE) (35). Fluorogenic esterase substrate is passively loaded into cell where it is converted by intracellular esterases into fluorescein analogs which are retained by cells. The strength of fluorescence corresponds to the enzymatic/metabolic activity. Labeling bacteria with esterified fluorogenic substrates followed by flow cytometric analysis offers a rapid measurement of metabolically active bacteria.

The rapid development of metabolomics techniques have successfully achieved high throughput and quantitative measures of small metabolites in complex biological matrices in biomedical studies for exploration of the metabolic effects of pharmaceutical (36, 37), environmental (38, 39) and dietary factors (40, 41). Mass spectrometry (MS) and nuclear magnetic resonance (NMR) spectroscopy are the most widely used platforms for global and targeting metabolomics research, and each technique has its own merits and limitations. MS-based metabolomics techniques like gas chromatography-mass spectrometry (GS-MS) and liquid chromatography-mass spectrometry (LC-MS) have excellent sensitivity and efficiency but relatively complicated extraction processes and less reproducibility; whereas NMR excels in high reproducibility and simple preparation procedure however is hampered by relative insensitivity (42, 43). Metabolome profiling

with combined MS and NMR techniques provides complementary insight into the characteristic changes of the metabolic, enzymatic pathways and networks following xenobiotic exposure. Metabolomics approaches also provide systemic tools to investigate global metabolites within microorganisms and monitoring the consequences of the interactions between microbiota and the external stressor (44, 45).

In the current study, microbial toxicity was evaluated physiologically and metabolically with isolated gut microbiota following short-term exposure to the xenobiotic tempol **(Figure 4-2)**. ^{1}H NMR and Orbitrap LC-MS global metabolomics and flow cytometric analysis were performed to characterize the metabolic and physiological changes following tempol exposure. Combining the accurate snapshot of the microbial physiological state provided by flow cytometry and the metabolic status profiled with global metabolomics, the study revealed the direct effect of tempol on microbial physiology and metabolism. Importantly, this study supports the potential of integrated multi-platform physiological and metabolic phenotyping for microbial toxicity.

MATERIALS AND METHODS

Microbiome Incubation and Collection

6-week-old wild-type male C57BL/6J mice (Jackson Laboratory, Bar Harbor, Maine) were transferred into anaerobic chamber (Coy Laboratory Products, Inc., Grass Lake, MI) following CO_2 asphyxiation. All the following procedures were performed under strict anaerobic conditions with an oxygen level below 20 ppm. The cecal content was collected and diluted 1:10 (1 g in 10 mL) with brain heart infusion (BHI) broth (Sigma, St. Louis, MO). Each suspension was prepared in triplicate (one for flow

experiment, the other two replicates for metabolomics analysis). The cecal content suspension was treated with tempol at a final concentration 0.01 mg/mL, 0.1 mg/mL and 1 mg/mL, following a brief centrifuge and incubation at 37 °C for 4 h in dark. The negative control group was treated with 12 mM HCl to reach a pH=4. After incubation, two sets of samples were stored at -80 °C for future metabolomics analysis. The other samples were centrifuged (700 g, 4 °C for 1 min). 600 µL of the microbial supernatant were transferred to a new tube and then centrifuged (6000 g, 4 °C for 3 min). Supernatant were discarded and the microbial pellet was washed with pre-filtered (0.2 µm) reduced PBS (1X PBS solution containing 137 mM sodium chloride, 2.7 mM potassium chloride, 10 mM phosphate buffer, 1 mg/mL L-cysteine and 1 µg/mL the oxygen indicator resazurin), centrifuged (6000 g, 4 °C for 2 min) and resuspended in 600 µL reduced PBS. The wash step was repeated two times until the microbial suspension was colorless. Then the microbial cell suspension was diluted 120 fold with reduced PBS. A 500 µL diluted microbial suspension was transfer to an FCM tube to be stained for physiology assessment.

Microbial Physiology Profiling with Flow Cytometry

Four distinct florescent dyes that stain cells based on nucleic acid content (SYBR Green I, final concentration 1×, 15 min), membrane damage (PI, final concentration 40 µg/mL, 15 min; and DiBAC, final concentration 1 µg/mL, 10 min) and biochemical activity (CFDA, final concentration 10 µM, 30 min) were applied to microbial suspension in the dark and under strict anaerobic condition. All cytometric analyses were made using an Accuri C6 flow cytometer (Becton Dickinson, Franklin Lakes, NJ)

equipped with a solid state 488 nm laser with standard filter setup. SYBR Green I (488/520), DiBAC (488/516), CFSE (488/517) fluoresce in the green channel (FL1) and PI (488/620) fluoresces in yellow channel (FL2). Data were analyzed with FlowJo software (V10, FlowJo, LLC). Cell growth and transcriptional activity was assessed by SYBR Green; metabolic activity was indicated by CFSE; PI and DiBAC were used as indicators of a compromised membrane and cell damage. Microbial suspension with a pH adjusted to pH=4 with 12 M HCl was used as a negative control for damaged microbial cell.

^{1}H NMR Metabolomics Profiling

The microbial suspension saved after 4h incubation were used for ^{1}H NMR spectroscopy. 1 mL of microbial suspension was centrifuged at low speed (700 g, 4 °C for 1 min) to pellet down large particles. Maximum volume of microbial supernatants were transferred to a new tube, centrifuged at high speed (6000 g, 4 °C for 3 min) to pellet down bacteria. The microbial pellet was washed two times with PBS. After the third wash, 1 mL of pre-cooled methanol:H_2O (v/v = 2:1) and 1.0 mm diameter zirconia/silica beads (BioSpec, Bartlesville,OK) were added to the microbial pellet, followed by homogenization (6500 rpm, 1 cycle, 60 s) using the Precellys tissue homogenizer ((Bertin Technologies, Rockville, MD). The homogenized sample was freeze-thawed three times with liquid nitrogen and 37 °C water bath, then was homogenized again and sonicated for 15 min at 250W (ultrasonic 1 min, stop 1 min, repeat 8 times) to rupture microbial cell walls and release intracellular metabolites. The sample was centrifuged (11180g, 4 °C, and 10 min) and the supernatants was transferred

to a new 2 mL tube. Another 1 mL methanol:H_2O (v/v = 2:1) was added to the pellets and the extraction procedure was repeated. All supernatants were combined, dried down and reconstituted in 600 μL of PBS (K_2HPO_4/NaH_2PO_4, 0.1M, pH 7.4, containing 50% D2O and 0.005% TSP-d4 as internal standard). Following centrifugation (13 000g, 4 °C, 10min), 550 μL of each extract was transferred into a 5 mm NMR tube for analysis.

^{1}H NMR spectra of extracted samples were acquired at 298 K on a Bruker NMR spectrometer (600 MHz for ^{1}H) configured a 5 mm inverse cryogenic probe as previously described (9). In brief, a standard one-dimensional NOESY – presaturation pulse sequence (Bruker 1D noesygppr1d pulse sequence) was employed with irradiation at the water frequency during the recycle and mixing time delays to suppress water signal. The 90° pulse length was adjusted to approximately 10 μs (9.6 dbW) and 64 transients were collected into 64 k data points for each spectrum with spectral width of 16 ppm. For the resonance assignment, a series of two-dimensional NMR spectroscopy were performed, including ^{1}H–^{1}H correlation spectroscopy (COSY), ^{1}H–^{1}H total correlation spectroscopy (TOCSY), ^{1}H- ^{13}C heteronuclear single quantum correlation (HSQC) and ^{1}H-^{13}C heteronuclear multiple-bond correlation (HMBC) spectra.

Quality of ^{1}H NMR spectra were improved by phase, baseline correction and calibration referenced to TSP-d4 (δ 0.0) using Topspin 3.0 (Bruker Biospin, Germany). The NMR spectra then were processed by AMIX 3.9.14 software (Bruker Biospin, Germany). The spectral region at δ 0.5- δ 9.0 was bucketed into 0.004 ppm bins. The residual water signal (region δ 4.2-5.2) was discarded prior to normalization. The binned spectral data were normalized to the sum of total intensity of the spectrum to compensate for the overall concentration differences. Multivariate data analysis was performed on the

normalized binned NMR data with SIMCA 13 (Umetrics, Sweden). Principal component analysis (PCA) was done first with the scores plots showing intergroup separation and the possible presence of outliers. Then orthogonal projection to latent structures with discriminant analysis (OPLS-DA) was performed with a 7-fold cross validation method using UV scaling. To perform OPLS-DA, a binary variable for Y is created and assigned when defining a class (in this case, control group is 0, tempol treatment group is 1) before importing to SIMCA. After the model fitting, R^2X and Q^2 values generated represent the predictive power and validity of the models, respectively. The validation of the OPLS-DA model was further confirmed by CV-ANOVA analysis (implemented in SIMCA 13). To facilitate interpretation of the results, color-coded loading plots using Pearson linear correlation coefficients of variables from OPLS-DA loadings were generated by MATLAB (The Mathworks Inc., Natwick, MA). The hotness of the color represents the significance of the metabolite contribution to intergroup separation, with a "hot/red" color being more significant than a "cold/blue" color. A cutoff value of $|r| > 0.754$ ($r > 0.754$ and $r < -0.754$) was used as significant based on the discrimination significance ($p \leq 0.05$).

LC-MS Metabolomics Profiling

600 µL of bacteria suspension after 4h incubation was centrifuged (700 g, 4 °C for 1 min) and supernatants were transferred to a new tube, centrifuged (6000 g, 4 °C for 3 min) and washed 3 times with PBS. After the final centrifuge, 1 mL cold 50% aqueous methanol containing 1 µM chlorpropamide and 1.0 mm diameter zirconia/silica beads (BioSpec, Bartlesville,OK) were added to the microbial pellet, following with the

homogenization (6500 rpm, 1 cycle, 60 s). The sample was freeze-thawed three times with liquid nitrogen to break tough microbial cell wall. Then the sample was centrifuged (max speed, 4 °C, and 10 min), supernatants were transferred to a new EP tube, dried down and resuspended in 200 µL 3% aqueous methanol. After a final spin (max speed, 4 °C, and 10 min), 150 µL supernatants were transferred to autosampler for LC-MS analysis.

Metabolomics profiling was performed with a Dionex Ultimate 3000 quaternary high-performance liquid chromatography (HPLC) pump, column compartment and autosampler coupled Exactive plus Orbitrap mass spectrometer controlled by Xcalibur 2.2 software (Thermo Fisher Scientific, Waltham, MA). LC-MS was run with a modified ion pairing reversed phase negative ion electrospray ionization method (46). A total volume of 10 µL sample is injected and separated on a Phenomenex (Torrance, CA) Hydro-RP C18 column (100 × 2.1 mm, 2.5 µm particle size) using a water/methanol gradient with tributylamine and acetic acid added to the aqueous mobile phase to enhance separation. The HPLC column is maintained at flow rate of 200 µL/min with the temperature of 30 °C. Solvents and gradient are as follows: Solvent A is 3% aqueous methanol with 10 mM tributylamine and 15 mM acetic acid; solvent B is 100% methanol. The gradient is 0 min, 0% B; 5 min, 20% B; 7.5 min, 20% B; 13 min, 55% B; 15.5 min, 95% B; 18.5 min, 95% B; 19 min, 0% B; and 25 min, 0% B. The Exactive plus is operated in negative ion mode at maximum resolving power (140,000), and scanned from m/z 72 -1000 for the first 90 sec and then from m/z 85-1000 for the remainder of the chromatographic run for the detection of small molecule metabolites. The automatic gain control target is 3E6 with a maximum injection time of 100 us, the nitrogen sheath gas

flow rate is set at 35, the auxillary gas at 10 and the sweep gas at 1. The capillary voltage is 3.2 kV and both the capillary and heater set at 200 °C, the S-lens was 55.

Orbitrap-LC-MS data was analyzed with the open-source software pipeline MS-Dial (47). An in-house library generated from 288 pure metabolite standards were used for peak identification with a strict accurate mass tolerance 0.002 Da (5 ppm at mass of 400) and retention time tolerance 0.5 min. Raw integrated data was normalized to chlorpropamide (m/z: 275.0262, RT:16.91). Filtering methods were applied to remove features with greater than 50 % gap-filling and their peak areas were less than background signal of blank injection. Chemical and biochemical similarity among identified compounds was calculated with MetaMapp (48). Biochemical mapping was calculated based on the KEGG reactant pairs database and chemical mapping was obtained from substructure comparison in PubChem database using Tanimoto chemical similarity. For the visualization of biochemical and chemical mapping, Cytoscape is used. P-value from statistical t-test and fold change can show node color (related to up- and down-regulation) and node size related to absolute value of fold change. MetaboAnalyst (http://metaboanalyst.ca)(49) is used for metabolite set enrichment analysis, which identify a collection of pre-curated metabolite pathways using KEGG pathway information. Significant pathway of globaltest's p-value less than 0.05 are selected for visualization by rendering PathView package (50). For the metabolic profile visualized with heatmap, Z-scores were created with the equation $z=((x- \bar{x}))/(sd(x))$. All shown identified metabolites are significant at $P<0.05$ from a student's t test in high tempol group relative to control. Heatmaps were created with the heatmap.2 function from the gplots package in R.

Quantitative PCR Analysis

Standard curve construction

E.coli (WT MG1655) was cultured in Luria Bertani media at 37°C, 220 rpm in the incubator overnight. Spectrophotometer readings at OD600 were obtained (Eon™ Microplate Spectrophotometer, BioTek) to estimate bacteria number. A series of diluted E.coli media (dilution degree is based on estimated bacteria number) were cultured on LB agar plates under the same conditions (24h at 37°C). All plate cultures analyzed in triplicate. The countable colonies counts were averaged to determine the total bacteria number, represented as colony-forming units (CFU). In parallel, DNA from the same E.coli culture was extracted using E.Z.N.A stool DNA kit (Omega BioTek). Quantitative PCR assays were carried out using 16S rRNA universal primers (8F: 5'-agagtttgatcctggctca-3', 338R: 5'-ctgctgcctcccgtaggagt-3') on serially diluted DNA with FastSYBR green QPCR master matrix on an ABI Prism 7900HT Fast Real-Time PCR sequence detection system (Applied Biosystems, Foster City, CA). The reactions were analyzed according to the ΔΔCT method. QPCR conditions were 95°C for 20 s; 95 °C for 3s; 60 °C for 30 s, 45 cycles. Standard curve was constructed with CT value versus microbial number.

Bacteria quantification

Microbial DNA from cecal content (50 mg) were extracted using E.Z.N.A stool DNA kit (Omega Bio-tek). DNA concentration was determined by Nanodrop and diluted in DEPC water at a concentration of 1 ng/μL. DNA was then subjected to quantitative

PCR using FastSYBR green with indicated universal 16S rRNA primers, PCR condition and ΔΔCT method above. Ct values were substituted into standard curve. Finally results were expressed as bacteria number per mg of microbial pellet. For relative specific bacteria quantification, specific primers were utilized instead of the universal primer.

Statistical Analysis

Graphical illustrations and statistical analyses were performed using Prism version 6. Microsoft Excel (2016) and R studio (1.1.419). All data values were expressed as mean ± sd. Statistical significance was defined as $p<0.05$. Pearson correlation analysis was used to investigate the relationships between stain intensity and metabolite levels across all three doses (low, medium and high). Statistical significance was determined by transforming the Pearson r values into t values and then using t distributions to determine P values. The equation used to find the statistical significant cutoff was r=t÷√((t^2+n-2)), where r is the correlation value and n is the number of subjects. In this experiment, n was equal to 24. The t value was found by using the Excel function tinv (0.05,22), where 0.05 represents a P value of 0.05 and 24 is the degrees of freedom for this experiment (n-2). Results were shown using the heatmap.2 function from the gplots package in R.

RESULTS

Short Term Exposure of Xenobiotic in Vitro Directly Impacts Microbial Physiology in a Dose-Dependent Manner

First, microbial physiology after short-term exposure of the xenobiotic tempol in vitro was examined using a flow cytometric approach **(Figure 4-3)**. Microbiota isolated directly from the mouse cecum were incubated in BHI broth containing different doses of tempol (0.01 mg/mL, 0.1 mg/mL and 1 mg/mL) under strict anaerobic condition for 4 hours. A pH=4 group was introduced as a positive control by treating microbiota with 12 mM HCl to reach a pH=4. Acid treatment caused direct, severe damage to microbial membranes indicated by a significant high percentage of PI+ cells (40.7% PI+ cells with pH=4 treatment versus 12.5% in control in average, $p<0.0001$, Student's t-test) and DiBAC+ cells (81.3% DiBAC+ cells in pH=4 group versus 39.2% in control group in average, $p<0.0001$, Student's t-test). Additionally, pH=4 group showed a significant slow growth rate indicated by a decrease of SYBR Green-stained cells (an average of 85.8 % SYBR+ cells in pH=4 group compared to 91.9% in control group; $p<0.0001$, Student's t-test), and drastically decreased metabolic activity revealed by very low percent of CFDA+ cells (2.3 % averaged CFDA+ cells in pH4 group comparing to 36.5% in control group; $p<0.0001$, Student's t-test). The negative control with the anticipated compromised physiology and metabolic activity validated the feasibility of the flow cytometry method. Flow cytometry analysis revealed a significant increase of DiBAC+ cells following high dose tempol exposure (1 mg/mL) and an marked elevation of PI+ cells at medium and high dose of tempol exposure (0.1 and 1 mg/mL) in vitro, indicating excessive membrane depolarization and loss of membrane integrity of microbiota in response to tempol. A significant decrease of CFDA+ cells were observed with all three different doses of tempol exposure (0.01 mg/mL, 0.1 mg/mL and 1 mg/mL) compared to control in vitro, suggesting the compromised metabolic activity of tempol-exposed microbiome. These

data together demonstrated tempol directly impacts membrane health and metabolic activity of microbiome in vitro without the involvement of host component. Notably, the impact of tempol on microbial physiology in vitro is dose-dependent with a 100-fold dose range (0.01 - 1 mg/mL).

Xenobiotic Tempol Directly Alters Microbial Metabolism in Vitro

We did metabolic profiling of tempol-exposed microbiota in vitro with global ^{1}H NMR metabolomics. NMR analysis revealed a dose-dependent decrease of microbial-derived metabolites including acetate, propionate, butyrate, valine, leucine and isoleucine, suggesting the inhibition of microbial fermentation by direct tempol exposure in vitro **(Figure 4-4)**. In addition, energy metabolites and the fermentation substrates glucose and oligosaccharides were at higher concentration in microbiota exposed at high dose tempol, consistent with the low metabolic activity of tempol-exposed microbiome revealed by decreased CFDA fluorescence by flow cytometric analysis in vitro. Moreover, a significant change in amino acid profiles characterized with a decrease of phenylacetate and an increase of aromatic amino acids including tyrosine and phenylalanine were identified. It has been reported microbial enzymes and genes participate in aromatic amino acid catabolism, emphasizing the significant role of microbiome in phenylalanine and tyrosine degradation (51). Moreover, It has been elucidated microbial enzymes involve in the anaerobic oxidation of phenylalanine to generate phenylacetate (52). Therefore, the compromised microbial metabolism with a low microbial enzyme activity after tempol exposure might explain the increased aromatic amino acid substrates phenylalanine and tyrosine, and decreased degradation

product phenylacetate in the metabolic profile. The most versatile amino acid threonine serving as a precursor for SCFAs synthesized by microbiome (53), was also significantly increased with tempol exposure, together with the low SCFAs production, confirms the compromised microbial metabolic activity. Interestingly, the integration of physiological and metabolic biomarkers revealed a unique, strong and direct correlation of microbial physiology and metabolites following direct tempol exposure in vitro **(Figure 4-5)**. Specifically, the inactivation physiological biomarkers (membrane damage indicators) PI and DiBAC are positively correlated with inactivation metabolic biomarkers (catabolism substrates) including glucose, oligosaccharides and amino acids, while negatively correlated with activation metabolic biomarkers (catabolism products) including SCFAs and branched-chain amino acids (BCAAs). These data suggested the compromised microbial metabolic activity is strongly correlated with the disrupted microbial membrane by direct xenobiotic exposure.

Agreed Physiological and Metabolic Profiles of Tempol-Exposed Microbiome in Vivo and in Vitro

To further validate the viability of the described multi-platform approach in vitro, an in vivo exposure model was developed by gavaging tempol to mice with a dose of 100 mg/kg. The in vivo effect of tempol on microbial physiology and metabolism was analyzed with the microbial isolates from the tempol-treated mouse cecum following the same procedure performed for in vitro analysis. Consistent with in vitro results, the microbial physiological status characterized by increased severe membrane damage (higher percentage of PI+ cells, $p<0.01$, Student's t-test) and decreased metabolic activity

(lower percentage of CFDA+ cells, $p<0.05$, Student's t-test) were observed in vivo with tempol treatment (**Figure 4-3B**). Noted, the proportion of DiBAC+ cells, which showed a significant increase in vitro, remained unchanged in vivo with a greater variation of staining percentage. As DiBAC stains for membrane depolarization which might be more sensitive to mild environmental stress, the likely additional mild environmental stress introduced during longer preparation procedure of in vivo samples results in observed larger variation and loss of statistical significance during DiBAC staining.

Microbial metabolic profiling after in vivo tempol exposure by ^{1}H NMR revealed similar metabolic fingerprints with in vitro exposure, characterized by a lower level of SCFAs and BCAAs and a higher level of glucose and oligosaccharides (**Figure 4-6B**). The consistent results in vitro and in vivo suggested the in vitro method could be a convenient and economic in vivo alternative to predict the in vivo microbial toxicity upon a xenobiotic exposure using flow cytometric and global metabolomics analysis.

Xenobiotics Tempol Modulates Microbial Composition Directly in Vitro

It is well-established that the microbiome composition is intimately related to microbial functional roles and host metabolic outcomes. Having defined the physiological and metabolic changes of tempol-exposed microbiome in vitro, we then investigated the microbial community composition following tempol exposure in vitro by QPCR analysis (**Figure 4-7**). First, total bacterial quantitation revealed a significant decrease in total bacterial population in medium and high dose of tempol exposure in vitro, consistent with the decreased total gut microbiota quantified in the in vivo model (54). Consistent with previous in vivo studies of tempol (4, 54), a significant decrease of

β-proteobacteria, *Clostridium coccoides*, *Closteridum leptum* Subgroup and *Lactobacillus* spp., were confirmed in the tempol-exposed in vitro model. This data suggested the observed microbial composition change in tempol-treated mice (54) is likely due to primary impact of tempol on microbiome directly without necessarily involvement of host components, as the tempol exposure in vitro have induced the similar modulatory effect on microbial quantitation and composition.

Orbitrap-LC-MS Revealed Metabolic Biomarkers in the Functional Networks

To provide an in-depth view of xenobiotic-altered microbial metabolic features and pathways, LC-MS was performed for additional metabolic biomarker identification and metabolic network assessment. Orbitrap-LC-MS analysis identified over 40 significantly changed microbial metabolites in the tempol-treated group, providing additional metabolic biomarkers for microbial membrane damage and metabolism disruption following tempol exposure (**Figure 4-8**). KEGG functional pathway analysis (**Table 4-1**) revealed a broad coverage of metabolic pathway being altered by tempol exposure, especially nucleotide, amino acid and sugar metabolism suggesting the compromised physiological and metabolic activity. Metabolite network suggested a dose-dependent change of the tempol-treated microbial profiles relative to control (**Figure 4-9**). Specifically, a significant downregulation of deoxyribose, ribose nucleotides and derivatives including dAMP, dCMP, dGMP, dTMP, GDP, uridine and uric acid was spotted. Nucleotides are used not only as backbone material for RNA and DNA synthesis, but also as energy donors for many cellular function including amino acid, proteins and cell membrane and component synthesis and transportation (55). The

downregulation of nucleotides with tempol exposure agreed with the altered aminoacyl-tRNA biosynthesis, amino acid, pyrimidine and purine metabolism annotated by KEGG. Moreover, a marked change in amino acids metabolism identified by KEGG pathway analysis was visualized in heatmap (**Figure 4-8**) and functional network metamap (**Figure 4-9**). High tempol exposure induced an overall decrease of essential amino acids (leucine, isoleucine, tryptophan, methionine), conditionally essential and non-essential amino acids (arginine, aspartate, taurine, proline, glutamate), amino acids derivatives (acetyl-glycine, acetyl-alanine, acetyl-glutamine, acetyl-ornithine, valyl-asparate). As amino acids carry out important nutritional and physiological roles in proteins and coenzymes synthesis, cell signaling and gene regulation (56), a perturbed amino acids pool serve as indicative biomarkers of the compromised physiological and metabolic function of microbiome with tempol exposure. In addition, a significant decrease of glucose-6-phosphate was seen in microbiome exposed with all three different tempol doses, suggesting a compromised glucose metabolism with tempol exposure as glucose-6-phosphate is the initiating molecule of two major glucose metabolic pathways including glycolysis and pentose phosphate pathway (57). Importantly, decreased glucose metabolism revealed by LC-MS is in agreement with the high level of sugar substrates like glucose and oligosaccharides detected by NMR, together suggesting compromised microbial energy source catabolism with tempol exposure. Moreover, significantly decreased hydroxyphenylacetate, phenylpyruvate and hydroxybenzoate revealed the decreased microbial anaerobic metabolism of aromatic compounds (58, 59), consistent with the NMR results showing a decrease of phenylacetate and an elevated aromatic substrates. Altogether, the tempol-disrupted microbial metabolism is revealed

with a wide range of biomarkers participating in nucleotide, amino acid and glucose metabolism by LC-MS in addition to NMR, suggesting a profound and extensive microbial toxicity of tempol. The compromised microbial metabolism revealed by metabolomics is in agreement with tempol-disrupted membrane physiology and metabolic rate characterized by flow cytometry, demonstrating the intimately direct relationship between microbial physiology and metabolism, as well as the feasibility of assessing microbial toxicity of xenobiotic exposure with the physiological and metabolic biomarkers by multi-platform functional phenotyping approach.

DISCUSSION

The well-established link between disease and disrupted gut microbiome-host interactions empowers the microbiota-targeted therapies (60). Thorough study of the potential toxicity of new compounds to the microbiome may identify new off target effects and improve risk assessment. This study took advantage of high-throughput metabolomics, combined with flow cytometry and in vitro bacteria culture, to extensively investigate the physiological and metabolic toxicity of the microbiome exposed with a typical xenobiotic tempol. The multi-platform functional phenotyping revealed a direct influence of short-term tempol exposure on microbial membrane health and metabolic activity, providing additional insight into the application of the gut microbiome as a screening tool to better understand the mode of action of xenobiotics to better inform risk assessment and drug screening.

A human microbiome study demonstrated that membrane damage indicated by membrane depolarization and integrity loss is significantly increased with environmental

hazards like high heat and oxygen exposure (61). In the current study, we observed disrupted membrane physiology characterized with excessive loss of polarity (DiBAC+) and integrity (PI+) by flow cytometry with xenobiotic tempol exposure, implying tempol directly targets the microbiome to introduce environmental stress to microbial membrane. Membrane physiology including membrane potential, integrity and energy metabolism is the prerequisite for its function, including ions, proteins, nucleic acids, nutrients and metabolites passive permeability and active transportation, extracellular environment and intercecullar communication and signal transduction (62). Thus, the disrupted membrane physiology could lead to profound and extensive physiological and metabolic consequences. We confirmed the disrupted biochemical and metabolic activity along with damaged membrane with both physiological and metabolic biomarkers using flow cytometry and metabolomics. With flow cytometric analysis, physiological biomarker CFDA, which is readily retained and fluorescent in cells with an intact membrane and highly active enzymatic activity (15), showed a significantly weaker fluorescent signal after tempol exposure, confirming the disrupted membrane physiology and subsequently compromised enzymatic and biochemical activity.

In addition to physiological biomarkers, informative microbial metabolic biomarkers and the altered metabolic functional pathways with tempol exposure were identified with high-throughput MS- and NMR-based metabolomics. The combination of MS- and NMR-based metabolomics surpasses the limitation of MS or NMR when performed alone (63) and permits a broader view of the metabolic alterations with improved metabolite identification confidence (64). NMR analysis identified significantly inhibited microbial fermentation and catabolic activity revealed by a

decrease of degradation products (SCFAs) and an increase of fermentation/degradation substrates (glucose, oligosaccharides) and precursors (threonine). More sensitive LC-MS analysis identified over 40 significantly changed metabolites with tempol exposure in addition to NMR. Many of the metabolites are involved in the critical metabolic pathways of nucleotide synthesis (dAMP, dCMP, dGMP, dTMP and UMP), amino acids (leucine, isoleucine, tryptophan, methionine, arginine, aspartate, taurine, proline, glutamate), amino acid derivatives (acetyl amino acid, dipeptide and tripeptide) and sugar derivatives (glucose-6-phosphate, lactate) identified with KEGG, suggesting the marked and profound systemic metabolic response of microbiota to tempol exposure. We have reported tempol promotes host energy homeostasis and glucose metabolism in mice by inhibiting microbial fermentation, hence shifts host energy balance from energy reserving to expenditure as an adaptive response of the host to the restricted intestinal microbial-derived SCFAs (54). Consistent with the in vivo finding, a significant inhibition of microbial fermentation activity with short-term tempol exposure was observed in vitro as well, demonstrating the tempol-induced host energy metabolism regulation via modulating microbiome is likely through direct microbiome-targeting mechanism rather than host-targeting mechanism. It has been suggested different microbial species contribute differently to the synthesis of essential amino acids and non-essential amino acids in response to the environmental stimulations (65). Given tempol modulates microbial composition readily in vivo (66) and in vitro **(Figure 4-7)**, the alterations in amino acids profile in vitro is anticipated. Tempol has been reported to scavenge reactive oxygen species to protect nucleic acid, protein and lipid against oxidative stress, and increase the NAD+/NADH ratio to promote energy metabolism against obesity in vivo

with animal models (67). This is the first time, the direct impact of tempol on microbial energy metabolism was reported. Notably, the altered metabolic pathways are functionally interconnected and mutually dependent. For example, nucleotides serve as both building blocks for nucleic acids synthesis and energy donors for cellular physiological and metabolic function. The altered nucleotide metabolism by tempol impacts the microbial growth revealed by total bacteria counts, and disturbs the energy supply that other metabolic pathways dependent on, leading to disrupted amino acids metabolism and sugar metabolism observed. On the other hand, nucleotide metabolism requires sugar units as the backbone component and amino acid-formed protein to catalyze the reaction, thus the alteration in sugar and amino acid metabolism due to tempol also cause perturbation in nucleotides metabolism. Sugars provide the critical energy source for microbiome, however requires nucleotide adenosine triphosphate (ATP) for energy storage to support cellular work. Therefore, the changed nucleotide metabolism with tempol exposure could interfere with the sugar metabolism. In addition, the compromised amino acid metabolism with tempol exposure could be either the result of the depleted energy supply due to disrupted nucleotide and carbohydrate metabolism, or the cause of the compromised energy metabolism, as the nucleotide and carbohydrate metabolic pathways are heavily dependent on the protein-based enzymes and co-factors triggered catalytic reactions, which are synthesized from amino acids.

The normal intracellular metabolism is dependent on healthy membrane for toxicant exclusion, nutrients and metabolites transportation, signaling transduction and intercellular communication, while replenish and maintenance of normal membrane physiology require biological molecules and energy fueled from metabolic activity. With

the in vitro model, direct and strong correlations between physiological and metabolic biomarkers were established in gut microbiome community. The physiological biomarkers indicating membrane damage (DiBAC+ and PI+) are positively correlated with inactivation metabolic biomarkers (energy substrates like glucose and oligosaccharides) and negatively linked to activation metabolic biomarkers (catabolism products like SCFAs and BCAAs). Similarly, the physiological biomarkers (CFDA+) and metabolic biomarkers, which indicates activation, are positively correlated. As the health membrane and normal metabolic activity are mutually dependent, the integrated physiological and metabolic profiles revealed by multi-platform approach provide informative functional assessment of the microbial response to xenobiotic in addition to the compositional change evaluated with sequencing or QPCR based techniques. Notably, the practical applicability of the described multi-platform approach for microbial toxicity in vitro was validated with in vivo mice model. The consistent results of the multi-platform functional phenotyping with in vitro and in vivo tempol exposure model demonstrated the in vitro method could be a convenient and economic alternative to represent and predict the microbial response to xenobiotic exposure in vivo.

The gut microbiome is extremely susceptible to modulation from environmental toxicants and orally ingested xenobiotics, indicating the gut microbiome can be used as a valuable screening tool to better understand the mode of action and potential toxicity of xenobiotics and drugs. The gut microbiome has been incorporated into drug screening recently with 40 human microbial stain representatives being selected to screen more than 1000 non-antibiotic drug (68). An astonishing 24% of non-antibiotic drugs presented antimicrobial or microbial modulatory effects, uncovering the potential risk of non-

antibiotics promoting antibiotic resistance. The current work confirmed the gut microbiome as a valuable drug and xenobiotic screening tool by assessing functionally informative physiological and metabolic phenotype of gut microbiome, and validating the translational application from in vitro to in vivo.

CONCLUSION

The gut microbiome can be associated with disease pathogenesis and is increasingly appreciated as promising therapeutic target. Using the gut microbiome as a screening tool opens the door for better understanding the underlying mechanism and potential toxicity of the microbiome-targeted xenobiotic/drug. This work presented a novel multi-platform functional phenotyping approach that combines in vitro culturing, flow cytometry and global metabolomics for the integrated characterization of the physiological and metabolic phenotype of the microbiome in response to xenobiotic exposure. The study discovered the physiological and metabolic biomarkers, demonstrated the direct correlation between physiology and metabolism in the response of gut microbiome to xenobiotic stimuli, and validated the in vitro multi-platform functional phenotyping as a feasible in vivo alternative to evaluate microbial toxicity.

REFERENCE

1. Mcneil NI. The Contribution of the Large-Intestine to Energy Supplies in Man. *Am J Clin Nutr.* 1984;39(2):338-42.
2. Bergman EN. Energy contributions of volatile fatty acids from the gastrointestinal tract in various species. *Physiological reviews.* 1990;70(2):567-90.
3. Schroeder BO, and Backhed F. Signals from the gut microbiota to distant organs in physiology and disease. *Nature medicine.* 2016;22(10):1079-89.
4. Li F, Jiang C, Krausz KW, Li Y, Albert I, Hao H, Fabre KM, Mitchell JB, Patterson AD, and Gonzalez FJ. Microbiome remodelling leads to inhibition of intestinal farnesoid X receptor signalling and decreased obesity. *Nature communications.* 2013;4(2384.
5. Cani PD, Bibiloni R, Knauf C, Waget A, Neyrinck AM, Delzenne NM, and Burcelin R. Changes in gut microbiota control metabolic endotoxemia-induced inflammation in high-fat diet-induced obesity and diabetes in mice. *Diabetes.* 2008;57(6):1470-81.
6. Kayagaki N, Wong MT, Stowe IB, Ramani SR, Gonzalez LC, Akashi-Takamura S, Miyake K, Zhang J, Lee WP, Muszynski A, et al. Noncanonical inflammasome activation by intracellular LPS independent of TLR4. *Science.* 2013;341(6151):1246-9.
7. Claus SP, Ellero SL, Berger B, Krause L, Bruttin A, Molina J, Paris A, Want EJ, de Waziers I, Cloarec O, et al. Colonization-induced host-gut microbial metabolic interaction. *MBio.* 2011;2(2):e00271-10.
8. Selmer T, and Andrei PI. p-Hydroxyphenylacetate decarboxylase from Clostridium difficile. A novel glycyl radical enzyme catalysing the formation of p-cresol. *Eur J Biochem.* 2001;268(5):1363-72.
9. Zhang L, Nichols RG, Correll J, Murray IA, Tanaka N, Smith PB, Hubbard TD, Sebastian A, Albert I, Hatzakis E, et al. Persistent Organic Pollutants Modify Gut Microbiota-Host Metabolic Homeostasis in Mice Through Aryl Hydrocarbon Receptor Activation. *Environ Health Perspect.* 2015;123(7):679-88.
10. Lamas B, Richard ML, Leducq V, Pham HP, Michel ML, Da Costa G, Bridonneau C, Jegou S, Hoffmann TW, Natividad JM, et al. CARD9 impacts colitis by altering gut microbiota metabolism of tryptophan into aryl hydrocarbon receptor ligands. *Nature medicine.* 2016;22(6):598-605.
11. Sousa T, Paterson R, Moore V, Carlsson A, Abrahamsson B, and Basit AW. The gastrointestinal microbiota as a site for the biotransformation of drugs. *Int J Pharm.* 2008;363(1-2):1-25.
12. Wagner J, Coupland P, Browne HP, Lawley TD, Francis SC, and Parkhill J. Evaluation of PacBio sequencing for full-length bacterial 16S rRNA gene classification. *BMC microbiology.* 2016;16(274.
13. Dhariwal A, Chong J, Habib S, King IL, Agellon LB, and Xia J. MicrobiomeAnalyst : a web-based tool for comprehensive statistical , visual and meta-analysis of microbiome data. 2017:1-9.
14. Pasolli E, Truong DT, Malik F, Waldron L, and Segata N. Machine Learning Meta-analysis of Large Metagenomic Datasets: Tools and Biological Insights. *PLoS Computational Biology.* 2016;12(1-26.
15. Forster S, Snape JR, Lappin-Scott HM, and Porter J. Simultaneous fluorescent gram staining and activity assessment of activated sludge bacteria. *Appl Environ Microbiol.* 2002;68(10):4772-9.
16. Foladori P, Bruni L, Tamburini S, and Ziglio G. Direct quantification of bacterial biomass in influent, effluent and activated sludge of wastewater treatment plants by using flow cytometry. *Water research.* 2010;44(13):3807-18.
17. Hammes F, Broger T, Weilenmann HU, Vital M, Helbing J, Bosshart U, Huber P, Odermatt RP, and Sonnleitner B. Development and laboratory-scale testing of a fully

automated online flow cytometer for drinking water analysis. *Cytometry Part A : the journal of the International Society for Analytical Cytology.* 2012;81(6):508-16.
18. Besmer MD, Weissbrodt DG, Kratochvil BE, Sigrist JA, Weyland MS, and Hammes F. The feasibility of automated online flow cytometry for in-situ monitoring of microbial dynamics in aquatic ecosystems. *Frontiers in microbiology.* 2014;5(265.
19. Peris-Bondia F, Latorre A, Artacho A, Moya A, and D'Auria G. The active human gut microbiota differs from the total microbiota. *PloS one.* 2011;6(7):e22448.
20. Ambriz-Avina V, Contreras-Garduno JA, and Pedraza-Reyes M. Applications of flow cytometry to characterize bacterial physiological responses. *BioMed research international.* 2014;2014(461941.
21. Steen HB, Boye E, Skarstad K, Bloom B, Godal T, and Mustafa S. Applications of flow cytometry on bacteria: cell cycle kinetics, drug effects, and quantitation of antibody binding. *Cytometry.* 1982;2(4):249-57.
22. Assuncao P, Antunes NT, Rosales RS, Poveda C, de la Fe C, Poveda JB, and Davey HM. Application of flow cytometry for the determination of minimal inhibitory concentration of several antibacterial agents on Mycoplasma hyopneumoniae. *Journal of applied microbiology.* 2007;102(4):1132-7.
23. Maurice CF, Haiser HJ, and Turnbaugh PJ. Xenobiotics shape the physiology and gene expression of the active human gut microbiome. *Cell.* 2013;152(1-2):39-50.
24. Cronin UP, and Wilkinson MG. Bacillus cereus endospores exhibit a heterogeneous response to heat treatment and low-temperature storage. *Food microbiology.* 2008;25(2):235-43.
25. Sunny-Roberts EO, and Knorr D. Evaluation of the response of Lactobacillus rhamnosus VTT E-97800 to sucrose-induced osmotic stress. *Food microbiology.* 2008;25(1):183-9.
26. Mols M, van Kranenburg R, van Melis CC, Moezelaar R, and Abee T. Analysis of acid-stressed Bacillus cereus reveals a major oxidative response and inactivation-associated radical formation. *Environ Microbiol.* 2010;12(4):873-85.
27. Gasol JM, Zweifel UL, Peters F, Fuhrman JA, and Hagstrom A. Significance of size and nucleic acid content heterogeneity as measured by flow cytometry in natural planktonic bacteria. *Appl Environ Microbiol.* 1999;65(10):4475-83.
28. Lebaron P, Servais P, Agogue H, Courties C, and Joux F. Does the high nucleic acid content of individual bacterial cells allow us to discriminate between active cells and inactive cells in aquatic systems? *Appl Environ Microbiol.* 2001;67(4):1775-82.
29. Terstappen LW, Shah VO, Conrad MP, Recktenwald D, and Loken MR. Discriminating between damaged and intact cells in fixed flow cytometric samples. *Cytometry.* 1988;9(5):477-84.
30. Haugland RP. *The handbook: A guide to fluorescent probes and labeling technologies (10th ed.).* Carlsband, California: Invitrogen Corp; 2005.
31. Jepras RI, Carter J, Pearson SC, Paul FE, and Wilkinson MJ. Development of a robust flow cytometric assay for determining numbers of viable bacteria. *Appl Environ Microbiol.* 1995;61(7):2696-701.
32. Mason DJ, Lopez-Amoros R, Allman R, Stark JM, and Lloyd D. The ability of membrane potential dyes and calcafluor white to distinguish between viable and non-viable bacteria. *The Journal of applied bacteriology.* 1995;78(3):309-15.
33. Kolek J, Branska B, Drahokoupil M, Patakova P, and Melzoch K. Evaluation of viability, metabolic activity and spore quantity in clostridial cultures during ABE fermentation. *FEMS Microbiol Lett.* 2016;363(6).
34. Collado S, Oulego P, Alonso S, and Diaz M. Flow cytometric characterization of bacterial abundance and physiological status in a nitrifying-denitrifying activated sludge system treating landfill leachate. *Environmental science and pollution research international.* 2017.

35. Ueckert JE, Nebe von-Caron G, Bos AP, and ter Steeg PF. Flow cytometric analysis of Lactobacillus plantarum to monitor lag times, cell division and injury. *Letters in applied microbiology.* 1997;25(4):295-9.
36. Lindon JC, Holmes E, and Nicholson JK. Metabonomics techniques and applications to pharmaceutical research & development. *Pharmaceutical research.* 2006;23(6):1075-88.
37. Wei R. Metabolomics and its practical value in pharmaceutical industry. *Current drug metabolism.* 2011;12(4):345-58.
38. Garcia-Sevillano MA, Garcia-Barrera T, and Gomez-Ariza JL. Environmental metabolomics: Biological markers for metal toxicity. *Electrophoresis.* 2015.
39. Rattray NJW, Charkoftaki G, Rattray Z, Hansen JE, Vasiliou V, and Johnson CH. Environmental influences in the etiology of colorectal cancer: the premise of metabolomics. *Current pharmacology reports.* 2017;3(3):114-25.
40. Gu H, Chen H, Pan Z, Jackson AU, Talaty N, Xi B, Kissinger C, Duda C, Mann D, Raftery D, et al. Monitoring diet effects via biofluids and their implications for metabolomics studies. *Anal Chem.* 2007;79(1):89-97.
41. Esko T, Hirschhorn JN, Feldman HA, Hsu YH, Deik AA, Clish CB, Ebbeling CB, and Ludwig DS. Metabolomic profiles as reliable biomarkers of dietary composition. *Am J Clin Nutr.* 2017;105(3):547-54.
42. Sumner LW, Mendes P, and Dixon RA. Plant metabolomics: large-scale phytochemistry in the functional genomics era. *Phytochemistry.* 2003;62(6):817-36.
43. Cai J, Zhang J, Tian Y, Zhang L, Hatzakis E, Krausz KW, Smith PB, Gonzalez FJ, and Patterson AD. Orthogonal Comparison of GC-MS and 1H NMR Spectroscopy for Short Chain Fatty Acid Quantitation. *Anal Chem.* 2017;89(15):7900-6.
44. Tang J. Microbial metabolomics. *Current genomics.* 2011;12(6):391-403.
45. Quinn RA, Phelan VV, Whiteson KL, Garg N, Bailey BA, Lim YW, Conrad DJ, Dorrestein PC, and Rohwer FL. Microbial, host and xenobiotic diversity in the cystic fibrosis sputum metabolome. *ISME J.* 2016;10(6):1483-98.
46. Lu W, Clasquin MF, Melamud E, Amador-Noguez D, Caudy AA, and Rabinowitz JD. Metabolomic analysis via reversed-phase ion-pairing liquid chromatography coupled to a stand alone orbitrap mass spectrometer. *Anal Chem.* 2010;82(8):3212-21.
47. Tsugawa H, Cajka T, Kind T, Ma Y, Higgins B, Ikeda K, Kanazawa M, VanderGheynst J, Fiehn O, and Arita M. MS-DIAL: data-independent MS/MS deconvolution for comprehensive metabolome analysis. *Nature methods.* 2015;12(6):523-6.
48. Barupal DK, Haldiya PK, Wohlgemuth G, Kind T, Kothari SL, Pinkerton KE, and Fiehn O. MetaMapp: mapping and visualizing metabolomic data by integrating information from biochemical pathways and chemical and mass spectral similarity. *BMC Bioinformatics.* 2012;13(1):99.
49. Xia J, and Wishart DS. Web-based inference of biological patterns, functions and pathways from metabolomic data using MetaboAnalyst. *Nature Protocols.* 2011;6(743.
50. Luo W, and Brouwer C. Pathview: an R/Bioconductor package for pathway-based data integration and visualization. *Bioinformatics.* 2013;29(14):1830-1.
51. Arias-Barrau E, Olivera ER, Luengo JM, Fernández C, Galán B, García JL, Díaz E, and Miñambres B. The Homogentisate Pathway: a Central Catabolic Pathway Involved in the Degradation of l-Phenylalanine, l-Tyrosine, and 3-Hydroxyphenylacetate in Pseudomonas putida. *Journal of bacteriology.* 2004;186(15):5062-77.
52. Aklujkar M, Risso C, Smith J, Beaulieu D, Dubay R, Giloteaux L, DiBurro K, and Holmes D. Anaerobic degradation of aromatic amino acids by the hyperthermophilic archaeon Ferroglobus placidus. *Microbiology.* 2014;160(Pt 12):2694-709.
53. Neis EPJG, Dejong CHC, and Rensen SS. The Role of Microbial Amino Acid Metabolism in Host Metabolism. *Nutrients.* 2015;7(4):2930-46.

54. Cai J, Zhang L, Jones RA, Correll JB, Hatzakis E, Smith PB, Gonzalez FJ, and Patterson AD. Antioxidant Drug Tempol Promotes Functional Metabolic Changes in the Gut Microbiota. *J Proteome Res.* 2016;15(2):563-71.
55. Alberts B, Johnson A, Lewis J, Raff M, Roberts K, and P W. *Molecular Biology of the Cell, 4th edition.* New York: Garland Science; 2002.
56. Wu G. Amino acids: metabolism, functions, and nutrition. *Amino Acids.* 2009;37(1):1-17.
57. Berg JM, Tymoczko JL, and L S. *Biochemistry 5th edition*. New York: W H Freeman; 2002.
58. Harwood CS, Burchhardt G, Herrmann H, and Fuchs G. Anaerobic metabolism of aromatic compounds via the benzoyl-CoA pathway. *FEMS Microbiology Reviews.* 1998;22(5):439-58.
59. Heider J, and Fuchs G. Microbial anaerobic aromatic metabolism. *Anaerobe.* 1997;3(1):1-22.
60. Lemon KP, Armitage GC, Relman DA, and Fischbach MA. Microbiota-Targeted Therapies: An Ecological Perspective. *Science translational medicine.* 2012;4(137):137rv5-rv5.
61. Maurice CF, and Turnbaugh PJ. Quantifying and identifying the active and damaged subsets of indigenous microbial communities. *Methods in enzymology.* 2013;531(91-107.
62. Remaut H, and Fronzes R. Norfolk, UK :: Caister Academic Press; 2014.
63. Sumner LW, Mendes P, and Dixon RA. Plant metabolomics: large-scale phytochemistry in the functional genomics era. *Phytochemistry.* 2003;62(6):817-36.
64. Cai J, Zhang J, Tian Y, Zhang L, Hatzakis E, Krausz KW, Smith PB, Gonzalez FJ, and Patterson AD. Orthogonal Comparison of GC-MS and (1)H NMR Spectroscopy for Short Chain Fatty Acid Quantitation. *Anal Chem.* 2017;89(15):7900-6.
65. Shoaie S, Ghaffari P, Kovatcheva-Datchary P, Mardinoglu A, Sen P, Pujos-Guillot E, de Wouters T, Juste C, Rizkalla S, Chilloux J, et al. Quantifying Diet-Induced Metabolic Changes of the Human Gut Microbiome. *Cell Metab.* 2015;22(2):320-31.
66. Li F, Jiang C, Krausz KW, Li Y, Albert I, Hao H, Fabre KM, Mitchell JB, Patterson AD, and Gonzalez FJ. Microbiome remodelling leads to inhibition of intestinal farnesoid X receptor signalling and decreased obesity. *Nature communications.* 2013;4(2384.
67. Yamato M, Kawano K, Yamanaka Y, Saiga M, and Yamada K-i. TEMPOL increases NAD(+) and improves redox imbalance in obese mice. *Redox Biology.* 2016;8(316-22.
68. Maier L, Pruteanu M, Kuhn M, Zeller G, Telzerow A, Anderson EE, Brochado AR, Fernandez KC, Dose H, Mori H, et al. Extensive impact of non-antibiotic drugs on human gut bacteria. *Nature.* 2018;555(623-8.

Figure 4-1

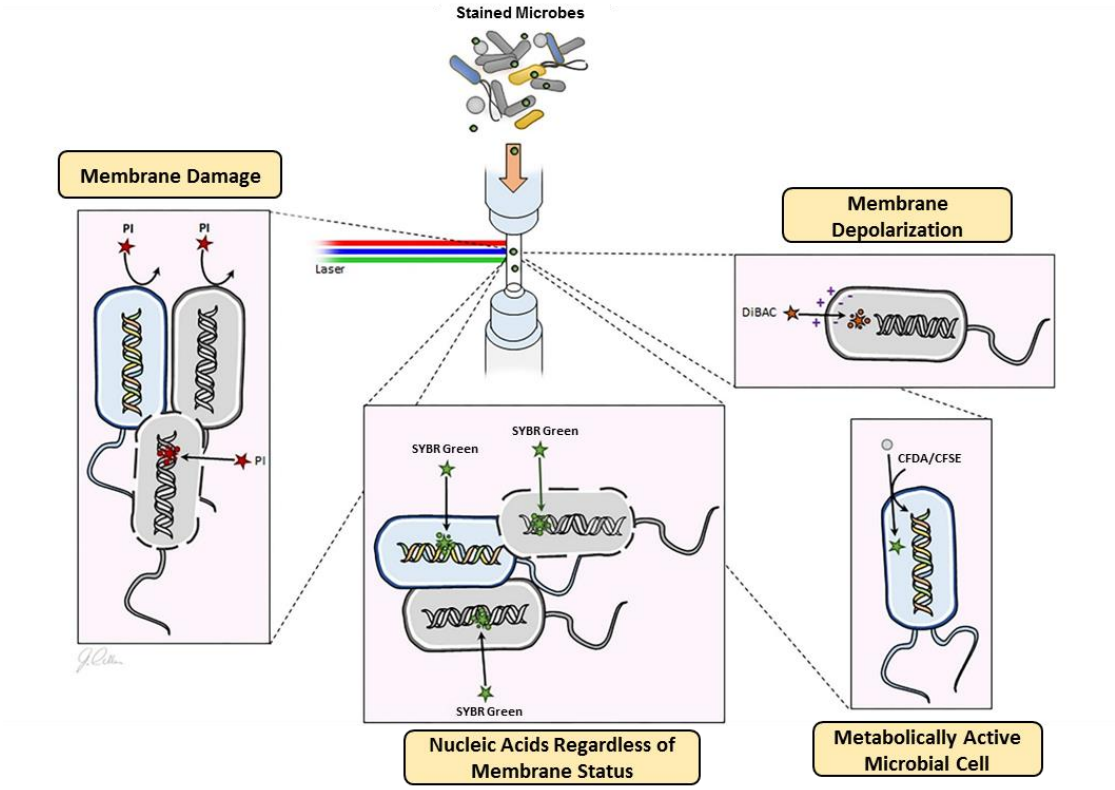

Figure 4-1. Flow Cytometry Provides a Snapshot of the Microbial Physiological States. Four fluorescent dyes are used to evaluating different physiological parameters. Nucleic acid-labeling fluorescent SYBR Green indicates growth rate, Bis-(1,3-Dibutylbarbituric Acid) Trimethine Oxonol (DiBAC) assesses membrane depolarization (moderate damage), Propidium iodide (PI) determines loss of membrane integrity (severe damage) , carboxyfluorescein diacetate (CFDA)/carboxyfluorescein diacetate succinimidyl ester (CFSE) measures metabolic activity.

Figure 4-2

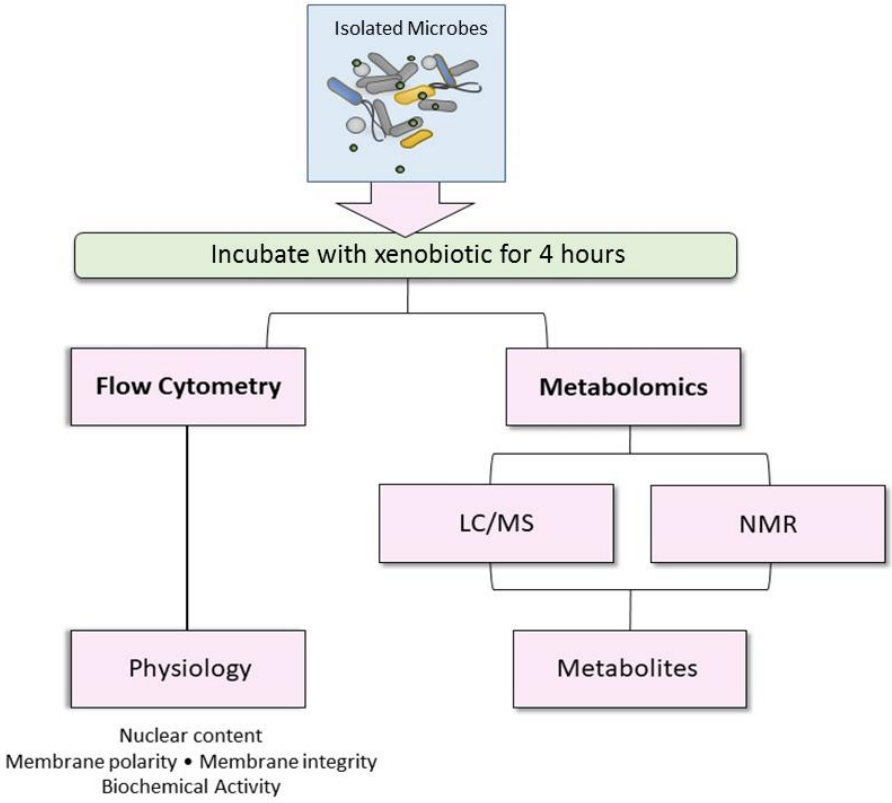

Figure 4-2. Experimental Scheme of the Microbial Toxicity Assessment. Microbes isolated from mouse gut are incubated with xenobiotic (tempol) for 4h under strict anaerobic conditions (O2 < 20 parts per million). Microbial toxicity is evaluated by characterizing microbial physiological and metabolic status. Microbial physiological status is evaluated by flow cytometry with different fluorescent dyes indicating membrane damage and biochemical activity. Microbial metabolism is assessed by global NMR- and LC-MS-based metabolomics.

Figure 4-3

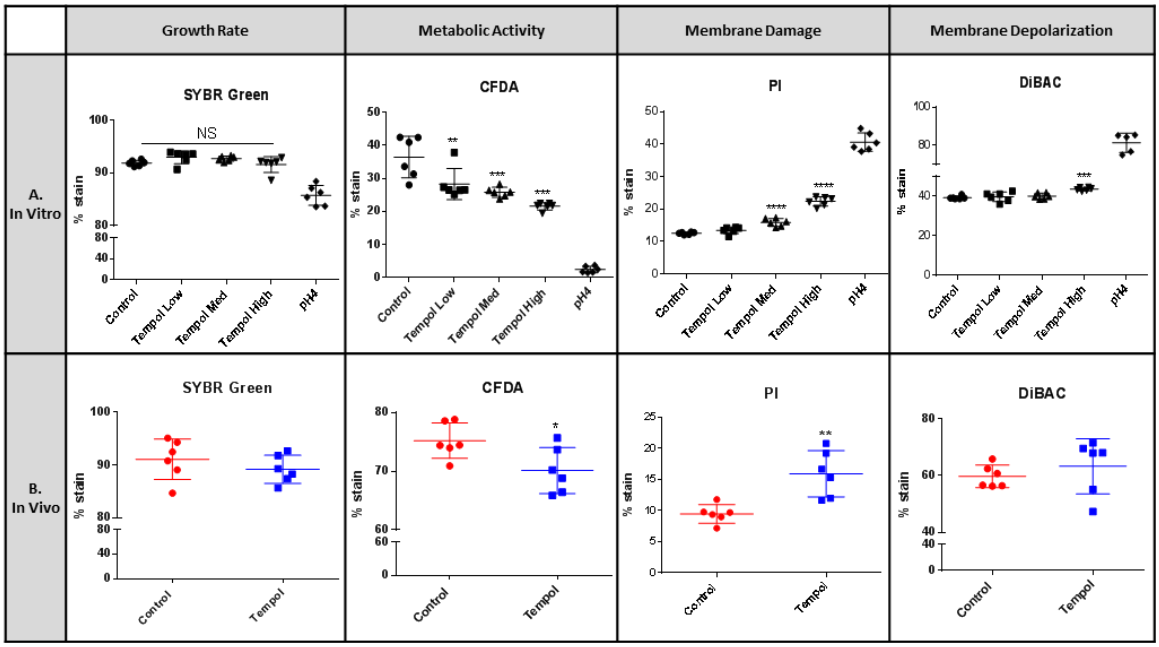

Figure 4-3. Xenobiotic Tempol Directly Impacts Microbial Physiology. Microbial physiology was evaluated by flow cytometry after tempol exposure via (A) 4h short-term incubation of microbial isolates with different doses of tempol (0.01, 0.1. 1 mg/mL) in vitro; (B) 5-day gavage of tempol (100 mg/kg) to mice in vivo. p**<0.01, p***<0.001, p****<0.0001. One-way ANOVA with Tukey's correction. pH4 group is introduced as a control. All data are presented as mean ± sd. (n=6 isolates per group)

Figure 4-4

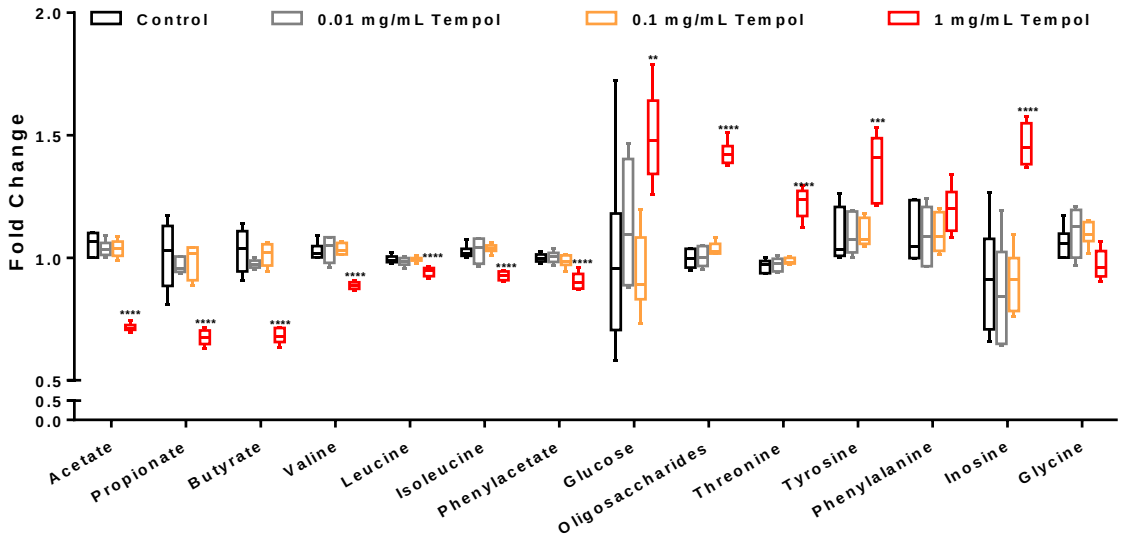

Figure 4-4. Xenobiotic Tempol Directly Impacts Microbial Metabolic Profiles Characterized by ^{1}H NMR. Relative concentration of microbial metabolites with different doses of tempol exposure in vitro were measured by 1H NMR analysis. p**<0.01, p***<0.001, p****<0.0001 compared to control. One-way ANOVA with Tukey's correction. All data are presented from min to max ranges with box and whisker plots. (n=6 isolates per group)

Figure 4-5

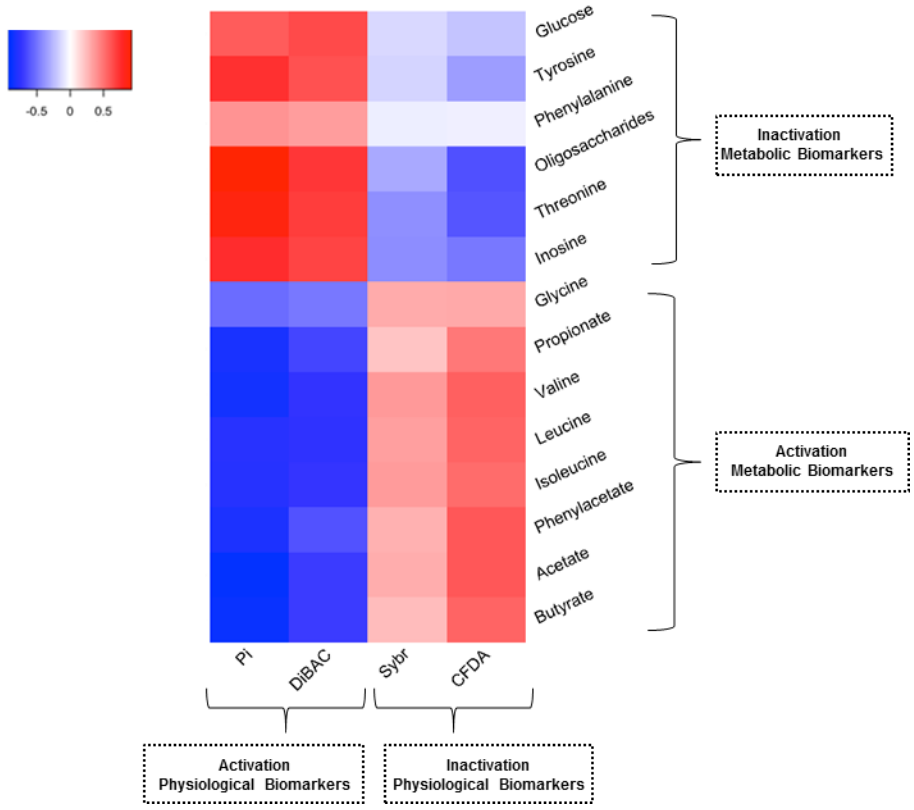

Figure 4-5. Strong Correlations Between Microbial Physiology and Metabolism. Pearson correlation analysis was performed between physiological biomarkers and metabolic biomarkers characterized with flow cytometric and NMR analysis, respectively and visualized using the heatmap.2 function from the gplots package in R. Positive correlation is indicated by "hot" color (e.g., red) while negative correlation is indicated by ""cold" color (e.g., blue).

Figure 4-6

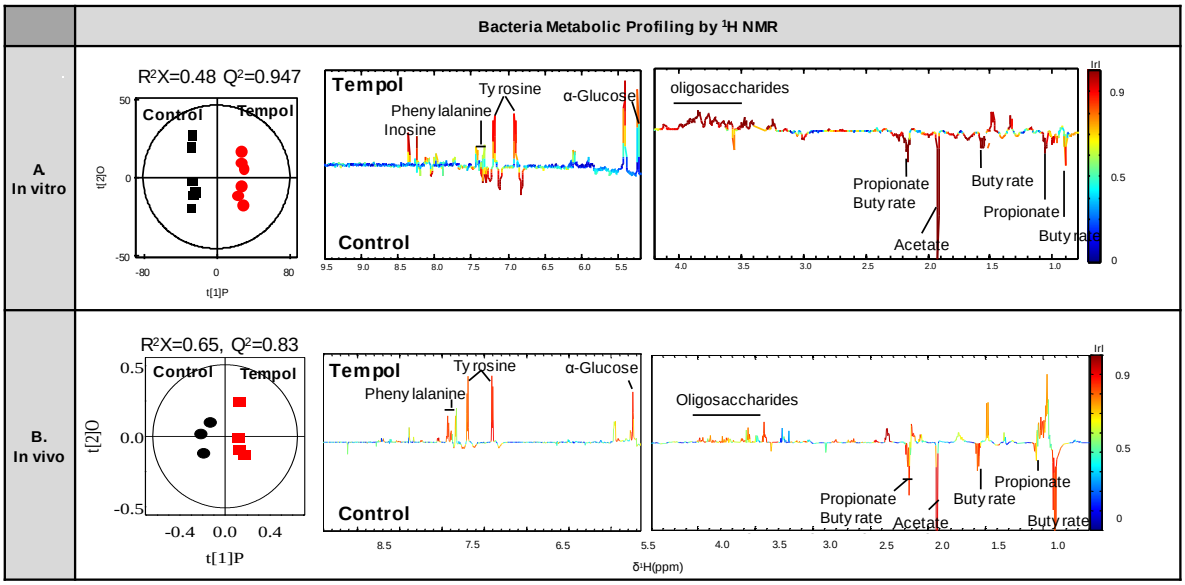

Figure 4-6. Similar Microbial Metabolic Fingerprints between in Vivo and in Vitro Exposure of Tempol Revealed by ^{1}H NMR. OPLS-DA scores plots (left) indicating model quality and coefficient plots (right) displaying metabolites changes, are generated using 1H NMR spectra of microbial extract from (A) microbial isolates after 4h short-term incubation with tempol (1 mg/ml) in vitro (n=6 isolates per group); (B) microbial isolates from mice gavaged tempol (100 mg/kg) in vivo (n=4 mice per group). The hotness of the color is corresponding to the discrimination significance of the metabolite contributed to the model separation. Positive peak indicates the metabolite presented in higher concentration in tempol treatment group, while negative peak indicates the metabolite is in higher level in control group.

Figure 4-7

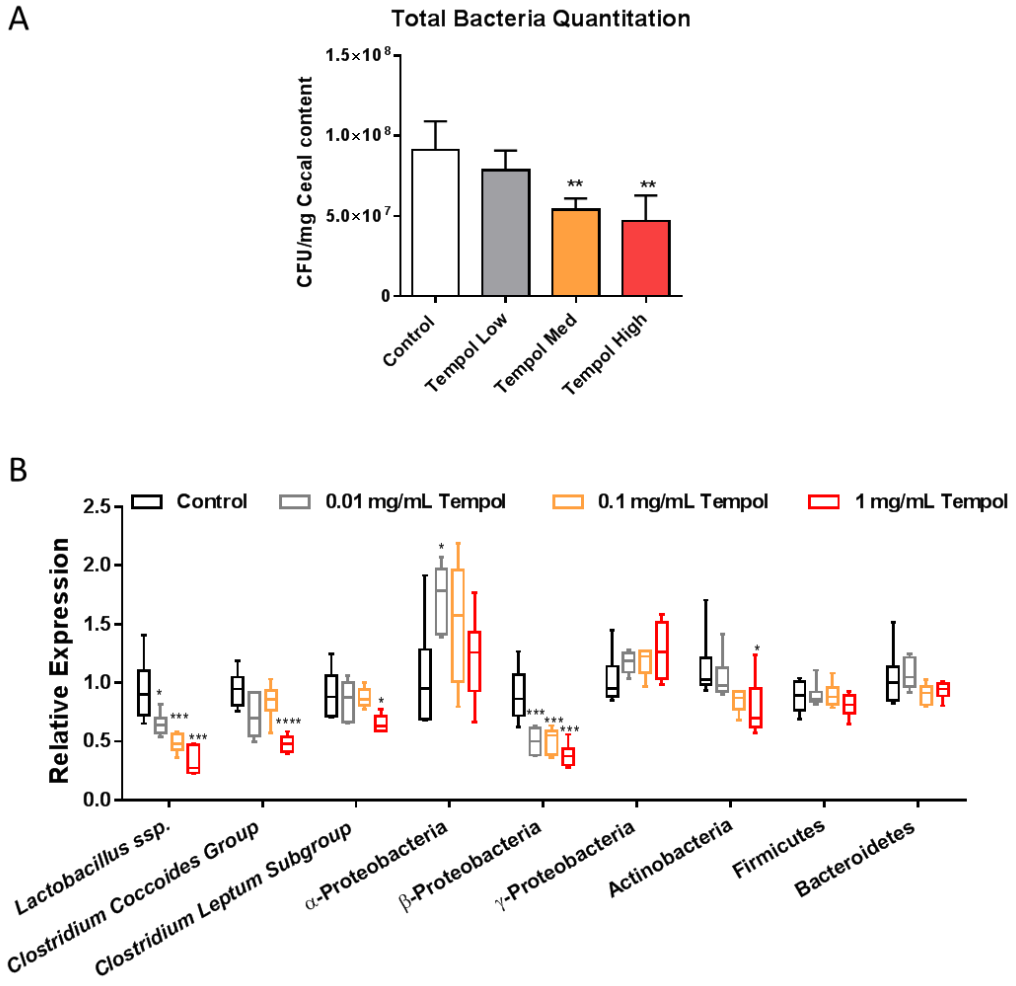

Figure 4-7. Xenobiotics Tempol Modulates Microbial Composition Directly in Vitro. Quantitative PCR analysis 16s rRNA gene in the microbial isolates exposed to tempol in vitro with (A) universal primers for absolute quantification of total bacteria with a standard curve (B) targeted primers for relative quantitation of specific bacteria. p*<0.05, p**<0.01, p***<0.001, p****<0.0001 relative to control. One-way ANOVA with Tukey's correction. All data are presented as mean ± sd. (n=6 isolates per group)

Figure 4-8

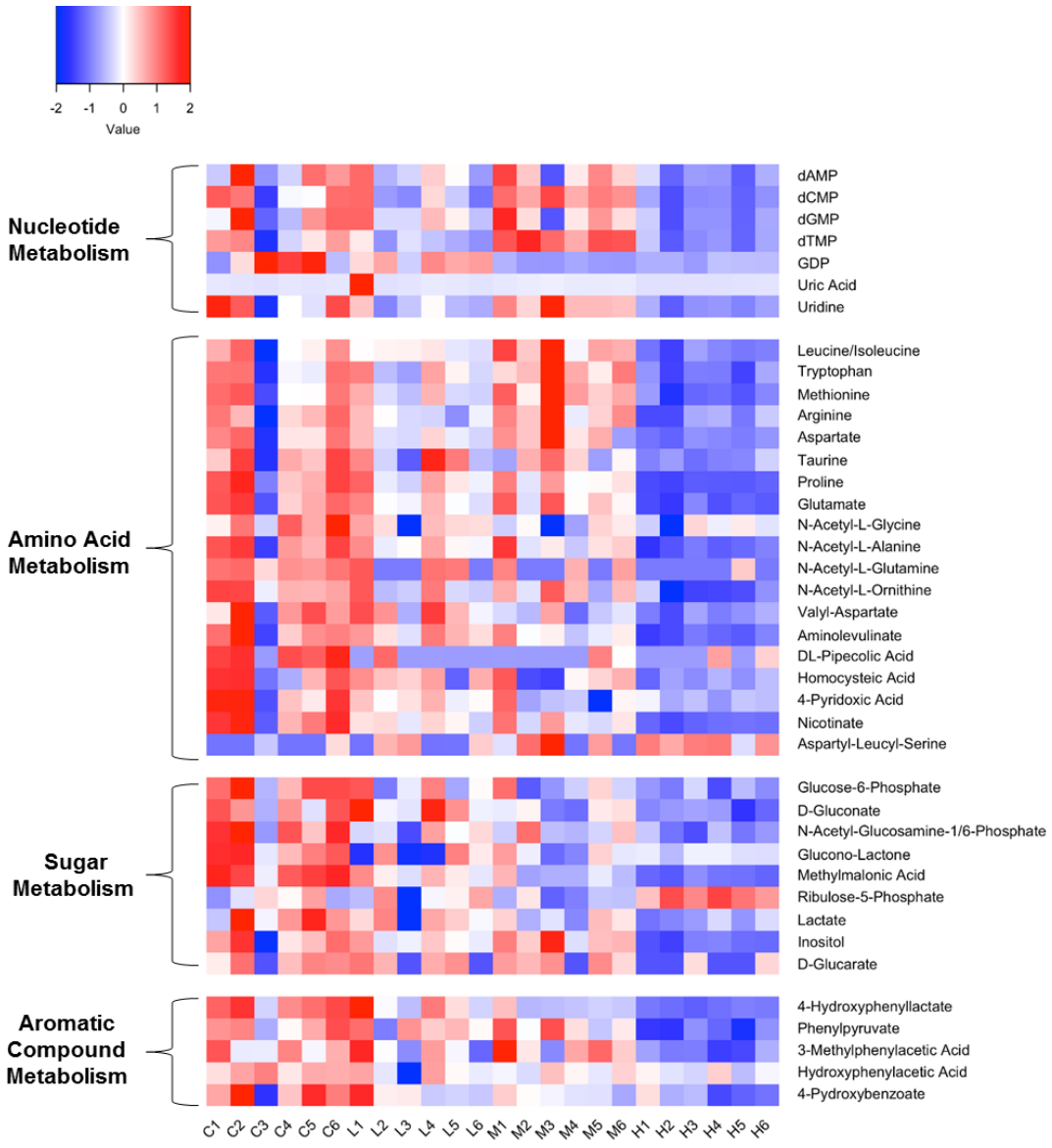

Figure 4-8. LC-MS Revealed Altered Microbial Metabolic Profile in Response to Tempol. Metabolomic changes are illustrated with z scores showing the number of standard deviations each metabolic level is away from the mean for each sample. Red colors represent metabolites that are increased or above the mean and blue colors represent metabolites that are decreased or below the mean.

Figure 4-9

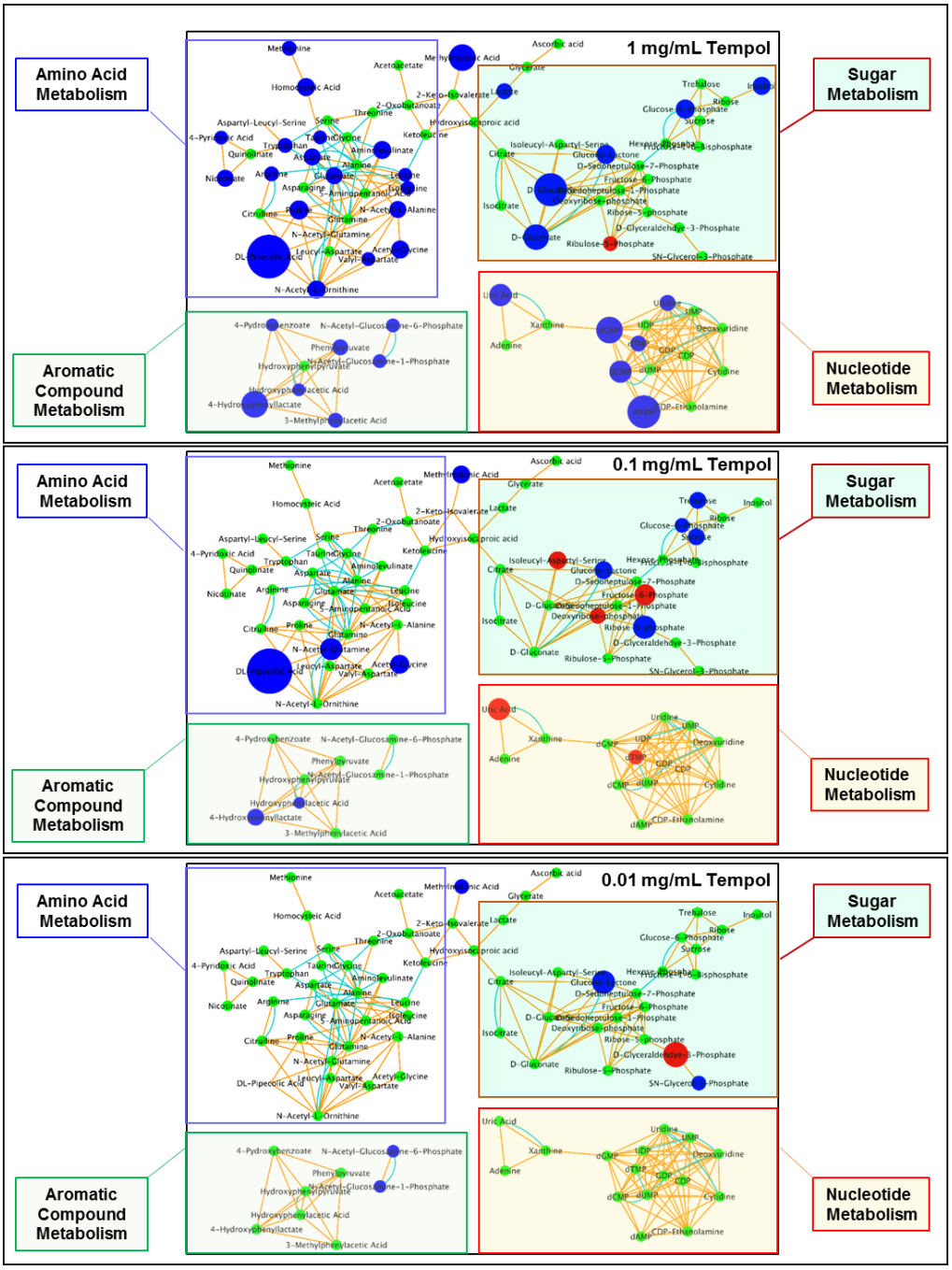

Figure 4-9. Metabolic Network Changes of Microbiome in Response to Tempol Exposure. Network map was drawn with MetaMapp (for chemical and biochemical similarity) and Cytoscape (for visualization) using normalized LCMS data (to internal standard). The blue and red of stand for significant down- and up-regulated compounds compared with control group respectively, but green color means no significant difference, which are calculated from T-test. The size of node is dependent on the absolute value of fold change. The orange peel (#FF9900) and Egg blue (#00CCCC) colors stands for Tonimoto coefficient and KEGG reaction pairs obtained from MetaMapp package, respectively.

Table 4-1. Primer Sequences of Bacteria for QPCR Analysis

target group	forward primer	reverse primer
Universal	**AGAGTTTGATCCTGGCTCAG (8F)**	**CTGCTGCCTCCCGTAGGAGT (338R)**
***Lactobacillus*.spp**	**AGCAGTAGGGAATCTTCCA (LabF362)**	**CACCGCTACACATGGAG (LabR677)**
αProteobacteria	**ACTCCTACGGGAGGCAGCAG (Eub338)**	**TCTACGRATTTCACCYCTAC (Alf685)**
βProteobacteria	**ACTCCTACGGGAGGCAGCAG (Eub338)**	**TCACTGCTACACGYG (Bet680)**
γProteobacteria	**CMATGCCGCGTGTGTGAA (γ395f)**	**ACTCCCCAGGCGGTCDACTTA (γ 871r)**
Actinobacteria	**CGCGGCCTATCAGCTTGTTG (Actino235)**	**ATTACCGCGGCTGCTGG (Eub518)**
Firmicutes	**GCAGTAGGGAATCTTCCG (Lgc353)**	**ATTACCGCGGCTGCTGG (Eub518)**
Bacteroidetes	**GTACTGAGACACGGACCA (Cfb319)**	**ATTACCGCGGCTGCTGG (Eub518)**
***Clostridium coccoides* group**	**AAATGACGGTACCTGACTAA (g-Ccoc-F)**	**CTTTGAGTTTCATTCTTGCGAA (g-Ccoc-R)**
***Clostridium leptum* subgroup**	**GCACAAGCAGTGGAGT (Sg-Clept-F)**	**CTTCCTCCGTTTTGTCAA (Sg-Clept-R3)**

Table 4-2. KEGG Functional Pathway Analysis.

Control vs Tempol High						
Pathway	Match Status	Raw p	-log (p)	Holm adjust	FDR	Impact
Aminoacyl-tRNA biosynthesis	8/69	0.000172	8.666	0.014133	0.014133	0
Ascorbate and aldarate metabolism	2/9	0.019142	3.9559	1	0.46498	0
Arginine and proline metabolism	4/44	0.02099	3.8637	1	0.46498	0.23975
Phenylalanine metabolism	2/11	0.028353	3.563	1	0.46498	0.24074
Valine, leucine and isoleucine biosynthesis	2/11	0.028353	3.563	1	0.46498	0.66666
Histidine metabolism	2/15	0.05089	2.9781	1	0.69549	0
Valine, leucine and isoleucine degradation	3/38	0.064532	2.7406	1	0.75477	0
Pyrimidine metabolism	3/41	0.077566	2.5566	1	0.75477	0.10996
Purine metabolism	4/68	0.08284	2.4908	1	0.75477	0.04842
Control vs Tempol Medium						
Pathway	Match Status	Raw p	-log (p)	Holm adjust	FDR	Impact
Pyrimidine metabolism	3/41	0.009695	4.6362	0.79497	0.74959	0.18496
Starch and sucrose metabolism	2/19	0.018283	4.0018	1	0.74959	0
Purine metabolism	3/68	0.037788	3.2758	1	1	0.04607
Control vs Tempol Low						
Pathway	Match Status	Raw p	-log (p)	Holm adjust	FDR	Impact
Amino sugar and nucleotide sugar metabolism	2/37	0.012832	4.3558	1	1	0.04649
beta-Alanine metabolism	1/17	0.081183	2.511	1	1	0
Glycerolipid metabolism	1/18	0.085777	2.456	1	1	0.0256

Normalized LCMS data (to internal standard) were mapped to the KEGG orthology database using MetaboAnalyst. The denominator and numerate are the number of compounds shown in each pathway and the number of compounds shown in the LCMS data. The p-value is estimated from global test based on hypergeometric test for the probability of having n-number metabolites of a pathway in the input list, and the Holm adjust and FDR are applied for multiple comparison. Here the top-ranked pathways are selected in each comparison.

Chapter 5

Discussion

The dissertation is a thorough investigation of the high-throughput metabolomics approaches including GC-MS, LC-MS and NMR, which covers method development, optimization, validation and extensive application combined with other biochemical and bioinformatics approaches to explore the impact of xenobiotics on the microbiome-metabolite-host interaction to fully elucidate the therapeutic and toxicity potential of microbiome-targeting xenobiotics.

NMR and MS-based metabolomics is one of the most powerful bioanalytical tools to study the biological and metabolic consequences of complex environmental stimuli like drugs, toxicants, and diet for the understanding the link between environment, gut microbiome, and health (1-3). The rapid development of metabolomics techniques in the past decade has permitted high throughput and efficient quantitative detection of small molecule metabolites within complex systems. Metabolomics represents an excellent option to study microbial-derived metabolites and microbiome-host co-metabolites to understand the metabolite chatter between the host and the gut microbiome (4-7). MS- and NMR-based approaches are extensively utilized in metabolomics, however the inherent insensitivity issue for NMR and low reproducibility problem for MS have raised accuracy and reliability concerns (8). In chapter 2, confident metabolomics methods using both NMR and GC-MS for SCFAs quantitation with improved analytical performance and comparable quantitation results were developed and confirmed. First, four different SCFAs quantitation methods were thoroughly investigated and optimized from extraction, instrumentation and data integration using two independent platforms. The optimized methods were applied to quantify the SCFAs level in pooled mice feces

and the comparable quantitation results from different methods demonstrated the methods are dependable and reliable. Second, the analytical performance including sensitivity, accuracy and reproducibility were compared orthogonally and suitable applications were assigned for each method accordingly (**Table 5-1**). The GC-MS-based derivatization method with superior sensitivity and accuracy yet slow sample preparation and data acquisition procedure is recommended for the trace/ultratrace SCFAs detection within small sample size. The MS-based acidified water method is the fastest method with relative high sensitivity thus is suitable for large-scale human studies with larger sample size. NMR-based methods exhibits higher repeatability with relative lower sensitivity, and more importantly yields global metabolic profiles beyond SCFAs, thus are most suitable for the studies with higher SCFAs concentration in samples, and with both global and target analysis purposes. Finally, a highly reliable and complementary approach was established by combining global NMR-based and targeted MS-based method and validated in germ free mice study. The consistent results from three mutually independent methods GC-MS, NMR and bomb calorimetry demonstrated significantly reduced SCFAs levels, increased fermentation substrates, and energy excretion in feces of germ free mice compared to conventionally-raised mice. These results correspond to the absence of bacteria that are responsible for fermenting fiber to produce SCFAs.

The gut microbiome impacts host metabolic status mainly through its control of intestinal energy availability by contributing to the fermentation of non-digestible dietary fiber (oligosaccharides) into absorbable and reusable short chain fatty acids (SCFAs) in the gut. SCFAs produced by bacterial fermentation contribute 5-10% to daily energy

intake of the host (9). The SCFAs feed back into the host metabolic system as energy source or anabolic substrates (10). Therefore, oligosaccharides and SCFAs are good indicators for microbial fermentation activity, host energy availability and metabolic phenotype. The combination of GC-MS, NMR and bomb calorimetry provides a reliable, complementary and comprehensive view of bacterial fermentation activity. Chapter 3 took advantage of the combined metabolomics approach aforementioned to study the impact of a xenobiotic tempol on microbiome fermentation and host energy metabolism. Nitroxide radical tempol is an antioxidant, exhibits beneficial metabolic improvements through modulating the gut microbiome composition, specifically inhibiting BSH producing bacteria *Lactobacillus*, which resulted in higher intestinal TβMCA level and stronger FXR antagonism (11). Focusing on the microbiome modulation effect of tempol, the bacteria fermentation activity of mice following 5-day gavage of tempol was evaluated by NMR and GC-MS metabolomics in combination with bomb calorimetry. The results suggested short-term tempol administration by gavage lead to the inhibition of bacteria fermentation characterized by decreased SCFAs and increased oligosaccharides level in the intestine in a dose dependent manner. As SCFAs serve as energy source and anabolic substrates for biosynthesis to the host (10), the restricted intestinal SCFAs availability due to tempol-inhibited bacteria fermentation profoundly impacts the host overall energy metabolism towards a catabolic state revealed by metabolic and gene expression profiles in the liver **(Figure 5-1**). The metabolic profiles were characterized with the depleted energy source pool and upregulated metabolites involved in catabolism. Analysis of the glucose and lipid metabolism associated gene expression further confirmed the promoted glycogenolysis and glycolysis, and suppressed

lipogenesis by tempol. Overall, metabolic pathways altered by tempol-modulated gut microbiome favor energy expenditure. Interestingly, tempol failed to induce any observed metabolism improvement in germ free mice, suggesting the metabolic regulatory function of tempol is mediated through microbiome. In summary, this study provides a microbiome-dependent mechanism of tempol, which achieves its beneficial metabolic improvement effects through inhibiting bacteria fermentation to decrease energy harvest of the host and shifts host energy homeostasis from energy reservation to expenditure. This work not only presented a promising strategy to target gut microbiome for obesity and metabolic disorder treatment and prevention, but also demonstrated the practical applicability of combined global NMR-based and targeted MS-based metabolomics approaches to generate a complementary and comprehensive view for a better understanding the crosstalk among gut microbiome, metabolites and host.

Xenobiotic refers to a foreign chemical substance that is not endogenously produced or expected to be present within the organism. Xenobiotics like environmental toxicants, antibiotics, drugs and other chemicals have been known to alter gut microbiome physiology, composition and gene expression (12), and the functional interactions between xenobiotics and gut microbiome has been implicated in drug efficacy, chemical toxicity, and human disease pathogenesis and progression (13). Microbiome-targeted therapies have been exploited in the treatment of diseases related to dysregulated xenobiotic-microbiome-host interactions. However, the functional interactions between xenobiotic and host-associated gut microbiome are never unidirectional. Gut microbiome affects xenobiotic/drug efficacy and toxicity through

direct modification of the chemical compound or indirect modulation of host xenobiotic/drug metabolism via bacterial-derived signaling. Xenobiotics also impact the gut microbiome composition and health which can cause profound microbial-associated metabolic consequences to the host (14). Therefore, a better understanding of how the xenobiotic impacts the host-associated microbiome will enlighten the molecular mechanism, pharmaceutical potential, as well as the toxicity of the xenobiotic for better microbiome-targeted therapy development and risk assessment.

Chapter 4 introduced a novel multi-platform in vitro approach that combines high throughput global metabolomics with in vitro microbial culturing and flow cytometry to evaluate the effect of xenobiotics on microbial toxicity characterized with functional physiological and metabolic indicators. Xenobiotic tempol was chosen as it is known to modulate microbial structure and improve host metabolism yet is microbiome modulating effects are unclear and unexplored (11, 15). Using flow cytometry, microbial physiology including nucleic acid content, membrane damage and enzymatic /biochemical activity was profiled with different florescent dyes. The flow cytometric analysis revealed a direct impact to microbial physiology in response to short-term tempol exposure in vitro, characterized with excessive membrane damage (higher percent Pi+ and DiBAC+ cells) and suppressed biochemical activity (lower percent CFDA+ cells). Taking advantage of combination of NMR- and MS- based metabolomics, a comprehensive and complementary metabolic profiles was created. The metabolic profiling with independent platforms revealed a consistent low microbial metabolic activity following tempol exposure in vitro, including decreased microbial fermentation, degradation, energy

generation and biosynthesis, which broadly covered many critical metabolic pathways like nucleotide, amino acid, sugar, and aromatic compounds anaerobic metabolism. Comprehensively, the disrupted microbial physiology and compromised microbial metabolism induced by tempol are highly correlated, demonstrating the mutually dependent relationship between a healthy membrane and normal metabolic activity. As the membrane provides a selective barrier against environmental hazardous substances from impacting normal intracellular metabolic activity, while the normal metabolic activity supplies molecular components and energy required for membrane synthesis and maintenance, the integrated physiological and metabolic profiles revealed by multi-platform approach provide informative functional assessment of the microbial response to xenobiotic. Critically, the application of the multi-platform physiological and metabolic phenotyping is further validated with the consistent results using in vitro and in vivo tempol exposure models. Together, the multi-platform functional phenotyping described in Chapter 4 represents a novel approach to evaluate microbial toxicity and xenobiotic risks in vitro, which holds great potential as a translational tool for drug screening and xenobiotic risk assessment.

Future Directions

Combining high-throughput metabolomics with other informative techniques, the work in the dissertation revealed the interplay between xenobiotic/drug and host-associated gut microbiome for mode of action characterization, toxicity evaluation and risk assessment. A recent study has started to incorporate the gut microbiome into drug screening, and discovered an astonishing 24% of human targeted, non-antibiotic

compounds exhibited antimicrobial or microbial modulatory effects, which is correlated with the antibiotic-like side effects in human studies. This finding reflects the off-target effects of non-antibiotic compounds on gut microbiome, implying the potential risk of the antibiotic resistance introduced by human-targeted drugs (16). Another study has attempted to use MS-based metabolomics as a prediction tool to classify the mode of the action of antimicrobial compounds for early drug discovery (17). Our study expanded on the idea of using the gut microbiome for drug screening and developed the multi-platform functional phenotype approach by using MS- and NMR- based metabolomics and flow cytometry. This multi-platform approach out-performs the single MS-metabolomics approach by providing the comprehensive and complementary functional phenotypic assessment containing physiological and metabolic profiles. This comprehensive approach opens up new paths for translational applications in risk assessment for existing drugs, and identification of the modes of action for new compounds. In fact, we have already expanded the investigation to generate the integrated functional phenotypic database of microbiome using the antibiotics with distinct mechanisms. The selected antibiotics include ampicillin, ciprofloxacin, tetracycline, and rifampin, with each having a distinct mechanism of action (**Figure 5-2**). Ampicillin prevents the synthesis of the bacterial cell wall by inhibiting the required enzyme transpeptidase and will cause a loss of membrane potential and cell damage. Ciprofloxacin inhibits DNA synthesis through inhibiting DNA gyrase and prevents bacteria from replicating. Tetracycline is a protein synthesis inhibitor, which prevents the binding of aminoacyl-tRNA to the mRNA-ribosome complex. Rifampin inhibits DNA-dependent RNA synthesis via inhibiting bacterial DNA-dependent RNA polymerase (18). In addition to the flow cytometry and

metabolomics to characterize the whole microbial community, it would be more informative to assess the physiological structure, taxonomic and functional changes of the microbial community subsets by introducing fluorescence-activated cell sorting and downstream sequencing based approaches. After introducing the different fluorescent dyes to the microbial community, a fluorescence-activated cell sorter will be used to sort microbes based on the physiological status indicated by fluorescent intensity. Then the taxonomic composition and gene expression profile of each physiological category subset community will be analyzed with downstream sequencing-based approaches including 16S rRNA gene sequencing, metagenomics, and metatrascriptomics. The physiological and metabolic profiles characterized with the novel multi-platform functional phenotyping approach, together with the incorporation of taxonomic and transcriptomic profiles characterized with sequencing-based approaches, will help screen and characterize future compounds of interest that have an unknown mode of action, or help identify current known compounds that have potential antimicrobial activity (**Figure 5-3**). Moreover, the multi-platform functional phenotyping approach could be applied to assess the effect of xenobiotic to specific bacteria strain associated with health and diseases such as *Clostridium difficile* (19), *Helicobacter pylori* (20) and *Lactobacillus* spp. (21), assist the elucidation of the xenobiotic mode of action as well as the health impact of xenobiotics the microbiome.

In summary, the findings in this dissertation demonstrated the valuable metabolomics tools in combination with other informative techniques enables the comprehensive and complementary understanding of the mechanistic interplay between

xenobiotic and host-associated microbiome, paving the ways to the discovery and development of potent and safe microbiome-targeted compounds for human disease treatment.

REFERENCE

1. Bonvallot N, Tremblay-Franco M, Chevrier C, Canlet C, Debrauwer L, Cravedi JP, and Cordier S. Potential input from metabolomics for exploring and understanding the links between environment and health. *Journal of toxicology and environmental health Part B, Critical reviews.* 2014;17(1):21-44.
2. Zhang L, Nichols RG, Correll J, Murray IA, Tanaka N, Smith PB, Hubbard TD, Sebastian A, Albert I, Hatzakis E, et al. Persistent Organic Pollutants Modify Gut Microbiota-Host Metabolic Homeostasis in Mice Through Aryl Hydrocarbon Receptor Activation. *Environ Health Perspect.* 2015;123(7):679-88.
3. Martin FP, Sprenger N, Montoliu I, Rezzi S, Kochhar S, and Nicholson JK. Dietary modulation of gut functional ecology studied by fecal metabonomics. *J Proteome Res.* 2010;9(10):5284-95.
4. Pinu FR, Villas-Boas SG, and Aggio R. Analysis of Intracellular Metabolites from Microorganisms: Quenching and Extraction Protocols. *Metabolites.* 2017;7(4).
5. Mashego MR, Rumbold K, De Mey M, Vandamme E, Soetaert W, and Heijnen JJ. Microbial metabolomics: past, present and future methodologies. *Biotechnology letters.* 2007;29(1):1-16.
6. Hou W, Zhong D, Zhang P, Li Y, Lin M, Liu G, Yao M, Liao Q, and Xie Z. A strategy for the targeted metabolomics analysis of 11 gut microbiota-host co-metabolites in rat serum, urine and feces by ultra high performance liquid chromatography–tandem mass spectrometry. *Journal of Chromatography A.* 2016;1429(207-17.
7. Yan S, Huang J, Chen Z, Jiang Z, Li X, and Chen Z. Metabolomics in gut microbiota: applications and challenges. *Science Bulletin.* 2016;61(15):1151-3.
8. Sumner LW, Mendes P, and Dixon RA. Plant metabolomics: large-scale phytochemistry in the functional genomics era. *Phytochemistry.* 2003;62(6):817-36.
9. McNeil NI. The contribution of the large intestine to energy supplies in man. *Am J Clin Nutr.* 1984;39(2):338-42.
10. Zambell KL, Fitch MD, and Fleming SE. Acetate and butyrate are the major substrates for de novo lipogenesis in rat colonic epithelial cells. *J Nutr.* 2003;133(11):3509-15.
11. Li F, Jiang C, Krausz KW, Li Y, Albert I, Hao H, Fabre KM, Mitchell JB, Patterson AD, and Gonzalez FJ. Microbiome remodelling leads to inhibition of intestinal farnesoid X receptor signalling and decreased obesity. *Nature communications.* 2013;4(2384.
12. Maurice CF, Haiser HJ, and Turnbaugh PJ. Xenobiotics shape the physiology and gene expression of the active human gut microbiome. *Cell.* 2013;152(1-2):39-50.
13. Claus SP, Guillou H, and Ellero-Simatos S. The gut microbiota: a major player in the toxicity of environmental pollutants? *Npj Biofilms And Microbiomes.* 2016;2(16003.
14. Wilson ID, and Nicholson JK. Gut microbiome interactions with drug metabolism, efficacy, and toxicity. *Translational Research.* 2017;179(204-22.
15. Cai J, Zhang L, Jones RA, Correll JB, Hatzakis E, Smith PB, Gonzalez FJ, and Patterson AD. Antioxidant Drug Tempol Promotes Functional Metabolic Changes in the Gut Microbiota. *J Proteome Res.* 2016;15(2):563-71.
16. Maier L, Pruteanu M, Kuhn M, Zeller G, Telzerow A, Anderson EE, Brochado AR, Fernandez KC, Dose H, Mori H, et al. Extensive impact of non-antibiotic drugs on human gut bacteria. *Nature.* 2018;555(623-8.
17. Zampieri M, Szappanos B, Buchieri MV, Trauner A, Piazza I, Picotti P, Gagneux S, Borrell S, Gicquel B, Lelievre J, et al. High-throughput metabolomic analysis predicts mode of action of uncharacterized antimicrobial compounds. *Science Translational Medicine.* 2018;10(429).
18. Kohanski MA, Dwyer DJ, and Collins JJ. How antibiotics kill bacteria: From targets to networks. *Nature Reviews Microbiology.* 2010;8(423-35.

19. Lessa FC, Mu Y, Bamberg WM, Beldavs ZG, Dumyati GK, Dunn JR, Farley MM, Holzbauer SM, Meek JI, Phipps EC, et al. Burden of Clostridium difficile infection in the United States. *N Engl J Med.* 2015;372(9):825-34.
20. Kao C-Y, Sheu B-S, and Wu J-J. Helicobacter pylori infection: An overview of bacterial virulence factors and pathogenesis. *Biomedical Journal.* 2016;39(1):14-23.
21. Martinez RM, Hulten KG, Bui U, and Clarridge JE. Molecular Analysis and Clinical Significance of Lactobacillus spp. Recovered from Clinical Specimens Presumptively Associated with Disease. *Journal of clinical microbiology.* 2014;52(1):30-6.

Figure 5-1

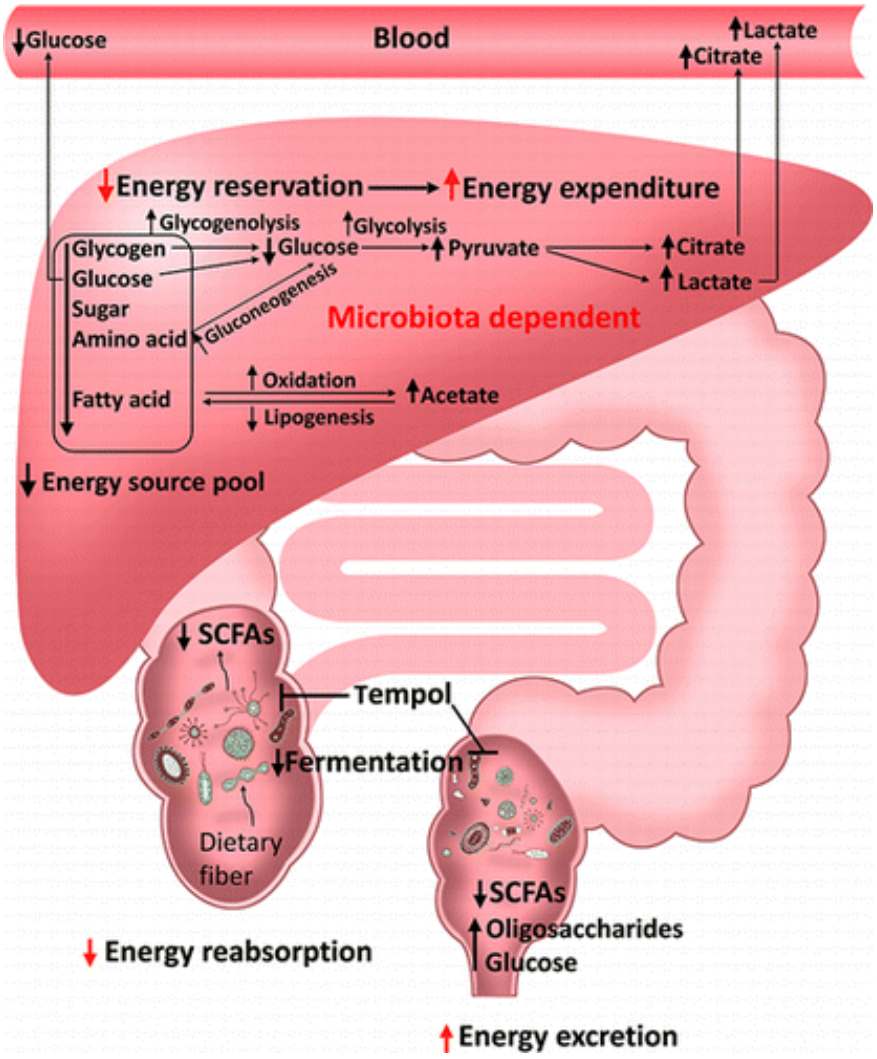

Figure 5-1 Metabolic Pathways Modulated by Tempol-Altered Functional Change of Gut Microbiome Favor Energy Expenditure and Catabolism.

Figure 5-2

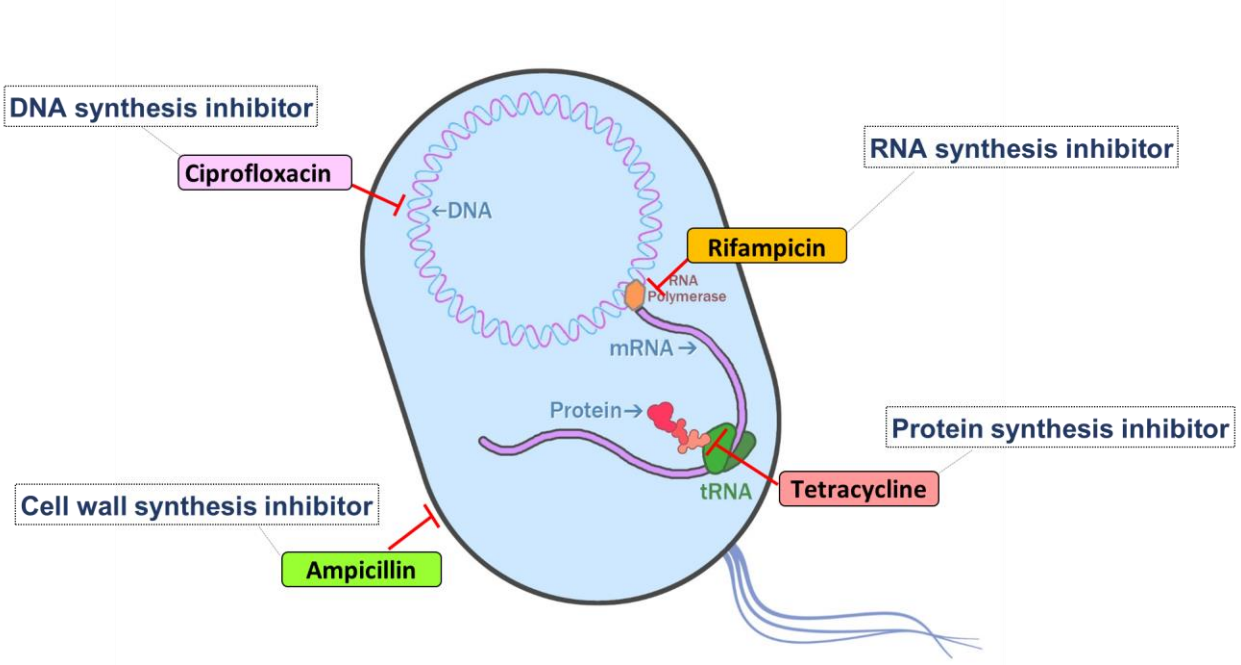

Figure 5-2 Mechanism of Action of Different Antibiotics. Ampicillin inhibits bacterial cell wall synthesis through inhibiting the required enzyme transpeptidase. Ciprofloxacin inhibits DNA synthesis and consequently cell division by inhibiting DNA gyrase. Rifampicin Inhibits DNA- dependent RNA synthesis thus preventing inhibiting bacterial DNA-dependent RNA polymerase. Tetracycline inhibits protein synthesis through inhibiting binding of aminoacyl-tRNA to the mRNA-ribosome complex.

Figure 5-3

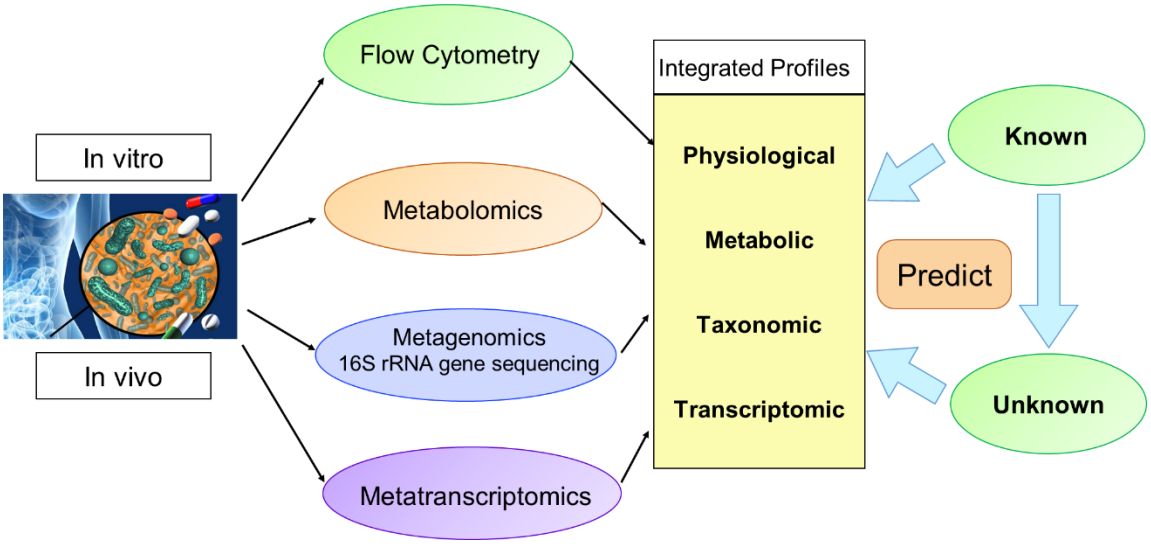

Figure 5-3. Combining Multi-Platform Tools to Study Xenobiotic Toxicity on Microbiome

Table 5-1 Orthogonal Comparison of SCFA Quantitation Methods.

	Linearity	Sensitivity	Matrix Effect	Repeatability	Sample Prep	Acquisition Time	Application
GC-MS Propyl Esterification Method	Good	High	Relative High	Good	Complicated	25 min	Trace SCFAs quantitation (bio-fluid / intracellular)
GC-MS Acidified Water Method	Good	Intermediate	Relative High	Good	Simplest	14 min	Large quantity samples from bio-digester or large-scale human studies
^{1}H NMR Quantification Method	Good	Relative Low	Relative Low	Great	Relative Simple	20 min	Cecal or fecal samples with the purpose of characterizing the overall metabolic status

Appendix

Structural and Functional Analysis of the Gut Microbiome for Toxicologists

Accepted in Current Protocols in Toxicology

Robert G. Nichols[1*]**, Jingwei Cai**[1*]**,** Iain A. Murray[1], Imhoi Koo[1], Philip B. Smith[2], Gary H. Perdew[1], and Andrew D. Patterson[1]

[*]Denotes shared authorship.

Affiliations: [1]Center for Molecular Toxicology and Carcinogenesis, Department of Veterinary and Biomedical Sciences, Pennsylvania State University, University Park, State College, Pennsylvania, 16802, USA; [2]Metabolomics Facility, Huck Institutes of Life Sciences, Pennsylvania State University, University Park, State College, Pennsylvania, 16802, USA

Contributions: RGN, JC and ADP conceived and coordinated the study and wrote the manuscript. RGN designed, performed and wrote the sequencing-based analysis part, including basic protocol 1-3 and trouble shooting. JC designed, performed and wrote the MS- and NMR- based metabolomics analysis part, including basic protocol 4-9. IAM, IK, PBS and GHP contributed to the data interpretation and preparation of the manuscript. All authors reviewed the results and approved the final version of the manuscript.

ABSTRACT

Characterizing the reciprocal interactions between toxicants, the gut microbiota and the host, holds great promise for improving our mechanistic understanding of toxic endpoints. Advances in culture-independent sequencing analysis (e.g., 16S rRNA gene amplicon sequencing) combined with quantitative metabolite profiling (i.e., metabolomics) have provided new ways of studying the gut microbiome and have begun to illuminate how toxicants influence the structure and function of the gut microbiome. Developing a standardized protocol is necessary for establishing robust, reproducible and importantly, comparative data. This protocol can be used as a foundation for examining the gut microbiome via sequencing-based analysis and metabolomics. Two main units follow: 1) Analysis of the gut microbiome via sequencing-based approaches; and 2) Functional analysis of the gut microbiome via metabolomics.

INTRODUCTION

Alterations to any area of the microbiome will occur in almost all toxicological studies. The gut microbiome will be altered with any oral exposure of xenobiotics (1). The microbiome protecting the lungs and airways will be altered when exposed to aerosolized compounds like polycyclic aromatic hydrocarbons (2). Even the resilient protective microbiome on the skin is being constantly altered by the xenobiotics individuals are exposed to every day (3). Despite the importance of the various microbiomes in toxicology, the majority of toxicological studies neglect to include an investigation of the appropriate microbiome. A major reason for the missing microbiome studies is the fact that there is no universal protocol to refer to when completing the microbiome analysis. Below is a step by step, nine-part protocol created to start the process of incorporating gut microbiome analysis into any applicable toxicological study. Even though this protocol only includes one area of the microbiome, it will provide an avenue for other complete protocols describing how to investigate the other areas of the microbiome.

The following unit describes the process of bacterial DNA extraction from mouse cecal contents. A flow chart describing the following unit can be seen in **Figure A-1**. The bacterial DNA isolation kit used in this protocol can also be used for bacterial DNA isolation of rodent fecal pellets or human stool samples and the data generation and analysis protocols also apply to human fecal bacterial DNA. Integration of microbiome analyses in to toxicology studies can provide insights into cryptic or previously uncharacterized toxic endpoints. It is a common misconception that only a computer scientist can conduct microbiome analyses, but the reality is that only basic terminal

commands and basic R programming are needed for a comprehensive microbiome analysis. There are many online resources that can be used; for example, the R cookbook, a comprehensive manual for R programming, is a freely available, (http://www.cookbook-r.com/) and there are many websites for terminal-based coding. This unit will cover 16S rRNA gene analysis using the mothur software package (4) and also metagenomic sequence analysis using the HUMAnN2 (**H**uman microbiome project **U**nified **Me**tabolic **An**alysis **N**etwork) software package (5). The resulting files from 16S rRNA gene analysis are a taxonomic distribution that can be used to create graphs illustrating significant changes. The resulting files from the metagenomic analysis represent pathways that are present in the gut microbiome and demonstrate if the relative abundance of these pathways have increased or decreased in response to a specific treatment. Importantly, sequence analyses revealing the presence of a given panel of genes associated with specific metabolic pathways does not imply phenotypic expression of the pathway, additional functional assessment is required. Such functional verification will be covered in Unit 2. Overall this unit will provide a comprehensive and easy to follow method of gut microbiome analysis.

Sample data, a script for the mother analysis, and a R mark down file for GUnifrac analysis have been included and made available to accompany this protocol in a zip file (test_data.zip). Other sample data can be found on the mothur wiki site (https://www.mothur.org/wiki/MiSeq_SOP) and sample data for HUMAnN2 can be found (**https://bitbucket.org/biobakery/humann2/wiki/Home**) on the HUMAnN2 bit bucket page. To run the included sample script, simply unzip the sample folder, open terminal, and navigate to the test_data directory. Type *./mothur/mothur*

./Mothur.test.batch.txt. This script should take roughly 15 min (script specifies two processors, it can be edited for more processors if more are available) and will result in a summary table, which includes the taxonomic distribution for the test data. It should be noted that the commands to make a phylogenic tree with mothur are included but will not run without removing the hashtags before the commands. These commands are not run because these commands will add an extra 30 min to the run time of this script and the resulting.tre and count files **WILL NOT** work for GUnifrac analysis due to the small size of the subset. Instead both a separate .tre file and a count file are provided to illustrate the GUnifrac analysis with the R mark down file in a folder called GUnifrac_data. Also, the included mothur script is a guide and each user should modify the file names and parameters as necessary.

SEQUENCING-BASED PROTOCOLS

Basic Protocol 1: Bacterial DNA Extraction

Introduction

Basic Protocol 1 explains the process of bacterial DNA isolation from mouse cecal contents. For information on how to extract cecal contents see **Support Protocol 1.** This protocol is adopted from the Omega-BioTek E.Z.N.A stool isolation kit and has been used extensively within our laboratory(6-9). The PowerSoil DNA Isolation kit (moBio) has also been used and can be implemented instead of the Omega-BioTek E.Z.N.A kit. A recent study has shown that the use of different bacterial DNA isolation kits leads to less variation than the use of different 16S rRNA gene primers (V3-V4

yields different results than V4-V5) (10). Listed below is a modified version of the protocol provided Omega-BioTek provided protocol.

Materials

Sterile 10 - 200 μL pipette (Denville)

Sterile 1000 μL pipette (Denville)

1 Omega-BioTek E.Z.N.A Stool DNA kit (200 preps)

1 Centrifuge (Eppendorf 5409 R)

1 set of sterile sample labeled 1.5 mL screw cap homogenizer tubes (VWR)

3 sets of sterile sample labeled 2 mL nuclease-free Eppendorf tubes (Eppendorf)

Benchmark Multi-Therm Shaker with Heating

Vortexer (any brand)

100% Ethanol (Any brand as long as it meets USP specifications)

Ice bath

Zirconia/Silica 1.0mm diameter homogenization beads (BioSpec Products)

Precellys 24 lysis and homogenization (Bertin Technologies) (Optional)

Protocol Steps

1. Dilute the *DNA Wash Buffer* from the E.Z.N.A kit with 80 mL of 100% Ethanol (only if the 200 prep kit is purchased). If this was previously done go to step three.

2. Dilute the *VHB Buffer* from the E.Z.N.A kit with 84 mL of 100% Ethanol (only if the 200 prep kit is purchased). If this was previously done go to step three.

3. Set one incubator to 70°C.

4. If a second incubator is available, set it to 95°C.

5. Place the *HTR Reagent* from the E.Z.N.A kit into the ice bath.

6. Take between 50 and 100 mg of cecal contents (can be as high as 200 mg) and deposit it into the labeled screw cap tubes.

7. Add 10 - 30 Zirconia/Silica beads to each tube and place tube into the ice bath.

8. Add 540 μL of the *SLX-Mlus Buffer* from the E.Z.N.A kit to each tube.

9. If homogenizer is available, homogenize samples at 6,500 rpm for 15 seconds, pause for 30 seconds, then homogenize for another 15 seconds. Samples will look foamy. Go to step 11.

10. If homogenizer is not available, vortex each sample for at least 10 min or until each sample is thoroughly homogenized.

11. Add 60 μL of the *DS Buffer* and 20 μL of the *Proteinase K Solution* from the E.Z.N.A kit. Vortex for 30 seconds to mix.

12. Place samples in the incubator (70 °C) for 10 min. Vortex each sample twice for 15 s during the incubation, once at minute 2 and once at minute 7.

13. Immediately after incubation place the samples in the 95 °C incubator for 5 min. This step is optional but improves DNA isolation from gram-positive bacteria.

14. Add 200 μL *SP2 Buffer* from the E.Z.N.A kit and vortex for 30 sec to mix. Place samples in ice bath for 5 min.

15. Centrifuge at maximum speed (at least 13,000 x g) for 5 min.

16. While the samples are spinning, transfer 5 mL of the *Elution Buffer* to separate Eppendorf tubes and incubate them at 65 °C until needed.
    a. Each sample requires 150 μL of elution buffer will be needed for each sample at the end of this protocol, so adjust the total amount of elution buffer accordingly.

17. Remove 400 μL of the supernatant from **step 15,** and transfer it to the first set of labeled Nuclease-free Eppendorf tubes. Be careful when transferring to not disturb the pellet.

18. Make sure the cap is secure on the *HTR Buffer* and shake it vigorously to completely mix the buffer. Cut the tip off of a 1000 μL pipette tip (this helps pipetting the *HTR Buffer*) and transfer 200 μL of the *HTR Buffer* to each sample.

19. Incubate at room temperature for 2 min and then centrifuge at maximum speed for 2 min.

20. Remove 250 μL of the supernatant, and place it in the second set of labeled Eppendorf tubes.

21. Add 250 μL of the *BL buffer* from the E.Z.N.A kit and 250 μL of 100% ethanol to each sample and vortex for 10 s to mix.

22. Place one *HiBind DNA Mini Column* into a 2 mL collection tube, both provided in the E.Z.N.A kit. Label each column appropriately.

23. Transfer the entire sample from **step 21** into each respective column (including any precipitates). Centrifuge at maximum speed for 1 min.

24. Discard the filtrate and collection tube. Transfer the column into a new collection tube and add 500 μL of *VHB Buffer* from the E.Z.N.A kit.

25. Centrifuge for 30 s at maximum speed. Discard the filtrate but reuse the collection tube.

26. Add 700 μL o f the *DNA Wash Buffer* to each sample. Centrifuge at maximum speed for 1 min. Discard the filtrate but reuse the collection tube.

27. Repeat step 26 to wash the DNA once again.

28. Centrifuge at maximum speed for 2 min to dry out the column and remove any excess wash buffer.

29. Transfer the column to the third set of labeled Eppendorf tubes.

30. Add 150 μL of the heated *Elution buffer* to each sample and incubate them at room temperature for 2 min.

31. Centrifuge at maximum speed for 1 min.
    a. Note: Do not be alarmed if some of the Eppendorf caps come off during the centrifugation. Since the caps of the Eppendorf tubes cannot be closed during the centrifugation, the g-force will sometimes rip them off.

32. Samples can be stored at -20 °C.

Basic Protocol 2: V4-V4 Amplification for 16S rRNA Gene Sequencing

After DNA isolation, samples can either be directly submitted for bacterial metagenomic shotgun sequencing (see **Alternative Protocol 1** for metagenomic analysis) or they can be further modified for 16S rRNA **gene** sequencing. Here the process for PCR amplification of the fourth variable region of the 16S rRNA gene is described. The V4 region of the 16S rRNA gene has been reported to provide the most taxonomic information of the 8 variable regions present in the 16S rRNA gene, but other variable regions like V5, and V6 can provide comparable results (11). Also, if there is access to a long read sequencer like the Pacbio Sequel II system, the entire variable region can be amplified and sequenced. Sequencing the entire variable region is the only way to get reliable species level taxonomy assignment (12). Using V4-V4 16S rRNA gene sequencing provides reliable genus level sequencing (4). This protocol will describe how to amplify the V4 region of the 16S rRNA gene by PCR and sequence it.

Materials

Ice bath

Isolated DNA from **Basic Protocol 1**

NanoDrop UV-Vis Spectrophotometer Lite (Thermo-Scientific)

Sterile 0.5 μL – 10 μL pipette (Denville)

Sterile 10 - 200 μL pipette (Denville)

Sterile 1000 μL pipette (Denville)

V4-V4 primer set (515F and 806R) (10 μM concentration)

Nuclease free water (Any Brand)

Invitrogen Platinum SuperFi Enzyme Kit (ThermoFisher Scientific)

Sterile 0.2 mL Thin Wall PCR Tubes, strips of 8 tubes (Denville)

T100 Thermocycler (Bio rad)

1X TAE (Tris base, acetic acid and EDTA) buffer

Omnipur Agarose (Calbiochem)

Gel electrophoresis box (Labnet)

GelRed dye (Biotium)

Gel loading dye 6X, no SDS (Biolabs)

100 bp DNA ladder (Omega)

ChemiDoc XRS+ (BioRad)

Protocol Steps

1. Thaw the isolated bacterial DNA from **Protocol 1**

2. Measure DNA concentration on the NanoDrop
    a. This requires only 1 μL of isolated bacterial DNA. Concentration values typically range from 100 ng/μL to 400 ng/μL. Also the NanoDrop gives only an estimate of the total bacterial DNA concentration. For a more accurate result, submit samples for quantification on a Bioanalyser.

3. Create a 100 μL aliquot at 10 ng/μL concentration.
    a. The easiest way to complete this is to first figure out how much original DNA to add and then subtract that from 100 to figure out how much nuclease free water to add. To find out how much original bacterial DNA to add simply divide 1,000 by the average concentration. For example, if the average concentration was 254 ng/μL, take 1000/254 = 3.94. Add 3.94 μl of original bacterial DNA sample to (100 - 3.94 = 96.06) 96.06 μL of nuclease free water.

4. Place aliquots on ice and create 10 μM solutions of forward (515F) and reverse primers (806R).

5. Place 10 μL of the Platinum Superfi Enzyme mix, 0.4 μL of the forward primer (10 μM), 0.4 μL of the reverse primer (10 μM) and 8.7 μL of nuclease free water to each PCR tube.
    a. It is important to prepare a master mix. As an example, a master mix for 20 samples can be prepared as follows: The 20 sample master mix should be prepared for 23 samples (for blanks as well as to account for imprecise pipetting) samples and would contain 230 μL (10 x 23) of Platinum Superfi enzyme mix, 9.2 μL (0.4 x 23) of forward primer, 9.2 μL (0.4 x 23) of reverse primer and 200.1 μL (8.7 x 23) of nuclease free water. Then 19.5 μL of the master mix is placed in each of the 21 PCR tubes (20 samples + 1 blank)

6. Add 0.5 μL of the 10 ng/μL aliquot of bacterial DNA and pipette to mix.

7. Place the caps on the PCR tubes and place the sealed tubes into the PCR machine. Run the PCR machine at these settings:

    a. 1 cycle at 98° C for 2 min
    b. 25 cycles of:
        i. 98 °C for 10 sec
        ii. 56.5 °C for 20 sec
        iii. 72 °C for 15 sec
    c. 1 cycle at 72 °C for 5 min
    d. Infinite hold at 4 °C
    e. Note that over amplification can affect the results. The more cycles of initial amplification completed, the more populated the abundant species become and it makes it much more difficult to observe the rare species. Also as the number of cycles increases, there is a greater chance of contamination amplification.

8. While the PCR is running, create a 1X agarose gel by mixing 1 g of Omnipur Agarose in 100 mL of 1X TAE buffer and microwaving for 2 min.

9. Before the gel sets, add 10 μL (10 μL per 100 mL of gel) of GelRed dye to the liquid gel.
    a. GelRed can be used instead of ethidium bromide for several reasons: First, it is much safer to use in the lab. Second, there is no need to add extra dye to the running buffer, so the buffer can be reused multiple times. Third, and most importantly, the gels are much clearer and there is no ethidium bromide band in the gel.

10. Once PCR is finished add 5 μL of the PCR sample to 4 μL of 6x loading dye (BioLabs) and 6 μL of nuclease free water in a separate tube.

11. Fill the gel electrophoresis box with 1X TAE buffer and add 5 μL of 100 bp DNA ladder to the edges of the gel. Add the entire sample from **step 10** to the empty wells. Run at 80 Volts for 50 min to an hour. The gel run will be complete when the purple band is ¾ of the way down the gel. The gel can also be placed back into the gel box for further running if the bands have not separated enough.

12. When the bands are at least ¾ the way down the gel, remove the gel and analyze it with the ChemiDoc. The correct band length should be 350 bp.
    a. Do not be alarmed if the bands are not very bright (**Figure A-2**). Duller bands are preferred because another round of PCR will be completed before sequencing.

13. Submit samples to a sequencing core or a sequencing company and request 250 x 250 paired end sequencing on the Illumina Miseq.
    a. **Important**: Each sequencing core or sequencing company is different and may require a different end product for sample submission. Most will take the sample after the first round of PCR because this generates amplicons of the 16S rRNA gene variable region of the users choosing. If they require more PCR follow the detailed instructions provided by the sequencing core or company of the users choosing.
    b. Depth is also an important specification to decide prior to sequencing. Typically, the Illumina Miseq will provide 10 million reads split across each of the user's samples. This means if the user has 50 samples in one run on the Illumina Miseq the user will get roughly 200,000 reads per sample. Depth preference is generally between 50,000 and 100,000 reads per sample (13)
    c. When the data is returned, it should be demultiplexed, generating two files for each sample in FASTQ format.

Basic Protocol 3: 16S rRNA Gene Amplicon Data Analysis

The following protocol is directly based on the mothur miseq SOP created by Dr. Patrick Schloss. The website can be found here, https://www.mothur.org/wiki/MiSeq_SOP, and if this method is used, the 2013 paper by Kozich *et al* **must** be cited (4). The following command progression is exactly how it appears in the Schloss SOP, but the file names, values and explanations are different. For a more detailed explanation, please see the above website and consult the Wiki. This

protocol covers the basic mothur analysis, normalization, identification of significantly different bacterial taxa, and Generalized unifrac analysis. If one chooses, QIIME is an alternative 16S rRNA gene sequence analysis pipeline, and more information can be found at https://qiime2.org/ (14).

This protocol requires that the analysis be performed within a Mac or PC Linux environment through the application terminal. PC environments do have a command line tool called command prompt, but the computing language the command prompt uses is very different from the terminal/Linux computing language. It is also recommended that at least 8 processors with at least 100 Gb of memory be used. This analysis can be done on a personal laptop, but it is extremely time consuming; therefore, the use of an external server or a computing cluster is highly recommended. Since mothur is terminal-based, basic command line knowledge is required for this analysis. Also, all graphing and some statistical analysis can be done with R studio, thus basic R knowledge or an alternative statistical/graphing software is required.

The mothur github site and SOP describes how to download and install this software on a PC (https://github.com/mothur/mothur/releases/tag/v1.39.5 and https://mothur.org/wiki/MiSeq_SOP). If one is using an external server or a computing cluster, the download is a little more complicated because the user does not have administrative privileges. The easiest way to "install" mothur on an external server is first by downloading the most recent version on the mothur github site. There are multiple options of how to download mothur, and the one used for this procedure is **mothur.linux_64.zip**. This file can be copied over to the external server of a cloud cluster and unzipped there. Then simply add the mother folder to the user's path with the

command export *PATH="$PATH:~/mothur"*. To run mothur, simply type *mothur* in the command line.

Also on the mothur miseq SOP, there are several files that are required for the analysis. The first is the SILVA alignment file, which can be found under the **Logistics** section of the mothur miseq SOP. This provides a zip file, and only the silva.bacteria.fasta file is needed for this analysis. The SILVA alignment file is regularly updated and new versions of this file can be downloaded from the Silva database website (https://www.arb-silva.de/). The next two necessary files can be found right below the SILVA link, in a link titled *mothur-formated version of RDP training set*. This will provide a second zip file that contains only two files; both are needed for this analysis. Like the SILVA alignment file, the RDP trainsets are also updated regularly and can be found at the RDP website (https://rdp.cme.msu.edu/misc/resources.jsp#aligns). Once all three files are obtained (silva.bacteria.fasta, trainset9_032012.pds.fasta, and trainset9_032012.pds.tax), create a work folder on the external server or computing cluster for the mother analysis and move these files into it. For this analysis the provided RDP trainsets and the provided SILVA alignment files from the mothur miseq SOP (version 9) will be used. For future use, RDP and SILVA regularly puts out new trainsets and alignment files, as mentioned above.

Materials

Mac computer (or Windows with Linux environment)

External server or computing cluster with an allocation of at least 100 GB and 8 processors (can use personal computer but will drastically increase computational time)

Sequenced data from **Protocol 2**

Protocol steps

1. Before the analysis, be sure to read the above information and have mothur installed and acquire all the necessary files.

2. With the raw data make a stability file. This is a file that will help mothur know what two paired end files to combine and name it according to the user created sample names.
    a. This file can be made with a text editor and will look like the example below (and an example stability file can be found in the provided sample data).

501 501_S21_L001_R1_001.fastq 501_S21_L001_R2_001.fastq
502 502_S22_L001_R1_001.fastq 502_S22_L001_R2_001.fastq
503 503_S23_L001_R1_001.fastq 503_S23_L001_R2_001.fastq
504 504_S24_L001_R1_001.fastq 504_S24_L001_R2_001.fastq
505 505_S25_L001_R1_001.fastq 505_S25_L001_R2_001.fastq

    b. The first column contains the sample names; in this case they are 501, 502, 503, 504, and 505. After each sample name, it is important to tab, not space, to the next column. The second column contains the first file name for each pair. In this case, 501_S21_L001_R1_001.fastq is the name of the first file of the 501 pair. Again tab to create the third column, the second file name for each pair. In this case 501_S21_L001_R2_001.fastq is the second file name for the 501 pair. Continue this for each sample in the run.
    c. This file should be named after the user's project. In this example this file will be named Test.stab.txt. This file should then be sent to the mothur work folder along with all the FASTQ data and the required files mentioned above.

3. Execute mothur and run *make.contigs(file=Test.stab.txt, processors=8)*
    a. Notice how the stability file created in the previous step is directly used and how mother needs to be told to use 8 processors. If mothur is not instructed how many processors to use, the default is 1.
    b. This process will take about 1 minute per sample and will result in six files. The only two required for this analysis are *Test.stab.trim.contigs.fasta* and *Test.stab.contigs.groups*

c. Notice how the first part of these file names are the name of the stability file. This is why it is important to name the stability file something related to the experiment.

4. With the output files, run a summary with the command summary.seqs(fasta= *Test.stab.trim.contigs.fasta)*
    a. The result will be a table that breaks down the fasta file from **step 3**. An example of this can be seen in **Table A-1**.
    b. The rows break down the data into various segments defined by the different columns. For example, the 25%-tile row says that 25% of the data has a start site at 1, an end site at 292, they are all at least 292 bases long with 0 ambiguous sites, an average of 3 polymers and has 670164 sequences in this group. This is typical, and the only column that is important from this specific summary file is the NBases column. Since the above protocol resulted in a 350 bp insert of the V4 region in **Protocol 2**, the user would expect the average base length of the sequences to be around 320 base pairs long.

5. Screen the sequences with the command *screen.seqs(fasta= Test.stab.trim.contigs.fasta, group=Test.stab.contigs.groups, maxambig=0, maxlength=320)*
    a. This command screens the data and trims off any bad reads. The maxambig=0 part of the command indicates that this command will cut any sequence with ambiguous bases. Referring back to the above table the user can see that 128 sequences have ambiguous bases. Also this command cuts anything larger than 320 bases (maxlength=320). 320 was picked because according to the above table, 97.5% of the data is 311 base pairs long or smaller and it is recommended on the mothur miseq wiki to go a few base pairs higher than the number at the 97.5% mark.
    b. The screen.seqs command specifications is very dependent on the data, so the max length will change depending on which variable region is used and the type of Illumina miseq run is completed (150x150 or 250x250). As a general rule, the user wants the max length to be at least the nBases number for the 97.5-tile group.

6. Remove duplicate sequences by running *unique.seqs(fasta= Test.stab.trim.contigs.good.fasta)*
    a. This step is included to save computational time by condensing the data. The resulting files represent a fasta file with only unique sequences and a name file that includes how many times each sequence occurred. This way when aligning and cleaning the data, each sequence is only seen once.

7. Combine the resulting name file from **step 6** and the group file from **step 3** to form a count table with the command *count.seqs(name= Test.stab.trim.contigs.good.names, group=Test.stab.contigs.good.groups)*
    a. This command will now create a count table that will have the names for every unique sequence and how many times they occur in each sample.

8. **Optional:** To save on computational time, the silva.bacteria.fasta file can be modified to only include alignment for the V4-V4 region of the 16S rRNA gene with the command *pcr.seqs(fasta=silva.bacteria.fasta, start=11894, end=25319, keepdots=F, processors=8)*
    a. This step will **only** work if the V4 region was sequenced but this step is not necessary for this analysis and will only save computational time.

9. Align the raw reads to the SILVA database with the command *align.seqs(fasta=Test.stab.trim.contigs.good.unique.fasta, reference= silva.bacteria.pcr.fasta, flip=t)*
    a. The reference file used in this example is the edited one from **Optional Step 8**. If **Optional Step 8** is not completed the file for the reference option will simply be *silva.bacter.fasta*
    b. With the optional step 8 the alignment time was about 9 min for 1618841 sequences.
    c. Without the optional step 8 the alignment time was 30 min to align 1618841 sequences.
    d. The flip=t option is included to attempt to align the reverse complement of sequences that do not align in the forward direction. This option will also produce more alignments and a more comprehensive look at the microbiome composition.

10. Investigate the alignment with another summary command, *summary.seqs(fasta=Test.stab.trim.contigs.good.unique.align, count= Test.stab.trim.contigs.good.count_table)*
    a. The purpose of this step is to further clean the data by picking reads that start and end at particular values.
    b. The summary table will be the same format as the one obtained in **step 4** but the values will be different**. Table A-2** provides an example of this summary table.
    c. When using the modified SILVA file, the start sequence will almost always be 1. The important variables to look at are the *End* and the *NBases* column. The *Nbases* column will show how large the sequences are and they should be similar to the cutoffs from step 4. In this case nothing should be larger than 320 and there should be no ambiguity. The end column will be used in the next step.

11. Screen the sequences again for poor alignment and any alignment errors with the command *screen.seqs(fasta=Test.stab.trim.contigs.good.unique.align, count=Test.stab.trim.contigs.good.count_table, start=1, end=13424, maxhomop=8)*
    a. The values for the start, end, and maxhomop options can be found in the summary file generated in **step 10**. The start option will select any sequence that starts at or before this value. The end value will select any sequence that ends at or after any value and the maxhomop removes any sequences that have more than 8 homopolymers. These details are important to know because occasionally the summary from **step 10** will show that 50% of the values have an end site of 13424 and 50% will have an end site of 13425. Picking the higher value makes logical sense but this command actually wants the lower value because it selects any sequence that ends at or after the selected value. Deciding the threshold of homopolymers is completely arbitrary and 8 is used in this methods paper because 8 are used in the miseq SOP (4).

12. Filter the raw data to remove any overhangs from the alignment with the command *filter.seqs(fasta=Test.stab.trim.contigs.good.unique.good.align, vertical=t)*
    a. The vertical option is used to ignore certain characters like the '-' and '.' to prevent them from being removed.

13. Remove any duplicate sequences that resulted from the alignment with a second unique command, *unique.seqs(fasta=Test.stab.trim.contigs.good.unique.good.filter.fasta, count=Test.stab.trim.contigs.good.good.count_table)*
    a. Like step 6, this step saves only the unique sequences and updates the count file with the number of times each sequence appears in each sample.

14. Further clean the data by addressing minor sequencing errors and combining sequences that are only different by 2 nucleotides with the command *pre.cluster(fasta=Test.stab.trim.contigs.good.unique.good.filter.unique.fasta, count=Test.stab.trim.contigs.good.unique.good.filter.count_table, diffs=2)*
    a. The pre.cluster command is based off an algorithm developed for pyrosequencing by Sue Huse (15).

15. Remove chimeras from the data with the command *chimera.uchime(fasta=Test.stab.trim.contigs.good.unique.good.filter.unique.precluster.fasta, count=Test.stab.trim.contigs.good.unique.good.filter.unique.precluster.count_table,* dereplicate*=t)*

a. Depending on the version of mothur, this command may be called something else. Later versions of mothur use the command chimera.vsearch, but the options within the command are the exact same.
b. If this command discovers a chimera present in one sequence in one sample, the default option is to remove that sequence from every other sample in the data set, regardless of the presence of chimeras. To prevent this, the dereplicate=t option is implemented. This pulls out all identified sequences with chimeras and what sample they are present in. The next command will remove the chimeric sequences only from the samples where they were discovered.

16. Remove the chimeras from the FASTA file with the command *remove.seqs(fasta=Test.stab.trim.contigs.good.unique.good.filter.unique.precluster.fasta, accnos=Test.stab.trim.contigs.good.unique.good.filter.unique.precluster.denovo.uchime.accnos)*

17. **Optional:** Change the file names to something smaller with the commands *system(cp Test.stab.trim.contigs.good.unique.good.filter.unique.precluster.pick.fasta test.final.fasta)* and *system(cp Test.stab.trim.contigs.good.unique.good.filter.unique.precluster.denovo.uchime.pick.count_table test.final.count)*
    a. This step is used to clean up the file names. Having long file names can lead to frustration and errors. At this point the data cleaning is completed and the file names can be shortened with the above commands if desired.
    b. Also at any time, instead of typing in the entire FASTA or count name, one can use "current" to call the most recent FASTA or count file. For example, instead of typing *summary.seqs(fasta=Test.stab.trim.contigs.good.unique.good.filter.fasta, count=Test.stab.trim.contigs.good.good.count_table)*, one could type *summary.seqs(fasta=current, count=current)* to get the same output.

18. Classify the sequences to the RDP trainsets with the command *classify.seqs(fasta=Test.stab.trim.contigs.good.unique.good.filter.unique.precluster.pick.fasta, count=Test.stab.trim.contigs.good.unique.good.filter.unique.precluster.denovo.vsearch.pick.count_table, reference=trainset9_032012.pds.fasta, taxonomy=trainset9_032012.pds.tax, cutoff=75)*
    a. The FASTA and count names can vary depending on whether **Optional step 17** was completed.

b. As mentioned in the introduction of **Basic protocol 3**, the taxonomy and reference files can vary depending on which version is used.
c. The cutoff value is, again, arbitrary. This value provides a threshold of classification. As it is now, only 75% of the sequence has to align to the RDP trainset to be classified. This value can be higher leading to a more stringent analysis, or lower leading to a less stringent analysis.

19. Create a text file of the taxonomic summary obtained from step 18 with the command *system(mv Test.stab.trim.contigs.good.unique.good.filter.unique.precluster.pick.pds.wang.tax.summary Test.summary.txt)*
    a. This command creates a text file that now can be opened on a personal computer.
    b. This file can be copied and pasted into excel for normalization. To normalize this data, simply divide all taxonomic values in each sample by the root value in each respective sample. This normalization will show the percentage each taxa for each taxonomic level. This means that the members of each taxonomic level (phyla, class, order, family, genus) will add up to 100%.
    c. Significance can be found with a students' T-test.

20. Proceed to **Support protocol 2** for population based gut microbiome analysis, if needed.

Support Protocol 1: Cecal Contents Extraction

The cecum is used in order to obtain the greatest concentration of intestinal microbiota. It is important to note that other protocols call for colonic contents instead of cecal contents because in humans the greatest concentration of intestinal microbiota is in the colon but when using mice, the cecum has the highest concentration of gut microbiota.

The mice are transferred to a euthanasia chamber (Patterson Scientific) for CO_2 asphyxiation which is then followed by cervical dislocation. The cecal contents are obtained immediately during the mouse dissection. The cecum is the intraperitoneal pouch connected to the junction of the small and large intestines. It is located at the

beginning of the ascending colon of the large intestine. Once the cecum is identified, it will be resected with a surgical scissors from the rest of the digestive tract and placed on a piece of foil. Then, roll the cecum using a sterile pipette tip (1000 μL tip works the best), and the contents will easily come out. Use the same pipette tip to then scrape up the cecal contents and place them in a 1.5 mL screw top vial. The foil allows for an easy collection of the cecal contents once they have been removed from the cecum. All procedures must be performed in accordance with the Institute of Laboratory Animal Resources guidelines and, in the case of this protocol, were approved by the Pennsylvania State University Institutional Animal Care and Use Committee.

Support Protocol 2: Community-Based Analysis of the Gut Microbiome

This protocol is intended to describe the steps for a Generalized Unifrac analysis with the R package GUniFrac. Generalized unifrac is a measure that combines weighted and unweighted unifrac (16). Weighted unifrac is a measure used to analyze differences in abundant species within several populations. Unweighted unifrac is a measure of the differences in rare species within several populations. Generalized unifrac combines these measures to look at both rare and abundant species between two or more populations. This algorithm works by aligning a table of raw sequence reads to a customized hierarchal phylogenic tree. The output will be a graph showing the two populations (control and treatment) and how distinctly different, or similar they are. This protocol will only address using two populations (control and treatment) but GUniFrac analysis can be done with many groups as well. As mentioned above a R markdown file and sample files have been included with this unit discussion to aide in understanding.

Materials:

Computer with R Studio installed

Analyzed raw sequence reads from **Protocol 3**

External server or computing cluster with an allocation of at least 100 GB and 8 processors (can use personal computer but will drastically increase computational time)

Protocol Steps:

1. Return to the folder with the mothur output files via terminal and create a new folder for GUnifrac analysis.

2. Move the *Test.stab.trim.contigs.good.unique.good.filter.unique.precluster.pick.fasta* (or *test.final.*fasta)and the *Test.trim.contigs.good.unique.good.filter.unique.precluster.denovo.vsearch.pick.count_table* (or *test.final.*count) file to the new folder.
    a. It is recommended to rename these files as described in **Basic Protocol 3 step 17**. Shortening the names of these files makes the downstream analysis much simpler.

3. Start mothur and create a distance table with the command *dist.seqs(fasta=test.final.fasta, output=lt, processors=8)*
    a. This command will take several hours and may crash. If it does crash, the command line will say "killed", and the mothur program will close. In the event that *dist.seqs* crashes, follow the following steps:
        i. Take a subsample of the fasta and the count files with the command *sub.sample(fasta=test.final.fasta, count=test.final.count)*
        ii. This command will take a random 10% of test.final.fasta and the same random 10% from test.final.count and create files with the name *test.final.subsample.fasta* and *test.final.subsample.count*.
        iii. If a larger subsample is desired, run the command *count.groups(count=test.final.count)*. This will show how many sequences are in each group and how many total sequences are present (shown below).

            501 contains 20554.
            502 contains 4474.
            503 contains 19336.
            504 contains 2101.

505 contains 11445.
601 contains 23595.
602 contains 22541.
603 contains 22195.
604 contains 12943.
605 contains 13733.

Total seqs: 152917.

iv. Note that the above sequences are uneven for each group. This occurs because the Illumina miseq provides 10 million reads, randomly distributed between the samples of the run. The above example data comes from a 50 sample run, giving each sample about 150,000 to 200,000 reads. Concordantly **step iii** takes a 10% subsample of the data. This means that each sample should have between 15,000 and 20,000 reads. The above data table is variable, but most samples are around that range.

v. The total sequences are 152917. For a 50% subsample take 50% of 152917, which is 76459. Run the command *sub.sample(fasta=test.final.fasta, count=test.final.count, size=76459)*

vi. The size option tells the command to take 76459 random sequences from both the files, thus resulting in a 50% random sampling.

vii. Rerun *dist.seqs(fasta=test.final.subsample.fasta, output=lt, processors=8)*

viii. If it crashes again, take a smaller subsample.

ix. Note this protocol will use file names that have not been subsampled. If a subsample is needed, change the names accordingly.

4. Create a phylogenic tree with the command *clearcut(phylip=test.final.phylip.dist)*
    a. When this command is running, it will appear that the command line is frozen, but that is completely normal. When it is complete, this command will result in *test.final.phylip.tre.*

5. Exit mothur and change directories on terminal to be in the directory with all the GUnifrac files. Convert the count file to a text file with the command *cp test.final.count test.final.count.txt*

6. Create a meta file containing sequence names and group identification.
    a. This can be done in excel where the first column, labeled ‘samples’, are the respective sample names and the second column, labeled ‘treatment’, are the treatment groups (control, treatment).

   b. For this analysis the meta file will be named *test.meta.txt.*

7. Open R studio and install the GUnifrac package.

8. Import the resulting tree file from **step 4** with the command *read.tree(file="//Users/setup/Desktop/mothur_files/test.final.phylip.tre")->test.tre.*
   a. The file path is where the tree file is on the computer.

9. Search the imported tree for nodes by typing *test.tre* in the R command line.
   a. This is very important because a tree with nodes will not work with the GUnifrac command.
   b. If a tree has nodes, it will be only one sequence and can be found under 'Node labels' in the output.
   c. If there are no 'Node labels' or if 'Node labels' does not show any sequence id's then proceed to step 11

10. Open *test.final.count.txt* and search (using command f) for the node label from **Step 9**. When found, delete this sequence and the entire row associated with it, and save.

11. Import *test.final.count.txt* into R studio, making sure the first column is used as row names with the command *read.delim("~/Desktop/mothur_files/test.final.count.txt", row.names=1)->test.count*.
   a. Again the file path will be different for everyone, adjust accordingly.
   b. This command imports the count table into the variable test.count.
   c. This file will also be referred to as the OTU table by the GUniFrac software.

12. Test the row names and column names with the commands *head(row.names(test.count))* and *colnames(test.count)* respectively.
   a. The head modifier is used with the row names because there will be over 100,000 rows in this file.
   b. The row names should look like "M00946_96_000000000-AEE8U_1_1119_3781_11413".
   c. The column names should be the sample names. If the sample names are numbers, for example: 501, 502, 503 … 605. They will appear different after the *colnames* command. They will look like "X501, X502, X503 … *X605*". This occurs because when importing, R puts an X in front of the column names to distinguish them from numbers. To fix this issue run the command *colnames(test.count)=c("501", "502", "503",…,"605).*

13. Transpose the rows and columns with the command *t(test.count)=test.transpose.count*. Check the column names with the command *head(colnames(test.transpose.count))*.
    a. A second check is required because occasionally the row names do not get transposed to the column names.
    b. If they did not get transferred, use the command *colnames(test.transpose.count) = row.names(test.count)*.

14. Run GUnifrac with the command *GUniFrac(test.transpose.count, test.tre, alpha=c(0,.5,1))$unifracs -> TestUni*
    a. This command will take roughly half an hour to run, and will most likely end in an error. If it immediately ends with the error "*Warning message: In GUniFrac(test.transpose.count, test.tre, alpha=c(0,.5,1)) : The tree has more OTU than the OTU table!*" there is a problem, please see the above troubleshooting, or the **Troubleshooting** section at the end of this protocol.
    b. If the above error is seen at the end of 10 to 30 min, then the command worked. This is because the command will work if there are less sequences in the count table then are represented on the tree, but it will not work if there are more sequences in the count table than are represented on the tree. When deleting the node label from the count table, the user is reducing the count table by 1. The count table is now one less than the mapped tree, thus this error will be reported at the end of the analysis.
    c. The alpha value is used to tell how much weight to put on abundance species, so in this example alphas of 0, 0.5, and 1 are being used. An alpha of 0 will put no weight on abundance species, an alpha of 0.5 will put half the weight on abundant species, and an alpha value of 1 will put all of the weight on abundant species. For this analysis the most important alpha value is 0.5 because this corresponds to a generalized unifrac measure.
    d. The resulting data frames will be in the variable TestUni.

15. Extract the generalized unifrac data frame with the command *TestUni[, , "d_0.5"]->TestGU*
    a. If interested, the weighted and unweighted unifrac analysis can be extracted with the command *TestUni[, , "d_1"]->TestW* and *TestUni[, , "d_UW"]->TestUW* respectively.

16. Import the meta file and create a meta variable with the command *read.delim("~/Desktop/mothur_files/test.meta.txt")*$treatment->meta.
    a. This command will import the treatment groups into a variable called meta.

17. Create a color and a shape variable with the commands *coul= coul<-c("red", "blue")* and *shape= c(15, 15, 15, 15, 15, 16, 16, 16, 16,16)* respectively.
    a. The colors can be changed to any color desired
    b. The shape codes come from the PCH table (http://www.endmemo.com/program/R/pchsymbols.php), which has numerical values for different shapes. In this case they are squares (15) and circles (16).

18. Plot the results with the command *s.class(cmdscale(TestGU, k=2), fac=meta, cpoint=1, pch=shape, col=coul).*
    a. An example of a GUniFrac graph can be seen in **Figure A-3**.
    b. Since there are no axes measurements, the "d=0.1" measurement represents the length of each axis in the graph space.

19. Check for statistical significance with the command *Adonis(as.dist(TestGU) ~ meta).*
    a. The Adonis command computes a multivariate analysis of variance using distance matrices. Since GUnifrac is a measurement of phylogenic distance, the Adonis command is the logical choice for statistical significance. Adonis is also recommended for use in the GUnifrac package details and will result in a p-value (16).

Alternative Protocol 1: Metagenomic Analysis of the Gut Microbiome

This protocol describes the process of metagenomic analysis with the HUMAnN2 software from the Huttenhower lab (5). HUMAnN2 is a powerful pipeline combining a taxonomic analysis through the software Metaphlan2 (17), alignment of raw sequences to a bacterial reference genome with Bowtie2 (18), and a secondary alignment to a protein database for unmapped reads with DIAMOND (19). Together these programs work together to produce a comprehensive list of metabolic pathways present in the gut microbiome. This information can be used to help predict and validate metabolic changes seen in the host. Significantly different pathways will be discovered with the use of LEfSe (**L**inear discriminant analysis **Ef**fect **S**iz**e**) which combines statistical significance and biological relevance with the Wilcoxon and the Kruskal-Wallace statistical tests,

respectively (20). This protocol uses the bacterial DNA isolated in **Protocol 1**.There is also an online manual for HUMAnN2 (https://bitbucket.org/biobakery/humann2/wiki/Home).

Materials

Bacterial DNA isolates from **Protocol 1**

Sequencing core facility or an Illumina Hiseq 2500

External server or computing cluster with an allocation of at least 100 GB and 8 processors (can use personal computer but will drastically increase computational time)

HUMAnN2 installed with all required dependencies (can be found at https://bitbucket.org/biobakery/humann2/wiki/Home#markdown-header-requirements)

Internet connection and access to the Huttenhower galaxy site

NanoDrop UV-Vis Spectrophotometer Lite (Thermo-Scientific)

Excel or Numbers

Protocol Steps:

1. Measure DNA concentration on the NanoDrop
    a. This requires only 1 μL of isolated bacterial DNA. Concentration values should range from 100 ng/μL to 400 ng/μL.
        i. If values exceed 400 ng/μL, this is not an issue and less input bacterial DNA will be used. Also most sequencing cores will test the quality of DNA before sequencing
        ii. If values are lower than 100 ng/μL, then PCR may be required to increase the input material before sequencing. This is not an issue but can introduce PCR bias into the results. PCR bias occurs when abundant species are amplified and end up masking rarer species. PCR can also amplify contaminants which can skew results
    b. With metagenomic shotgun sequencing, no PCR is needed before submission as long as there is at least 1-2 μg of DNA.

2. Submit the DNA isolates to a sequencing core or an independent company for Illumina hiseq 150x150 sequencing with the PCR-free library construction kit.
    a. Please note that HUMAnN2 **cannot** run both partners of a paired end read simultaneously. This protocol will go through using only one partner from each pair. Due to this, single end sequencing can be completed instead of paired end sequencing if HUMAnN2 is the only analytical pipeline being used. If, however, further analysis is required, it is recommended to use the paired end sequencing because most analytical pipelines require paired end sequencing.

3. Install HUMAnN2 according to instructions, making sure that all dependencies are installed.
    a. The dependencies include: MetaPhlAn2, Bowtie2, Diamond, and python (at least version 2.7). They should be automatically installed when installing HUMAnN2.
    b. This can be difficult without administrative permissions. This will be the case if an external server or a computing cluster is being used for analysis.
        i. To get around this, import the latest humann2.tar.gz file on to the server.
        ii. Decompress the file, enter the resulting directory and run *python setup.py install --user.*
        iii. This will put all the dependencies in a /.local directory, bypassing the need for administrative permissions
        iv. The user must also run *export PATH="$PATH:~/.local/bin"*

4. Install the chocophlan and uniref databases using the commands *humann2_databases –download chocophlan full $Path_to_install* and *humann2_databases –download uniref uniref90_diamond $Path_to_install.*
    a. The $Path_to_install will be modified to the path of the desired location of the database. This is important because the configuration file that is used to run HUMAnN2 will be updated with this command, so do not move the databases once installed.
    b. Also together both databases are about 20 GB
    c. It is also important to make sure that the version of HUMAnN2 being used is v 0.11.1 or higher. This command will not work with earlier versions of HUMAnN2.

5. Import raw sequence file from the Illumina Hiseq to the server or computer cluster being used.

6. Create a directory for the output.

7. Run HUMAnN2 with the command *humann2 --input ./Raw_sequence_files/Test1.R1.fastq --output ./output_files --metaphlan ./metaphlan2/ --threads 8*
    a. The paths to the input and the output depends on the environment being used and will be different for everyone.
    b. It is important to tell HUMAnN2 where to find metaphlan2, because when running on the external server adding the location of metaphlan2 to the /.local directory does not work. Thankfully, the HUMAnN2 command allows the user to specify where the metaphaln2 dependencies are.
    c. At any point HUMAnN2 crashes and has an error describing that bowtie2 or diamond cannot be found, they can also be added to the above HUMAnN2 command.
        i. The resulting command could potentially read, *humann2 --input ./Raw_sequence_files/Test.R1.fastq --output ./output_files --metaphlan ./metaphlan2/--bowtie2 ~/bowtie2-2.2.5 --diamond ~/diamond-0.7.9/bin --threads 8*
        ii. This will work as long as the bowtie and diamond dependencies are at the ~ (home) location.
    d. With 8 processors, this process will take 12 hours to run. The run time can be shortened with more available processors.
    e. The resulting files will be a pathway abundance file, a pathway coverage file and a gene families file. The pathway abundance file has abundance values for all HUMAnN2 identified pathways. The pathway coverage file contains the percentage of each pathway present. This is represented with a value from 0-1, with 1 being 100% covered and every gene family present in the pathway. The gene families file contains all the gene families identified with HUMAnN2.
        i. This analysis will not utilize the gene families file but the gene families file could be used for *de novo* pathway creation.

8. Transport all pathway abundance files and all coverage files off of the external server and onto the desktop.

9. Install the latest version of HUMAnN2 onto the computer in use, but do not install the databases.

10. Combine the pathway abundance and pathway coverage file for each sample with the command *humann2_join_tabels --input ./test.1 --output ./test.1.combo.txt*.
    a. Each sample should get its own directory and each respective pathway abundance and pathway coverage file will be placed into that directory. In this case the directory is called *test.1*. This

directory contains the files *test.1.pathwayabundance.txt* and *test.1.pathwaycoverage.txt*.

b. When combined the resulting file will be called *test.1.combo.txt* and will contain the pathway abundances and respective coverages for all pathways discovered in sample test.1.

11. Copy and paste the contents of the combo files into Excel or Numbers. Sort the table by coverage (high to low), remove all pathways below a 0.3 (30%) coverage and create a new text file with the trimmed data.
    a. The 0.30 (30%) cut off is completely arbitrary and can be higher or lower depending on the needs of the experiment.
    b. The reason a cutoff value is needed is because multiple gene familes can belong to multiple pathways, so the less the coverage is, the less likely the pathway is to be actually present.
    c. The edited combo file should be placed in a directory called *test.edits*.

12. Combine all edited combo files into one file which contains all the pathway abundances with at least a 30% coverage with the command *humann2_join_tabels --input ./test.edits --output ./Test.whole.txt.*
    a. Test.whole.txt contains all the pathway abundances with at least a 30% coverage for the experiment.
    b. Depending on the version of HUMAnN2, the coverages may or may not be combined with the pathway abundances. If this is the case just delete the coverage columns, leaving only the pathway abundances.

13. Open *Test.whole.txt* and clean up the labels by replacing the column names with the sample names (test1, test2, test3 … testn). Also add a new row directly below the column names and title the row 'Treatment' and add the appropriate treatments to each sample.
    a. The *Test.whole.txt* file example can be seen in **Table A-3**.
    b. A cleaned version can be seen in **Table A-4**.

14. Export the cleaned version of *Test.whole.txt* as *Test.whole.clean.txt* and import it to the Huttenhower galaxy page (https://huttenhower.sph.harvard.edu/galaxy/)

15. Go to LeFSe tab A) and select the uploaded file. Make sure that rows are selected as the *vector* option and select 'Treatment' for the *class* option and 'Sample' as the *subject* option. Click execute.

16. Move to LeFSe tab B) and select the file created from the previous step. Adjust the alpha values if needed (default is p = 0.05). Click execute.

17. Move to LeFSe tab C) select the resulting file from B and adjust the DPI if necessary and click execute.
    a. The resulting file will show the significantly different and biologically relevant pathways from the gut microbiome.

METABLOMICS-BASED PROTOCOLS

Basic Protocol 4: Cecal Content Extraction for LC-Orbitrap-MS

LC-Orbitrap-MS offers high throughput, high-resolution, accurate-mass performance, and has been extensively utilized as a powerful metabolomics tool to detect a wide range of compounds, especially small metabolic molecules during global and target analysis. Cecal content contains most abundant and active bacteria, thus metabolic profile of cecal content indicates not only bacterial activity and host metabolism, but also informs the co-metabolic status of the host and bacteria. This protocol describes an untargeted hydrophilic phase extraction method of cecal content for LC-Orbitrap-MS (Thermo) analysis.

Materials

10 - 200 μL pipette (Denville)

1000 μL pipette (Denville)

1 Centrifuge (Eppendorf 5430R)

1 set of sample labeled 2 mL screw cap homogenizer tubes (VWR)

1 sets of sample labeled 1.5 mL Eppendorf tubes (Eppendorf)

250 μL autosampler vials (Thermo Fisher)

Vortexer (Any Brand)

Precellys 24 lysis and homogenization (Bertin Technologies)

Savant SPD121P SpeedVac Concentrator (Thermo Scientific)

37 °C water bath

Liquid nitrogen

1 mm Silica homogenization beads (BioSpec)

HPLC graded methanol (Sigma-Aldrich)

HPLC graded water (Sigma-Aldrich)

Chlorpropamide (Sigma-Aldrich)

Protocol Steps

1. Cecal content (~50 mg) is mixed with 10 - 15 1 mm silica homogenization beads first, then extracted with 1 mL of ice-cold methanol (50% v/v) containing 1 μM chlorpropamide.

2. Vortex the sample briefly, then homogenize thoroughly (after homogenizing for 1 min, stop for 2 min to prevent overheating).

3. Freeze and thaw three times with liquid nitrogen.

4. Centrifuge for 10 min, 12,000 x g, 4 °C.

5. Transfer the supernatants to a new 1.5 mL tube.

6. Re-extract cecal contents by adding an additional 500 μL of ice-cold methanol (50% v/v) containing 1 μM chlorpropamide, repeat step 2 - 4.

7. Combine the supernatants.

8. Dry down the samples in speedvac (takes about 3 hours).

9. Suspend the pellet in 200 μL 3% methanol.

10. Centrifuge for 10 min, 13000xg, 4 °C.

11. Transfer 150 μL of the supernatants to a 250 μL autosampler vials and store at -20°C until ready to be run.

12. Pool 10 μL of each sample to a new tube for quality control. Pooled samples are prepared in triplicate.

13. See **support protocol 3** for how to set up the LC-Orbitrap-MS.

Support Protocol 3: LC-Orbitrap-MS Instrumentation Settings

The LC-MS system consists of a Dionex Ultimate 3000 quaternary HPLC pump, a Dionex 3000 column compartment, a Dionex 3000 autosampler, and an Exactive plus Orbitrap mass spectrometer controlled by Xcalibur 2.2 software (all from Thermo Fisher Scientific, Waltham, MA). Extracts are analyzed by LC-MS using a modified version of an ion pairing reversed phase negative ion electrospray ionization method (21). A volume of 10 μL sample is injected and separated on a Phenomenex (Torrance, CA) Hydro-RP C18 column (100 × 2.1 mm, 2.5 μm particle size) using a water/methanol gradient with tributylamine and acetic acid added to the aqueous mobile phase. The HPLC column is maintained at 30 °C, and at flow rate of 200 μL/min. Solvent A is 3% aqueous methanol with 10 mM tributylamine and 15 mM acetic acid; solvent B is methanol. The gradient is 0 min, 0% B; 5 min, 20% B; 7.5 min, 20% B; 13 min, 55% B; 15.5 min, 95% B; 18.5 min, 95% B; 19 min, 0% B; and 25 min, 0% B. The Exactive plus is operated in negative ion mode at maximum resolution (140,000) and scanned from *m/z* 72 to *m/z* 1000 for the first 90 sec and then from *m/z* 85 to *m/z* 1000 for the remainder of the chromatographic run. The AGC target is 3 x 106 with a maximum injection time of 100 ms, the nitrogen sheath gas is set at 35, the auxillary gas at 10 and the sweep gas at 1. The capillary voltage is 3.2 kV and both the capillary and heater set at 200 °C, the S-lens was 55. To aid in the detection of metabolites, a homemade database generated from 288 pure metabolite standards using the same instrument and method to determine detection capability, mass/charge ratio (m/z), and retention time for each metabolite is used as a primary database for metabolites identification.

Basic Protocol 5: LC-Orbitrap-MS Data Analysis with MS-Dial

MS-DIAL, an open-source software pipeline is used for untargeted metabolomics analysis (22).

1. Start up a project
   a. Before performing analysis, LC-Orbitrap-MS Data (.raw) needs to be converted to mzML format with open source software Proteowizard (23).
   b. In the MS-DIAL interface, click "File-New project" and open "Start up a project" window. Select a directory that contains the converted mzML format MS files. Choose the "Soft Ionization" as ionization type; "Conventional LC/MS or data dependent MS/MS" as method type; "Profile data" as data type for MS1 and MS/MS; choose "Negative ion mode" as ion mode and "Metabolomics" as target omics, click next.
   c. Browse the analysis file paths, change the file format to mzML file (*.mzml) and select all the mzML format files to be analyzed. Choose the correct type for each sample (sample, standard, quality control or blank). Then based on the group information, add the corresponding Class ID for each sample (Control, low dose treatment, high dose treatment, etc.). Uncheck any samples under "Included" for exclusion if necessary, then click next.

2. Peak detection, identification, and alignment setting
   a. Under "Analysis parameter setting" window, click "Identification" tab, select the "MSMS-AllPublic-Curated-Neg" MSP file from Public MSPs folder included in the software package.
   b. Based on the accuracy of mass and retention time of the Orbitrap instrument, select the retention time tolerance within range of 0.2~0.5 min, accurate mass tolerance from 0.001~0.005 Da (2~10 ppm at 200 m/z).
   c. If an in-house library generated from a list of pure metabolite standards using the same instrument and methods, then select the text file (an accurate database) containing name, mass-to-charge ratio (m/z) and retention time for each metabolite. Select the stricter tolerance setting such as retention time tolerance $\leq$ 0.2 min and accurate mass tolerance $\leq$ 0.002 Da.
   d. Click "Alignment" tab, choose a non-blank sample as a reference file for alignment. Recommended reference file: a pooled sample, or intermediate sample in injection sequence order. Recommended tolerance setting: RT tolerance of 0.2~0.5 min and MS1 tolerance of 0.0025~0.003 Da.

e. Click “Finish” and peak detection, identification and alignment starts. Those processing steps take several hours based on sample number and computer capacity.

3. Browse the result window and export alignment results
   a. Double click “Alignment navigator” at the left bottom of the result window.
   b. Apply normalization method by clicking statistical analysis-normalization (optional).
   c. Perform PCA analysis by clicking statistical analysis-principal component analysis (optional).
   d. At the Peak spot navigator window, select “Identified display filter” (identified peaks with the database generated from a list of pure metabolite standards using the same instrument and method). Check the number of the alignment in “Peak spot navigator “with identified display filter. If the number is too low, check the “Annotated display filter” (identified the peaks with the public MSP file without MS/MS) or return to 2c and 2d to increase accurate mass and retention time tolerance.
   e. Click individual spot in “Alignment spot viewer” window at the middle bottom, check the peak and compound information (right top window), bar chart of aligned spots (middle top window) and the MS1 spectrum (left bottom).
   f. Click export-alignment result, select a folder for import, choose export format as “txt”, the most important files for import are “Raw data matrix (Area)”, “Parameters” and “normalized data matrix” (If normalization method is applied).

4. Post processing alignment result
   a. Check the data quality.
      i. Check Coefficient of variation value of the internal standard (chlorpropamide) and replicated pooled samples.
      ii. Check if the pooled samples are close to biological averaging.
      iii. Check the fill % (Percentage of samples having good shape, otherwise, apply “Gap Filling”).
   b. Apply additional filter if necessary to clean the data.
      i. Subtract blank values from averaged sample values and filter the compound only with positive values.
      ii. Filter the compound with fill % > 0.3 - 0.5 (good alignment).

Basic Protocol 6: Cecal Content Extraction for NMR

^{1}H NMR is a reliable, stable and cost-effective tool for global metabolomics analysis. The non-destructive, non-invasive and instrument-independent nature of NMR techniques guarantees high reproducibility. The protocol below describes a cecal content extraction, data processing, and statistical analysis protocol for NMR spectroscopy.

Materials

10-200 μL pipette (Denville)

1000 μL pipette (Denville)

1 Centrifuge (Eppendorf 5430 R)

1 set of sample labeled 2 mL screw cap homogenizer tubes (VWR)

1 sets of sample labeled 1.5 mL Eppendorf tubes (Eppendorf)

5 mm NMR tube and lid (Norell)

Vortexer (Any Brand)

Precellys 24 lysis and homogenization (Bertin Technologies)

Liquid nitrogen

1 mm silica homogenization beads (BioSpec)

Potassium phosphate dibasic (K_2HPO_4) (Sigma-Aldrich)

Sodium phosphate monobasic (NaH_2PO_4) (Sigma-Aldrich)

3-(Trimethylsilyl)propionic-2,2,3,3-d_4 acid sodium salt (TSP-d_4) (Sigma-Aldrich)

Distilled Water

Deuterium oxide (D_2O) (Cambridge Isotope Laboratories)

Protocol Steps

1. Extract cecal content (~50 mg) with 1 mL of phosphate buffer (K_2HPO_4/NaH_2PO_4, 0.1 M, pH 7.4, 50% v/v D_2O) containing 50 μg/mL (290 μM) TSP-d4 as a chemical shift reference (δ 0.00).

2. Freeze-thaw three times with liquid nitrogen.

3. Homogenize for 1 min, 6,500 rpm, 1 cycle and centrifuge for 10 min, 11,180 x g, 4 °C.

4. Transfer the supernatants to a new 1.5 mL tube

5. Add another 600 μL PBS to the pellets, vortex for 1 min.

6. Centrifuge for 10 min, 11,180 x g, 4 °C.

7. Transfer the additional supernatants to the 1.5 mL (combined supernatants are around 1.2 mL in total volume).

8. Centrifuge the combined supernatants for 10 min, 11,180 x g, 4 °C.

9. Transfer the supernatants to a 5 mm NMR tube, and store at 4 °C until performing NMR spectroscopy.

10. See **Support Protocol 4** for information on acquisition settings.

Support Protocol 4: NMR Spectra Acquisition Setting

All ^1H spectra are recorded at 298K on a Bruker NMR spectrometer (600 MHz for ^1H) configured with a 5-mm inverse cryogenic probe. A standard one-dimensional pulse sequence noesypr1d (recycle delay-90°-t1-90°-tm-90°-acquisition) is used with a 90 pulse length of approximately 10 μs (-9.6 dbW) and 64 transients are recorded into 32k data points with a spectral width of 9.6 KHz. For quantitation purposes, a relaxation delay (5s) and a recycle delay (4s) are added to the cycle to ensure the total repetition time (relaxation time, recycle delay and acquisition time) is more than 5 times the longitudinal relaxation time (T1) of the compounds (24). Quantitation analysis is performed based on either TSP-d4 reference with known concentration (25) or calibration

curve. To facilitate NMR resonance assignments, two-dimensional (2D) NMR spectra including ^{1}H-^{1}H total correlation spectroscopy (TOCSY), ^{1}H-^{1}H correlation spectroscopy (COSY), J-resolved (JRES), ^{1}H-^{13}C heteronuclear single quantum correlation (HSQC), and ^{1}H-^{13}C heteronuclear multiple bond correlation (HMBC) are acquired. Chemical shifts are reported in ppm from TSP ($\delta = 0.00$).

Basic Protocol 7: NMR Spectra Processing

Protocol Steps

1. NMR spectra processing with Topspin 3.0 (Bruker Biospin, Germany)
    a. Before performing statistical analysis, an exponential window function (command code: efp) is applied with a line-broadening factor of 1 Hz (command code: lb 1) prior to Fourier Transformation.

    b. Then all ^{1}H NMR spectra qualities are improved by correcting the phase (command code: ph), baseline (command code: bas) and referencing to TSP (δ 0.00) (command code: cal) automatically or manually (manually recommended).

2. Further process the spectra with AMIX software version: 3.9.14 (Brucker Biospin, Germany)
    a. Import the data and check quality
        i. Open Amix-File-Open TOPSPIN 1D file, choose the right directory where the ^{1}H NMR spectra are stored and select all the spectra for analysis.
        ii. Check the layered spectra for proper overlay. If the spectra are not overlaid properly, repeat 1b to improve spectra phase, baseline, and calibration.

    b. Bucketing
        i. Click "Amix-Tools-Bukcets,Statistics-Statistics-Bucket Table-New".
        ii. Choose 1D NMR and simple rectangular buckets.
        iii. Change bucket width to 0.004 ppm (2.4 Hz).
        iv. Change the scaling mode to either scaling to total intensity (non-quantitative purpose) to compensate the overall concentration differences (26), or no scaling then normalize to the tissue weight later (for quantitative purpose) (24).
        v. Select "edit exclusions" and remove the interference signals including the residual water signal (region δ 4.2 -

5.2), other contamination signal, like methanol (region δ 3.3 - 3.4), ethanol (region δ 1.1 - 1.2, 3.6 - 3.7) and Polyethylene glycol (δ 3.6 - 3.8).

vi. Select a directory to save the bucket table.
vii. Select data source from TOPSPIN data tree and reselect all the spectra again.
viii. Choose "no" for "select next" window, close the file display window.
ix. Click "Statistic-Bucket table-Import", rename the txt file, choose "table (spectrum per column)" as "output format"; Choose "blanks, commas, tables" as "delimiters used in table output".
x. The imported txt file is under default path of Bruker-Amix directory.

Basic Protocol 8: Universal Profiling of NMR Data

Multivariate data analysis is performed with SIMCA 13 (Umetrics, Sweden). Before performing statistical analysis, import the bucketed .txt file into Excel, delete the regions with a number 0 (the exclusion regions edited in Amix), save as "Excel 2003-2007 workbook" as other formats cannot be recognized by SIMCA.

Protocol Steps

1. Principal component analysis (PCA)
    a. Open SIMCA, create a new regular project, select the saved Excel file as data source.
    b. At import data wizard window, click "Edit-Transpose" to transpose the spread sheet. Now the first column is the data ID and first row is the ppm ID
    c. Click the arrows on the first column and row, choose primary observation ID and primary variable ID, respectively. Click "File-Save as-Finish import".
    d. Click "New model", under "observations" tab, select all the samples from one treatment group, click "Set class", then select another group click "Set class", until all samples are assigned. Under "Scale" tab, select "Ctr" as scaling type, choose "PCA-X" as "Model type".
    e. Click "Two First" to calculate the first two components.
    f. Click "Overview" to create summary plots.

i. Check Score Scatter Plot for outliers and other abnormalities.
ii. If a sample is significantly away from the rest of the samples, check loading scatter plot for the contributed specific primary IDs (ppm IDs). Confirm this abnormality by checking the ppm regions from the original spectra with topspin. The data points could be removed if the signals are contamination or external signals.
iii. Loading plot also reveals the significant contributors (metabolites) for the group separation. Future targeted analysis could be applied if necessary.

2. Orthogonal projection to latent structure-discriminant analysis (OPLS-DA)
    a. Follow the same step described in 1a-c. Before import, insert one new column at position 2, select the column name as "Y variable". This binary variable Y is created and assigned to defining a group. (For example control group is 0, treatment group is 1).
    b. Same as 1d, select "UV" instead of "Ctr" as scaling type for OPLS-DA analysis. A 7-fold cross validation method is employed to validate the OPLS-DA models. The quality of the model is indicated by the parameters R^2X (predictive power) and Q^2 (validity of the model). The validity of the OPLS-DA model is further assessed with CV-ANOVA tests by clicking "Analyze-CV-ANOVA" for significance with $p < 0.05$(27).

Basic Protocol 9: Quantitative Analysis of NMR Data

Quantitative analysis is performed with the software Chenomx NMR suite (Chenomix, Inc).

Protocol Steps

1. Converting and processing native spectra in a batch with Chenomx Processor
    a. Convert native spectrum formats to Chenomx file format with the application named Chenomx processor within Chenomx NMR suite.

i. Click “Tools-Batch Import” and select files or a fold that contains all native spectra to be processed. Click next.
ii. Choose “Bruker 1r” as the type of data. Click next.
iii. Select “TSP” as a Chemical Shape Indicator (CSI), the concentration is 0.29 mM. Click next.
iv. Select “Automatic Phase Correction” and “Automatic Baseline Correction- Spline”. Click next.
v. Choose a folder to save the converted files.

b. Manually check the batch-processed spectra for ensured quality.
i. Click “File-Open” and select the converted files generated from last step.
ii. Click “Processing history-Files”, a list of converted spectra shows at the left window. Go through those spectra to make sure the quality of the spectra are satisfied. If necessary, click the “Phase Correction” and “Baseline correction” below the spectrum window to adjust the processing parameters manually to improve the quality of the spectrum.
iii. Click “File-Send to Profiler” for metabolites identification and quantitation.

2. Identifying and quantifying the metabolites in a batch with Chenomx Profiler
a. The converted NMR spectra are transferred to Chenomx Profiler, a function named “batch fit” allows to identify and quantify the metabolites across whole datasets with sophisticated computer-assisted fitting routines using a default Chenomx's spectral library or a library with only targeted metabolites generated by the user manually.
i. Click “Tools-Batch Fit-Add Folder” and select a folder that contains all processed spectra. Click next.
ii. Choose a list of interested compounds from:
1. A profiled spectrum (a library with only targeted metabolites generated by the user manually).
2. Chenomx Reference Compounds at 600 HZ (Default Chenomx's spectral library). Click next (if choosing ii-1, jump to 3 to learn how to generate a library with only targeted metabolites manually).
iii. Refine the previous compound selection by moving the interested compounds from the left to the right window. Click next and finish. It takes from several min to

several hours to process, depending on the number of compounds selected and the computer's capacity.

b. Manually check the batch-fitted spectra for accurate quantitation.
    i. Review the fitted spectra list on the left to make sure the peak fitting is correct. Adjust the fitting manually if necessary.
    ii. Click "File-Export-Compound Table" to export the quantified results.

3. Manually generate a profiled spectrum with only targeted metabolites (Do this step first if choose a-ii-1)
    a. Open a good representative spectrum within the spectra batch with Chenomx Profiler.
    b. Search for targeted compounds either by typing the metabolite name or the reference chemical shift at the "Find in Table" input box below the spectrum.
    c. Select the targeted compound name in the candidate list below the spectrum. Once a compound name is selected, a corresponding reference peak in purple will appear in the spectrum window. Zoom in to adjust the purple arrow vertically and horizontally to fit the peak.
    d. After fitting all targeted compounds, click "File-Save as", name the file as "targeted library".
    e. Follow all of step 2, except in a-ii, choose a-ii-2, use the profiled spectrum generated in this step as a reference.

Reagents and Solutions:

50X TAE:

Tris	121 g
Acetic Acid	28.55 mL
0.5 M EDTA	50 mL
Distilled Water	500 mL

Mix all ingredients and stir until fully dissolved (about 1-2 hours). Dilute to 1X by adding 20 mL of the 50X solution to 980 mL of distilled water.

COMMENTARY

Background Information

There is a growing importance surrounding microbiome analyses and coupling them with toxicological studies. This, combined with the misconception that microbiome analyses are only for computational biologists, is creating missed opportunities in novel pathway discovery, toxic effects, and risk factors. The above microbiome analysis is also not the only way to investigate the microbiome; QPCR methods have been established to analyze specific phyla or species of bacteria, and how they change with a given treatment. QPCR methods can and should be coupled with the above protocol because they can validate the bioinformatics results. Also, QPCR can use fecal pellets as a source of bacterial DNA if a study has run out of cecal contents. If a group wants a deeper analysis of the microbiome RNAseq studies have started to become a more popular way to investigate the metatranscriptome of the gut microbiome. This does involve an extensive isolation protocol and a 16S **rRNA** degradation protocol. Current metatranscriptomic results only report microbial transcripts expressed as a whole, but there is the potential to link mRNA expression to specific gut bacterial species. The key to this linkage is a combination of classical metabolomic strategies and bioinformatics. The above protocol is the first step in wide spread implementation of bioinformatics in classical toxicology labs.

This wide spread implementation is important to growing the knowledge base for the gut microbiome. As it stands now, microbiome analysis is still in its infancy, meaning there is not a standard protocol, reference base, or even a normal gut composition. The more research put into microbiome analysis, helps this knowledge base grow. It is also important for toxicologists to implement microbiome analysis to help validate results.

Most labs will do either a toxicological study or a bioinformatics microbiome analysis, making it almost impossible to link the two. With this protocol, combining classic toxicological studies and new microbiome analyses should become more common, which will lead to more validation and a better understanding of the microbiome's role in drug metabolism, dietary changes, and other toxicological studies.

Critical Parameters

As previously discussed, some basic training in terminal-based coding and R programming is needed to get the most out of a microbiome analysis. This training does not need to be extensive. For terminal coding, all that is needed are the skills to connect to and move around an external server or computing cluster within terminal and how to move files to and from a server. R coding should be used for graphing and statistics, but any software can be used instead of R. Also it is highly recommended that this analysis be done on a server or a computing cluster. Microbiome analyses can be done on a personal computer but it could take up to a month to complete, compared to a few hours on a server or computing cluster. Most major schools and universities have a computing cluster to be used for computationally intensive commands, like microbiome analyses. If there is not a computing cluster available, the amazon cloud is cost-affordable and will work just as well as a university computing cluster.

It is also extremely important to use blanks and method controls. The method controls will show what is picked up during the extraction and amplification. Also since 16S rRNA gene sequencing uses PCR, a very small amount of contamination could grow exponentially. To account for this, sequence the method blank to make sure the contamination seen in the blank is not in the samples. Also, if possible, run a mock

community with the samples on the sequencer. A mock community involves a known quantity of bacteria, usually about 12 - 15 different species. Mothur uses the mock community from BEI resources and is called HM-782D. Another mock community that can be used is from ZymoBIOMICS called the Microbial Community DNA Standard #D6305. These mock communities can be used to validate any other methods of 16S rRNA gene classification. Mothur has certain commands in the software that can be used to obtain an error rate based on the composition of mock communities. This can also help discover any sequence errors or any human errors in the analytic pipeline.

Troubleshooting

As with most computational workflows, there will be errors not mentioned in this protocol. If an error is not mentioned in this protocol, refer back to the miseq wiki (https://www.mothur.org/wiki/MiSeq_SOP), the HUMAnN2 bitbucket page (https://bitbucket.org/biobakery/humann2/wiki/Home), or the HUMAnN2 google group (https://groups.google.com/forum/#!forum/humann-users). This next section will discuss common errors that were not discussed in the above protocols.

1. **"X…num.temp is blank. Please correct." Error from mothur**. This is a very common error that results in a segmentation fault and an exit from the mothur program. When this error occurs, it is a notification that the server or the computer has run out of space. This happens more times on a personal computer than a server, but it has happened on a server. The best way to fix this is to delete all the files that are not needed any more, especially dist files. Dist files can sometimes be over 100 GB, so deleting them will free up a lot of space.
2. **After any command in mothur, there is an error of X sequence that is not present in Y file but is present in Z file.** This could also have to do with memory but can usually be fixed by deleting all the files in the working directory expect for the starting files (raw FASTQ files, stability file, silva.bacteria.fasta, and the two trainsets). When rerunning, this error should go away. This also sometimes occurs after a subsample has been taken. If this is the case, delete the subsample files and take a new

subsample. If this error is obtained multiple times, delete the files and start over from the beginning.

3. **Negative sequence lengths after summary.seqs command in mothur.** This will not give a segmentation fault but the results will be corrupted. This is caused by a mistake in the first step (*make.contigs*) and is usually due to one of the FASTQ files missing or misspelling in the stability file. There is an error present with this, but it usually comes up too quickly to notice. This is another important reason to do summary.seq commands with every run. To fix this, double check all the FASTQ files and make sure that both parts of the pair are present. Also check the stability file to make sure the format and the spelling are correct.
4. **OTU's do not match the tree error from GUnifrac.** This was briefly mentioned in the above sections, but a different way to solve this can be done all in R. Use the following commands to fix the problem within R.

```
Test.count <- read.delim("~/Desktop/count_table.txt", row.names=1)
row.names(Test.count)->A
Test.tre$tip.lable->B
setdiff(A,B)->C
Test.count.update<-Test.count [! row.names(Test.count) %in% C,]
```

These commands will find all the different names between the count table and the tree file and remove them. This sometimes works better than the steps outlined in **Support Protocol 2**, because, occasionally, there are more sequence differences in the count_table than just the tree node. The above commands will find these difference and remove them.

Anticipated Results

As mentioned above, this protocol will result in a summary file that has the taxonomic distribution of the gut microbiome. This file can be used for statistical tests to adequately describe the taxonomic shifts. If the alternative protocols are completed, a figure will be generated showing how different the two populations are based on distances mapped onto a phylogenic tree, as well as a list of pathways that are significantly different between a control and treatment group. With these outputs, many other applications can be done. A popular application is correlations between taxonomic

changes and metabolomic changes. This can show relationships between bacterial genera and metabolites and can be used to validate the metagenomic results. Also this information can be used for modeling and predictive software.

Time Constraints

Basic Protocol 1 will take about 5 - 8 hours of bench work, depending on the number of samples. **Basic Protocol 2** will take about 3 - 4 hours. The sequencing can take 1 week to 4 weeks, depending on the queue or if samples are sent to private sequencing companies. **Basic Protocol 3** will take between a day and a month depending on what is used for the analysis. If performed on an external server or computing cluster, **Basic Protocol 3** will only take about a day but if the analysis is done on a personal laptop, then it could take up to a month to complete. **Support Protocol 3** will take another day to a week, depending on the number of samples, size of the subsample, and what is being used to do the analysis. Dist.seqs is a command that can take a while and may be killed if the file being created is too large. Again this also depends on the computing power used for this analysis. **Alternative Protocol 1** will take 1 week to a month. The Illumina Hiseq takes considerably more time to sequence than the Illumina Miseq, one should factor in at least twice the Illumina Miseq sequencing run time for an Illumina Hiseq run. Also the actual analysis is easier but each HUMAnN2 command can take between 12 hours and a day on an external server. A time estimate for a HUMAnN2 run on a personal computer cannot be provided. NMR sample preparation for 30 samples will take approximately 5 hours. NMR sample acquisition for 30 samples will take

approximately 15 hours and the analysis of the 30 samples will take an additional 5 hours.

REFERENCES

1. Spanogiannopoulos P, Bess EN, Carmody RN, and Turnbaugh PJ. The microbial pharmacists within us: a metagenomic view of xenobiotic metabolism. *Nature Reviews Microbiology.* 2016.
2. Hosgood DH, Sapkota AR, Rothman N, Rohan T, Hu W, Xu J, Vermeulen R, He X, White JR, Wu G, et al. The Potential Role of Lung Microbiota in Lun Cancer Attributed to Household Coal Burning Exposures. *Environmental Molecular Mutagenesis.* 2015;55(643-51.
3. Lee HJ, Jeong SE, Lee S, Kim S, Han H, and Jeon CO. Effects of cosmetics on the skin microbiome of facial cheeks with different hydration levels. *MicrobiologyOpen.* 2017:1-14.
4. Kozich JJ, Westcott SL, Baxter NT, Highlander SK, and Schloss PD. Development of a dual-index sequencing strategy and curation pipeline for analyzing amplicon sequence data on the miseq illumina sequencing platform. *Applied and Environmental Microbiology.* 2013;79(5112-20.
5. Abubucker S, Segata N, Goll J, Schubert AM, Izard J, Cantarel BL, Rodriguez-Mueller B, Zucker J, Thiagarajan M, Henrissat B, et al. Metabolic reconstruction for metagenomic data and its application to the human microbiome. *PLoS Computational Biology.* 2012;8(
6. Zhang L, Xie C, Nichols RG, Chan SHJ, Jiang C, Hao R, Smith PB, Cai J, Simons MN, Hatzakis E, et al. Farnesoid X Receptor Signaling Shapes the Gut Microbiota and Controls Hepatic Lipid Metabolism. *mSystems.* 2016;1(e00070-16.
7. Murray IA, Nichols RG, Zhang L, Patterson AD, and Perdew GH. Expression of the aryl hydrocarbon receptor contributes to the establishment of intestinal microbial community structure in mice. *Scientific Reports.* 2016;6(33969.
8. Li G, Xie C, Lu S, Nichols RG, Tian Y, Li L, Patel D, Ma Y, Brocker CN, Yan T, et al. Intermittent Fasting Promotes White Adipose Browning and Decreases Obesity by Shaping the Gut Microbiota. *Cell Metabolism.* 2017;26(672-85.e4.
9. Hubbard TD, Murray IA, Nichols RG, Cassel K, Podolsky M, Kuzu G, Tian Y, Smith P, Kennett MJ, Patterson AD, et al. Dietary broccoli impacts microbial community structure and attenuates chemically induced colitis in mice in an Ah receptor dependent manner. *Journal of Functional Foods.* 2017;37(685-98.
10. Rintala A, Pietilä S, Munukka E, Eerola E, Pursiheimo JP, Laiho A, Pekkala S, and Huovinen P. Gut microbiota analysis results are highly dependent on the 16s rRNA gene target region, whereas the impact of DNA extraction is minor. *Journal of Biomolecular Techniques.* 2017;28(19-30.
11. Yang B, Wang Y, and Qian P-Y. Sensitivity and correlation of hypervariable regions in 16S rRNA genes in phylogenetic analysis. *BMC Bioinformatics.* 2016;17(135.
12. Martínez I, Muller CE, and Walter J. Long-term temporal analysis of the human fecal microbiota revealed a stable core of dominant bacterial species. *PLoS One.* 2013;8(7):e69621.
13. Jovel J, Patterson J, Wang W, Hotte N, O'Keefe S, Mitchel T, Perry T, Kao D, Mason AL, Madsen KL, et al. Characterization of the gut microbiome using 16S or shotgun metagenomics. *Frontiers in Microbiology.* 2016;7(1-17.
14. Caporaso JG, Kuczynski J, Stombaugh J, Bittinger K, Bushman FD, Costello EK, Fierer N, Peña AG, Goodrich K, Gordon JI, et al. QIIME allows analysis of high-throughput community sequencing data. 2010;7(335-6.

15. Huse SM, Welch DM, Morrison HG, and Sogin ML. Ironing out the wrinkles in the rare biosphere through improved OTU clustering. *Environmental Microbiology*. 2010;12(1889-98.
16. Chen J, Bittinger K, Charlson ES, Hoffmann C, Lewis J, Wu GD, Collman RG, Bushman FD, and Li H. Associating microbiome composition with environmental covariates using generalized UniFrac distances. *Bioinformatics.* 2012;28(2106-13.
17. Truong DT, Franzosa EA, Tickle TL, Scholz M, Weingart G, Pasolli E, Tett A, Huttenhower C, and Segata N. MetaPhlAn2 for enhanced metagenomic taxonomic profiling. *Nature Methods.* 2015;12(902-3.
18. Fonslow BR, Stein BD, Webb KJ, Xu T, Choi J, Kyu S, and Iii JRY. Fast gapped-read alignment with Bowtie 2. 2013;10(54-6.
19. Buchfink B, Xie C, and Huson DH. Fast and sensitive protein alignment using DIAMOND. *Nature methods.* 2015;12(59-60.
20. Segata N, Izard J, Waldron L, Gevers D, Miropolsky L, Garrett WS, and Huttenhower C. Metagenomic biomarker discovery and explanation. *Genome Biology.* 2011;12(R60.
21. Lu W, Kimball E, and Rabinowitz JD. A high-performance liquid chromatography-tandem mass spectrometry method for quantitation of nitrogen-containing intracellular metabolites. *Journal of the American Society for Mass Spectrometry*. 2006;17(37-50.
22. Tsugawa H, Cajka T, Kind T, Ma Y, Higgins B, Ikeda K, Kanazawa M, VanderGheynst J, Fiehn O, and Arita M. MS-DIAL: data-independent MS/MS deconvolution for comprehensive metabolome analysis. *Nature methods.* 2015;12(6):523-6.
23. Kessner D, Chambers M, Burke R, Agus D, and Mallick P. ProteoWizard: open source software for rapid proteomics tools development. *Bioinformatics.* 2008;24(21):2534-6.
24. Cai J, Zhang J, Tian Y, Zhang L, Hatzakis E, Krausz KW, Smith PB, Gonzalez FJ, and Patterson AD. Orthogonal Comparison of GC-MS and 1H NMR Spectroscopy for Short Chain Fatty Acid Quantitation. *Anal Chem.* 2017;89(15):7900-6.
25. Dai H, Xiao C, Liu H, and Tang H. Combined NMR and LC-MS analysis reveals the metabonomic changes in Salvia miltiorrhiza Bunge induced by water depletion. *J Proteome Res.* 2010;9(3):1460-75.
26. Cai J, Zhang L, Jones RA, Correll JB, Hatzakis E, Smith PB, Gonzalez FJ, and Patterson AD. Antioxidant Drug Tempol Promotes Functional Metabolic Changes in the Gut Microbiota. *J Proteome Res.* 2016;15(2):563-71.
27. Eriksson L, Trygg J, and Wold S. CV-ANOVA for significance testing of PLS and OPLS (R) models. *J Chemometr.* 2008;22(11-12):594-600.

Figure A-1

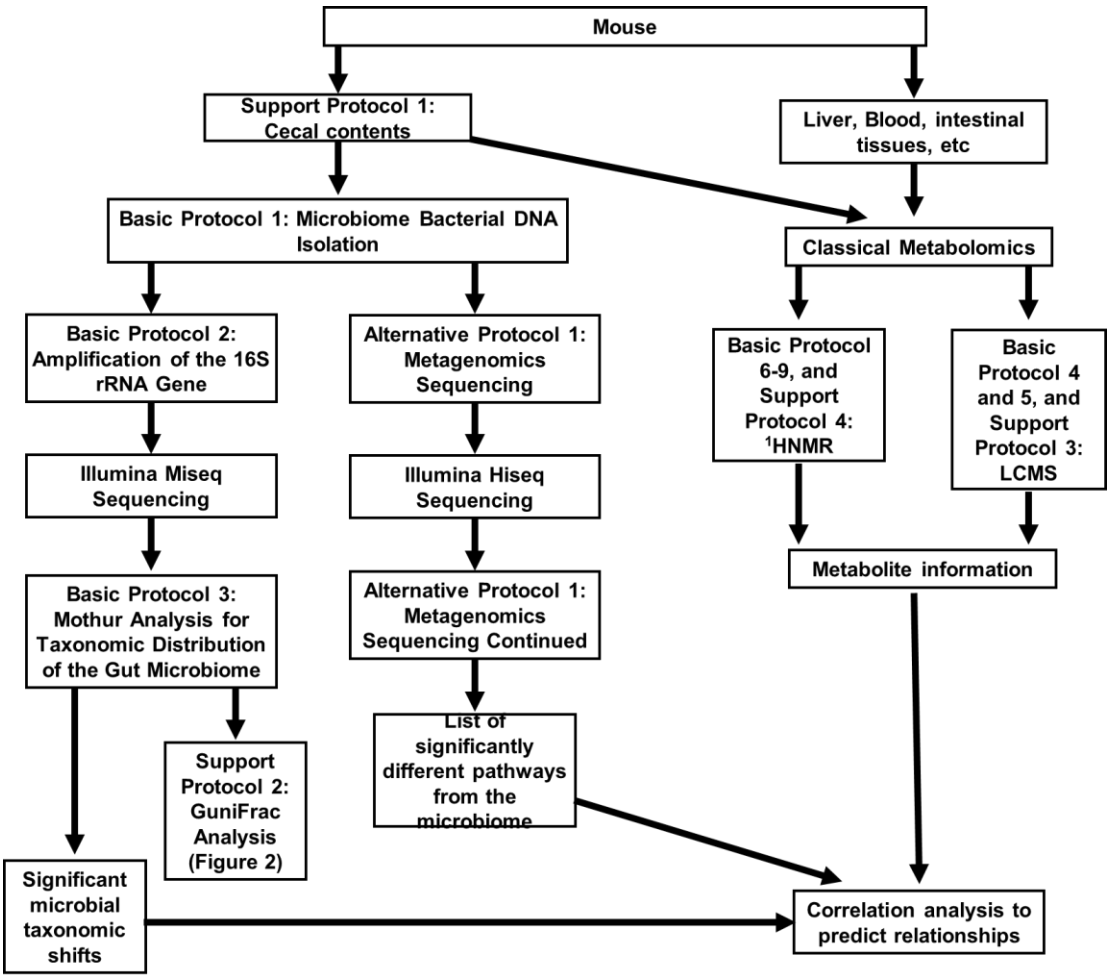

Figure A-1. Microbiome Analysis Flow Chart. Analysis flow chart using sequence- and metabolomics-based analysis to uncover structural and functional changes in the gut microbiome.

Figure A-2

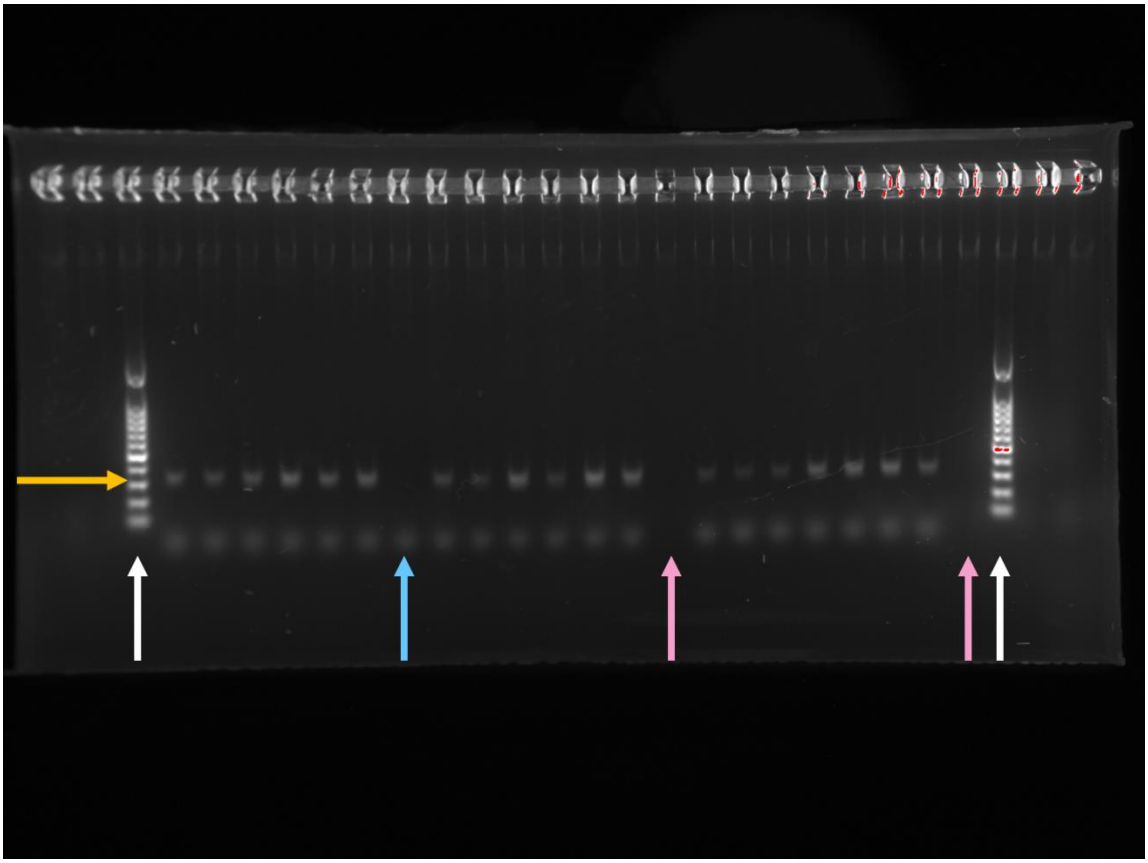

Figure A-2. An Example of the 1X Gel Used to Check the Size of the Amplified 16S V4V4 Region. The white arrows show the 100 base pair ladder used to check the length of the amplicons. The orange arrow show the 350 base pair location and all amplicons are 350 base pairs long. The blue arrow shows the method blank sample with no amplification and the pink arrows show wells with no material added.

Figure A-3

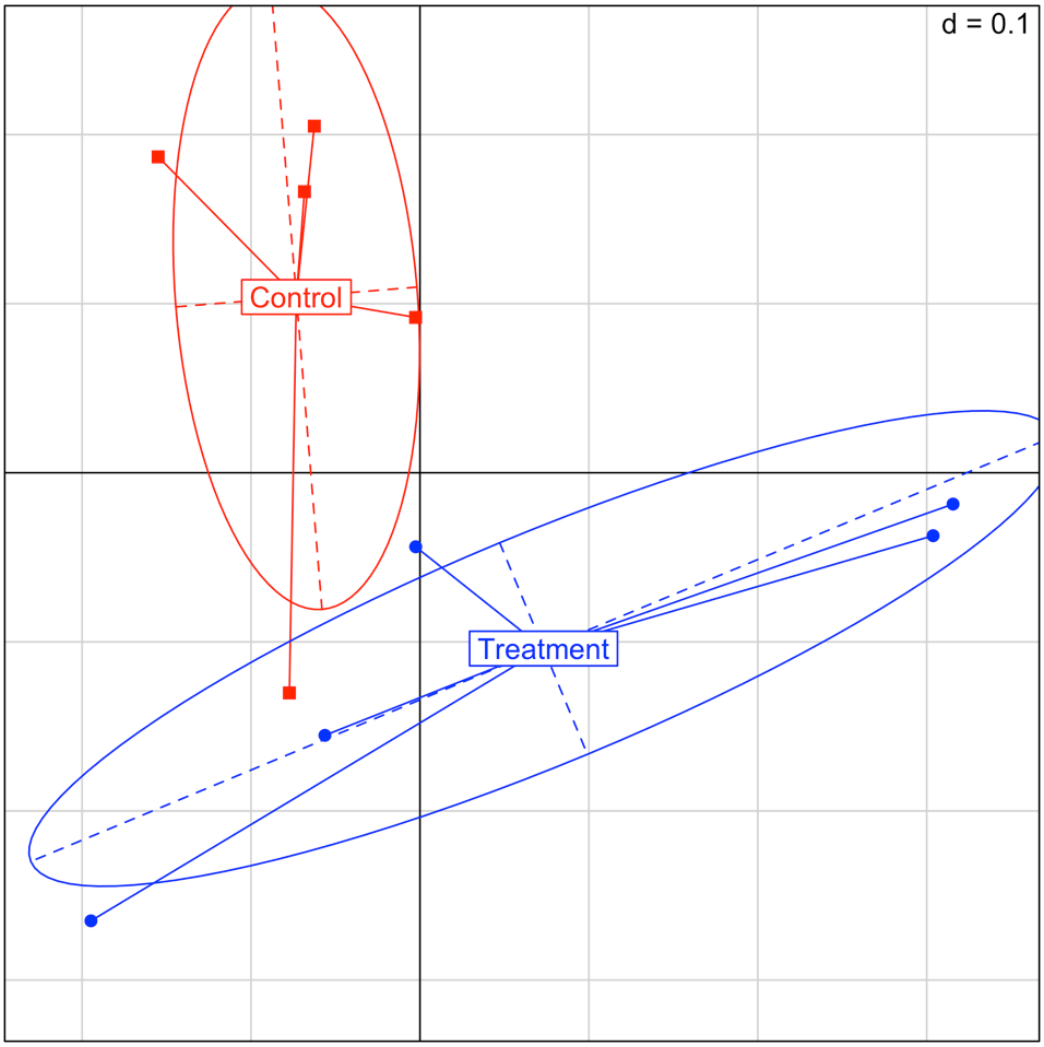

Figure A-3. An Example of Gunifrac Output. The use of different colors and shapes make the population level differences clear and easy to see. The p-value must be manually added to the graph after running adonis.

Table A-1. Example of Output From the Summary.seqs Command Described in Basic Protocol 3 Step 4

	Start	End	NBases	Ambigs	Polymer	NumSeqs
Minimum	1	90	90	0	3	1
2.5%-tile	1	292	292	0	3	67017
25%-tile	1	300	300	0	4	670164
Median	1	301	301	0	4	1340328
75%-tile	1	307	307	1	5	2010492
97.5%-tile	1	311	311	13	6	2613639
Maximum	1	602	602	128	300	2680655
# of Seqs	2680655					

Table A-2. Example of Output From the Summary.seqs Command Described in Basic Protocol 3 Step 10

	Start	End	NBases	Ambigs	Polymer	NumSeqs
Minimum	1	1984	25	0	3	1
2.5%-tile	1	13424	290	0	3	46530
25%-tile	1	13424	292	0	4	465299
Median	1	13424	292	0	4	930597
75%-tile	1	13424	292	0	5	1395895
97.5%-tile	1	13425	293	0	5	1814663
Maximum	10024	13425	312	0	10	1861192
# of Seqs	1618841					

Table A-3. Example of the First Four Rows of Test.Whole.txt

	Test1_R1_abundance	Test2_R1_abundance	Test3_R1_abundance	Test4_R1_abundance
PWY-6531: mannitol cycle	1795.5782225069	1725.7504704103	2029.9612805819	2440.9453481149
PWY-5097: lysine biosynthesis VI	2323.3379572841	2022.8473314703	1611.7329672909	1280.1021528578
PWY-5100: pyruvate fermentation to acetate and lactate II	1675.2226101548	1792.6844298156	2250.1729447694	2139.3626834727
VALSYN-PWY: valine biosynthesis	1577.5178609018	1469.8751222891	1902.6320681466	2261.7115189351

Table A-4: Example of the First Four Rows of Test.whole.clean.txt

Sample	Test 1	Test 2	Test 3	Test 4
Treatment	Control	Control	Treatment	Treatment
PWY-6531: mannitol cycle	1795.5782225069	1725.7504704103	2029.9612805819	2440.9453481149
PWY-5097: lysine biosynthesis VI	2323.3379572841	2022.8473314703	1611.7329672909	1280.1021528578
PWY-5100: pyruvate fermentation to acetate and lactate II	1675.2226101548	1792.6844298156	2250.1729447694	2139.3626834727
VALSYN-PWY: valine biosynthesis	1577.5178609018	1469.8751222891	1902.6320681466	2261.7115189351

Jingwei Cai

Education

Ph.D., Molecular Toxicology (2013-2018) The Pennsylvania State University
Minor, Genomics and Bioinformatics

B.S., Biological Sciences (2008-2012) Soochow University

Publications (Selected)

1. **Cai, J.**; Zhang, J.; Tian, Y.; Zhang, L.; Hatzakis, E.; Krausz, K. W.; Smith, P. B.; Gonzalez, F. J.; Patterson, A. D., Orthogonal Comparison of GC-MS and ^{1}H NMR Spectroscopy for Short Chain Fatty Acid Quantitation. *Anal Chem* 2017, 89 (15), 7900-7906.

2. **Cai, J.**; Zhang, L.; Jones, R. A.; Correll, J. B.; Hatzakis, E.; Smith, P. B.; Gonzalez, F. J.; Patterson, A. D., Antioxidant Drug Tempol Promotes Functional Metabolic Changes in the Gut Microbiota. *J Proteome Res* 2016, 15 (2), 563-71.

3. Nichols, R. G*.; **Cai, J*.**; Murray, I. A.; Koo, I.; Smith, P. B.; Perdew, G. H.; Patterson, A. D., Structural and Functional Analysis of the Gut Microbiome for Toxicologists. *Curr Protoc Toxicol* 2018 (*Denotes shared authorship)

4. Tian, Y.; Nichols, R. G.; Roy, P.; Gui, W.; Smith, P. B.; Zhang, J.; Lin, Y.; Weaver, V.; **Cai, J.**; Patterson, A. D., Cantorna, M. T., Prebiotic Effects Of White Button Mushroom (*Agaricus bisporus*) Feeding On Succinate And Intestinal Gluconeogenesis. *J Funct Foods* 2018, 45, 223-232.

5. Tian, Y,; Nichols, R.G.; **Cai, J.**; Patterson, A. D.;.Cantorna, M.T., Vitamin A Deficiency In Mice Alters Host And Gut Microbial Metabolism Leading To Altered Energy Homeostasis. *J. Nutr. Biochem.* 2018, 54, 28-34.

6. Zhang, L.; Xie, C.; Nichols, R. G.; Chan, S. H.; Jiang, C.; Hao, R.; Smith, P. B.; **Cai, J.**; Simons, M. N.; Hatzakis, E.; Maranas, C. D.; Gonzalez, F. J.; Patterson, A. D., Farnesoid X Receptor Signaling Shapes the Gut Microbiota and Controls Hepatic Lipid Metabolism. *mSystems* 2016, 1 (5).

7. Singh, V.; Chassaing, B.; Zhang, L.; San Yeoh, B.; Xiao, X.; Kumar, M.; Baker, M. T.; **Cai, J.**; Walker, R.; Borkowski, K.; Harvatine, K. J.; Singh, N.; Shearer, G. C.; Ntambi, J. M.; Joe, B.; Patterson, A. D.; Gewirtz, A. T.; Vijay-Kumar, M., Microbiota-Dependent Hepatic Lipogenesis Mediated by Stearoyl CoA Desaturase 1 (SCD1) Promotes Metabolic Syndrome in TLR5-Deficient Mice. ***Cell Metab*** 2015, 22 (6), 983-96.

8. Jiang, C.; Xie, C.; Li, F.; Zhang, L.; Nichols, R. G.; Krausz, K. W.; **Cai, J.**; Qi, Y.; Fang, Z. Z.; Takahashi, S.; Tanaka, N.; Desai, D.; Amin, S. G.; Albert, I.; Patterson, A. D.; Gonzalez, F. J., Intestinal Farnesoid X Receptor Signaling Promotes Nonalcoholic Fatty Liver Disease. *J Clin Invest* 2015, 125 (1), 386–402.

Awards (Selected)

- 2018 Paul Hand Research Achievement Award
- 2017 Graduate Student Travel Award
- 2016 Huck Graduate Research Innovation Awards
- 2015 National Institutes of Health T32 Training Grant, Animal Models of Inflammation
- 2013 Pennsylvania State University Excellence in Graduate Recruitment Award

Presentations (Selected)

- 2017 Mid-Atlantic Regional Meeting (MARM) in Hershey, PA
- 2016 Modern Methods in Metabolomics Seminar in University Park, PA
- 2015 Metabolomics Society Conference in San Francisco, CA
- 2014 Microbiome Workshop in University Park, PA